

# Implementing process analytical technology (PAT) tools for the analysis and control of manufacturing processes during hot-melt extrusion

By

Muhammad Tariqul Islam [B.Pharm (Hons.), MSc]

A thesis submitted to the University of Greenwich in partial fulfilment for  
the Degree of Doctor of Philosophy

December, 2014

Faculty of Engineering & Science, University of Greenwich, UK



## DECLARATION

“I certify that this work has not been accepted in substance for any degree, and is not concurrently being submitted for any other degree than that of Doctor of Philosophy being studied at the University of Greenwich. I also declare that this work is result of my own investigations except where otherwise identified by references and that I have not plagiarised the works of others”.

Signed:

**Muhammad Tariqul Islam** (Candidate)

.....

### PhD Supervisors

Dr Dionysios Douroumis

Prof. Babur Z Chowdhry

Date:

## ACKNOWLEDGEMENTS

These past three years turned out to be an overwhelming experience, coloured by the people around me. Completing this PhD could not have been possible without the help, patience, support and encouragement of numerous people, who inspired me and each of them contributed to this work in their own way.

Firstly, I would like to take the opportunity to extend my gratitude to almighty “ALLAH” who helped me numerous times to make this thesis possible (Alhamdulillah). I would also like to thank my parents, siblings, uncle, aunt and cousins for their continuous support and help throughout the past years and being with me during my research and giving me lots of inspiration and support.

I would like to express my sincerest appreciation to my supervisor, Dr Dionysios Douroumis and Prof. B. Z. Chowdhry for their guidance at each step of my progress. I am particularly indebted to my first supervisor Dr Dionysios Douroumis whose help, stimulating suggestions and encouragement helped me throughout my research.

I would also like to thank the School of Science of the University of Greenwich for giving me the opportunity to undertake this doctoral research and to use department facilities. I am grateful to Mrs Devyani Amin for her help with the HPLC experiments and Dr Ian Slipper of the School of Science whose assistance during this project is greatly appreciated.

Furthermore I would like to acknowledge Mrs. Sheelagh Halsey and Mr. Mark Arrowsmith from Thermofisher scientific UK for their enormous support during my study. And, I would like to express my gratitude to Dr Mohammed Maniruzzaman for his support during the studies.

Moreover, I would like to say a big thank you to my friend and colleague Dr Md Jasim Uddin for introducing me to my supervisors. I am grateful to my fellow PhD colleagues (Dr Hiren Moradiya, Mushfiq Akanda, and Uttam Roy) and friends for their assistance and mental support during my project work.

I am grateful to all of my well-wishers, teachers, and friends from my ex-universities “University of Science and Technology Chittagong, Bangladesh and Sheffield Hallam University, UK.”

And finally, my deepest gratitude goes out to my family and in particular to my parents and my uncle for their moral and financial support to upgrade me to this level of my career. Thank you for your endless support and encouragements, and for the many opportunities you have given me.

***Muhammad Tariqul Islam [B.Pharm(Hons.), MSc]***

## ABSTRACT

---

In the research reported in this thesis, hot-melt extrusion (HME) was coupled with process analytical technology (PAT) tools in order to investigate drug interactions during processing, identify drug/excipient interactions and monitor the quality of the extruded products. In order to ensure the quality of the products, X-ray powder diffraction (XRPD), differential scanning calorimetry (DSC), near infrared (NIR) spectroscopy, variable temperature x-ray powder diffraction (VTXRPD) and dissolution studies were implemented in various drug delivery systems manufactured by HME.

Paracetamol (PMOL) was processed with ethyl cellulose (EC) - Compritol 888 ATO (C888) polymer/lipid blends to produce sustained release drug formulations. The aim of this study was to optimize HME processing by using design of experiment (DoE) and to monitor the process using in-line NIR spectroscopy. Input variables such as drug loading, screw speed and feeding rate were investigated and in-line NIR spectra were collected during extrusion. A partial least squares calibration model and PCA plots were used to identify the optimum processing parameters. It was proved that drug loading has a significant effect on the final product while the PMOL dissolution rates were identified as a quality attribute for the development of sustained release formulations.

Extruded pharmaceutical cocrystals were manufactured by using carbamazepine (CBZ) as a model drug with saccharine (SCH) and *trans*-cinnamic acid (TCA) as cofomers at a 1:1 molar ratio. In-line NIR was employed to monitor the cocrystallization process along the HME barrel while off-line DSC and XRPD were used to characterise the extrudates. NIR analysis showed that cocrystal formation occurred gradually starting at the 2<sup>nd</sup> mixing zone and this was confirmed via DSC and XRPD analysis. Cocrystallization occurred via the formation of H-bonds between the drug and cofomers facilitating enhanced drug release rates compared to the prototype cocrystals produced via solvent evaporation.

Three sugar alcohols namely mannitol, sorbitol and xylitol were extruded at various weight ratios to produce sugar cocrystals. In-line NIR, employed for process monitoring, showed that cocrystal formation occurred by the formation of H-bonds. The extruded materials were compressed into orally disintegrating tablets and compared with tablets made using Starlac (as a binder) and the sugar alcohols. Characterization of the tablets showed that there is no significant difference - in terms of weight variation, thickness and hardness - of the tablets prepared from both extruded sugar cocrystals and the Starlac. However, tablets prepared from

the extruded sugar cocrystals demonstrated faster disintegration times and better friability compared with those compressed with Starlac.

In another study reflectance and transmission in-line NIR probes were coupled to HME to monitor the transformations of crystalline indomethacin (IND) to molecular solutions in the presence of Soluplus and Kollidon VA64 polymers. The analysis of the transmission and reflectance NIR data revealed that crystalline IND was completely transformed into molecular solutions while Raman analysis showed that it was homogeneously distributed in the polymer matrices. PCA analysis showed that the screw speed, during HME, affects the recorded spectra but not the homogeneity of the embedded drug in the films. Enhanced drug release, compared with bulk IND, was also attained using ground, hot-melt extruded films.

VTXRPD was used as a predictive tool to monitor the polymorphic behaviour of physical blends of PMOL and Soluplus polymer in comparison to HME processed blends. By using VTXRPD it was found that at temperatures above 120°C Form I PMOL transforms to Form II and significant 2-theta value shifts were detected using VTXRPD. The in-line NIR analysis confirmed that the polymorphic transformations taking place during HME processing were identical to those observed in VTXPRD. Thus, VTXRPD can be used as a predictive tool for HME processing.

## TABLE OF CONTENTS

<b>Contents</b>	<b>Page N°</b>
COVER PAGE	i
DECLARATION	ii
ACKNOWLEDGEMENT	iii-iv
ABSTRACT	v-vi
TABLE OF CONTENTS	vii
CONTENTS	viii-xiii
LIST OF TABLES	xiv-xv
LIST OF FIGURES	xv-xxi
ABBREVIATIONS	xxii-xxiii
PUBLICATIONS/CONFERENCE PRESENTATIONS	xxiv-xxv

# CONTENTS

---

<b>Chapter 1 : Introduction .....</b>	<b>1</b>
1.1. Hot-melt extrusion.....	1
1.1.1. Advantages and disadvantages of HME .....	2
1.1.2. Instrumentation .....	2
1.2. Quality by design (QbD).....	5
1.3. Process analytical technology (PAT) .....	6
1.3.1. Advantages of PAT.....	7
1.3.2. PAT tools .....	8
1.3.3. Near-infrared (NIR) spectroscopy .....	8
1.3.4. Principles of NIR spectroscopy .....	10
• Molecular vibrations .....	12
• Stretching vibrations .....	12
• Bending vibrations .....	13
1.3.5. NIR instrumentation.....	14
1.3.6. NIR measurement modes.....	15
1.4. Introduction to chemometrics: data mining .....	17
1.4.1. Pre-processing of signals .....	17
1.4.2. Pattern recognition example .....	18
1.4.3. Multivariate regression example.....	18
1.5. NIR as a PAT tool applied to pharmaceutical HME.....	18
1.6. Summary .....	20
1.7. References .....	20

**Chapter 2 : Development of sustained release formulations processed by hot-melt extrusion using a quality by design approach .....26**

2.1. Introduction .....	26
2.2. Materials and methods .....	28
2.2.1. Materials .....	28
2.2.2. Hot-melt extrusion .....	28
2.2.3. Thermal analysis .....	29
2.2.4. X-ray powder diffraction .....	29
2.2.5. NIR spectroscopy .....	30
2.2.6. Particle size analysis .....	31
2.2.7. Flow properties and compressibility .....	31
2.2.8. Tablet preparation .....	31
2.2.9. Tablet characterisation .....	31
2.2.10. <i>In-vitro</i> drug release studies .....	31
2.2.11. HPLC analysis .....	32
2.3. Results and discussion.....	32
2.3.1. HME processing.....	32
2.3.2. Thermal analysis .....	33
2.3.3. X-ray powder diffraction .....	36
2.3.4. In-line NIR monitoring .....	38
2.3.5. <i>In-vitro</i> drug release studies.....	40
2.4. Conclusions .....	43
2.5. References .....	43

## Chapter 3 : Monitoring cocrystallization processing via HME using in-line NIR spectroscopy48

3.1.	Introduction .....	48
3.2.	Materials and methods .....	50
3.2.1.	Materials .....	50
3.2.2.	Hot-melt extrusion processing .....	50
3.2.3.	Differential scanning calorimetry (DSC) analysis .....	51
3.2.4.	X-ray powder diffraction (XRPD) analysis .....	51
3.2.5.	In-line NIR spectroscopy monitoring .....	51
3.2.6.	Molecular modelling.....	52
3.2.7.	<i>In-vitro</i> dissolution studies.....	52
3.2.8.	HPLC analysis .....	52
3.3.	Results and Discussion.....	53
3.3.1.	HME processing.....	53
3.3.2.	Thermal analysis .....	53
3.3.3.	XRPD analysis .....	56
3.3.4.	In-line NIR monitoring .....	57
3.3.5.	<i>In-vitro</i> dissolution studies.....	60
3.3.6.	HME processing.....	61
3.3.7.	Thermal analysis .....	62
3.3.8.	XRPD analysis .....	64
3.3.9.	In-line NIR monitoring .....	67
3.3.10.	<i>In-vitro</i> dissolution studies.....	71
3.4.	Conclusions .....	72
3.5.	References .....	73

**Chapter 4 : Development and characterization of orally disintegrated tablets (ODTs) prepared by using sugar based cocrystals processed via hot-melt extrusion.....76**

4.1.	Introduction .....	76
4.2.	Materials & methods .....	78
4.2.1.	Materials .....	78
4.2.2.	HME.....	78
4.2.3.	Scanning electron microscopy .....	79
4.2.4.	Thermal analysis .....	79
4.2.5.	X-ray powder diffraction .....	79
4.2.6.	Near-infrared spectroscopy .....	79
4.2.7.	Particle size analysis .....	80
4.2.8.	Flow properties and compressibility .....	80
4.2.9.	Tablet preparation .....	80
4.2.10.	Tablet characterisation .....	81
4.3.	Results and discussion.....	81
4.3.1.	HME.....	81
4.3.2.	Scanning electron microscopy .....	82
4.3.3.	Differential scanning calorimetry .....	82
4.3.4.	X-ray powder diffraction .....	89
4.3.5.	In-line NIR monitoring .....	93
4.3.6.	Particle size analysis .....	97
4.3.7.	Tablet preparation .....	98
4.3.8.	Tablet characterization.....	100
4.4.	Conclusions .....	102
4.5.	References .....	103

**Chapter 5 : Implementation of transmission NIR as a PAT tool for monitoring drug transformation during HME processing .....106**

5.1. Introduction .....	106
5.2. Materials and methods .....	108
5.2.1. Materials .....	108
5.2.2. Hot-melt extrusion process .....	108
5.2.3. Thermal analysis .....	110
5.2.4. X-ray powder diffraction .....	110
5.2.5. Near-infrared spectroscopy (NIR) .....	111
5.2.6. Confocal Raman spectroscopy.....	112
5.2.7. <i>In-vitro</i> drug release studies.....	112
5.2.8. HPLC analysis .....	113
5.3. Results and discussion.....	113
5.3.1. Hot-melt extrusion process .....	113
5.3.2. X-ray powder diffraction (XRPD).....	114
5.3.3. Differential scanning calorimetry .....	116
5.3.4. In-line NIR monitoring .....	119
5.3.5. Confocal Raman spectroscopy.....	125
5.3.6. <i>In-vitro</i> drug release studies.....	127
5.4. Conclusions .....	128
5.5. References .....	128

**Chapter 6 : Prediction of polymorphic transformations of paracetamol in solid dispersions 133**

6.1.	Introduction .....	133
6.2.	Materials and methods .....	134
6.2.1.	Materials .....	134
6.2.2.	Hansen solubility parameters ( $\delta$ ) and Flory–Huggins interaction parameter ( $\chi$ ): drug–copolymer miscibility .....	134
6.2.3.	HME process.....	136
6.2.4.	Thermal analysis (DSC and MTDSC) .....	136
6.2.5.	Hot-stage microscopy .....	136
6.2.6.	Variable-temperature X-ray powder diffraction .....	137
6.2.7.	In-line NIR spectroscopy .....	137
6.3.	Results and discussion.....	138
6.3.1.	Solubility parameters .....	138
6.3.2.	(F–H) theory for the prediction of drug/polymers interaction parameter .....	138
6.3.3.	Thermal analysis .....	140
6.3.4.	Variable-temperature X-ray powder diffraction .....	144
6.3.5.	In-line NIR spectroscopy monitoring .....	150
6.4.	Conclusions .....	151
6.5.	References .....	152
<b>Chapter 7 : Overall conclusions and future work.....</b>		<b>156</b>
7.1.	Overall conclusions .....	156
7.2.	Future work .....	159

## LIST OF TABLES

### **Chapter 2: Development of sustained release formulations processed by hot-melt extrusion using a quality by design approach**

- Table 2.1.** Experimental design of PMOL/C888/EC formulations using drug loading, screw speed and feed rate as independent variables and PMOL release (%), particle size D(0, 5) as dependent variables. ....28
- Table 2.2.** ANOVA analysis for the % release of PMOL ( $T_{6hr}$ ,  $T_{12hr}$ ) and particle size of the extrudates according to the response surface design. ....42

### **Chapter 4: Development and characterization of orally disintegrated tablets (ODTs) prepared by using sugar based cocrystals processed via hot-melt extrusion**

- Table 4.1.** Compositions of formulations used for HME. ....781
- Table 4.2.** Composition of tablet formulations blended with PMOL as an API (PMOL loaded formulations, PLFs) ..... 102
- Table 4.3.** Compressibility properties of placebo formulations and PMOL loaded formulations. .... 102
- Table 4.4.** Tablet characterization of placebo formulations and Starlac (no PMOL). .... 100
- Table 4.5.** Tablet characterization of PMOL loaded formulations composed of extruded sugar cocrystals and Starlac. .... 102

### **Chapter 5: Implementation of transmission NIR as a PAT tool for monitoring drug transformation during HME processing**

- Table 5.1.** Composition of IND extruded formulations with SOL and VA64 at various drug: polymer ratios. .... 109
- Table 5.2.** Melting endotherms and glass transition temperatures for bulk IND, SOL, VA64 and extrudates (EX). .... 118

## **Chapter 6: Prediction of polymorphic transformations of paracetamol solid dispersions**

<b>Table 6.1.</b> Calculated Hansen solubility parameters for PMOL and polymers.....	138
<b>Table 6.2.</b> F–H interaction parameters for different melt extruded drug–polymer formulations. .....	139
<b>Table 6.3.</b> DSC data for PMOL, copolymers and HME extruded formulations.....	140
<b>Table 6.4.</b> Polymorphic transformation temperatures of formulations physical mixtures (PMs) and extruded formulations (EX).....	150

## **LIST OF FIGURES**

### **Chapter 1: Introduction**

<b>Fig. 1.1.</b> Schematic of different dosage forms that can be produced by HME [60]......	2
<b>Fig. 1.2.</b> Ram extruder [1]. .....	3
<b>Fig. 1.3.</b> HME equipment and process parameters traditionally monitored during pharmaceutical HME (1. feeding system, 2. feeding hopper, 3. temperature controlled barrel with one or twin screws, 4. die and 5. screw driving unit) [59]......	4
<b>Fig. 1.4.</b> HME extruder barrel (ThermoFisher). .....	4
<b>Fig. 1.5.</b> Schematic diagram of HME with downstream equipment. ....	4
<b>Fig. 1.6.</b> Location of the NIR spectral region in the electromagnetic spectrum.....	10
<b>Fig. 1.7.</b> Different regions of the electromagnetic spectrum and the related spectroscopic techniques; the wavelength and wavenumber limits of each region are shown [55]. .....	11
<b>Fig. 1.8.</b> Electromagnetic wave propagation [47]......	12
<b>Fig. 1.9.</b> Molecular vibrations.....	13
<b>Fig. 1.10.</b> Energy level diagrams showing the basic transitions involved in a) MIR and b) NIR [55]. .....	13
<b>Fig. 1.11.</b> A diagram of an FT NIR spectrometer (ThermoNicolet).....	15

## **Chapter 2: Development of sustained release formulations processed by hot-melt extrusion using a quality by design approach**

<b>Fig. 2.1.</b> Thermograms of the pure PMOL, pure EC and C888 ATO. ....	33
<b>Fig. 2.2.</b> Thermograms of the physical mixtures containing 40%, 60% and 80% PMOL and equal amounts of EC and C888 ATO.....	34
<b>Fig. 2.3.</b> Thermograms of the extrudates (F1-F5) containing 40%, 60% and 80% PMOL and equal amounts of EC and C888 ATO.....	35
<b>Fig. 2.4.</b> Thermograms of the extrudates (F6-F11) containing 40%, 60% and 80% PMOL and equal amounts of EC and C888 ATO.....	35
<b>Fig. 2.5.</b> X-ray diffractograms of pure materials, a physical mixture containing 80% PMOL and extrudates.....	36
<b>Fig. 2.6.</b> X-ray diffractograms of a physical mixture containing 60% PMOL and extrudates. ....	37
<b>Fig. 2.7.</b> X-ray diffractograms of a physical mixture containing 40% PMOL and extrudates. ....	38
<b>Fig. 2.8.</b> NIR spectra of PMOL (bulk), EC (bulk), C888 ATO (bulk) and PMOL/EC/C888 ATO extruded formulations.....	38
<b>Fig. 2.9.</b> PLS calibration curve obtained using 40%, 60% and 80 % PMOL with varying processing parameters.....	39
<b>Fig. 2.10.</b> Principal component plot obtained after PCA on the pre-processed in-line collected NIR spectra during extrusion of mixtures containing 40%, 60% and 80% PMOL extruded with EC and C888 ATO. ....	40
<b>Fig. 2.11.</b> Dissolution profiles for PMOL/EC/C888 formulations at 40%, 60% and 80% drug content, extruded at different processing parameters ( <b>Table 2.1</b> ).....	41

## **Chapter 3: Monitoring cocrystallization processing via HME using in-line NIR spectroscopy**

<b>Fig. 3.1.</b> Schematic diagram of the screw in TSE indicating the collection zones.....	53
<b>Fig. 3.2.</b> DSC thermograms of bulk CBZ, bulk TCA, cocrystals processed at TSE135°C and the physical mixture. ....	54
<b>Fig. 3.3.</b> DSC thermograms of samples collected from different zones in the TSE.....	55
<b>Fig. 3.4.</b> X-ray diffractograms of CBZ (bulk), TCA (bulk), CBZ-TCA physical mixture, samples from TSE barrel zones (A, B and C) and final extrudates.....	56
<b>Fig. 3.5.</b> NIR spectra of bulk CBZ, bulk TCA, and a physical mixture of CBZ and TCA. ....	57
<b>Fig. 3.6.</b> Second derivative NIR spectra of CBZ (bulk), TCA, and a physical mixture of CBZ and TCA in the 4600-5300 cm <sup>-1</sup> wavenumber region. ....	58
<b>Fig. 3.7.</b> Second derivative spectra of the PM and the extruded cocrystals in the wavenumber regions between 4600 and 5300 cm <sup>-1</sup> . ....	58
<b>Fig. 3.8.</b> Second derivative in-line NIR spectra in the mixing zones (A, B, C), the TSE extruded cocrystals and the PM.....	59
<b>Fig. 3.9.</b> 3D-molecular modelling of the developed CBZ-TCA cocrystals illustrating the hydrogen-bonding between the functional groups. ....	60
<b>Fig. 3.10.</b> Dissolution profiles of bulk CBZ, prototype and extruded cocrystals (pH 1.2, n=3). ....	61
<b>Fig. 3.11.</b> DSC thermograms of bulk CBZ, bulk SCH, cocrystals processed by TSE and the PM. ....	62
<b>Fig. 3.12.</b> DSC thermogram of CBZ-SCH prototype. ....	63
<b>Fig. 3.13.</b> DSC thermograms of samples were collected from different zones in the TSE, final extrudates and the PMs.....	64
<b>Fig. 3.14.</b> X-ray diffractogram of CBZ-SCH prototype.....	65
<b>Fig. 3.15.</b> X-ray diffractograms of CBZ (bulk), SCH (bulk), and CBZ-SCH cocrystal extrudates.....	65

<b>Fig. 3.16.</b> X-ray diffractograms of the CBZ-SCH physical mixture, samples from the TSE barrel zones (A, B and C) and final extrudates.....	66
<b>Fig. 3.17.</b> NIR spectra of CBZ (bulk), SCH, and CBZ/SCH PM.....	67
<b>Fig. 3.18.</b> Second derivatives NIR spectra of CBZ (bulk), SCH, and CBZ/SCH PM in the 6400-7100 cm <sup>-1</sup> wavenumber region. ....	68
<b>Fig. 3.19.</b> Second derivative spectra of CBZ/SCH (PM) and the extruded cocrystals in the 6400-7100 cm-1 wavenumber region.....	68
<b>Fig. 3.20.</b> Second derivative of in-line NIR spectra in the mixing zones (A, B, C), the TSE extrudates and the PM. ....	69
<b>Fig. 3.21.</b> Molecular modelling of the developed CBZ-SCH form I cocrystals depicting the hydrogen-bonding between the functional groups. ....	70
<b>Fig. 3.22.</b> Dissolution profiles of bulk CBZ and CBZ/SCH PM.....	71
<b>Fig. 3.23.</b> Dissolution profiles of CBZ/SCH prototype and CBZ/SCH cocrystals processed via TSE. ....	72

**Chapter 4: Development and characterization of orally disintegrated tablets (ODTs) prepared by using sugar based cocrystals processed via hot-melt extrusion**

<b>Fig. 4.1.</b> Schematic of the extruder screw, indicating the mixing and collection zones (ZA-ZC) of the HME. ....	81
<b>Fig. 4.2.</b> SEM micrographs of bulk pearlitol, sorbitol, xylitol, physical mixtures (PMs) and the extruded formulations of FA, FB and FC.....	82
<b>Fig. 4.3.</b> DSC thermograms for pure (bulk) pearlitol, sorbitol and xylitol.....	83
<b>Fig. 4.4.</b> DSC thermograms of a physical mixture of F1 and the extrudate. ....	83
<b>Fig. 4.5.</b> DSC thermograms of a physical mixture of F2 and the extrudate. ....	84
<b>Fig. 4.6.</b> DSC thermograms of physical mixtures of F3-F4 and the extrudates. ....	84
<b>Fig. 4.7.</b> DSC thermograms of physical mixtures of F5-F6 and the extrudates. ....	85

<b>Fig. 4.8.</b> DSC thermograms of physical mixtures of F7-F9 and the extrudates. ....	85
<b>Fig. 4.9.</b> DSC thermograms of the physical mixtures of FA, FB and FC.....	86
<b>Fig. 4.10.</b> DSC thermograms of samples collected from different mixing zones of the extruder barrel and the final extrudates of FA. ....	87
<b>Fig. 4.11.</b> DSC thermograms of samples collected from different mixing zones of the extruder barrel and the final extrudates of FB. ....	88
<b>Fig. 4.12.</b> DSC thermograms of samples collected from different mixing zones of the extruder barrel and the final extrudates of FC. ....	88
<b>Fig. 4.13.</b> XRPD profiles of pure (bulk) pearlitol, sorbitol and xylitol. ....	89
<b>Fig. 4.14.</b> XRPD profiles of the physical mixtures of F1-F4 and the extrudates. ....	90
<b>Fig. 4.15.</b> XRPD profiles of the physical mixtures of F5-F8 and the extrudates. ....	90
<b>Fig. 4.16.</b> XRPD profiles of a physical mixture and samples collected from three different mixing zones of extruder and final extrudates of FA. ....	91
<b>Fig. 4.17.</b> XRPD profiles of a physical mixture and samples collected from three different mixing zones of extruder and final extrudates of FB. ....	92
<b>Fig. 4.18.</b> XRPD profiles of a physical mixture and samples collected from three different mixing zones of extruder and final extrudates of FC. ....	92
<b>Fig. 4.19.</b> Off-line NIR spectra of the pure (bulk) sugars pearlitol, sorbitol, xylitol and the physical mixtures of FA, FB and FC. ....	93
<b>Fig. 4.20.</b> Second derivative NIR spectra of raw materials (pearlitol, xylitol and sorbitol), a physical mixture and the extrudate of FA in the 5800 – 4300 cm <sup>-1</sup> wavenumber region. ....	94
<b>Fig. 4.21.</b> Second derivative off-line NIR spectra of a physical mixture, in-line NIR spectra collected from different mixing zones during extrusion and the final extrudates of FA. ....	95

**Fig. 4.22.** Second derivative off-line NIR spectra of a physical mixture, in-line NIR spectra collected from different mixing zones during extrusion and the final extrudates of FB..96

**Fig. 4.23.** Second derivative off-line NIR spectra of a physical mixture, in-line NIR spectra collected from different mixing zones during extrusion and the final extrudates of FC..96

**Fig. 4.24.** Particle size distribution for the extruded formulations (FA-FC). .....97

**Fig. 4.25.** Particle size distribution of micronized sugar cocrystals of the extrudates of FA-FC. ....98

**Chapter 5: Implementation of transmission NIR as a PAT tool for monitoring drug transformation during HME processing**

**Fig. 5.1.** The special die (A) made for in-line NIR monitoring via a transmission NIR probe and (B) an example of an extruded film. .... 109

**Fig. 5.2.** In-line NIR probes (transmission and reflectance) attached to the HME. .... 112

**Fig. 5.3.** XRPD profiles of bulk IND, SOL and VA64. .... 114

**Fig. 5.4.** XRPD profiles of physical mixtures of IND/SOL and IND/VA64..... 115

**Fig. 5.5.** XRPD profiles of IND/SOL and IND/VA64 extrudates..... 115

**Fig. 5.6.** DSC thermograms of bulk IND, SOL and VA64. .... 116

**Fig. 5.7.** DSC thermograms of physical mixtures of IND/VA64 and extruded formulations. .... 117

**Fig. 5.8.** DSC thermograms of physical mixtures of IND/SOL and extruded formulations. 117

**Fig. 5.9.** Calibration plot (top) and second derivative NIR spectra (bottom) collected from extruded IND/SOL mixtures at different weight ratios and bulk IND. .... 119

**Fig. 5.10.** Principal component score plot of NIR spectra from the in-line transmission probe data. .... 120

**Fig. 5.11.** Unprocessed and second derivative NIR spectra of IND/VA64 (20/80). .... 121

<b>Fig. 5.12.</b> Unprocessed and second derivative NIR spectra of IND/SOL (20/80, w/w). .....	122
<b>Fig. 5.13.</b> Unprocessed and second derivative NIR spectra of IND/VA64 (40/60, w/w). ....	123
<b>Fig. 5.14.</b> Unprocessed and second derivative NIR spectra of IND/SOL (40/60, w/w). .....	124
<b>Fig. 5.15.</b> Unprocessed and second derivative NIR spectra of IND/SOL (50/50). .....	124
<b>Fig. 5.16.</b> Raman spectra of pure IND and VA64. ....	125
<b>Fig. 5.17.</b> a) Variation of eigenvalues with the principal components, b) comparison of first three PCs c) comparison of first PC with the spectra of IND and VA64 and d) chemical map of PC1. ....	126
<b>Fig. 5.18.</b> Drug release profile of bulk IND, IND/SOL (50/50) and IND/VA64 (40/60). ....	127

## **Chapter 6: Prediction of polymorphic transformations of paracetamol solid dispersions**

<b>Fig. 6.1.</b> DSC thermal transitions of PMOL and polymers. ....	141
<b>Fig. 6.2.</b> Thermal transitions of PMOL-VA64 extruded formulations. ....	142
<b>Fig. 6.3.</b> HSM of pure PMOL and PMOL/SOL, PMOL/VA64 extruded formulations. ....	143
<b>Fig. 6.4.</b> VT XR PD diffractograms of bulk PMOL as a function of temperature. ....	145
<b>Fig. 6.5.</b> VT XR PD diffractograms of PMOL/SOL 40% physical mixture (PM) and extruded formulations (EXT) at different temperatures (from ambient to 122°C). ....	146
<b>Fig. 6.6.</b> VT XR PD diffractograms of PMOL/SOL 60% extruded formulations at different temperatures (100-120°C; cooling and heating).....	147
<b>Fig. 6.7.</b> VT XR PD diffractograms of PMOL-VA64 60% extruded formulations as a function of temperatures (from ambient to 122°C). ....	148
<b>Fig. 6.8.</b> VT XR PD diffractograms of PMOL-VA64 40% and 60% physical mixture (PM) at different temperatures (from ambient to 122°C). ....	149
<b>Fig. 6.9.</b> (a) NIR spectra of PMOL pure Form I and PMOL extrudate at 120°C; (b) 2nd derivative NIR spectra. ....	151

## ABBREVIATIONS

<b>Abbreviation</b>	<b>Meaning</b>
C888	Compritol 888 ATO
CBZ	Carbamazepine
CMC	Chemistry, manufacturing and controls
CPP	Critical process parameter
CQAs	Critical quality attributes
DoE	Design of experiment
DSC	Differential scanning calorimetry
EC	Ethyl cellulose
EVA	Ethyl vinyl acetate
FDA	Food and Drug Administration
F-H	Flory Huggins
FT-IR	Fourier-transform infrared
HME	Hot-melt extrusion
HSM	Hot stage microscopy
IBU	Ibuprofen
ICH	International conference on harmonisation
IND	Indomethacin
MAPP	Manual of policies and procedures
MSC	Multiplicative scatter correction
NIC	Nicotinamide
NIR	Near infra-red
PAT	Process analytical technology
PCA	Principal Component Analysis
PEG	Polyethylene glycol
PEO	Polyethylene oxide
PLS	Partial least square

PM	Physical mixture
PMOL	Paracetamol
QbD	Quality by design
SCH	Saccharine
SEM	Scanning electron microscopy
SFP	Supercritical fluid processing
SNV	Standard normal variate
SOL	Soluplus
TCA	<i>Trans</i> -cinnamic acid
TPP	Target product profile
TSE	Twin screw extruder
VA64	Kollidon VA64
VTXRPD	Variable temperature X-ray powder diffraction
XRPD	X-ray powder diffraction

## PUBLICATIONS/CONFERENCE PRESENTATIONS

### Original Research Articles

- **Islam MT**, Maniruzzaman M, Halsey S, Chowdhry B, Douroumis D, Development of sustained release formulations processed by hot-melt extrusion by using a quality by design approach, *Drug Delivery and Translational Research*, 2014; 4: 377-387.
- Moradiya H, **Islam MT**, Woollam GR, Slipper IJ, Halsey S, Snowden MJ, Douroumis D, Continuous cocrystallization for dissolution rate optimization of a poorly water-soluble drug, *Crystal Growth & Design*, 2014; 14: 189-198.
- Moradiya H, **Islam MT**, Halsey S, Maniruzzaman M, Chowdhry B, Snowden MJ, Douroumis D, Continuous cocrystallization of carbamazepine and *trans*-cinnamic acid via melt extrusion processing, *CrystEngComm*, 2014; 16: 3573-3583.
- Maniruzzaman M, **Islam MT**, Moradiya H, Halsey S, Slipper I, Chowdhry B, Snowden M, Douroumis D, Prediction of polymorphic transformation of paracetamol in solid dispersions. *Journal of Pharmaceutical Sciences*, 2014; 103(6): 1819-1828.
- **Islam MT**, Moradiya HG, Scoutaris N, Halsey SA, Bradley M, Chowdhry B, Douroumis D, Implementation of Transmission NIR as a PAT tool for monitoring drug transformation during HME processing, *European Journal of Pharmaceutics and Biopharmaceutics*, 2015 (submitted).
- **Islam MT**, Scoutaris N, Chowdhry B, Douroumis D, Investigating the stability of sustained release tablets prepared by using various lipids as a carrier via melt extrusion processing. *Drug Delivery and Translational Research*, 2015 (submitted).

### Conference (oral presentations) Proceeding (Selected)

- **Islam MT**, Online process monitoring of continuous hot-melt extrusion, PhD research seminar 2013-14, University of Greenwich, UK.
- **Islam MT**, Halsey S, Douroumis D, Implementation of NIR spectroscopy as a process analytical tool in hot-melt extrusion processing, UKPharmSci 2013, Edinburgh, UK.
- **Islam MT**, Moradiya H, Halsey S, Douroumis D, Investigation of the potential of NIR spectroscopy as a PAT tool carbamazepine-*trans*-cinnamic acid cocrystal formation, UKPharmSci 2013, Edinburgh, UK.
- **Islam MT**, Moradiya H, Halsey S, Douroumis D, Implementing NIR spectroscopy as a process analytical technology (PAT) tool in hot-melt extrusion (HME) processing

followed by quality by design (QbD) approach, BIT's 3<sup>rd</sup> Annual Symposium of Drug Delivery Systems, 2013. Haikou, China.

- **Islam MT**, Douroumis D, Spectroscopic hot-melt extrusion in-process monitoring and evaluation, ThermoFisher Scientific user meeting 2012, Stratford Upon-Avon, UK.

#### **Conference (Poster presentation) Proceeding (Selected)**

- Maniruzzaman M, **Islam MT**, Douroumis D, Inorganic excipients to develop solid dispersions in continuous process, UKPharmSci 2014, Hertfordshire, UK.
- **Islam MT**, Halsey S, Douroumis D, Implementation of NIR spectroscopy as a process analytical tool in hot-melt extrusion processing, UKPharmSci 2013, Edinburgh, UK.
- **Islam MT**, Moradiya H, Halsey S, Douroumis D, Investigation of potential of NIR spectroscopy as a PAT tool carbamazepine-*trans*-cinnamic acid cocrystal formation, UKPharmSci 2013, Edinburgh, UK.
- Maniruzzaman M, **Islam MT**, Moradiya H, Halsey S, Slipper I, Chowdhry B, Snowden M, Douroumis D, Prediction of polymorphic transformation of paracetamol in solid dispersions, UKPharmSci 2013, Edinburgh, UK.
- **Islam MT**, Douroumis D, Spectroscopic hot-melt extrusion in-process monitoring and evaluation, UoG-AAPS student chapter conference 2013, London, UK.
- **Islam MT**, Halsey S, Douroumis D, Implementation of NIR spectroscopy as a process analytical tool in hot-melt extrusion processing, Faculty research symposium 2013, University of Greenwich, UK.

# Chapter 1: Introduction

---

## 1.1. Hot-melt extrusion

Since the 1930's, hot-melt extrusion (HME) is one of the most extensively used processes in industry e.g. plastic and food manufacturing [1]. Almost all of the plastic products including plastic bags, sheets, pipes [2] and lots of food items-for example pastas, cereals or pet food-are manufactured via this technique. HME is a method of producing raw materials into a uniform shape and density by pushing it through an opening (extrusion die) under controlled conditions for example temperature, pressure and feed rate [3, 4].

Widespread interest in HME for pharmaceutical applications has been increasing rapidly over the last few years and numerous patents regarding HME have been recorded since the 1980's [4]. HME has been used to prepare pharmaceutical drug delivery systems including transdermal [5, 6], sustained release tablets [7- 9], sustained release capsules [10], colonic delivery system [11], pellets [12], floating gastro-retentive devices [13], enteric tablets [14, 15], granules [16], implants [17, 18] and taste masking of bitter APIs [19]. Furthermore, HME was used to enhance the bioavailability of poorly soluble drugs by the development of solid dispersions [20, 21].

During hot-melt processing, polymer, active ingredient(s) and other processing materials are fed into a heated barrel and the polymer-drug blend is transported through the instrument towards the end (extrusion die); the ingredients melt or soften at the high temperature, the softened mass is continuously rubbed and pressurized, and finally the homogeneous melt is pumped through the die attached to the end of the barrel. As material passes through the die, the material acquires the shape of the die opening and the material solidifies; the extruded product is referred to as the extrudate. The shape of the die is important for the final product. Varying the shape of the die may vary the final product. The final product could be pellets, films, granules, cylinders or tubes depending on the die shape (**Fig. 1.1**).

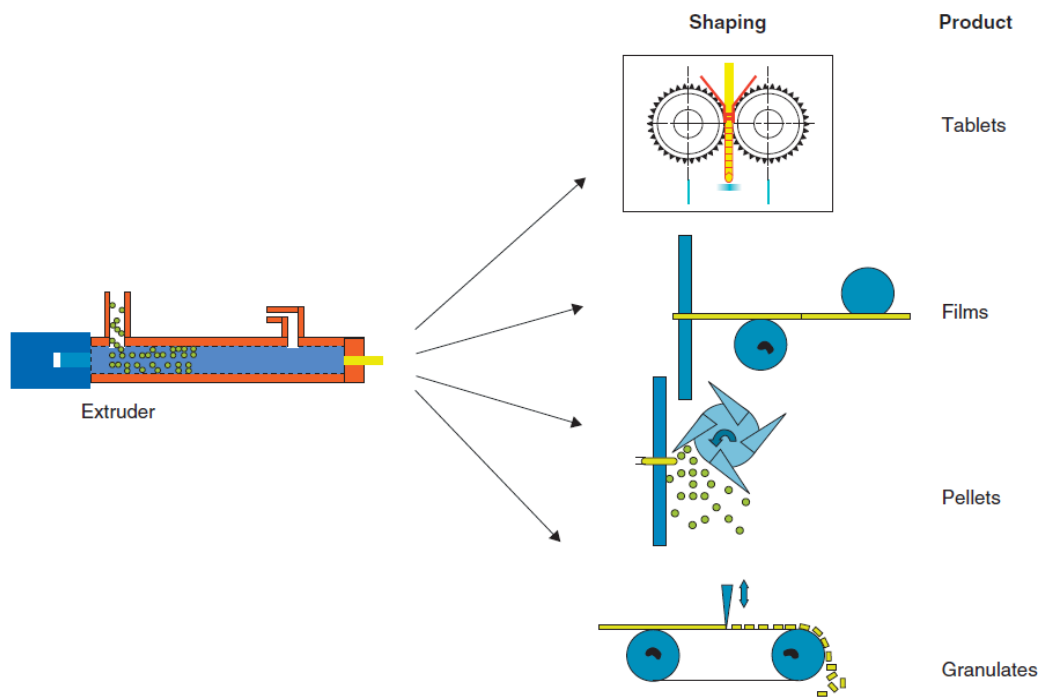


**Fig. 1.1.** Schematic of different dosage forms that can be produced by HME [60].

### 1.1.1. Advantages and disadvantages of HME

There are several benefits of processing materials via HME compared to conventional methods (e.g., spray drying, roll milling etc.). This is a continuous process; extruders can be used for blending, mixing, melting or softening and extruding or reacting of materials [22]. No solvent is required for HME processing, which potentially avoids the breakdown of the materials present. In-line monitoring is possible by using PAT tools during extrusion. By avoiding the solvent elimination step, toxicity and energy costs are potentially reduced. Furthermore, poorly compactable materials can be shaped as pellets by using the pelletizer i.e. by cutting the extrudates. Labour costs can be reduced, for HME processing, via automation.

The temperature and pressure needs to be optimized during HME processing in order to avoid degradation of the materials used. Initially, investment in HME instruments can be high due to the cost of contemporary automated instrumentation.

### 1.1.2. Instrumentation

There are two categories of hot-melt extruders namely: (i) ram extruders and (ii) screw extruders.

- **Ram extruder**

The design is very simple in the case of ram extrusion and the mode of operation is not continuous which considered to be a disadvantage of this. Extreme pressure is produced via the positive movement of the ram which pushes the materials through the die (**Fig. 1.2**). Inside the cylinder, materials start to heat until they melt, soft materials are formed; thus extrusion through a preferred shape die is forced by using a ram [23]. There are a few limitations of the ram extrusion method including limited melting capacity and poor temperature uniformity [1]. Additionally, the extruded materials are less homogeneous than those produced using screw extrusion [4].

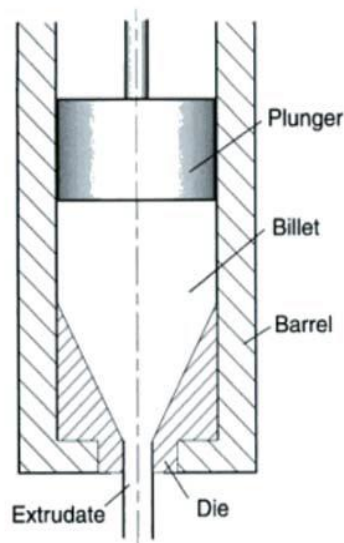


**Fig. 1.2.** Ram extruder [1].

- **Screw extruder**

Screw extrusion involves the use of a rotating screw inside the heated barrel of the HME. Screw extruders produce high shear stress and powerful mixing. The extruder consists of a feed hopper, temperature controlled barrel (contains mixing, milling, melting zones), rotating screw inside the barrel and a shape die at the extruder end (**Fig. 1.3**). Some other parts of an extruder include the cooling system, conveyor equipment as well as cutting and collecting equipment for the extruded products.

A powder blend usually contains API, polymer(s) or lipid(s) as matrix carriers and other functional excipients such as plasticizers, release modifying agents, super disintegrating agents, thickening agents, antioxidants, thermal lubricants, bulking agents, as well as other

possible additives [4, 24] which are fed via the feeder into the barrel. This barrel contains different zones and each zone is set at a specific temperature. **Fig. 1.4** shows a schematic view of the inside of the extruder barrel.

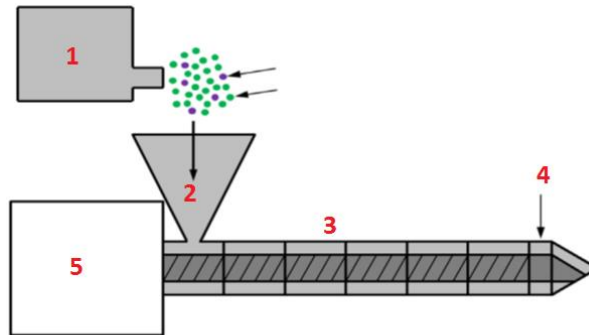


**Fig. 1.3.** HME equipment and process parameters traditionally monitored during pharmaceutical HME (1. feeding system, 2. feeding hopper, 3. temperature controlled barrel with one or twin screws, 4. die and 5. screw driving unit) [59].



**Fig. 1.4.** HME extruder barrel (ThermoFisher).

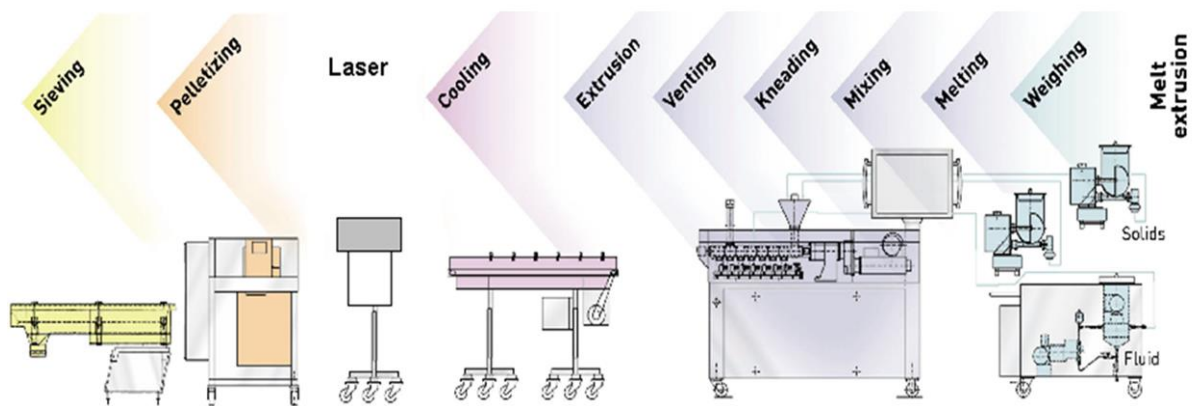


**Fig. 1.5.** Schematic diagram of HME with downstream equipment.

The rotating screws inside the extruder barrel pass the powder blends towards the die. The powder blend usually melts inside the barrel due to the high shear produced as a result of the screws and the barrel wall, and the temperature inside the barrel. The melted sample is then pumped through the die and subjected to further downstream processing (**Fig. 1.5**).

## **1.2. Quality by design (QbD)**

Recently, the Food and Drug Administration (FDA) agency and pharmaceutical industries have moved towards quality by design (QbD) approaches [25]. According to ICH guidelines, QbD is a systematic approach to pharmaceutical development that begins with pre-defined objectives and emphasizes product/process understanding and process control, based on science and quality risk management. This means designing and developing formulations and manufacturing processes to ensure a pre-defined product quality. According to the ICH Q8 annex, a QbD development process begins with a target product profile (TPP) which basically explains the use, safety, and efficacy of the product. After defining the TPP, relevant information is gathered regarding the drug substance(s) and excipients to be used. Thereafter, the critical quality attributes (CQAs) have to be identified prior to designing the pharmaceutical formulation. Critical process parameters (CPPs) are exceedingly important for identifying/controlling the CQAs and for obtaining the final product. In order to control the composition of the formulation during manufacturing a control strategy is required which allows the manufacturing process to be monitored. DoE and PAT tools are required to implement QbD. Furthermore, ICH indicates that as long as the process and formulation parameters are kept within the defined design space, no regulatory post approval change is needed. Moreover, the design space of a process also guarantees its reliability and robustness, supporting the quality risk management system.

Elements related to QbD for pharmaceutical development include the following.

- ***Target product profile (TPP)***

A TPP is literally the characteristics of a drug product that, ideally, will be achieved to ensure the desired quality by considering the safety and efficacy of the drug product.

- ***Critical process parameter (CPP)***

A process parameter whose variability has an impact on a critical quality attribute and therefore should be monitored or controlled to ensure the process produces the desired quality.

- **Critical quality attributes (CQAs)**

A CQA is a physical, chemical, biological or microbiological property or characteristic that should be within an appropriate limit, range, or distribution to ensure the desired product quality.

- **Design space**

This is defined as the multidimensional combination and interaction of input variables (e.g., CQAs) and process parameters that have been demonstrated to provide assurance of quality. Working within the design space is not considered as a change. Movement out of the design space is considered to be a change and would normally initiate a regulatory post approval change process. The design space is proposed by the applicant(s) and is subject to regulatory assessment and approval (ICH Q8) [25].

### **1.3. Process analytical technology (PAT)**

Pharmaceutical manufacturing is usually accomplished using batch processing with laboratory testing carried out on randomly collected samples for qualitative analysis. This approach literally slows down the batch processing step, because most of the conformity tests are conducted on end product samples. To ensure the final quality of the product at the end of manufacturing process, the FDA approved a new concept: process analytical technology (PAT) which can be defined as ***“a system for designing, analysing, and controlling manufacturing through timely measurements (i.e., during processing) of critical quality and performance attributes of raw and in-process materials and processes, with the goal of ensuring the final product quality”*** [26] The aim is to introduce PAT in the pharmaceutical industry in order to strengthen the process understanding of the manufacturing methods which can support a shift from conventional methods to science based manufacturing and to be a part of a larger cGMP initiative [27]. A timely measurement according to the FDA guidance includes in-line, on-line and at-line measurements, which are defined as follows.

- In-line: a measurement where the sample is not removed from the process stream and can be invasive or non-invasive.
- On-line: a measurement where the sample is diverted from the manufacturing process, and may be returned to the process stream.
- At-line: a measurement where the sample is removed isolated from and analysed in close proximity of the process stream.

The PAT measurements presented and discussed in this thesis are carried out in-line.

### **1.3.1. Advantages of PAT**

There are three major advantages of implementing PAT in pharmaceutical manufacturing processes, these are: scientific, regulatory and industrial benefits.

Industrial related benefits involve minimising risks and decreasing costs [28]. Risks can be connected to safety and decreasing costs arise when improvement of “in process control” has been developed. A reduced transfer time from the early development to industrial manufacturing by using PAT tool is quite possible. Development of in process control using PAT tools defined during the manufacturing process leads to an increase in the product yield by decreasing out-of-specification production tests and thus minimising the consumption of expensive ingredients. Furthermore, implementing PAT not only potentially reduces the cycle times and facilitates continuous processing but can also result in the omission of laborious finished product testing.

Regulatory benefits involve increasingly high demand from the regulatory authorities toward the pharmaceutical industries to improve in depth knowledge and understanding of particular manufacturing processes together with accuracy, robustness and reliability. The regulatory authorities have published guidelines to meet the requirements rather than providing solutions. The suggested improvements helps both industry and regulatory authorities with running, controlling, and monitoring processes on a well assessed science and risk based level. Process understanding is based upon process control and ensures the quality of the final product. According to ICH Q8 (R2) guidelines on pharmaceutical development, which emphasizes the “quality by design” concept, stating the quality shouldn’t be tested into products, but should be built in.

The scientific benefits of PAT result from understanding specific processes and improvement of product quality by introducing in-line PAT measurements. Predictive models have to be built which have to be in place in order to respond to the process derivation and consequently obtain consistent product quality. In comparison with conventional in-process controls, in-line PAT measurements allow monitoring of the manufacturing process in real time rather than collecting single data points at different time intervals.

In addition to being highly encouraging to manufacturers, the key concepts and recommendations appearing in the ICH Q8 (R2), Q9 and Q10 guidance to industry has,

recently, become more and more mandatory; this is stated in the recent manual of policies and procedures (MAPP) 5016.1 document for the chemistry, manufacturing, and controls (CMC) reviews (FDA, MAPP 5016.1, 2011). The document is effective since the 2<sup>nd</sup> of August, 2011 and clearly highlights the use of PAT and QbD as follows:

*“Reviewers should determine whether an application includes sufficient enhanced knowledge that demonstrates the applicant’s understanding of materials attributes, manufacturing processes, and controls for product quality to support the proposed flexible regulatory approaches. Examples of flexible regulatory approaches are as follows.*

- Manufacturing process improvements without regulatory notification (e.g., changes within a design space).

- In-process tests *in lieu* of end product testing, including real time release testing approaches (e.g., “PAT – A Framework for Innovative Pharmaceutical Development, Manufacturing, and Quality Assurance,” September 2004”).

### **1.3.2. PAT tools**

PAT is comprised of different techniques/methodologies and includes multivariate tools for design, data acquisition and analysis e.g. design of experiment (DoE); process analysis includes in-line and on-line measurement techniques, process control tools and continuous improvement and knowledge management.

A number of techniques are available which are able to meet the PAT requirements. The best known is NIR spectroscopy which is very useful tool and is applied to e.g. the identification and quality control of raw materials, granulation [29], blending and coating thickness measurements [30], tableting [31, 32], analysis of tablet hardness, dissolution of matrix tablets [33-35] and investigations of polymer-drug interactions [36].

The aim of the work reported in this thesis is to use in-line NIR spectroscopy as a PAT tool in HME processing for the development of pharmaceutical formulations. Importance will be mostly placed on NIR spectroscopy as a process analytical tool, while a potential application using Raman spectroscopy will also be considered.

### **1.3.3. Near-infrared (NIR) spectroscopy**

Sir William Herschel was a successful musician turned astronomer who noticed in 1800 that the area below the red end of the visible spectrum provided significant heating effect when

he diffracted sunlight through a glass prism [37]; thus near infrared (NIR) radiation was discovered. Abney and Festing [38], in 1881, used a photographic plate to record the NIR spectra of organic liquids in the range between 1000 to 1200 nm. The aforementioned work is of significance in spectroscopy not only because it represents the first NIR measurement but also the first interpretation of an NIR spectrum. Abney and Festing recognised both atomic groupings and the importance of H-bond in the NIR spectrum. The first NIR spectrometer was developed by Coblenz using a rock-salt prism and a thermopile connected to a mirror galvanometer which was highly susceptible to both vibrational and thermal disturbances. He noticed each compound had a unique “fingerprint” [40].

NIR spectroscopy was first used for quantitative measurements by Fowle in 1912 [57] to determine the moisture content in the atmosphere at the Mount Wilson observatory. Later on, in 1938, Ellis and Bath [58] used NIR to determine the amount of water in gelatin. In the 1930s, lead sulphide (PbS) was being studied as a compound semiconductor, and the advent of the World War II stimulated its development as an infrared detector for heat-sensing purposes. In the 1950s, PbS became available for commercial applications as a very sensitive detector for the 1 to 2.5- $\mu\text{m}$  wavelength region. The NIR region, at last, had a good detector. NIR research underwent a slow evolution in comparison with mid-infrared (MIR) field due to the difficulties in interpretation of spectra of, what were considered, lots of confusing and overlapping spectral bands. However, two aspects of NIR technology were initially overlooked. First, the PbS detector was very sensitive and because tungsten filament lamps (particularly quartz halogen) were a good source of NIR radiation, diffuse reflection measurements were possible. Second, relatively low-cost instruments could be manufactured because detectors, light sources, and, importantly, optics made from glass were inexpensive. Later developments in NIR spectroscopy were initiated by using advances in microcomputing which enabled data analysis to be undertaken, more efficiently and data mining could also be used based on chemometrics software [47].

In the last few decades, NIR and Raman vibrational spectroscopic techniques have been the main tools used for the chemometric analysis of multicomponent pharmaceutical formulation samples [39]. Due to the improvements in chemometric analysis, NIR spectroscopy became the first choice vibrational spectroscopic method compared with other spectroscopic tools e.g. Raman, FT-IR etc. Arguably, the-relatively-user friendly chemometrics software is advantageous for data exploration and interpretation. NIR

spectroscopy is now often routinely used in different pharmaceutical applications including research and development as well as process monitoring and is a popular analytical tool in the food [41, 42], fuel and pharmaceutical industries [43-45].

### 1.3.4. Principles of NIR spectroscopy

The near-infrared region lies between the visible and mid-infrared wavelength regions of the electromagnetic spectrum. According to European Pharmacopoeia the NIR bands extend from the 780 to the 2500 nm region. Wavenumber is another way to refer to the spectral range which means the spectral range of NIR is located between 12500 and 4000  $\text{cm}^{-1}$  **Fig. 1.6**.

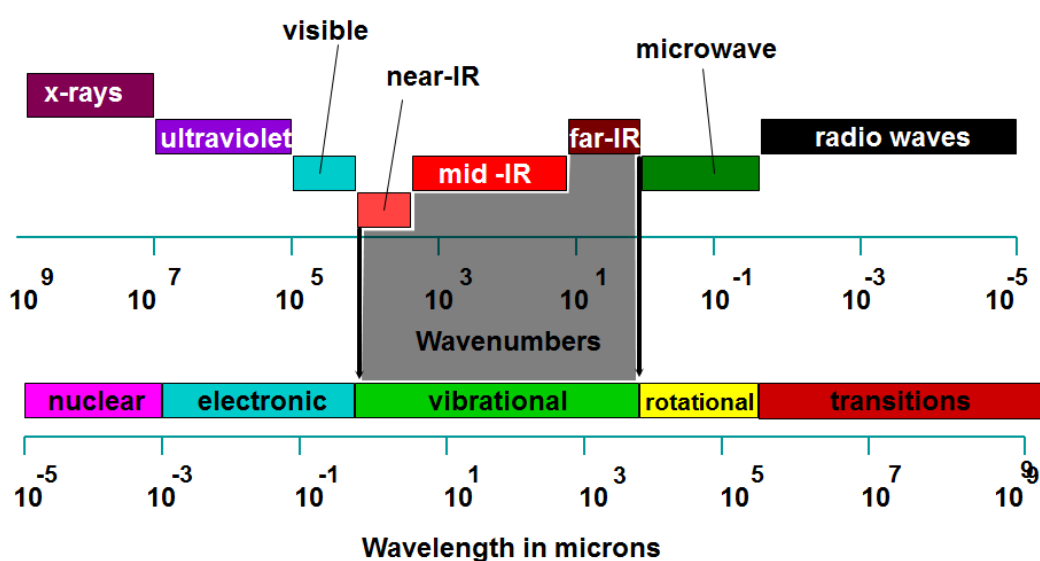


**Fig. 1.6.** Location of the NIR spectral region in the electromagnetic spectrum.

**Fig. 1.7** shows different regions of electromagnetic spectrum, the spectroscopic techniques used and the energetic transition involved. The Figure also shows the wavelengths and wavenumbers associated with each region. Each part of the electromagnetic spectrum corresponds to one or more spectroscopic techniques that exploit the phenomenon which occurs when the electromagnetic radiation of a pre-determined energy interacts with the molecule. Two complementary theories have been put forward to explain the properties of electromagnetic radiation: the classical theory (electromagnetic radiation is a wave) and the quantum theory (electromagnetic radiation is a stream of energetic particles).

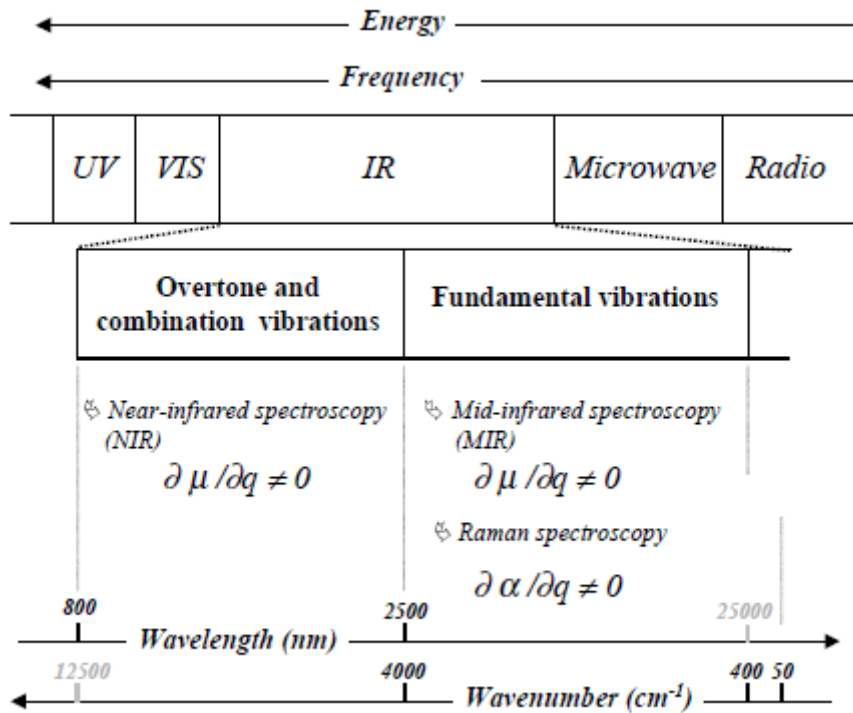


**Fig. 1.7.** Different regions of the electromagnetic spectrum and the related spectroscopic techniques; the wavelength and wavenumber limits of each region are shown [55].

- **Classical theory**

Light are a radiation consisting of combination of an electric and magnetic field perpendicular to each other and also perpendicular to the propagation direction corresponding to the light direction (**Fig. 1.8**). Both electric and magnetic fields exhibit a sinusoidal variation in space which can be defined by the following equation:

$$Y = A \sin 2 \pi \nu t \quad (1)$$

Where,  $Y$  is the displacement with a maximum is designated by the amplitude  $A$ ,  $\nu$  is the wave frequency and  $t$  is time.

The wavelength,  $\lambda$ , is defined by the distance between two successive wave minima or maxima; it can be defined by the following equation:

$$\lambda = c / \nu \quad (2)$$

Where,  $c$  is the universal constant of the velocity of light in vacuum.

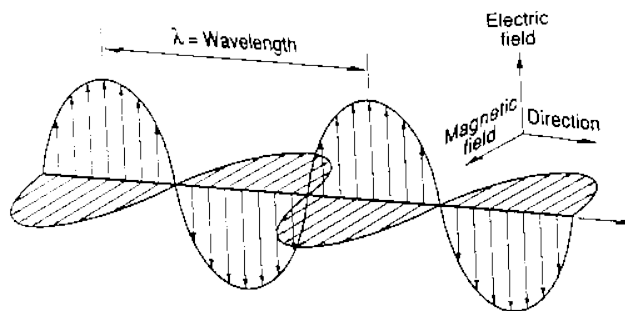


**Fig. 1.8.** Electromagnetic wave propagation [47].

NIR spectra are usually represented as the absorbance as a function of the wavenumber “ $\nu$ ” which is expressed by the following equation:

$$\nu = 1 / \lambda \quad (3)$$

- **Quantum Theory**

The classical theory does not explain all the properties of electromagnetic radiation and its interaction with matter, and fails to account for phenomena associated with the absorption or emission of energy. It is necessary to view electromagnetic radiation as a stream of discrete particles. Planck was the first to put forward the hypothesis that the electromagnetic wave was not continuous but composed of corpuscular units called quanta [56]. The energy of a quantum of radiation is expressed as follows:

$$E = h \nu \quad (4)$$

Where, E is the energy,  $\nu$  the frequency and h the Planck constant.

- **Molecular vibrations**

NIR and MIR spectroscopy are both vibrational spectroscopic techniques which are used to detect absorption of radiation due to vibrations of atomic bonds. The uptake of specific energy quanta induces e.g., stretching and deformation vibrations of atomic bonds and a change in the respective dipole moment. In contrast, changes in the dipole moment due to molecule rotations are induced and detected in far infrared spectroscopy region.

- **Stretching vibrations**

The change of the inter-atomic distance along the bond-axis is termed a stretching vibration. Stretching vibrations of several atomic bonds can be either symmetric or asymmetric. A schematic illustration of these two stretching vibrations is presented in **Fig. 1.9**.

- **Bending vibrations**

Bending or deformation vibrations change the angle between two atomic bonds. These changes occur as in-plane or out-of plane vibrations. The differences are illustrated in **Fig. 1.9**.

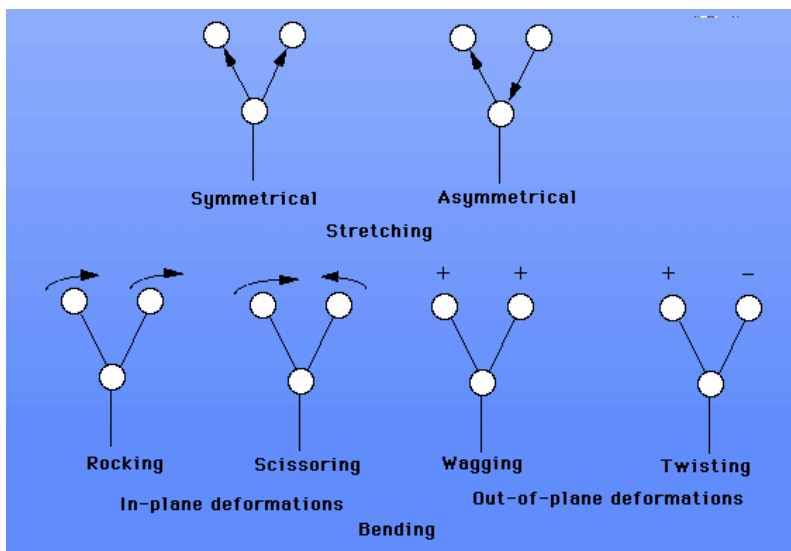


**Fig. 1.9.** Molecular vibrations.

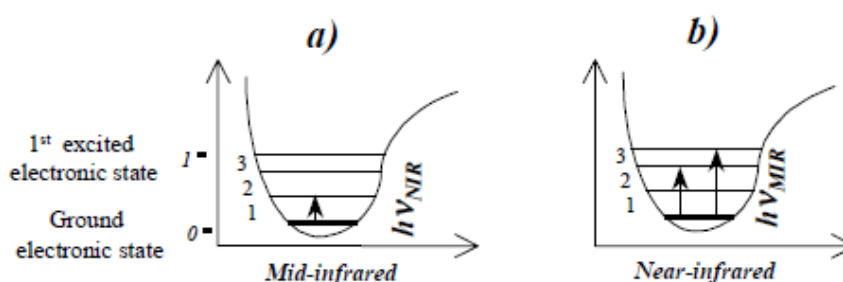


**Fig. 1.10.** Energy level diagrams showing the basic transitions involved in a) MIR and b) NIR [55].

- ***The absorption phenomenon of NIR spectroscopy***

The interactions of electromagnetic radiation with molecules give rise to several spectroscopic techniques based on absorption, emission or scattering processes. NIR and MIR spectroscopies are based on absorption. **Fig. 1.10** describes the different phenomena that occur in the infrared regions. For the sake of simplification, only two electronic states (the ground and the first excited) are shown.

MIR spectroscopy concerns the region of the electromagnetic spectrum lying between 2500 and 25000 nm ( $4000\text{-}400\text{ cm}^{-1}$ ). When radiation with energy corresponding to the MIR range interacts with a molecule, the energy at defined frequencies can be partially absorbed. The absorption of the incident electromagnetic radiation at a particular frequency ( $\nu_i$ ) is related to specific vibrational excitation energy ( $\Delta E=h\nu_i$ ). The frequencies of these vibrations are related to molecular parameters such as bending force constants and masses of the atoms involved in this vibration. The vibrations under consideration in MIR are mostly fundamentals (i.e., from the stable vibrational state to the first excited vibrational state in the electronic ground state) (**Fig. 1.10a**).

NIR spectroscopy involves radiation with energy higher than in MIR (**Fig. 1.6**). The NIR region lies between 780 and 2500 nm ( $12800\text{-}4000\text{ cm}^{-1}$ ). Electromagnetic radiation of this region is absorbed at frequencies corresponding to overtone (i.e., corresponding to the transition from the stable vibrational state to the second [first harmonic] or the third [second harmonic] excited vibrational state, or a higher vibrational state), or a combination vibration of different vibrations of the molecule under consideration (**Fig. 1.10b**).

### 1.3.5. NIR instrumentation

There are two types of NIR spectrometers available, dispersive and Fourier-transform (FT) NIR spectrometers.

- ***Dispersive NIR spectrometer***

In the case of dispersive NIR instruments, the NIR beam is usually emitted by the source which is separated sequentially into wavelength bandwidths by a moving grating. The grating then directs each wavelength to the detector via a slit. Therefore, each wavelength is analysed separately and the entire spectrum is measured when the movable grating has selected the entire spectral range [47].

- ***Fourier-transform (FT) NIR spectrometer***

FT-IR spectrometry was developed in order to overcome the limitations encountered with dispersive instruments. The main difficulty was the slow scanning process. A method for measuring all of the infrared frequencies simultaneously, rather than individually, was needed. A solution was developed which employed a very simple optical device called an interferometer (**Fig. 1.11**).

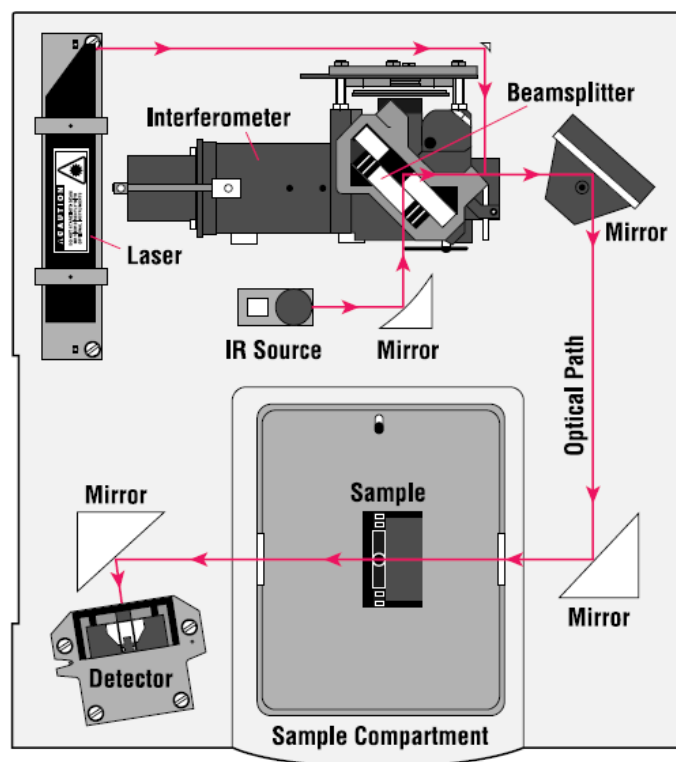


**Fig. 1.11.** A diagram of an FT NIR spectrometer (ThermoNicolet).

The NIR beam emitted from the source is divided into two beams by a beam-splitter. One beam is forwarded to a moving mirror while another one is towards to a fixed mirror. Furthermore, the separated beams are reflected and recombined at the beam splitter. According to the difference in distance travelled between the two beams, constructive and destructive interference occurs, leading to a global interference pattern termed an interferogram. The interferogram then passes through the sample. Some of the energy is absorbed, some is transmitted. The transmitted part containing all the spectral range finally goes to the detector. The data are then sent to a computer which converts the interferogram into a spectrum by performing the Fourier-transform algorithm [47].

### 1.3.6. NIR measurement modes

There are two different measurement modes available in NIR spectroscopy; these are transmission and reflectance modes.

- **Transmission mode**

The transmission mode allows the measurement of the light transmitted through a sample. This mode is advantageous for analysing the entire sample. It involves a detector at the opposite side of the measurement point. However, this measurement mode might not be helpful for

measuring the spectra of solid forms of a sample and might not be adequate for in-process measurement.

Transmittance  $T$  is defined by the light fraction passes through the sample:

$$T = I_T/I_0$$

Where,  $I_T$  is the intensity of the transmitted light and  $I_0$  is the intensity of incident light.  $I_T < I_0$  as part of the light has been absorbed by the sample.

So the absorbance will be,

$$A = \log (1/T) = \log (I_0/I_T)$$

- ***Reflection mode***

A reflection measurement typically reflects the NIR light source when it interacts with the sample and is then returned to the detector. Two types of reflection measurement are available. These are specular and diffuse reflection. Specular reflection corresponds to NIR light which is directly reflected at the surface of the sample. This type of reflection measurement only contains the physical property of the sample. Whereas diffuse reflection not only contains physical information, but also chemical features by penetrating into the sample and subjected to molecular absorption, diffraction and reflection of light scattering. Part of the light then goes to the detector.

Reflectance  $R$  is defined by the following equation, where  $I_R$  is the intensity of light reflected by the sample and  $I_0$  is the intensity of the incident NIR light:

$$R = I_R/I_0$$

The absorbance is defined by the following equation,

$$A = \log (1/R) = \log (I_0/I_R)$$

In comparison, the reflection mode is much more favourable than the transmission mode because it is not necessary to use a detector on the other side of the measurement. However, the penetration depth of the NIR beam is lower which is dependent on the sample density. And, the reflection mode is the most useful measurement for in-process analysis.

## 1.4. Introduction to chemometrics: data mining

Chemometrics, first invented by Wold in 1974; it is a mathematical and statistical tool used to extract relevant information, both chemical and physical, from the data produced in chemical experiments [46]. NIR spectra contains lots of chemical and/or physical information which is produced by the overlapping of absorption bands. It is difficult to undertake visual interpretation of the NIR spectra. Each spectral wavelength is associated with one absorbance value and the amount of data is huge as lots of variables are co-linear, there is also a need to reduce the number of variables to the most significant ones which are of interest for a particular investigation.

### 1.4.1. Pre-processing of signals

- ***Multiplicative scatter correction (MSC)***

MSC is a well-recognised signal pre-processing option which reduces the effect of scattered light on the diffuse reflectance spectra [48]. MSC is usually performed prior to calibration. A reference spectrum is selected which is typically a mean spectrum of the calibration set. All of the calibrations set spectra are then compared to the reference spectrum. The slope and Y intercept values of the calibration plot are estimated. All the experimental spectra are then corrected according to the slope and intercept of the calibration plot. The relevant chemical information is represented by the extracted spectra.

- ***Standard normal variate (SNV)***

Standard normal variate (SNV) analysis is used to correct for uncontrolled spectral variations [49]. For a sample spectrum, it works as follows: each variable absorbance is first corrected by the mean absorbance of the spectrum. The previous result is then divided by the standard deviation of the variable under investigation.

- ***Smoothing and derivative signal pre-processing***

The aim of smoothing is to reduce spectral noise. Spectral noise can hide the relevant physical and chemical information so smoothing is a necessary tool to gain information. The most widely used smoothing technique is Savitzky-Golay smoothing and the Norris derivative filter.

### **1.4.2. Pattern recognition example**

- ***Principal component analysis (PCA)***

PCA is the most widely used multivariate chemometric technique and is used because of the importance of multivariate measurements in chemical analysis techniques. PCA is a way of identifying patterns in data, and expressing the data in such a way as to highlight their similarities and differences. Since patterns in data can be hard to find in data of high dimensions, where the graphical representation is unavailable, PCA is a powerful technique for analysing data. PCA decomposes a data table with correlated measurements (e.g. spectra) into a new set of uncorrelated variables. These variables are called principal components/ factors/ eigenvectors/loadings. Each variable is also assigned a set of scores which corresponds to the weighting of each component. PCA data is usually presented in graphical form by plotting the projections of the units onto the components and the loading variables [48].

### **1.4.3. Multivariate regression example**

- ***Partial least squares (PLS) regression***

PLS is a quantitative spectral decomposition technique where the information pertaining to the spectral matrix and the data scores are decomposed. The objective of PLS regression is to combine some reference measurements with their corresponding spectral data in order to create a model that will, further, only need spectral data to predict some reference measurements. Reference measurements represents the analytical results obtained with the conventional analytical method, in the case of an API content determination method, the reference method could, for example, be a HPLC method. PLS is one of the mostly used multivariate regression methods, mainly in the application of PAT. Other multivariate regression method includes principal component regression (PCR), multi-linear regression (MLR), classical least squares regression (CLS) etc. [48].

## **1.5. NIR as a PAT tool applied to pharmaceutical HME**

In-line NIR spectroscopy has been used to understand polymer-drug behaviour during HME by Saerens *et al.*, [36]. A diffuse reflectance NIR probe was implemented in the extrusion die of a twin screw HME extruder. A PLS model was developed regressing the in-line NIR spectra collected during extrusion of reference physical mixtures containing 20%, 30% and 40 % (w/w) metoprolol tartrate (MPT) in Kollidon SR. The method was validated with the new extrusion experiments consisting of other concentrations of the API. Thereafter, a physical

mixture containing 40% (w/w) MPT was extruded at both 105°C and 135°C. The collected in-line NIR spectra, during extrusion, were compared with the spectra of the physical mixtures. NIR band shifts were detected after HME extrusion which demonstrated drug-polymer interactions during extrusion and it was found that the band shifts were more intense at 135°C than 105°C, which also showed that drug-polymer interactions were greater at higher temperature.

A different application of HME is the production of pharmaceutical cocrystals. Kelly *et al.*, [50] and Moradiya *et al.*, [51] demonstrated the use of NIR spectroscopy to confirm cocrystal formation during HME. Ibuprofen-nicotinamide (IBU-NIC) cocrystals were used by Kelly *et al.*, whereas Moradiya *et al.*, used carbamazepine-saccharine (CBZ-SCH) cocrystals. The cocrystals were produced by using a 1:1 molar ratio of drug and co-formers. In-line NIR monitoring was used during CBZ-SCH cocrystal formation whereas off-line NIR was used during IBU-NIC cocrystal formation. For the CBZ-SCH cocrystal formation experiments a high temperature NIR reflectance probe with a sapphire window was fitted at three different mixing zones of the extruder to monitor the changes occurring during HME processing. It was reported that the CBZ-SCH cocrystal formation occurred gradually from the 2<sup>nd</sup> mixing zone to the 3<sup>rd</sup> mixing zone by formation of H-bonds between the drug and co-formers. Formation of H-bonds was detected by the occurrence of a new FT-NIR band at 6885 cm<sup>-1</sup> which is a shifted band from 6802cm<sup>-1</sup> and is corresponds to N-H stretching first overtone. Temperature, screw configuration and screw speed are the critical process parameters during extrusion and an improved dissolution rate of the CBZ-SCH cocrystals was found compared with the prototype cocrystals which had not been produced by HME, but by the solvent evaporation method.

Transmission in-line NIR spectroscopy has been used to study the impact of process design and scale up residence time distributions [52] and for the determination of the composition of a multicomponent melt stream at the exit of a twin screw extruder [53]. Tumuluri *et al.*, [54] applied NIR spectroscopy to predict the amount of clotrimazole necessary for the production of HME processed polyethylene oxide (PEO) films by developing a PLS model.

## 1.6. Summary

HME has already proved to be a robust method of producing numerous drug formulation systems and therefore it has been found to be useful in the pharmaceutical industry enlarging the scope to include a range of polymers and APIs that can be processed with or without plasticizers. NIR spectroscopy is a fast, non-destructive analytical technique, which requires no sample preparation. In-line NIR probes, made with a sapphire window, have a high resistance to temperature and therefore gives the flexibility to work at high temperatures during HME process. In the 12500-4000  $\text{cm}^{-1}$  NIR region the main vibrational modes which can be detected are those due to CH, OH, SH and NH vibrations which overlap due to overtone and combination bands. Therefore, chemometric tools are often required to extract the information from the NIR spectra. Due to the unique properties of NIR (i.e., its non-invasive nature, minimal sample preparation, non-destructiveness and the ability to employ user friendly fibre optic probes) the technique is a good choice for in-line monitoring during HME processing of materials.

## 1.7. References

1. Rauwendaal C, Different types of extruder, in: Rauwendaal C, (Ed.), Polymer extrusion, 4 ed. Hanser Gardner Publications, Inc., Ohio, 2001; 11-35.
2. Kaufman HS, & Falcetta JJ, Introduction to polymer science and technology: an SPE textbook (1st Ed.). New York: John Wiley & Son, 1977.
3. Breitenbach J, Melt extrusion: from process to drug delivery technology, European Journal of Pharmaceutics and Biopharmaceutics, 2002; **54**(2): 107-117.
4. Crowley MM, Zhang F, Repka MA, Thumma S, Upadhye SB, Kumar BS, McGinity JW, Martin C, Pharmaceutical applications of hot-melt extrusion: Part I, Drug Development and Industrial Pharmacy, 2007; **33**(9): 909-926.
5. Repka MA, McGinity JW, Bioadhesive properties of hydroxypropylcellulose topical films produced by hot-melt extrusion, Journal of Controlled Release, 2001; **70**(3): 341-351.
6. Repka MA, McGinity JW, Influence of chlorpheniramine maleate on topical hydroxypropylcellulose films produced by hot-melt extrusion, Pharmaceutical Development and Technology, 2001; **6**(3): 297-304.

7. Brabander CD, Vervaet C, Bortel LV, Remon J, Bioavailability of ibuprofen from hot-melt extruded mini-matrices, *International Journal of Pharmaceutics*, 2004; **271**(1–2): 77-84.
8. Özgüney I, Shuwisitkul D, Bodmeier R, Development and characterization of extended release Kollidon® SR mini-matrices prepared by hot-melt extrusion, *European Journal of Pharmaceutics and Biopharmaceutics*, 2009; **73**(1): 140-145.
9. Verhoeven E, Vervaet C, Remon JP, Xanthan gum to tailor drug release of sustained-release ethylcellulose mini-matrices prepared via hot-melt extrusion: *in vitro* and *in vivo* evaluation, *European Journal of Pharmaceutics and Biopharmaceutics*, 2006; **63**(3): 320-330.
10. Mehuys E, Remon J, Vervaet C, Production of enteric capsules by means of hot-melt extrusion, *European Journal of Pharmaceutical Sciences*, 2005; **24**(2–3): 207-212.
11. Bruce LD, Shah NH, Waseem MA, Infeld MH, McGinity JW, Properties of hot-melt extruded tablet formulations for the colonic delivery of 5-aminosalicylic acid, *European Journal of Pharmaceutics and Biopharmaceutics*, 2005; **59**(1): 85-97.
12. Young CR, Dietzsch C, McGinity JW, Compression of controlled-release pellets produced by a hot-melt extrusion and spheronization process, *Pharmaceutical Development and Technology*, 2005; **10**(1): 133-139.
13. Fukuda M, Peppas NA, McGinity JW, Floating hot-melt extruded tablets for gastroretentive controlled drug release system, *Journal of Controlled Release*, 2006; **115**(2): 121-129.
14. Andrews GP, Advances in solid dosage form manufacturing technology, *Philosophical Transactions of the Royal Society A: Mathematical, Physical and Engineering Sciences*, 2007; **365**: 2935-2949.
15. Yang R, Wang Y, Zheng X, Meng J, Tang X, Zhang X, Preparation and evaluation of ketoprofen hot-melt extruded enteric and sustained-release tablets, *Drug Development and Industrial Pharmacy*, 2008; **34**(1): 83-89.
16. Albers J, Alles R, Matthée K, Knop K, Nahrup JS, Kleinebudde P, Mechanism of drug release from polymethacrylate-based extrudates and milled strands prepared by hot-melt extrusion, *European Journal of Pharmaceutics and Biopharmaceutics*, 2009; **71**(2): 387-394.

17. Ghalanbor Z, Körber M, Bodmeier R, Improved lysozyme stability and release properties of poly(lactide-co-glycolide) implants prepared by hot-melt extrusion, *Pharmaceutical Research*, 2010; **27**: 371-379.
18. Gosau M, Müller B, Release of gentamycin sulphate from biodegradable PLGA-implants produced by hot melt extrusion, *Die Pharmazie*, 2010; **65**: 487-492.
19. Maniruzzaman M, Bonnefille M, Aranyos A, Snowden MJ, Douroumis D, An in-vivo and in-vitro taste masking evaluation of bitter melt-extruded drugs, *Journal of Pharmacy and Pharmacology*, 2014; **66**(2): 323-337.
20. Hülsmann S, Backensfeld T, Keitel S, Bodmeier R, Melt extrusion—an alternative method for enhancing the dissolution rate of 17 $\beta$ -estradiol hemihydrate, *European Journal of Pharmaceutics and Biopharmaceutics*, 2000; **49**(3): 237-242.
21. Rambali B, Verreck G, Baert L, Massart DL, Itraconazole formulation studies of the melt-extrusion process with mixture design, *Drug Development and Industrial Pharmacy*, 2003; **29**(6): 641-652.
22. Mollan M, Historical overview, in: Ghebre-Sellassie, I. (Ed.), *Pharmaceutical extrusion technology*, Marcel Dekker, Inc., New York, 2003:1-18.
23. Perdikoulis J, Dobbie T, Die design, in: Ghebre-Sellassie, I., Martin, C. (Eds.), *Pharmaceutical extrusion technology*, Marcel Dekker, Inc., New York, 2003: 99-110.
24. Madan S, Hot melt extrusion and its pharmaceutical application, *Asian Journal of Pharmaceutical Sciences*, 2012; **7**: 123–133.
25. Food and Drugs Administration, Applying ICH Q8 (R2), Q9, and Q10 principles to CMC Review, MAPP 5016.1, 2011.
26. United States Food and Drug Administration (FDA), Guidance for industry PAT-A framework for innovative pharmaceutical manufacturing and quality assurance, 2004.
27. Balboni ML, Process analytical technology concepts and principles, *Pharmaceutical Technology*, 2003; **27**: 54-67.
28. Guenard R, Thureau G, Implementation of process analytical technologies: in *Process Analytical Technology* John Wiley & Sons Ltd, 2010:17-36.
29. Burggraeve A, Monteyne T, Vervaet C, Remon JP, Beer TD, Process analytical tools for monitoring, understanding, and control of pharmaceutical fluidized bed granulation: A review, *European Journal of Pharmaceutics and Biopharmaceutics*, 2013; **83**(1): 2-15.

30. Moes JJ, Ruijken MM, Gout E, Frijlink HW, Ugwoke MI, Application of process analytical technology in tablet process development using NIR spectroscopy: Blend uniformity, content uniformity and coating thickness measurements, *International Journal of Pharmaceutics*, 2008; **357**(1–2): 108-118.
31. Karande AD, Heng PWS, Liew CV, In-line quantification of micronized drug and excipients in tablets by near infrared (NIR) spectroscopy: Real time monitoring of tableting process, *International Journal of Pharmaceutics*, 2010; **396**(1–2): 63-74.
32. Porfire A, Rus L, Vonica AL, Tomuta I, High-throughput NIR-chemometric methods for determination of drug content and pharmaceutical properties of indapamide powder blends for tableting, *Journal of Pharmaceutical and Biomedical Analysis*, 2012; **70**(0): 301-309.
33. Tabasi SH, Moolchandani V, Fahmy R, Hoag SW, Sustained release dosage forms dissolution behavior prediction: A study of matrix tablets using NIR spectroscopy, *International Journal of Pharmaceutics*, 2009; **382**(1–2): 1-6.
34. Freitas MP, Sabadin A, Silva LM, Giannotti FM, do Couto DA, Tonhi E, Medeiros RS, Coco GL, Russo VFT, Martins JA, Prediction of drug dissolution profiles from tablets using NIR diffuse reflectance spectroscopy: A rapid and nondestructive method, *Journal of Pharmaceutical and Biomedical Analysis*, 2005; **39**(1–2): 17-21.
35. Hattori Y, Otsuka M, NIR spectroscopic study of the dissolution process in pharmaceutical tablets, *Vibrational Spectroscopy*, 2011; **57**(2): 275-281.
36. Saerens L, Dierickx L, Quinten T, Adriaensens P, Carleer R, Vervaet C, Remon JP, De Beer T, In-line NIR spectroscopy for the understanding of polymer–drug interaction during pharmaceutical hot-melt extrusion, *European Journal of Pharmaceutics and Biopharmaceutics*, 2012; **81**(1): 230-237.
37. Herschel W, Experiments on the refrangibility of the invisible rays of the sun, By William Herschel, LL. D. F. R. S., *Philosophical Transactions of the Royal Society of London*, 1800; **90**: 284-292.
38. Abney W, Festing ER, *Philos. Philosophical Transactions of the Royal Society*, 1881; **172**: 887.
39. Moros J, Garrigues S, de la Guardia M, *Trends in Analytical Chemistry*, 2010; **29**: 578.
40. Coblentz WW, *Investigations of infrared spectra Part 1*, Carnegie Institute of Washington, 1905:35.

41. Huang H, Yu H, Xu H, Ying Y, Near infrared spectroscopy for on/in-line monitoring of quality in foods and beverages: A review, *Journal of Food Engineering*, 2008; **87**(3): 303-313.
42. Chen Q, Zhao J, Chaitep S, Guo Z, *Food Chemistry*, 2009; **113**: 1272.
43. Roggo Y, Chalus P, Maurer L, Lema-Martinez C, Edmond A, Jent N, A review of near infrared spectroscopy and chemometrics in pharmaceutical technologies, *Journal of pharmaceutical and biomedical analysis*, 2007; **44**(3): 683-700.
44. De Beer T, Burggraefe A, Fonteyne M, Saerens L, Remon JP, Vervaet C, Near infrared and Raman spectroscopy for the in-process monitoring of pharmaceutical production processes, *International Journal of Pharmaceutics*, 2011; **417**(1–2): 32-47.
45. Saerens L, Vervaet C, Remon JP, De Beer T, Process monitoring and visualization solutions for hot-melt extrusion: a review, *Journal of Pharmacy and Pharmacology*, 2014; **66**(2): 180-203.
46. Wold S, *Chemometrics; what do we mean with it, and what do we want from it? Chemometrics and Intelligent Laboratory Systems*, 1995; **30**(1): 109-115.
47. Burns DA, Ciurczak EW, *Handbook of near-infrared analysis*, third ed., CRC Press, New York, 2008.
48. Geladi P, MacDougall D, Martens H, Linearization and scatter-correction for near-infrared spectra of meat, *Applied Spectroscopy*, 1985; **39**(3): 491-500.
49. Barnes RJ, Dhanoa MS, Lister SJ, Standard normal variate transformation and detrending of near-infrared diffuse reflectance spectra, *Applied Spectroscopy*, 1989; **45**(5): 772-777.
50. Moradiya H, Islam MT, Woollam GR, Slipper IJ, Halsey S, Snowden MJ, Douroumis D, Continuous cocrystallization for dissolution rate optimization of a poorly water-soluble drug, *Crystal Growth & Design*. 2014; **14**: 189-198
51. Kelly AL, Gough T, Dhumal RS, Halsey SA, Paradkar A, Monitoring ibuprofen–nicotinamide cocrystal formation during solvent free continuous cocrystallization (SFCC) using near infrared spectroscopy as a PAT tool, *International Journal of Pharmaceutics*, 2012; **426**(1–2): 15-20.
52. McKelvey C, Luke S, Mike L, Greg T, Applying extrusion to pharmaceutical formulation design, *Society of Plastic Engineers*, 2008: 54.
53. Troup GM, Process analytical technology for improved process understanding and control of a hot melt extrusion process, *Society of Plastic Engineers*, 2010: 56.

54. Tumuluri SVS, Prodduturi S, Crowley MM, Stodghill SP, McGinity JW, Repka MA, Avery BA, The Use of Near-Infrared Spectroscopy for the Quantitation of a Drug in Hot-Melt Extruded Films, *Drug Development and Industrial Pharmacy*, 2004; **30**(5): 505-511.
55. Baeten V, Dardenne P, *Spectroscopy: developments in instrumentation and analysis*, Grasasy Aceites, 2002; **53**(1): 45-63.
56. Osborne BG, Fearn T, *Near-infrared spectroscopy in food analysis*; Longman, Wile:NY, USA, 1986.
57. Fowl, FE, *Astrophysical Journal*, 1912; **35**: 149-162.
58. Ellis JW, Bath J, Modifications in the near infra-red absorption spectra of protein and of light and heavy water molecules when water is bound to gelatin, *The Journal of Chemical Physics*, 1938; **6**: 723-729.
59. Saerens L, Vervae C, Remon JP, De Beer T, Process monitoring and visualization solutions for hot-melt extrusion: a review, *Journal of Pharmacy and Pharmacology*, 2014; **66**(2): 180-203.
60. Repka MA, Shah S, Lu J, Maddineni S, Morott J, Patwardhan K, Mohammed NN. Melt extrusion: Process to product. *Expert Opinion on Drug Delivery*, 2012; **9**(1): 105-125.

## **Chapter 2: Developement of sustained release formulations processed by hot-melt extrusion using a quality by design approach**

---

### **2.1. Introduction**

Hot melt extrusion (HME) is one of the most widely applied continuous processing technologies in the plastic, food and rubber industry, which is now rapidly, increased its interest in pharmaceutical research for the development of various drug delivery systems. [1]. Being a versatile technique HME does not require solvents or water [2, 3], can be operate as a continuous process for the development of multiple drug delivery systems. HME has been successfully used for the taste masking purposes of various bitter drugs [4] and to enhance the dissolution rate and bioavailability of poorly water soluble drugs via the formation of solid dispersions of drugs in polymeric matrices during HME [5, 6]. Furthermore, HME also produce extrudates with sustained release property. In previous studies HME has been used to prepare matrix mini-tablets which was further investigated to characterize the property sustained release mini-matrices produced from ethyl cellulose, HPMC and ibuprofen [7, 8]. Extruded mini tablets showed several advantages such as, minimum risk of dose dumping and reduction of the inter- and intra-subject variability. Recently, vegetable calcium stearate was used for the development of retarded release pellets using a thermoplastic excipient processed via HME, and found that pellets with a paracetamol loading of 20% showed a release of only 11.54% of the drug after 8 hours due to the significant densification of the pellets. As expected, the drug release was influenced by the pellet size and the drug loading [9]. Recently oral sustained release formulation has been produced via HME using ethylene vinyl acetate (EVA) and polyethylene oxide as a polymeric carrier with metoprolol tartrate as an active pharmaceutical ingredient has also been reported [10].

Due to the advent of rapid developments in pharmaceutical research and manufacturing, pharmaceutical industries are moving towards vast changes in the product and process development bypassing the so called conventional univariate trial approach as well as risk based development process [11, 12]. The new approach that is being highly encouraged by the FDA to be adopted is known as “Quality by Design” (QbD) which is described in various ICH guidelines [13-15]. The aim of the QbD approach is to focus on science based paradigm to design and develop pharmaceutical formulations and manufacturing processes in order to

ensure predefined product quality [16]. Recently, QbD approach was used to predict quality attributes of continuously produced granules using complementary PAT tools [17]. Raman and NIR spectroscopy were coupled together with a photometric imaging technique to acquire solid-state information and granule size data, furthermore, these data were then used to predict the moisture content of the granules, tapped and bulk density and flowability. It has been used to monitor and map the state of the pharmaceutical co-precipitation process characterization [18-19], and to examine the effects of testing parameters and formulation variables on the segregation tendency of pharmaceutical powders, enhancement of the bioavailability of BCS class II drugs [20-21] and in pharmaceutical tablet imaging [22].

Process analytical technology (PAT) has been introduced by FDA agency to control, monitor and understand the manufacturing process [24]. Near-infrared (NIR) spectroscopy is one of the most commonly used technique which is suitable for an increased number of PAT applications and has been applied in several studies in the pharmaceutical research. NIR spectroscopy enables quantitative (*e.g.* concentration determination) and qualitative analysis including determination of drug crystallinity and identification of polymer-drug or polymer-polymer interactions used during HME process [25-27]. NIR spectroscopy was used as a PAT tool to monitor and understand cocrystal formation during solvent free continuous cocrystallization [28]. NIR spectroscopy has also been applied to test blend uniformity, content uniformity, coating thickness and hardness [29], quality attributes of continuously produced granules [17] and, more importantly, for scaling up hot melt extruded formulations [30].

The work presented in this chapter describes the application of NIR spectroscopy as a PAT tool during HME by combining with QbD and design of experiment (DOE) approach. In-line reflectance NIR probe was used to monitor the effects of the critical processing parameters such as feed rate, screw speed and drug loading during extrusion in order to identify the best HME processing conditions for the extrusion of PMOL in polymer/lipid matrices. Drug loading was included as an input/dependent variable in the DOE experiment and the obtained data were analyzed to identify the significant input variables. The drug release profiles of the sustained release formulations were selected as independent variable.

## 2.2. Materials and methods

### 2.2.1. Materials

Paracetamol (PMOL), ethyl cellulose (EC) and glyceryl dibehenate/Compritol 888 ATO (C888) were kindly donated by Mallinckrodt Chemical Ltd (Canada), Colorcon (Dartford, UK) and Gattefosse (Saint-Priest, France), respectively. The HPLC solvents, acetonitrile, acetic acid were of analytical grade and purchased from Fisher Chemicals (UK).

### 2.2.2. Hot-melt extrusion

HME was performed by using a Eurolab 16 mm twin screw extruder (Thermo Fisher Scientific, Germany) which was equipped with a DD Flexwall® 18 feeder (Brabender Technology, Germany), set in its gravimetric feeding mode (gravimetric feeding systems generally use a volumetric feeder associated with a weighing system to control the discharge of powder from a storage hopper at a constant weight per unit time – for example kg/min).

Three different drug/lipid/polymer blend ratios were extruded, consisting of equal amounts of ethylcellulose (EC) and Compritol-888 ATO (C888) with 40%, 60% and 80% (w/w) paracetamol (PMOL), respectively. Prior to HME, the drug, polymer and lipid were blended, for 10 min, using a Turbula TF2 mixer (100 rpm) (Basel, Switzerland), in order to obtain a homogeneous mixture. The temperature profile used in the HME barrel was set at (50 /100 /140/140/140/140/140/100)°C (from feeder to die) for all batches.

**Table 2.1.** Experimental design of PMOL/C888/EC formulations using drug loading, screw speed and feed rate as independent variables and PMOL release (%), particle size D(0, 5) as dependent variables.

Run No.	Independent Variables			Dependent variables		
	Drug Loading (% w/w)	Screw Speed (rpm)	Feed rate (gm/h)	PMOL Release (T <sub>6hr</sub> %)	PMOL Release (T <sub>12hr</sub> %)	Particle size D(0,5)
F1	80	150	400	62	87	274
F2	60	150	700	48	76	251
F3	40	150	700	38	51	203

<b>F4</b>	80	50	1000	64	90	209
<b>F5</b>	80	250	700	67	93	164
<b>F6</b>	60	150	1000	47	74	606
<b>F7</b>	40	250	1000	41	59	530
<b>F8</b>	40	50	400	35	48	467
<b>F9</b>	60	50	700	50	79	252
<b>F10</b>	60	150	700	46	73	283
<b>F11</b>	60	250	400	48	75	227

Extrudates with different processing parameters were obtained by incorporating a two-factor response surface fraction factorial design (DoE) in randomized order (**Table 2.1**) by using Fusion One software (D.o.E Fusion One™, US). Three centerpoint experiments were performed as well, resulting in  $2^3 + 3 = 11$  experiments, where, 2 is the two factorial design, and 3 is denoted as three variables and three centre points. Drug loading (% w/w), screw speed and feed rate (gm/h) were considered as variables whereas drug release rate was measured as a dependent variable/response.

### 2.2.3. Thermal analysis

The physical state of the pure drug, physical mixtures and the extruded granules were studied by differential scanning calorimetry (DSC) by using a Mettler-Toledo 823e (Greifensee, Switzerland) differential scanning calorimeter. Accurately weighed samples (2-3 mg) were placed in aluminium pans and sealed. Measurements were carried out under an atmosphere of nitrogen. The flow rate of dry nitrogen gas was (50 mL/min). Samples were subjected to heating scans only. The pans were heated at a heating rate of 10.0°C/min from 0°C to 220°C in the heating cycle.

### 2.2.4. X-ray powder diffraction

XRPD was used to assess the crystalline state of the active substance in the extruded formulations. All formulations including pure PMOL, physical mixtures and extruded formulations were evaluated using a Bruker D8 Advance in theta–theta mode, Cu anode at 40 kV and 40 mA, parallel beam Goebel mirror, 0.2 mm exit slit, LynxEye Position Sensitive Detector with 3° opening and LynxIris at 6.5 mm and sample rotation at 15 rpm. The samples

were scanned from 2 to 40° 2-theta with a step size of 0.02° 2-theta and a counting time of 0.2 s per step; 176 channels active on the PSD making a total counting time of 35.2 s per step.

### **2.2.5. NIR spectroscopy**

Diffuse reflectance NIR spectra were continuously collected in-line and non-invasively during HME using a Fourier-transform NIR spectrometer (Antaris MX NIR, analyzer Thermo Fisher Scientific, United Kingdom) equipped with an InGaAs detector, a quartz halogen lamp, and a fibre optic probe which was attached in the extrusion die. Spectra were collected every 1 min in the 10000-4000 cm<sup>-1</sup> region with a resolution of 16 cm<sup>-1</sup> and the scans averaged over 32 scans.

Data (NIR spectra) collection was carried out using the Result Software (Version 3.0, Thermo Fisher Scientific, UK) and the data analysis was performed via TQ analyst software (Version 3.0, Thermo Fisher Scientific, UK). Spectra collected in the diffuse reflectance mode usually require spectral pre-treatment before analysis. The degree of scattering depends on the wavelength of the light and the refractive index of the sample, which causes an unequal scatter over the whole spectrum. This can result in a baseline shift [31]. Therefore, standard normal variate (SNV) correction was used before chemometric analysis of the spectra. Using SNV, unwanted scatter was removed from the raw spectra to prevent it from dominating over chemical information within the spectra. The result of SNV pre-processing is that each spectrum has the same offset and amplitude, eliminating difference in light scatter in the spectra from different samples, before developing the calibration model. Furthermore, second derivative pre-processing was undertaken after SNV correction. Second derivative NIR spectra magnify differences in spectral features, provide baseline normalisation and remove data offsets due to scattering effects and path length variation [32]. For principal component analysis (PCA) and for the development of a partial least square (PLS) model, 5 spectra of each drug-polymer-lipid mixture were used. Prior to PCA and PLS, spectra were mean centred. The PLS model was developed by regressing the PMOL concentration (*Y*) versus the corresponding in-line collected spectra (*X*). This model was validated by using new NIR spectra collected for each drug-polymer-lipid mixture. These validation spectra were used to evaluate the predictive performance of the PLS model.

### **2.2.6. Particle size analysis**

The particle size distribution was measured by laser diffraction (Mastersizer 2000, Malvern, UK) where 5 g of powder was placed in the dry powder feeder. Sampling time was set at 15 s, and each sample was measured three times.

### **2.2.7. Flow properties and compressibility**

Compressibility index (Carr's index) values of different formulations were determined by measuring the tapped and bulk densities of the powders after subjecting them to 100 taps in a graduated measuring cylinder using the following relationship:

$$Carr's\ index = \left(1 - \frac{\rho_b}{\rho_t}\right) \times 100$$

Where  $\rho_b$  is the bulk density and  $\rho_t$  is the tapped density.

### **2.2.8. Tablet preparation**

For the tablet compression, all extruded batches were cutter milled to produce granules and then tablets were produced using of 500 mg dose of the PMOL from extruded granules. All excipients were passed through a mesh sieve with an aperture of 500  $\mu$ m before use. The batches were blended with magnesium stearate (1%) and silicon dioxide (0.25%) in a Turbula TF2 mixer (Basel, Switzerland) for 5 min. Blends were directly compressed on a Flexitab tablet press (Oystar-Manesty, Germany) using 13 mm normal flat punches. Dwell time was set at 30 ms and the compaction force was varied from 8-12 kN to obtain the final tablets with a hardness of 5.0-6.0 kP.

### **2.2.9. Tablet characterisation**

Freshly prepared sustained release PMOL tablets were characterized according to the United States Pharmacopeia (USP 30-NF 25, 2007). For the weight uniformity test, ten tablets were weighed individually and the results were expressed as a mean value of the individual determinations. The thickness of 10 tablets was measured using a screw meter. The tablet hardness was measured with a Erweka hardness tester (Erweka, Germany).

### **2.2.10. *In-vitro* drug release studies**

*In-vitro* drug release studies were carried out in 750 ml of 0.1 M hydrochloric acid for 2 hours using a Varian 705 DS dissolution paddle apparatus (Varian Inc. North Carolina, US) at

100 rpm and  $37\pm 0.5^{\circ}\text{C}$ . After 2 hours of operation, 150 ml of 0.20 M solution of trisodium phosphate dodecahydrate were added to each of the vessels (buffer medium: pH 6.8) that had been equilibrated at  $37^{\circ}\text{C}\pm 0.5^{\circ}\text{C}$ . At predetermined time intervals 5 mL of samples were withdrawn for HPLC assay and 5 mL of fresh dissolution medium was added to the dissolution vessel to refill. All dissolution studies were performed in triplicate.

### **2.2.11. HPLC analysis**

The amount of PMOL released from the tablets during the dissolution studies was determined by using an Agilent Technologies HPLC 1200 series system equipped with a HICROM S50DS2,  $5\ \mu\text{m} \times 150\ \text{mm} \times 4\ \text{mm}$  column. The UV wavelength used for the analysis was set at 276 nm for the PMOL HPLC assay [39]. The mobile phase consisted of acetonitrile/water (1% acetic acid) (50:50, v/v). The flow rate was adjusted to 1.5 ml/min and the retention time of PMOL was about 4 min. The PMOL calibration curve plotted with the concentrations varying from 10–50  $\mu\text{g}/\text{ml}$  were used to evaluate all the samples with 20  $\mu\text{l}$  injection volume.

## **2.3. Results and discussion**

### **2.3.1. HME processing**

The objective of this study was not only to develop sustained release PMOL tablets processed by HME but also to investigate the effects of the processing parameters which would eventually help to identify the critical quality attributes (CQAs) and define the design space. For the formulation and process optimization a DOE was implemented where the process parameters (screw speed, feed rate) and the drug loading were used as inputs, while PMOL dissolution rates were the dependent variables (response). The relationship and the effect of the three inputs on the dissolution rate were further explored. In order to reduce the number and time needed to conduct experiments as well as the number of processing parameters we did not include temperature in the DOE but the optimized temperature profile was used for all experiments. C888 acted as a plasticizer resulting in reduced extrusion temperatures ( $140^{\circ}\text{C}$ ) compared to PMOL/EC binary blends ( $>150^{\circ}\text{C}$ ).

The rationale for the co-processing of lipid-polymer formulations is not uncommon and has been reported by Windbergs *et al.*, by using trilaurin/polyethylene glycol (PEG) blends with various drugs to adjust the release profiles (e.g. increased rates) [33-34]. In our case, C888 was introduced in order to reduce the burst release in PMOL/EC extrudates. All formulations were

easily processed even at 80% PMOL loadings. The particle size distributions were measured for all extruded formulations while the Carr's indexes were varied from 5-12%. Despite the fact that HME processing was conducted at different settings, the compressed tablets were robust with low friability (<0.1%) and the hardness varied from 5.0 to 6.0 kP.

### 2.3.2. Thermal analysis

DSC was used to study the solid state behaviour of PMOL within the EC/C888 matrices. The melting peak of bulk PMOL was detected at 172.41°C ( $\Delta H = 144.40 \text{ Jg}^{-1}$ ) whilst that for the C888 occurred at 72.47°C ( $\Delta H = 139.05 \text{ Jg}^{-1}$ ) (**Fig. 2.1**). The DSC thermogram of EC presented a  $T_g$  at 117.61°C due to its amorphous nature. It has been previously reported [35-36] that PMOL presents three polymorphic forms such as the stable Form I (m.p. 170°C), Form III which is highly unstable (m.p. 148°C) and the metastable Form II (m.p. 160°C). Based on the data obtained from the DSC analysis, it can be seen that the polymorphic form of PMOL used in the current study was Form I.

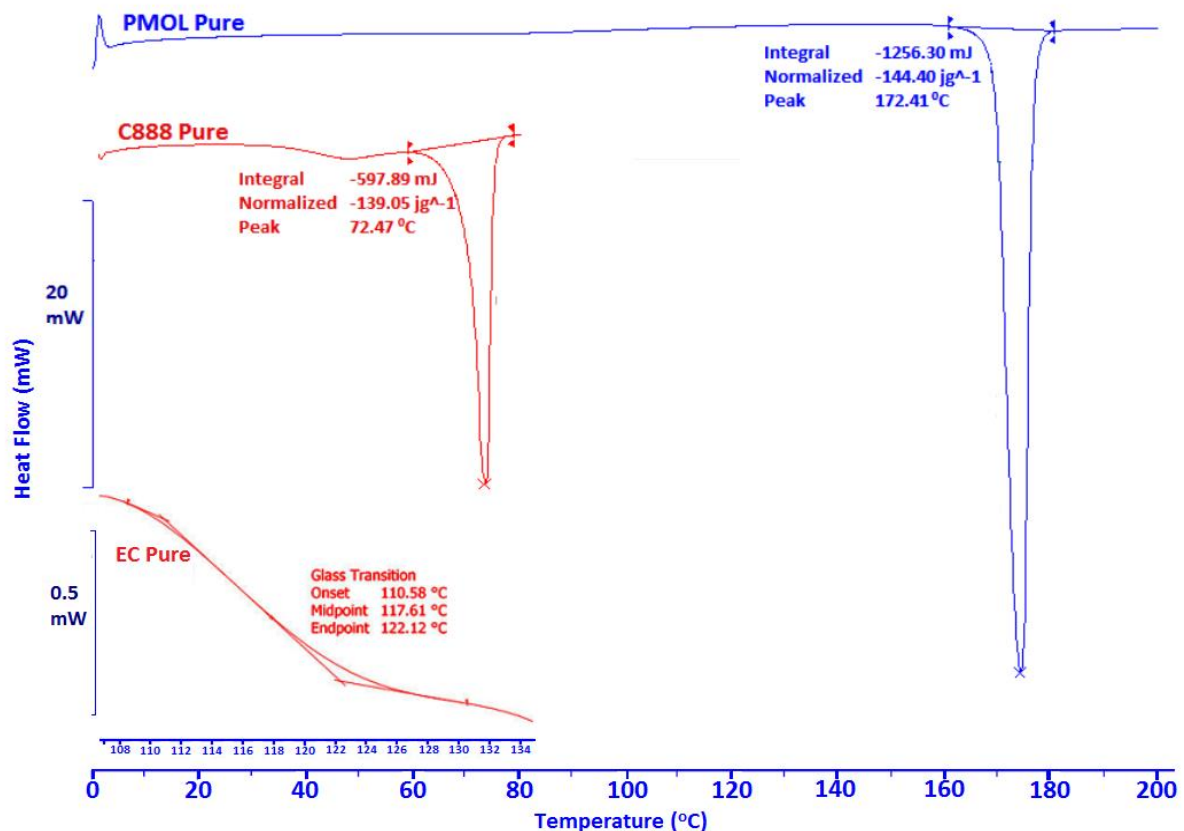


**Fig. 2.1.** Thermograms of the pure PMOL, pure EC and C888 ATO.

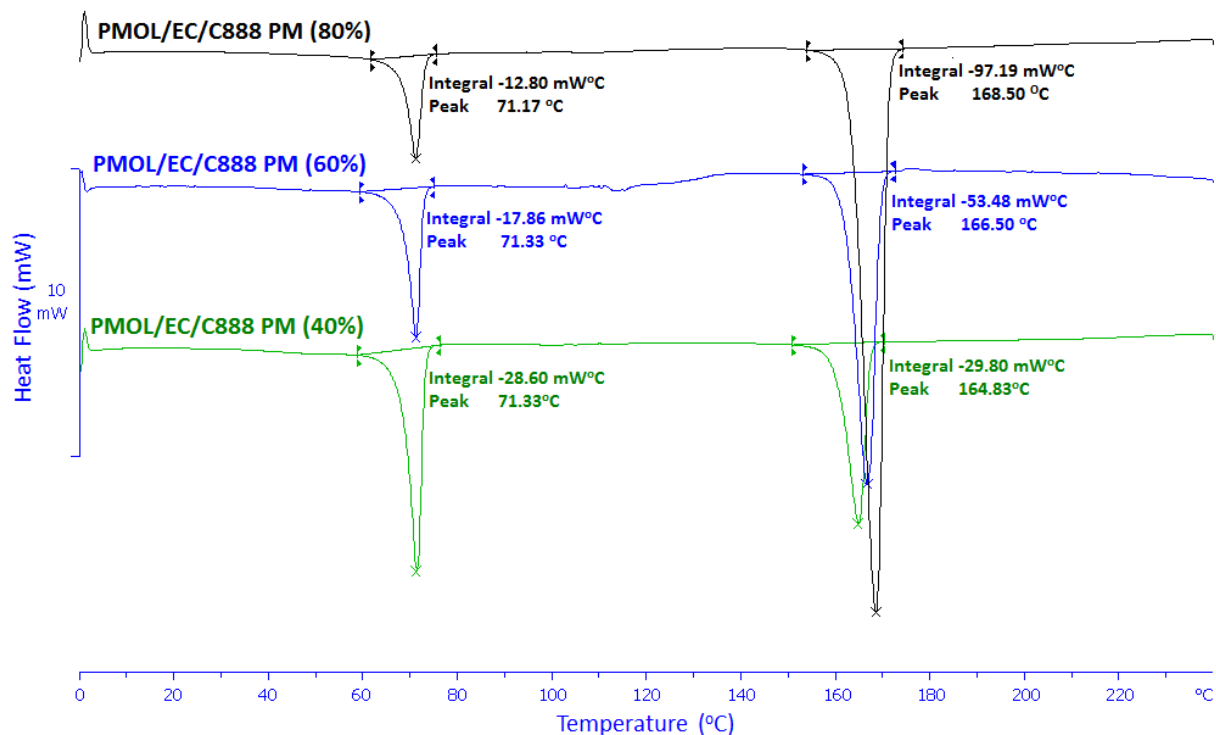


**Fig. 2.2.** Thermograms of the physical mixtures containing 40%, 60% and 80% PMOL and equal of amounts of EC and C888 ATO.

The DSC scans of the PMOL/EC/C888 extrudates (**Fig. 2.3** and **Fig. 2.4**) showed melting endotherms at 167°C, 166°C and 165°C corresponding to 80%, 60%, and 40% (w/w) PMOL loadings, respectively. The observed melting peaks are shifted to lower temperatures and the peak shapes are broader compared to those of pure PMOL suggesting the presence of less crystalline PMOL after extrusion, but nevertheless the observed melting peaks of PMOL between 165-167°C indicate the presence of Form I in the lipid-polymer matrices. The shifts of the melting points in all the drug/polymer/lipid physical mixtures (**Fig. 2.2**) as well as in the extruded formulations are attributed to the solubilisation effect of the lipid and the small amorphous PMOL content.

Sweeney *et al.*, showed that partial drug solubilisation can take place due to the slow DSC heating rates which provides sufficient time for C888 to solubilize PMOL [37]. However, the broad PMOL melting endotherms suggest the presence of small amorphous drug content due to possible PMOL/EC interactions or the processing conditions. This was confirmed by the variability in the  $\Delta H$  values of the processed formulations at the same drug loadings.

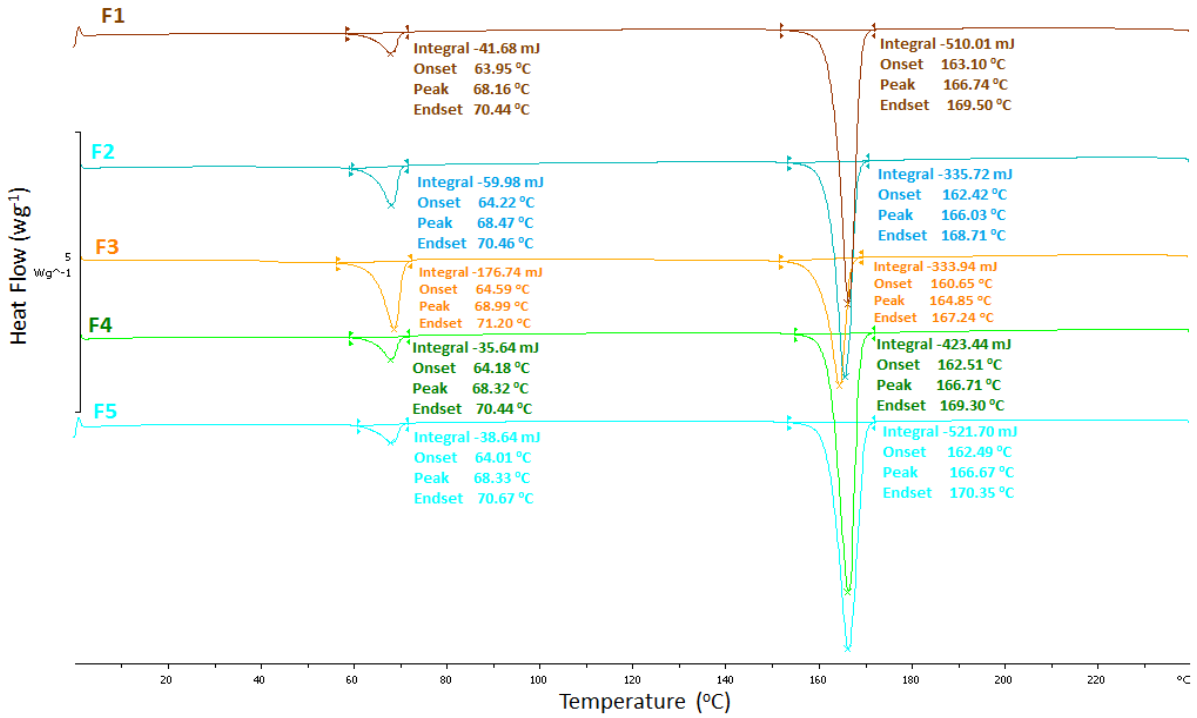


**Fig. 2.3.** Thermograms of the extrudates (F1-F5) containing 40%, 60% and 80% PMOL and equal amounts of EC and C888 ATO.

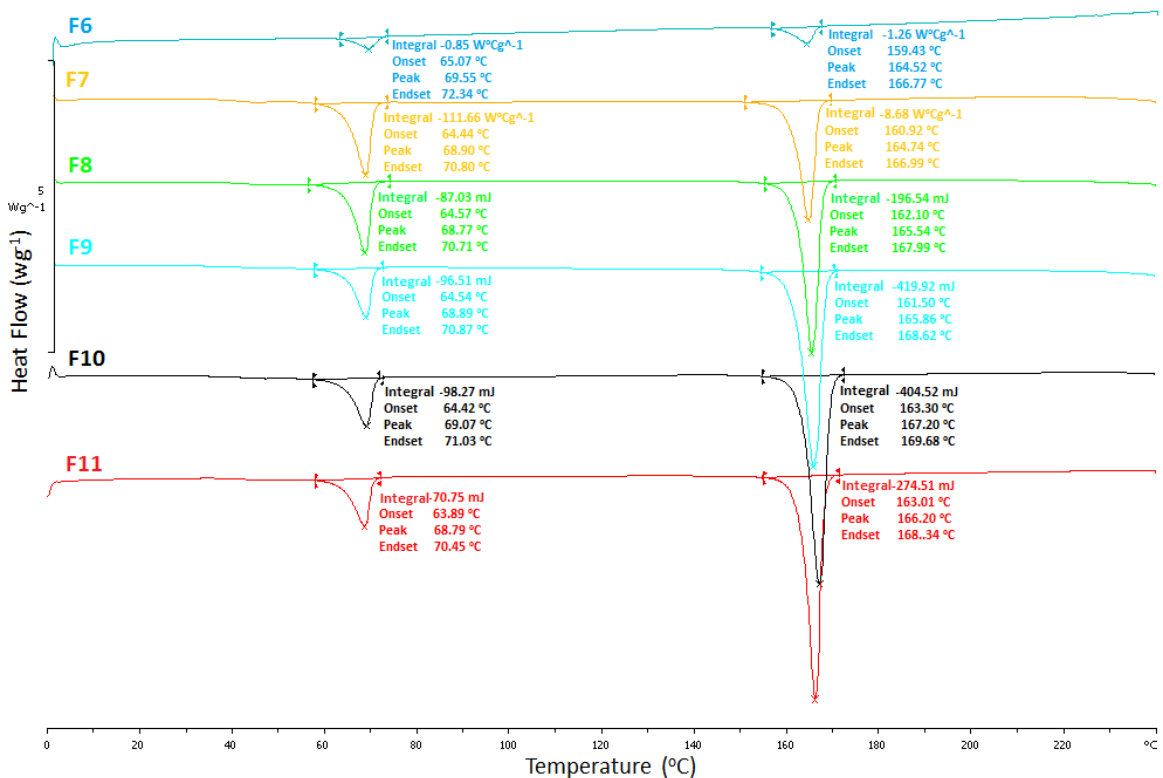


**Fig. 2.4.** Thermograms of the extrudates (F6-F11) containing 40%, 60% and 80% PMOL and equal amounts of EC and C888 ATO.

### 2.3.3. X-ray powder diffraction

XRPD was used to investigate the crystalline state of PMOL within the lipid-polymer matrices. The standard XRPD patterns of pure PMOL, physical mixtures with EC/C888 ATO, and extrudates are depicted in **Fig. 2.5**, **Fig. 2.6** and **Fig. 2.7**, respectively. The bulk PMOL showed distinct peaks at  $12.09^\circ$ ,  $13.78^\circ$ ,  $15.5^\circ$ ,  $18.17^\circ$ ,  $20.35^\circ$ ,  $23.46^\circ$ ,  $24.74^\circ$ , and  $26.52^\circ$   $2\theta$  values and a series of smaller peaks ranging from  $27.16^\circ$  to  $39.50^\circ$   $2\theta$ . C888 peaks appeared at  $4.13^\circ$ ,  $21.14^\circ$  and  $23.33^\circ$   $2\theta$  values whereas EC showed diffuse peaks indicating the amorphous nature of the polymer.

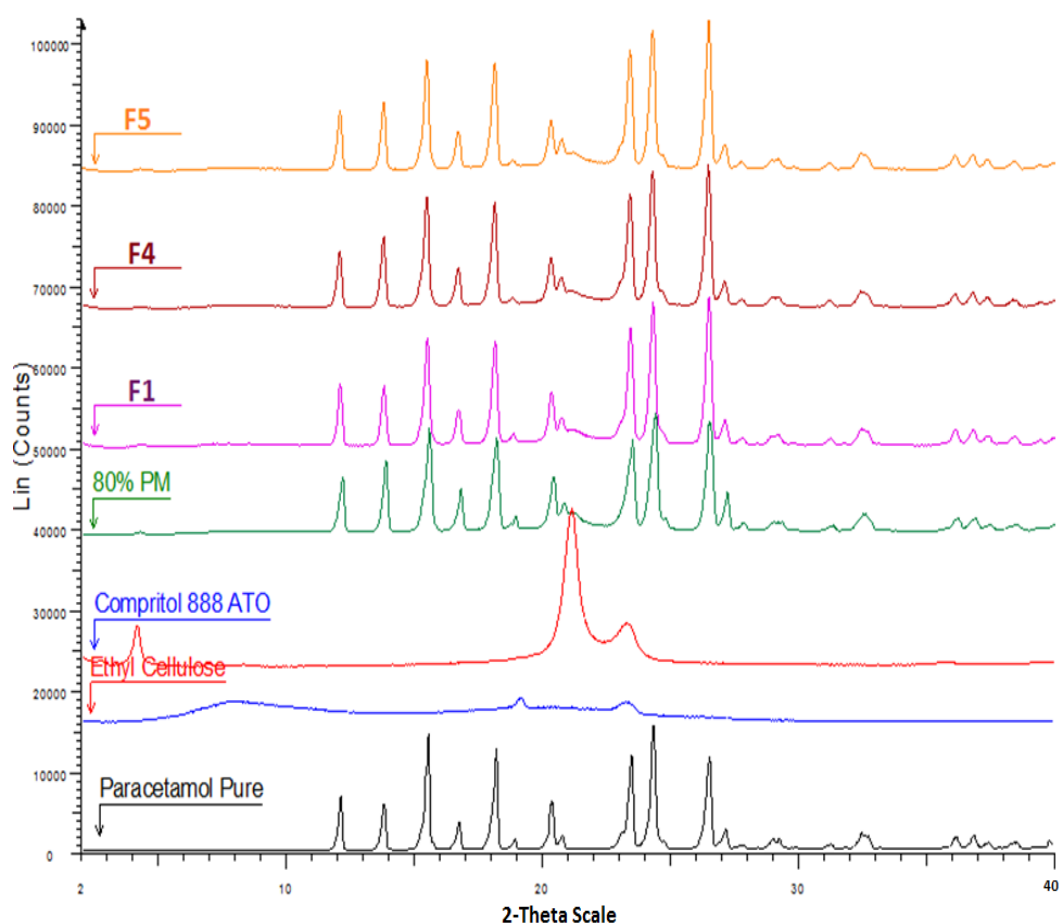


**Fig. 2.5.** X-ray diffractograms of pure materials, a physical mixture containing 80% PMOL and extrudates.

The diffraction patterns of the physical mixtures at three different ratios (40%, 60% and 80%) presented identical crystalline peaks to those of pure PMOL but with relatively lower intensities. The XRPD patterns of extruded formulations showed characteristic peaks corresponding to bulk PMOL, which indicates the presence of crystalline PMOL in the solid

dispersion prepared via HME. Furthermore, the diffractions patterns of the all the extrudates confirmed the presence of PMOL Form I within the polymer matrices and no new distinct crystalline peaks at different  $2\theta$  values were found [35]. In addition the peak intensities of the extruded formulations appear smaller than those of the respective physical mixtures with equal drug loadings, suggesting a different content of amorphous PMOL. This observation is in agreement with the DSC results, and confirmed the co-existence of low amorphous PMOL content. Previous studies [38] showed that C888 cannot facilitate PMOL amorphicity during HME processing and thus it should be attributed to the presence of EC. Indeed, Windbergs *et al.*, [33-34] confirmed that the presence of polyethylene glycol (PEG) affected the solid state of theophylline due to the drug-polymer interactions, which led to changes in the drug crystalline state (anhydrous). The same research group showed that the processing parameters (e.g. temperature) could significantly affect the physical state of the drug and consequently the dissolution rates. In our case EC presented a small solubilisation capacity leading to a small PMOL amorphous content, which is also affected by the HME processing parameters (e.g. screw and feed rates) when the same PMOL loadings were processed. Nevertheless, stable PMOL solid dispersions were manufactured with reproducible solid-state characteristics.

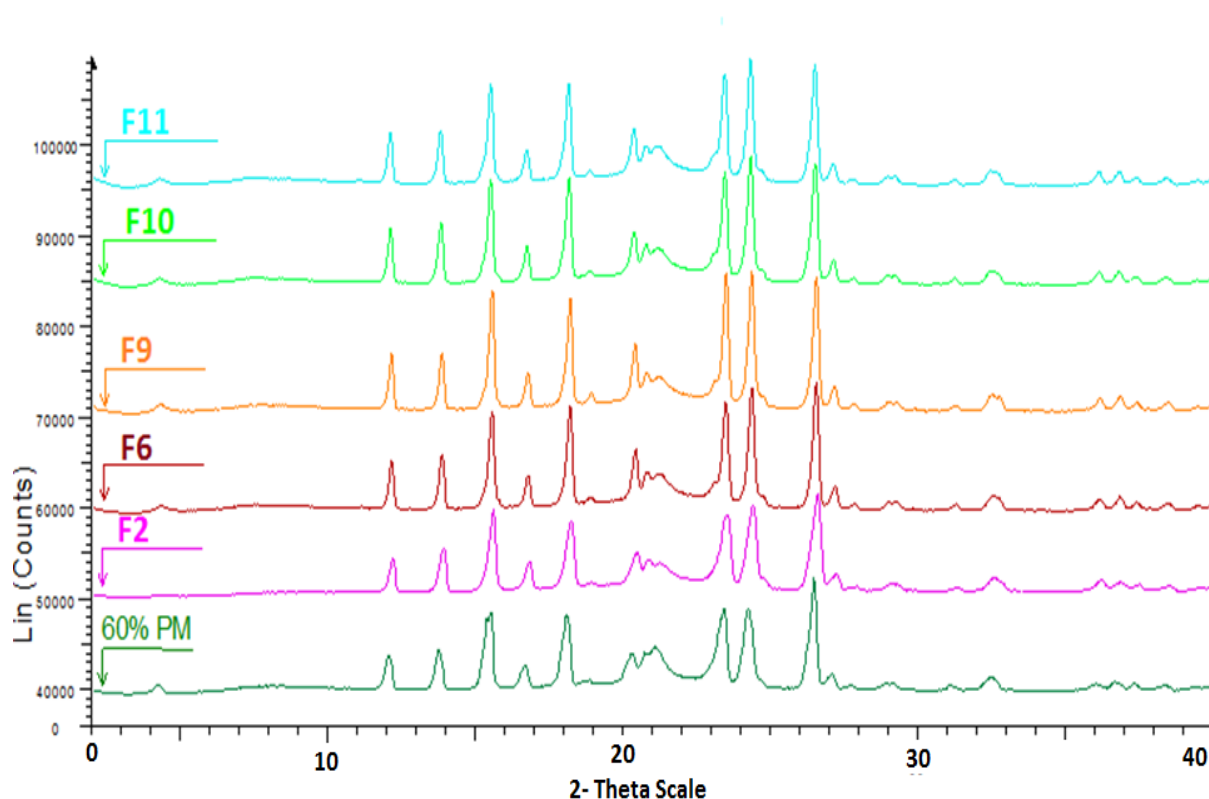


**Fig. 2.6.** X-ray diffractograms of a physical mixture containing 60% PMOL and extrudates.

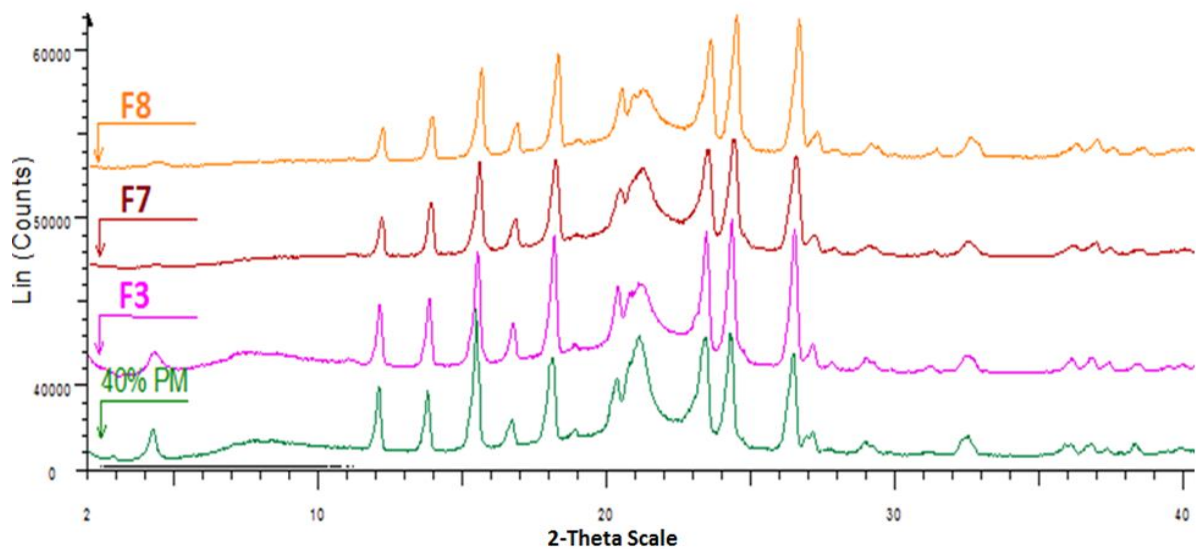


**Fig. 2.7.** X-ray diffractograms of a physical mixture containing 40% PMOL and extrudates.

### 2.3.4. In-line NIR monitoring

Off-line NIR spectra of PMOL, EC, C888 and the physical mixture (PM) were measured to identify the characteristic vibrational bands attributed to the pure samples. It can be easily observed that the NIR spectra of pure samples have characteristic bands at different wavenumbers (**Fig. 2.8**).

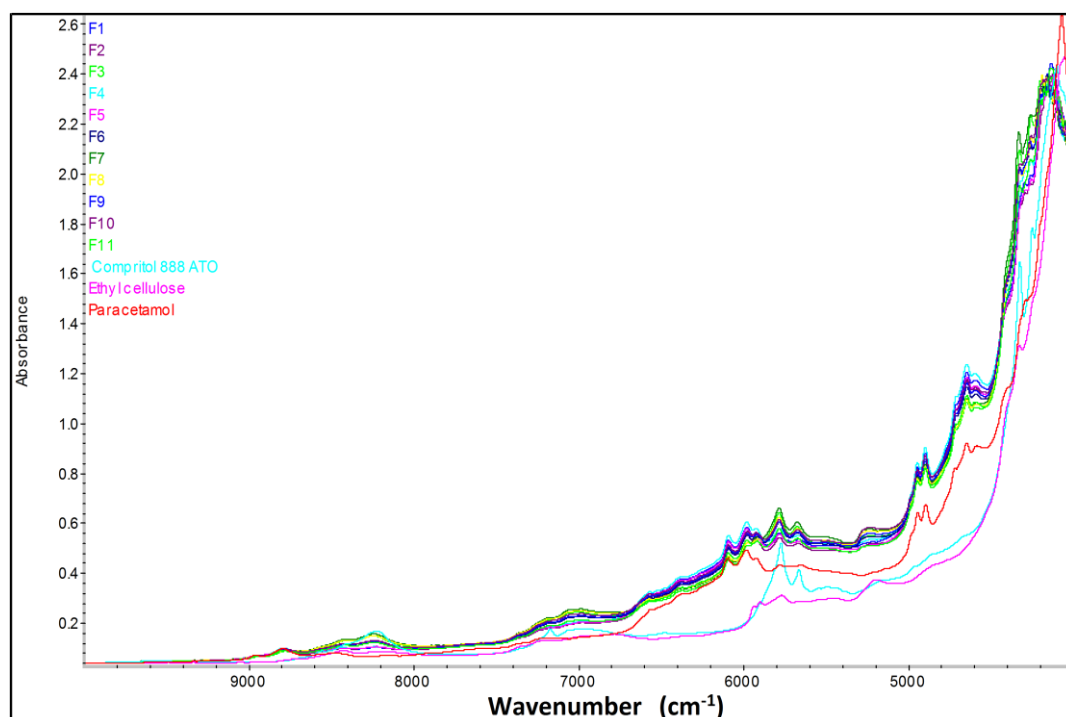


**Fig. 2.8.** NIR spectra of PMOL (bulk), EC (bulk), C888 ATO (bulk) and PMOL/EC/C888 ATO extruded formulations.

All extrudates containing 40%, 60% and 80% PMOL (w/w) blends (**Table 2.1**) with EC and C888 matrices were monitored with the in-line near infrared probe where the HME processing parameters (screw speed and feed rate), drug loading and percent drug release of the active substance were taken into account as critical processing parameters (CPP) and critical quality attributes (CQA) of the PAT processing, respectively. The typical in-line NIR spectra collected during extrusion processing (9091-4085  $\text{cm}^{-1}$ ) are shown in **Fig. 2.8**. A partial least square (PLS) calibration model (**Fig. 2.9**) was developed to allow prediction of PMOL concentration in unknown samples during HME processing ( $r^2 = 0.99$ ). The in-line NIR spectra were regressed versus the known PMOL concentrations, thus establishing the rationale of the foregoing claims.

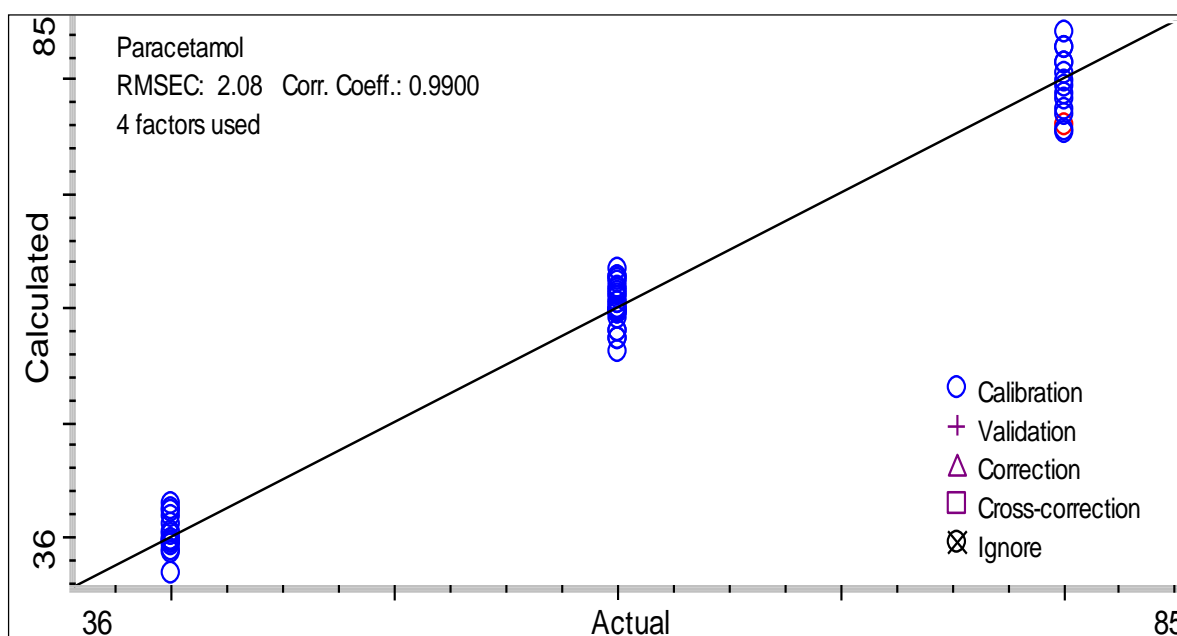


**Fig. 2.9.** PLS calibration curve obtained using 40%, 60% and 80 % PMOL with varying processing parameters.

PCA was applied to all 55 NIR spectra (5 spectra for each extruded formulation) leading to a model with two principal components covering nearly all spectral variations. The first principal component (PC1) captures 83.98% of the variation while the second component (PC2) covers 7.30% extra variation (**Fig. 2.10**). The PC score plot for spectra with the same process conditions with three different PMOL loadings describes the changes in PMOL concentration very well. The sizes of the ellipses for each concentration varied, which indicates that possibility that there is extra variation attributed with PMOL concentration. In most of the instances, the ellipses are smaller at high drug loading compared to that of the lower loading,

which demonstrates that the low drug loading introduces more variability into the spectra of the extruded formulations. For that reason, all formulations with 80% PMOL loadings (right part of the PC score plot) showed relatively lower variability compared to that of 60% PMOL loaded formulations. Similarly, all formulations with 60% PMOL loadings showed less variability compared to that of 40% loadings but, as expected, slightly higher than the 80% loading. The foregoing reasons also account for the observed smaller variation due to the feeding rate in PC2. F2 shows extra variation on PC1 which could be due to the effect of screw speed and feed rate.

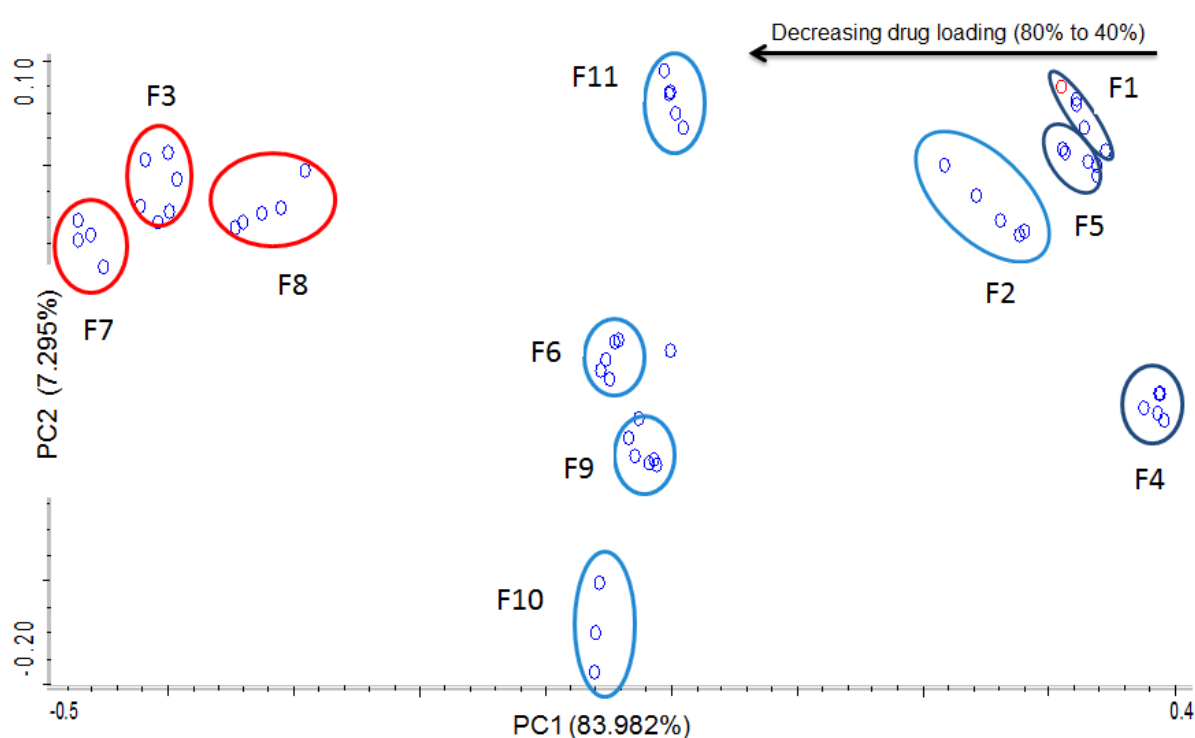


**Fig. 2.10.** Principal component plot obtained after PCA on the pre-processed in-line collected NIR spectra during extrusion of mixtures containing 40%, 60% and 80% PMOL extruded with EC and C888 ATO.

These data showed the sensitivity of NIR spectroscopy to the processing conditions during HME. Furthermore, the data also show the potential implementation and modern application of NIR spectroscopy to optimize critical process conditions.

### 2.3.5. *In-vitro* drug release studies

*In-vitro* dissolution studies were carried out for the compressed PMOL tablets produced from extruded granules, at equal doses of 500 mg, to assess their performance. Tablets with

high drug loaded formulations (F1, F4 and F5) showed higher dissolution rates with more than 60% and 80% of the drug being dissolved after 6 h and 12 h, respectively (**Fig. 2.11**). In contrast, tablets with 40 and 60% PMOL loadings showed sustained release but at much lower rates at 6 and 12 hr. It is obvious that PMOL release rates depend on the final drug loading due to the highly hydrophilic nature of the drug. The combination of EC/C888 matrices could be used to successfully control PMOL release rates while it worth noticing the absence of burst release for all formulations.

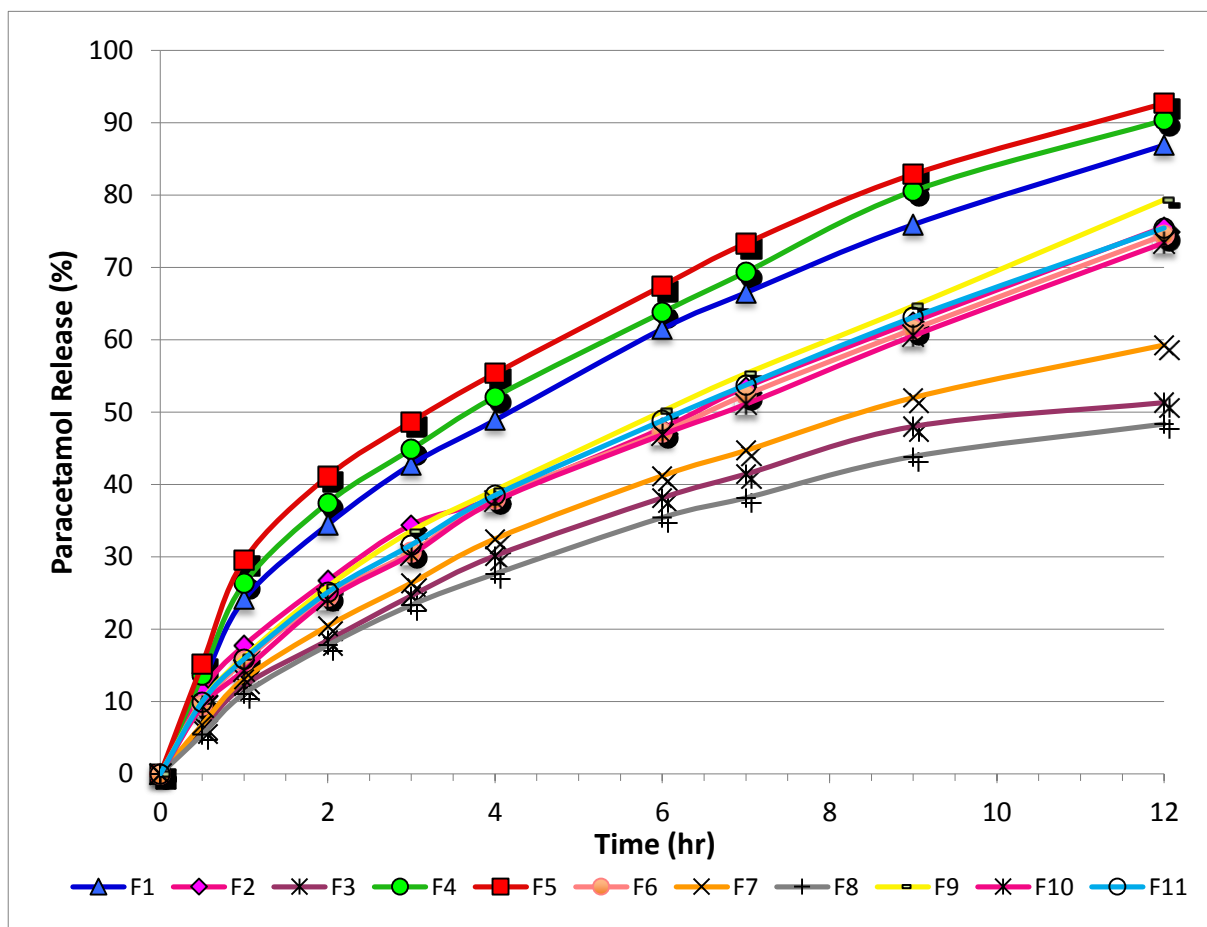


**Fig. 2.11.** Dissolution profiles for PMOL/EC/C888 formulations at 40%, 60% and 80% drug content, extruded at different processing parameters (**Table 2.1**).

The fractions of PMOL release at 6 and 12 hr were used as independent variables in the DoE analysis in order to assess the effect of the processing parameters and the drug loading. As shown in the data in **Table 2.2** the ANOVA statistical analysis revealed that only drug loading has a significant effect on PMOL dissolution rates with probability values ( $p$ ) less than 0.05. None of the processing parameters showed a significant effect on both dissolution rates and particle size distribution.

The PC score plot showed that only F4, F5 and F6 fulfil the criteria for HME processing as clusters are condensed with very little relative standard deviation among the each scan and the processing parameters introduce low variability during processing. In contrast, as shown from the DOE analysis only F1, F4 and F5 provide the desired PMOL release rates and sustained release above 80% can be obtained after 12 hr. The QbD approach introduced in this study, whereas DoE experimentation and in-line PAT tools are combined, helped to identify a CQA and optimize the extrusion processing. Eventually, the employed QbD approach helped to identify the design space for this particular dosage form. Nevertheless, the same strategy could be used in future for other formulations by introducing additional independent and dependent variables.

**Table 2.2.** ANOVA analysis for the % release of PMOL ( $T_{6hr}$ ,  $T_{12hr}$ ) and particle size of the extrudates according to the response surface design.

Coded Variable Name	P-values for Correlation Coefficients		
	PMOL Release ( $T_{6hr}$ )	PMOL Release ( $T_{12hr}$ )	Particle size D(0,5)
X1	0.0239	0.0396	0.1900
X2	0.5660	0.9815	0.3293
X3	0.1788	0.3199	0.1819
(X1) <sup>2</sup>	0.0921	0.1484	0.1704
(X2) <sup>2</sup>	0.0926	0.1469	0.5916
(X3) <sup>2</sup>	0.1683	0.3136	0.0825
X1 * X2	0.3979	0.9027	0.2045
X1 * X3	0.2372	0.3555	0.2374
X2 * X3	0.3418	0.9169	0.5401

X1= drug loading, X2= Screw speed, X3= Feed rate

## 2.4. Conclusions

HME was used to develop PMOL/EC/C888 sustained release formulations and to investigate the effect of screw rate, feed rate and drug loading. In-line NIR was successfully used to monitor PMOL/EC/C888 extrusion process. A fraction factorial design was used to produce the design of the experiment prior to extrusion considering screw speed, feed rate and drug loading as dependant variables. The NIR probe was inserted in to HME die in order to monitor and collect spectra during HME process. After SNV pre-processing a PLS calibration model was developed to predict unknown PMOL concentration using collected spectra from the HME die. A PCA plot model has also been prepared to demonstrate the repeatability of the process and demonstrates that only three formulations (F1, F4 and F5) shows better repeatability. Collected extrudates were milled using a cutter mill to produce less than 250  $\mu\text{m}$  particle size, blended with excipients to produce 500 mg PMOL tablets. The freshly prepared tablets were then subjected to drug release test to evaluate their drug release pattern, and it was found that only three formulations (F1, F4 and F5) showed sustained release PMOL after 12 hours compared with extruded formulations. The dissolution data were used for the statistical analysis to understand the effect of critical processing parameters during HME process, and found that only drug loading has got significant effect on the drug release pattern whereas screw speed and feed rate doesn't have any effect on the quality (drug release) of the final products. This paradigm of the QbD approach can be used in the future for process optimization and better understanding of the developed pharmaceutical formulations.

## 2.5. References

1. Gavin PA, David SJ, Osama AD, Daniel NM, Mark SMc, Hot-melt extrusion: an emerging drug delivery technology, *Pharmaceutical Technology Europe*, 2009; **21**(1).
2. Crowley MM, Zhang F, Repka MA, Thumma S, Upadhye SB, Battu SK, McGinity, JW, Martin C, *Pharmaceutical Applications of Hot-Melt Extrusion: Part I, Drug development and industrial pharmacy*, 2007; **33**(9): 909-926.
3. Repka MA, Battu SK, Upadhye SB, Thumma S, Crowley MM, Zhang F, *Pharmaceutical applications of hot-melt extrusion: Part II, Drug Development and Industrial Pharmacy*, 2007; **33**(10): 1043-1057.
4. Maniruzzaman M, Boateng JS, Bonnefille M, Aranyos A, Mitchell JC, Douroumis D, *Taste masking of paracetamol by hot-melt extrusion: An in vitro and in vivo evaluation*, *European Journal of Pharmaceutics and Biopharmaceutics*, 2012; **80**(2): 433-442.

5. Cilurzo F, Cupone IE, Minghetti P, Selmin F, Montanari L, Fast dissolving film made of maltodextrins, *European Journal of Pharmaceutics and Biopharmaceutics*, 2008; **70**(3): 895-900
6. Kalivoda A, Fischbach M, Kleinebudde P, Application of mixtures of polymeric carriers for dissolution enhancement of fenofibrate using hot-melt extrusion, *International Journal of Pharmaceutics*, 2012; **429**(1–2): 58-68
7. De Brabander C, Vervaet C, Fiermans L, Remon JP, Matrix mini-tablets based on starch/microcrystalline wax mixtures, *International Journal of Pharmaceutics*, 2000; **199**: 195-203.
8. De Brabander C, Vervaet C, Remon JP, Development and evaluation of sustained release mini-matrices prepared via hot melt extrusion, *Journal of Control Release*, 2003; **89**: 235–247.
9. Roblegg E, Jäger E, Hodzic A, Koscher G, Mohr S, Zimmer A, Khinast J, Development of sustained-release lipophilic calcium stearate pellets via hot melt extrusion, *European Journal of Pharmaceutics and Biopharmaceutics*, 2011; **79**: 635–645.
10. Almeida A., Possemiers S, Boone MN, De Beer T, Quinten T, Van Hoorebeke L, Ethylene vinyl acetate as matrix for oral sustained release dosage forms produced via hot-melt extrusion, *European Journal of Pharmaceutics and Biopharmaceutics*, 2011; **77**(2): 297-305.
11. Burcham CL, Roginski RT, Correlating powder flowability to particle size distribution using chemometric techniques, In: talk held in QbD Topical Conference at the 2009 AIChE Annual Meeting, Nashville, TN
12. Garcia-Munoz S, Gierer D, Film coating end-point determination for colored immediate release tablets using multivariate image analysis, In: talk held in QbD Topical Conference at the 2009 AIChE Annual Meeting, Nashville, TN
13. International Conference on Harmonisation (ICH) of technical requirements for registration of pharmaceuticals for human use, Topic Q8 (R2): Pharmaceutical development, Geneva, 2009.
14. International Conference on Harmonisation (ICH) of technical requirements for registration of pharmaceuticals for human use, Topic Q9: Pharmaceutical quality system, Geneva, 2005.

15. International Conference on Harmonisation (ICH) of technical requirements for registration of pharmaceuticals for human use, Topic Q10: Pharmaceutical quality system, Geneva, 2008.
16. Yu LX, Pharmaceutical Quality by Design: Product and Process Development, Understanding, and Control, *Pharmaceutical Research*, 2008; **25**(4): 781-791.
17. Fonteyne M, Soares S, Vercruyssen J, Peeters E, Burggraeve A, Vervaeke C, Remon JP, Sandler N, De Beer T, Prediction of quality attributes of continuously produced granules using complementary PAT tools, *European Journal of Pharmaceutics and Biopharmaceutics*, 2012; **82**(2): 429-436.
18. Wu H, White M, Khan MA, Quality-by-Design (QbD): An integrated process analytical technology (PAT) approach for a dynamic pharmaceutical co-precipitation process characterization and process design space development, *International journal of pharmaceutics*, 2011; **405**(1-2): 63-78.
19. Wu H, Khan MA, Quality-by-Design (QbD): An integrated process analytical technology (PAT) approach for real-time monitoring and mapping the state of a pharmaceutical coprecipitation process, *Journal of Pharmaceutical Sciences*, 2010; **99**(3): 1516-1534
20. Adam S, Suzzi D, Radeke C, Khinast JG, An integrated Quality by Design (QbD) approach towards design space definition of a blending unit operation by Discrete Element Method (DEM) simulation, *European Journal of Pharmaceutical Sciences*, 2011; **42**(1-2): 106-115.
21. Xie L, Wu H, Shen M, Augsburger LL, Lyon RC, Khan MA, Hussain AS, Hoag SW, Quality-by-design (QbD): Effects of testing parameters and formulation variables on the segregation tendency of pharmaceutical powder measured by the ASTM D 6940-04 segregation tester, *Journal of pharmaceutical sciences*, 2008; **97**(10): 4485-4497.
22. Awa K, Okumura T, Shinzawa H, Otsuka M, Ozaki Y, Self-modeling curve resolution (SMCR) analysis of near-infrared (NIR) imaging data of pharmaceutical tablets, *Analytica Chimica Acta*, 2008; **619**(1): 81-86.
23. Kenett RS, Kenett DA, Quality by Design applications in biosimilar pharmaceutical products, *Accreditation and Quality Assurance*, 2008; **13**: 681-690.
24. Food and Drug Administration CDER. Guidance for industry, PAT—A framework for innovative pharmaceutical development, manufacturing, and quality assurance, September 2006.

25. Saerens L, Dierickx L, Lenain B, Vervaet C, Remon JP, De Beer T, Raman spectroscopy for the in-line polymer–drug quantification and solid state characterization during a pharmaceutical hot-melt extrusion process, *European Journal of Pharmaceutics and Biopharmaceutics*, 2011; **77**(1): 158-163.
26. Saerens L, Dierickx L, Quinten T, Adriaensens P, Carleer R, Vervaet C, In-line NIR spectroscopy for the understanding of polymer–drug interaction during pharmaceutical hot-melt extrusion, *European Journal of Pharmaceutics and Biopharmaceutics*, 2012; **81**(1): 230-237.
27. De Beer T, Burggraeve A, Fonteyne M, Saerens L, Remon JP, Vervaet C, Near infrared and raman spectroscopy for the in-process monitoring of pharmaceutical production processes, *International Journal of Pharmaceutics*, 2011; **417**(1–2): 32-47.
28. Kelly AL, Gough T, Dhumal RS, Halsey SA, Paradkar A, Monitoring ibuprofen–nicotinamide cocrystal formation during solvent free continuous cocrystallization (SFCC) using near infrared spectroscopy as a PAT tool, *International Journal of Pharmaceutics*, 2012; **426**(1–2): 15-20.
29. Moes JJ, Ruijken MM, Gout E, Frijlink HW, Ugwoke MI, Application of process analytical technology in tablet process development using NIR spectroscopy: Blend uniformity, content uniformity and coating thickness measurements, *International journal of pharmaceutics*, 2008; **357**(1–2): 108-118.
30. Almeida A, Saerens L, De Beer T, Remon JP, Vervaet C, Up scaling and in-line process monitoring via spectroscopic techniques of ethylene vinyl acetate hot-melt extruded formulations, *International Journal of Pharmaceutics*, 2012; **439**(1–2): 223-229.
31. Fischer D, Bayer T, Eichhorn KJ, Otto M, In-line process monitoring on polymer melts by NIR-spectroscopy, *Fresenius' Journal of Analytical Chemistry*, 1997; **359**: 74–77
32. Honigs DE, Near infrared analysis, *Analytical Instrumentation*, 1985; **14**: 1–62
33. Windbergs M, Strachan CJ, Kleinebudde P, Understanding the solid-state behaviour of triglyceride solid lipid extrudates and its influence on dissolution, *European Journal of Pharmaceutics and Biopharmaceutics*, 2009; **71**(1): 80-7.
34. Windbergs M, Strachan CJ, Kleinebudde P, Influence of structural variations on drug release from lipid/polyethylene glycol matrices, *European Journal of Pharmaceutics and Biopharmaceutics*, 2009; **37**(5): 555-62.
35. Rossi A, Savioli A, Bini M, Capsoni D, Massarotti V, Bettini R, Gazzaniga A, Sangalli ME, Giordano F, Solid-state characterization of paracetamol metastable polymorphs

- formed in binary mixtures with hydroxypropylmethylcellulose, *Thermochimica Acta*, 2001; **406**: 55–67.
36. Martino PD, Guyot-Hermann AM, Conflant P, Drache M, Guyot JC, A new pure paracetamol for direct compression: the orthorhombic form, *International Journal of Pharmaceutics*, 1996; **128**: 1–8.
  37. Sweeney G, (PhD thesis), Queen’s Belfast University, 2012.
  38. Vithani K, Maniruzzaman M, Slipper IJ, Mostafa S, Miolane C, Cuppok Y, Marchaud D, Douroumis D, Sustained release solid lipid matrices processed by hot-melt extrusion (HME), *Colloids and Surfaces B: Biointerfaces*, 2013; **110**: 403–410.
  39. Maniruzzaman M, Boateng JS, Bonneille M, Aranyos A, Mitchell JC, Douroumis D, Taste masking of paracetamol by hot-melt extrusion: An *in vitro* and *in vivo* evaluation, *European Journal of Pharmaceutics and Biopharmaceutics*, 2012; **80**(2): 433-442.

## Chapter 3: Monitoring cocrystallization processing via HME using in-line NIR spectroscopy

---

### 3.1. Introduction

Cocrystals are defined as crystalline materials that are comprised of two or more components that are solids at room temperature (in order to distinguish them from hydrates and solvates) held together by non-covalent interactions such as hydrogen bonding, ionic interactions, van der Waals interactions and  $\pi$ -interactions [1-2]. Cocrystals are an emerging formulation approach in pharmaceutical drug development; the aims being to e.g., improve solubility, dissolution and bioavailability [3-5] of various poorly water soluble drugs. Trask *et al.*, (2006) reported that cocrystallization of caffeine and theophylline led to physical stability enhancement [6] whereas Karki *et al.*, (2009) and Sun *et al.*, (2008) showed the improvement of mechanical properties of the drug(s) by cocrystallization [7-8]. In addition to the physicochemical improvements of the drug molecules, cocrystals can highly be patentable as a completely new drug entity. Cocrystals can be viewed from a supramolecular perspective, which involves an understanding of the intermolecular interactions between the API and the coformer candidates [9-10]. Cocrystals are held together by low energy non-covalent interactions without changing physiological action of the drug compounds. Cocrystals are formed as homogenous phases between two or more molecular components in the crystalline lattice, which consists of a drug substance and a coformer [11]. Moreover, according to the FDA guidelines, “pharmaceutical cocrystals are crystalline materials, composed of two or more molecules in the same crystalline lattice” [12].

Traditionally cocrystals are prepared by solvent crystallization and mechanical/melt grinding of the constituents [13-14]. In recent times, liquid assisted grinding has been developed as a more effective method to make cocrystals [15-16], but in reality all of these techniques are time consuming and difficult to scale-up. Excessive use of solvents can be harmful and costly and a small residue of the solvent or impurities [17] can be toxic which can, again, raise regulatory issues. The solubility of the active compounds in organic solvents can lead to undesired solvate formation [18]. Some other techniques such as spray drying [19], ultra-sonication [20], supercritical fluid techniques [21] hydration [22], ink-jet printing [23] and microfluidic anti-solvent [24] crystallization have also been used for the development and engineering of various pharmaceutical cocrystals. In recent years significant progress has been

made towards designing simple procedures for using solution crystallization to scale-up the production of cocrystals [25]. However, use of solution crystallization requires drying of solvent from the final product to acceptable levels and also introduces the risk of forming solvates. We have presented hot-melt twin screw extrusion (TSE) of cocrystal components as a scalable and solvent free process that provides a viable alternative to solution crystallization [26].

HME has been introduced in the pharmaceutical industry and it is now broadly applicable as a highly versatile and robust process. HME has found several applications in formulation development including solubility and bioavailability enhancement or taste masking of bitter APIs via the manufacture of amorphous solid dispersions. Recently, HME has gained significant interest in pharmaceutical research for the manufacture and engineering of cocrystals [27-28]. HME is considered a continuous process with excellent scalability, high throughput efficacy, intense mixing capacity and low residence time compared to traditional technologies. The absence of any organic solvents or water during processing makes HME an environmental friendly technology.

The ability to monitor and to some extent to potentially control the quality attributes of cocrystals in real-time would be an effective tool aligning with the current regulatory initiatives towards continuous monitoring. In recent years, process understanding has been strongly supported by the FDA, through the implementation of quality by design (QbD) and process analytical technology (PAT) tools (CDER 2004) [29]. As a result, the scope of the real time data interpretation, continuous quality monitoring and control has led PAT to enjoy a renaissance in continuous manufacturing and product development. Nowadays, various PAT tools such as UV-visible, NIR and Raman spectroscopic techniques are being employed in the area of crystallization [30]. Raman spectroscopy has been reported as a cocrystallization characterization technique which probes the effect of crystal structure on bond vibrations [31]. This is a non-invasive and rapid measurement technique which can also be used for high throughput screening. Near infrared (NIR) spectroscopy is also non-destructive technique which has been used to show the spectral difference in bulk materials and cocrystals [32].

The aim of the current work was to investigate the use of NIR spectroscopy to monitor the formation of cocrystals produced, continuously, during twin screw HME. The ability to monitor and potentially control the purity of cocrystals in real-time would represent a highly useful process which would align well with the current regulatory drive towards continuous

monitoring and real-time quality control. Carbamazepine (CBZ) was used as a model drug and *trans*-cinnamic acid (TCA) and saccharine (SCH) used as co-formers in case studies A and B, respectively. Results were correlated with off-line evaluation of purity using XRPD and DSC techniques. The rationale to choose the drug and coformers is due to these two formulations were highly studied in pharmaceutical cocrystal formulation development.

## **3.2. Materials and methods**

### **3.2.1. Materials**

Pure carbamazepine form III (CBZ, purity  $\geq 98\%$ ), *trans*-cinnamic acid (TCA, purity  $\geq 99\%$ ) and saccharin (SCH, purity  $> 99\%$ ) were purchased from Sigma Aldrich (Gillingham, UK) and used as received. All solvents (acetonitrile, Na monophosphate) used for HPLC analysis were of analytical grade and purchased from Sigma Aldrich (Gillingham, UK).

### **3.2.2. Hot-melt extrusion processing**

The extrusion was performed by using Eurolab 16 twin screw extruders (TSE) (Thermofisher, Germany) without the die. Equimolar amounts of CBZ-TCA (Case A) and CBZ-SCH (Case B) (1:1 molar ratio) were weighed and blended thoroughly in a TF2 Turbula mixer (Willy A. Bachofen AG, Switzerland) for 10 min. Optimization of processing temperature for the both cases (A and B) was crucial as high temperature could degraded the materials inside the HME barrel whereas low temperature could produce high shear stress and pressure which possibly create blockade inside the HME barrel and lead to stop the HME process. So to optimise the processing temperature, HME process was started with 125°C to 130°C along with all zones of the extruder barrel except the feeding zone (50°C) during the extrusion of case studies A, observed that the extruder stopped during the process which indicates the production of high shear stress and pressure which stopped the process. On the other hand when 140°C used along the barrel to produce cocrystal, degradation of the product has been observed visually such as colour changes which is due to the high temperature burnt the processing materials inside the barrel. So, final processing temperature should not exceed (50/90//135/135/135/135/135/120)°C for TSE processes for CBZ-TCA (case A) extrusion because at these temperature profile the materials neither degraded nor stopped the extrusion process and the screw speed was kept at 10 rpm. To extrude CBZ-SCH (case B), typical temperature profiles used within different zones of the extruder from hopper to extruder were:

(70/95/110/120/120/120/120/115)°C. However, the maximum temperature was adjusted in order to optimize the cocrystal quality and was varied from 120 to 140°C.

### **3.2.3. Differential scanning calorimetry (DSC) analysis**

DSC was used to evaluate the solid state properties of the samples including bulk substances (CBZ, TCA and SCH), physical blends (CBZ-TCA and CBZ-SCH) and the extruded formulations collected from different mixing zones of the HME barrel. Accurately weighed, 3-5 mg, samples were placed into an aluminium pan and crimped, and heated from 25°C to 200°C (Mettler Toledo 823e, Greifensee, Switzerland) at a heating rate of 10°C/min. Pure nitrogen gas was used as a purge gas and was supplied at 20 ml/min. The Star evaluation software was used for post-experimental analysis.

### **3.2.4. X-ray powder diffraction (XRPD) analysis**

XRPD was used to determine the solid state properties of bulk materials, physical mixtures and extrudates using a Bruker D8 Advance (Germany) in theta-theta mode. For the study purposes a Cu anode at 40 kV and 40 mA, parallel beam Goebel mirror, 0.2 mm exit slit, LynxEye Position Sensitive Detector with 3° opening (LynxIris at 6.5 mm) and sample rotation at 15 rpm were used. Each sample was scanned from 2 to 40° 2 $\theta$  with a step size of 0.02° 2 $\theta$  and a counting time of 0.3 seconds per step; 176 channels active on the PSD were used making a total counting time of 52.8 s per step.

### **3.2.5. In-line NIR spectroscopy monitoring**

Diffuse reflectance near infrared (NIR) spectroscopy was continuously performed in-line and non-invasively during HME using an Antaris MX Fourier Transform NIR spectrometer (Thermo Scientific, UK). A fibre optic NIR probe was fitted in three different zones of the extruder barrel for in-line monitoring. Spectra were collected in the 10000-4000 cm<sup>-1</sup> region with a resolution of 16 cm<sup>-1</sup>. Each spectrum taken was an average of 32 individual scans which took around 16 s to complete. In addition to real-time monitoring, the extruded cocrystal spectra were measured off-line. Off-line NIR spectra were also collected for the bulk carbamazepine, bulk saccharin and the physical mixture of both. Data analysis was performed by using the RESULT software (version 3.0, Thermo Scientific, UK).

### **3.2.6. Molecular modelling**

ACD/ChemSketch 11.01 and the ACD/3DViewer 11.01 (Ontario, Canada) software were used to model the intermolecular interactions between CBZ and TCA cocrystals.

### **3.2.7. *In-vitro* dissolution studies**

Dissolution studies were carried out using USP II paddle apparatus (Varian 705, US). Equal amounts of 200 mg of bulk CBZ, CBZ-TCA, CBZ-SCH extruded powders and prototype were placed into 900 ml of 0.1 M (pH 1.2) HCl in each dissolution vessel (n=3). The temperature of the media was maintained at 37°C with a paddle rotation of 100 rpm. About 2-3 ml of samples were withdrawn at 15, 30, 60 and 120 min intervals and filtered with a 200 µm filter prior to HPLC analysis. Furthermore the GraphPad InStat® (GraphPad Software Inc.) was applied to assist the analysis of the dissolution profiles between the cocrystals and the bulk drug, respectively.

### **3.2.8. HPLC analysis**

HPLC analysis was carried out using an Agilent 1200 series HPLC (USA) instrument equipped with an autosampler. The mobile phase was prepared using 60:40 ratios of Na monophosphate buffer (pH 7.3) and acetonitrile. A Zorbax Eclipse C8 (4.6 × 150 mm × 5 µm) column (Agilent, USA) was used at a flow rate of 1 ml/minute and detection at a wavelength of 254 nm. The calibration curve was constructed by varying the standard solution concentration from 10–50 µg/ml.

### 3.3. Results and Discussion

#### Case study A: Monitoring by NIR spectroscopy as a PAT tool in carbamazepine-*trans*-cinnamic acid cocrystal formation using HME process.

##### 3.3.1. HME processing

Extruded cocrystals were collected in powder form from the extruder end as the die, which is normally placed at the end of the extruder to shape the extrudates, was removed. It has been reported that temperature plays an important role in the properties of cocrystals produced using HME [27]. During HME processing, the screw configuration was adjusted to achieve homogenous mixing by assembling the kneading elements in three separate “mixing zones”, as shown in **Fig. 3.1**. The mixing zones were designed to obtain high mixing capacity whereas conveying elements have minimal mixing ability. Extruded samples were collected from each zone to investigate the effect of the kneading elements and provide a better understanding of the cocrystallization process (discussed in following sections).

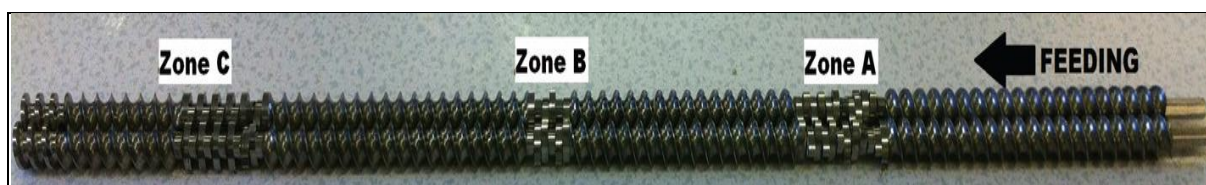


**Fig. 3.1.** Schematic diagram of the screw in TSE indicating the collection zones.

##### 3.3.2. Thermal analysis

DSC was employed to evaluate the solid state of the pure components as well as the extruded cocrystals. Analysis of the thermal transition of bulk CBZ indicated the existence of polymorphic form III as the melting peak appeared at 175.14°C ( $\Delta H = 15.40$  J/g) followed by a subsequent phase transformation leading to the melt at 192.39°C ( $\Delta H = 99.93$  J/g) (**Fig. 3.2**) [35]. The thermogram of bulk TCA showed an endothermic thermal transition due to its melting at 134.55°C ( $\Delta H = 145.47$  J/g) (**Fig. 3.2**).

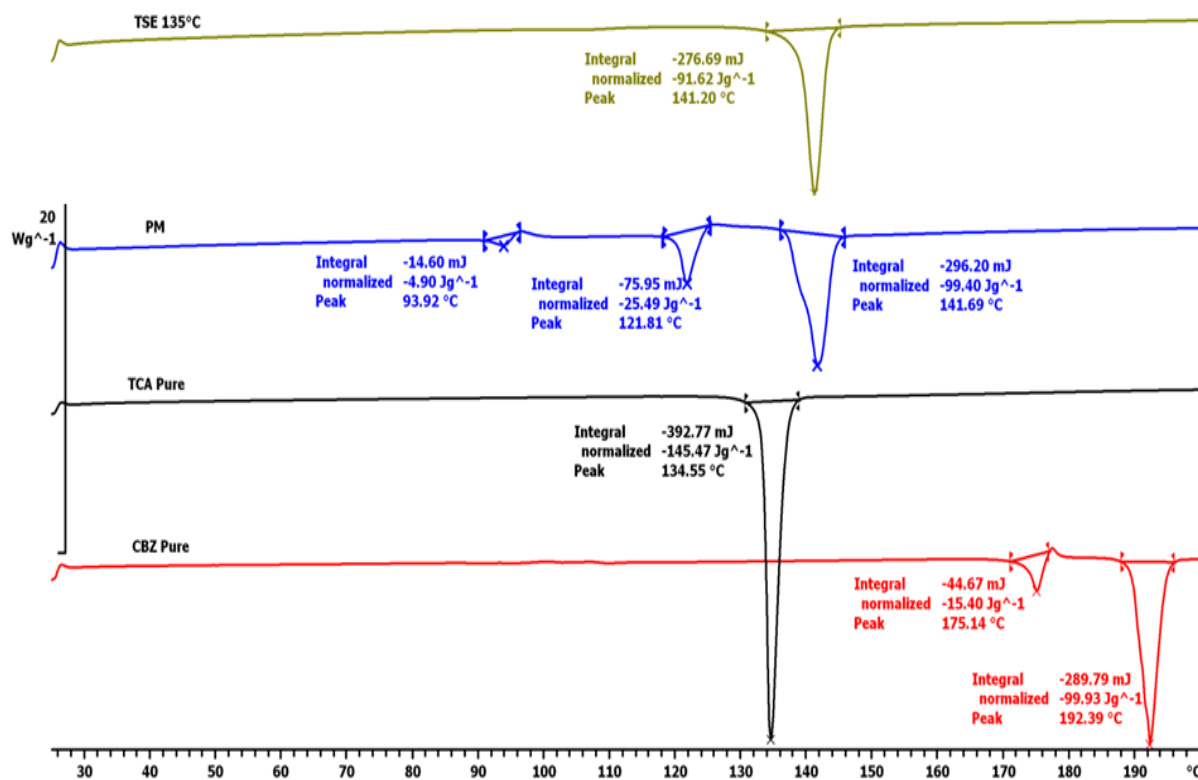


**Fig. 3.2.** DSC thermograms of bulk CBZ, bulk TCA, cocrystals processed at TSE135°C and the physical mixture.

The physical blend of CBZ-TCA at a 1:1 molar ratio showed one minor endotherm at 93.92°C ( $\Delta H = 4.90$  J/g) and two other main endotherms at 121.81°C ( $\Delta H = 25.49$  J/g) and 141.69°C ( $\Delta H = 99.40$  J/g), respectively (**Fig. 3.2**). The first transition at 121.81°C corresponds to the shifted peak of TCA while the second endothermic peak represents the eutectic of the cocrystal made from the melting of CBZ in TCA [11].

A single, sharp endothermic peak was observed in the thermogram (**Fig. 3.2**) of the extruded cocrystals processed with TSE which is quite similar to that of the prototype cocrystals. The thermogram of the CBZ-TCA cocrystals processed via TSE showed a sharp melting transition at 141.20°C ( $\Delta H = 92.62$  J/g) while the transition for the prototype occurred at 143.08°C ( $\Delta H = 114.46$  J/g). The TSE cocrystals were of high purity (>99%) and very similar to the prototype.

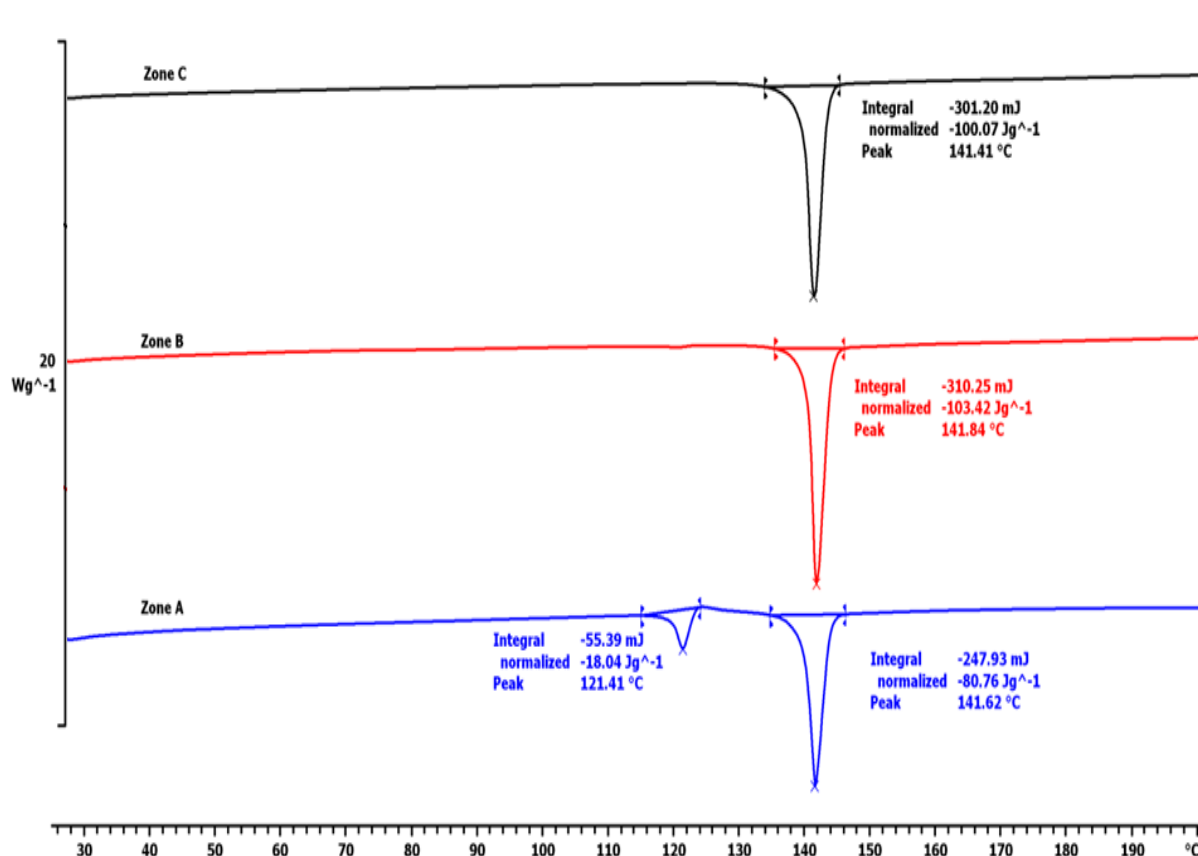


**Fig. 3.3.** DSC thermograms of samples collected from different zones in the TSE.

Furthermore, the data in **Fig. 3.3** shows the DSC thermograms of the materials collected in three different mixing zones during TSE processing. By comparing the thermograms of the sample collected from zone A and the PM it can be seen that they are almost identical (except the peak at 93.92°C) suggesting no major crystal transformation of the processed blends.

In contrast, the thermal transitions of the processed materials collected from zone B presented a sharp melting peak at 141.84°C which corresponds to the final melting point of the stable cocrystals but with some evidence of unreacted material at 121.41°C which corresponds to the unreacted TCA. The complete formation of CBZ-TCA cocrystals occurred in zone C where the absence of the small endothermic peak is evident.

### 3.3.3. XRPD analysis

X-ray diffractograms of physical blends, pure components, and processed cocrystals at different extrusion zones are illustrated in **Fig. 3.4**.

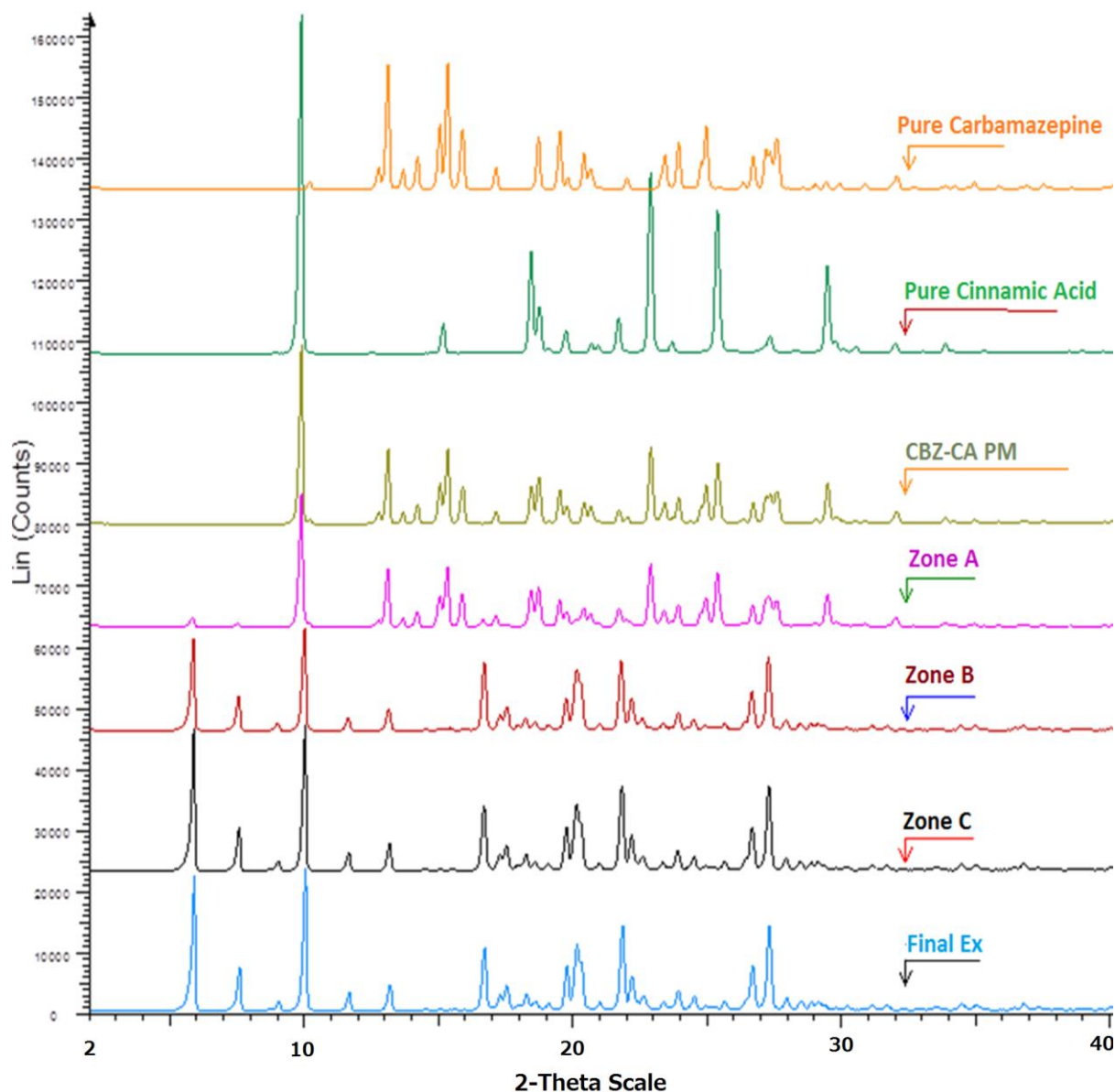


**Fig. 3.4.** X-ray diffractograms of CBZ (bulk), TCA (bulk), CBZ-TCA physical mixture, samples from TSE barrel zones (A, B and C) and final extrudates.

It can be clearly observed that the development of cocrystals begins in the 2<sup>nd</sup> mixing zone of the HME barrel with the appearance of new intensity peaks at 5.78° and 7.57°  $2\theta$  values (**Fig. 3.4**). Both peaks with low intensity were also observed in the 1<sup>st</sup> mixing zone together with other characteristic peaks of bulk CBZ and TCA. It is clear that the interactions between the

drug and co-former started in the 1<sup>st</sup> mixing zone while in the 2<sup>nd</sup> mixing zone, the peaks at 15.30°, 15.87°, 24.94°  $2\theta$  disappeared. Finally, the cocrystals were successfully formed at the 3<sup>rd</sup> mixing zone with the appearance of diffraction peaks at 5.83°, 7.57°, 9.91°, 16.66°, 21.82°, and 27.33°  $2\theta$  values which are identical to those of the prototype. Apparently, the screw configuration in mixing zone B plays a crucial role in the initiation of the cocrystallization process as well as temperature and residence time, whilst the placing the mixing elements at angles of 60 and 90° in zone C resulted in cocrystals with improved crystallinity.

### 3.3.4. In-line NIR monitoring

Off-line NIR spectra of CBZ, TCA and the physical mixture (PM) were measured to identify the characteristic bands attributed to the cocrystals. The NIR spectra of CBZ and TCA present characteristic vibrational bands at different wavenumbers (**Fig. 3.5**). The spectrum of the PM is represented by the combined spectra of the bulk materials.

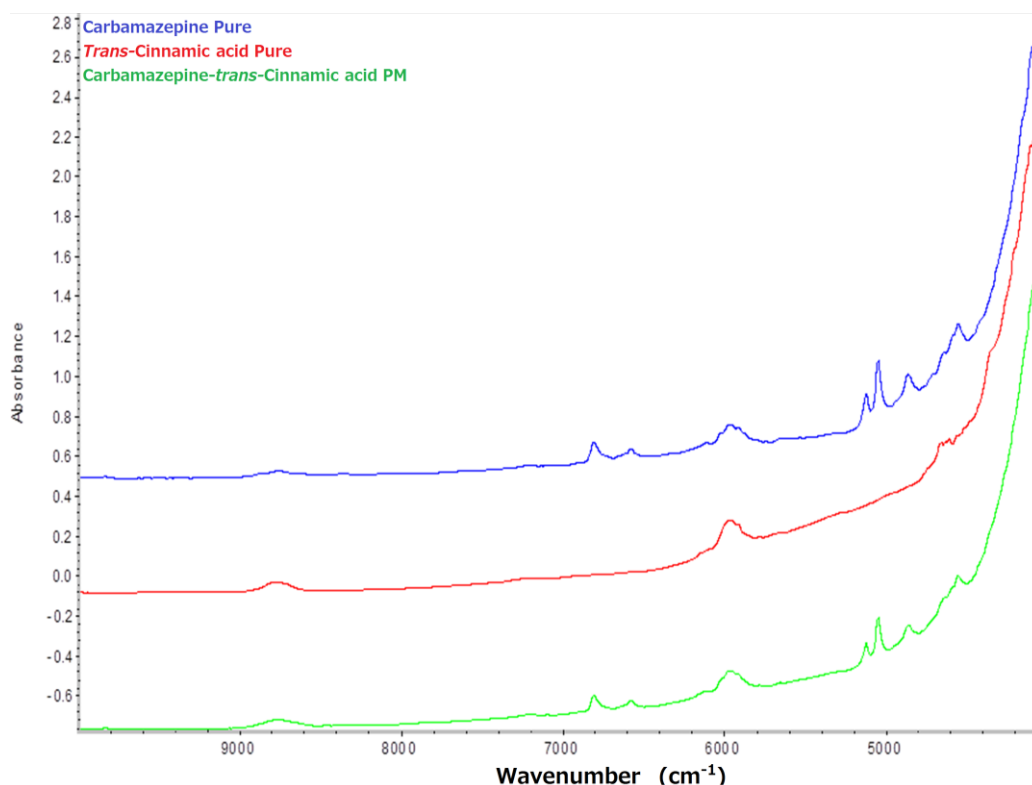


**Fig. 3.5.** NIR spectra of bulk CBZ, bulk TCA, and a physical mixture of CBZ and TCA.

The second derivative NIR spectra of the PM, CBZ and the co-former in the 4600-5300 cm<sup>-1</sup> region are shown in **Fig. 3.6**. The spectrum of TCA displays few bands at 4700-4600 cm<sup>-1</sup> whereas those of CBZ and the PM are identical as the spectra can be overlapped and only the band intensities are different.

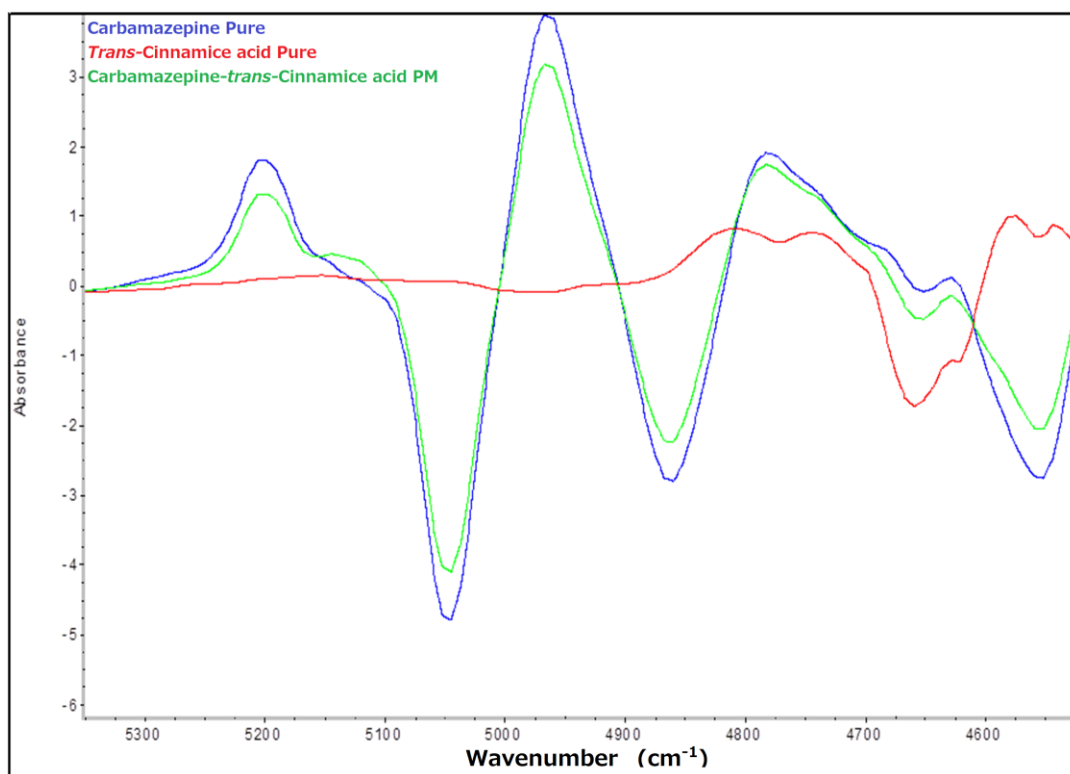


**Fig. 3.6.** Second derivative NIR spectra of CBZ (bulk), TCA, and a physical mixture of CBZ and TCA in the 4600-5300  $\text{cm}^{-1}$  wavenumber region.

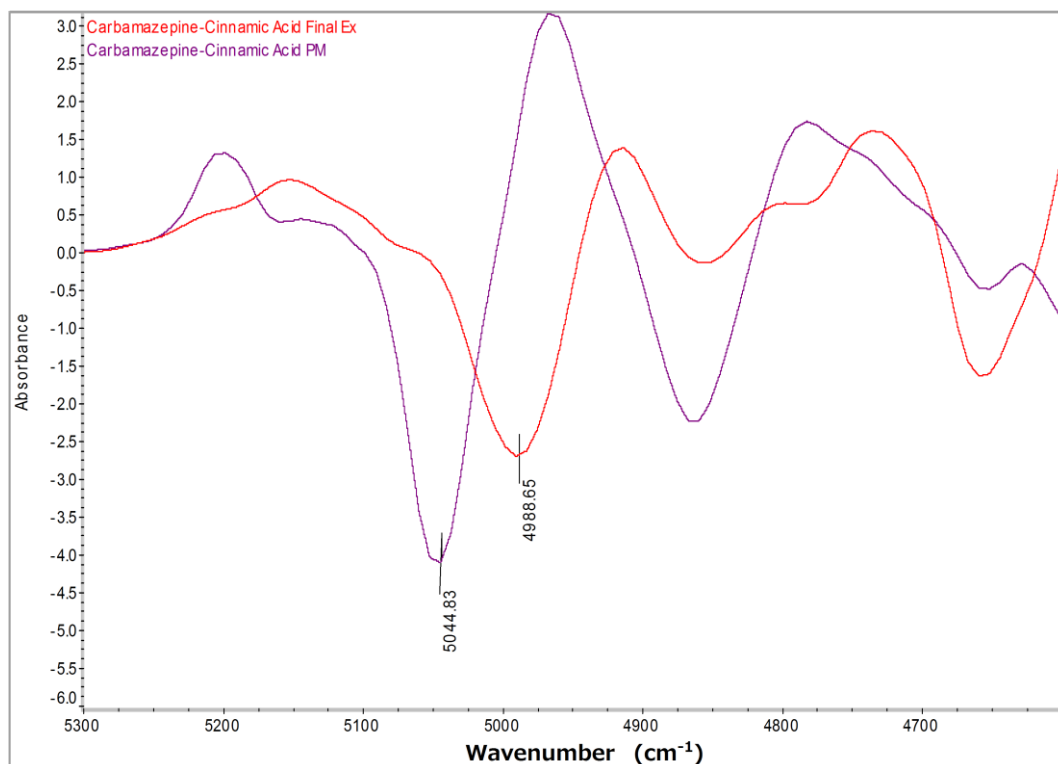


**Fig. 3.7.** Second derivative spectra of the PM and the extruded cocrystals in the wavenumber regions between 4600 and 5300  $\text{cm}^{-1}$ .

**Fig. 3.7** depicts the second derivative spectra of the PM and the extruded cocrystals that show significant differences due to vibrational band shifts. The band at  $5044\text{ cm}^{-1}$  is due to N-H stretching. This was found to shift to  $4988\text{ cm}^{-1}$  as the H-bond formed between CBZ and TCA. The new band became more intense as cocrystallization proceeded. The band shift at lower wavenumbers can be attributed to the formation of hydrogen bonds as a result of the formation of cocrystals between CBZ and TCA.

As the CBZ-TCA blends are transferred within the conveying and mixing zones, the formation of cocrystals is expected to gradually take place along the barrel. In order to further study cocrystal formation, the NIR probe was carefully placed in the three mixing zones and the in-line scans were collected [33]. **Fig. 3.8** shows the second derivative spectra of the three different mixing zones, the final extruded cocrystals in comparison to the PM. Formation of CBZ-TCA cocrystals starts in the second mixing zone and a band appears at  $4988\text{ cm}^{-1}$ . The spectra obtained for zones B and C show an increase in the intensity of the new band as the extrudate moves towards the end of the extruder. The off-line scan of the final extruded CBZ-TCA cocrystals showed the highest intensity bands suggesting the completion of the process.

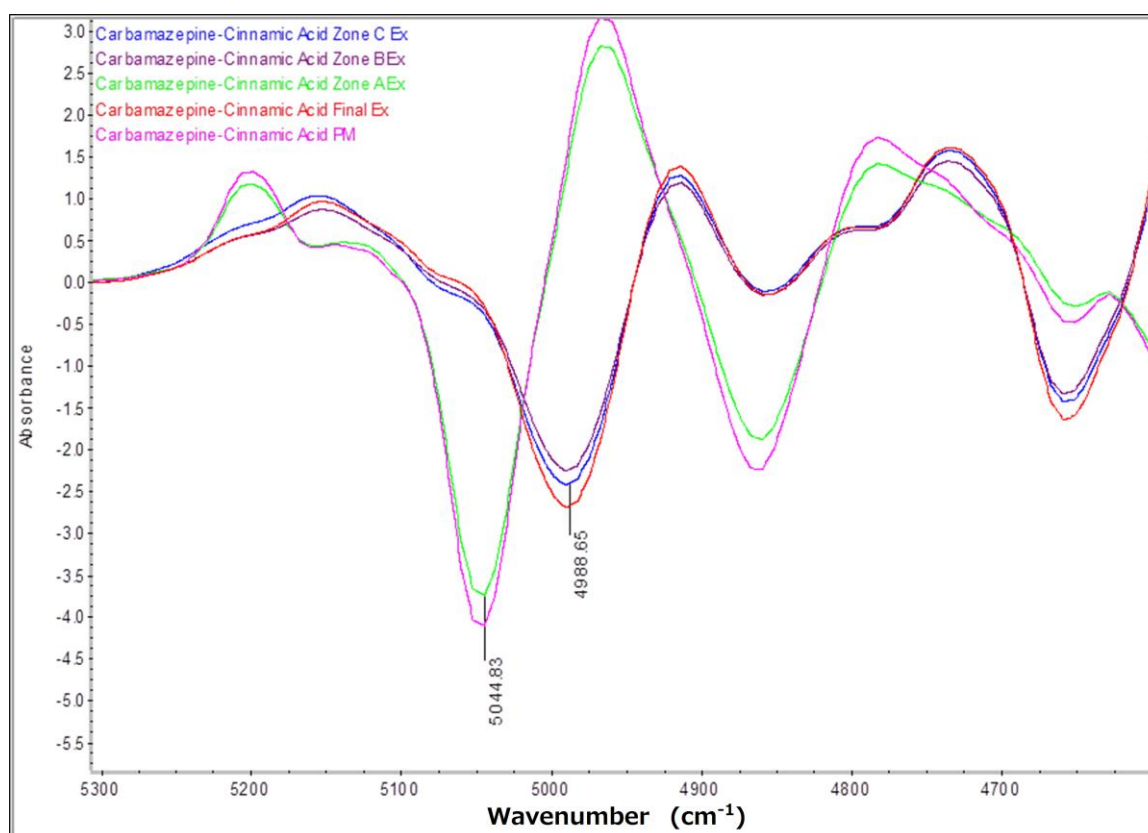


**Fig. 3.8.** Second derivative in-line NIR spectra in the mixing zones (A, B, C), the TSE extruded cocrystals and the PM.

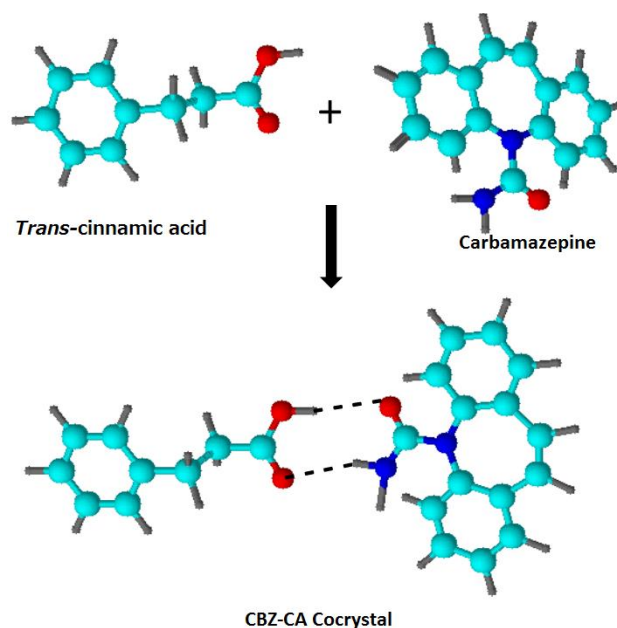


**Fig. 3.9.** 3D-molecular modelling of the developed CBZ-TCA cocrystals illustrating the hydrogen-bonding between the functional groups.

These findings suggest that cocrystals were formed gradually due to the increasing mixing capacity across the three mixing zones. A schematic representation of the H-bonding between the CBZ and TCA molecules is depicted in **Fig. 3.9**.

### 3.3.5. *In-vitro* dissolution studies

*In-vitro* dissolution studies were conducted to assess the performance of the cocrystals produced compared to the bulk CBZ. As shown in the data in **Fig. 3.10** a slow dissolution rate of 49% after 2 hr was observed for bulk CBZ. In contrast, the TSE 135°C cocrystals presented the higher rates with 50% CBZ dissolution within the first 10 min and 70% after 1 hr. Eventually, 90% CBZ release was observed after 120 min, compared to 81% of the prototype. As a result the faster dissolution rates are related to the higher purity of the developed cocrystals.

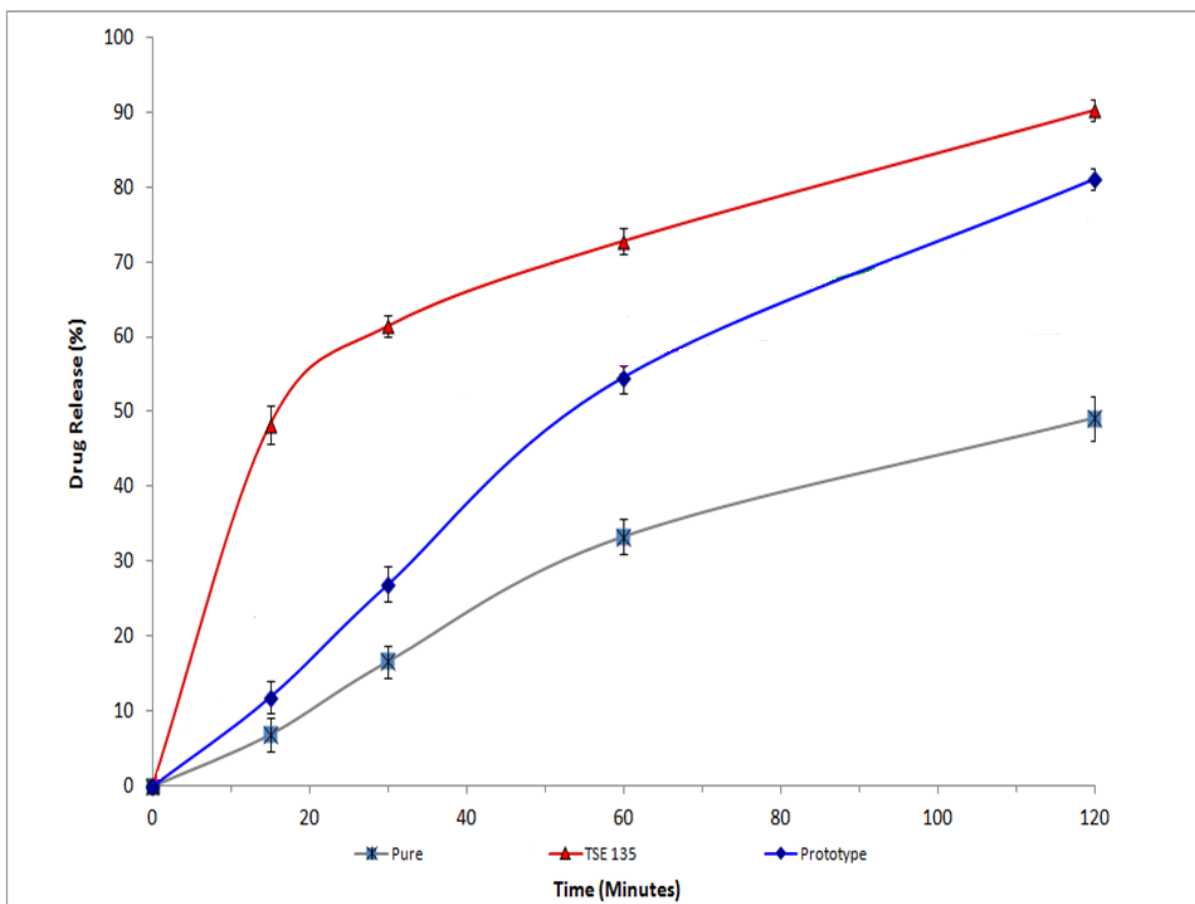


**Fig. 3.10.** Dissolution profiles of bulk CBZ, prototype and extruded cocrystals (pH 1.2, n=3).

## Case study B: In-line NIR monitoring as a PAT tool in carbamazepine-saccharine cocrystal formation using HME processing

### 3.3.6. HME processing

In this study, HME a continuous manufacturing process was explored for the development of cocrystals by co-processing CBZ/SCH blends at a 1:1 molar ratio. The cocrystals were optimized by using twin screw (TSE) extrusion in parallel as processing parameters play a key role in the quality of the obtained materials. As previously reported, the screw type, configuration and temperature profile were the critical processing parameters (CPP) [27]. In these TSE studies the die was removed from the extruder as the extrudates were not produced in the form of strands or melted material but rather as granular powders. CBZ was decomposed when extrusion temperatures above 145°C were used.

### 3.3.7. Thermal analysis

The thermo physical properties of the bulk powders (CBZ and SCH) and the extruded materials were analyzed using DSC (Fig. 3.11). Analysis of thermal transition of bulk CBZ indicated the existence of polymorphic form III as the melting peak appeared at 175.08°C ( $\Delta H = 17.58 \text{ J/g}$ ) followed by a subsequent phase transformation leading to the melt at 191.35°C ( $\Delta H = 96.47 \text{ J/g}$ ). The bulk SCH thermogram showed a sharp melting peak at 225.18°C ( $\Delta H = 131.16 \text{ J/g}$ ). The physical mixture of CBZ-SCH at 1:1 molar ratio showed a shift of the CBZ endothermic peaks at 153.24°C and 173.48°C was observed, respectively while the SCH endotherm was not observed. According to Enxian *et al.*, (2008) the melting endotherm at 153.24°C is attributed to the eutectic melt followed by cocrystal melting at 173.48°C [36] which is close to the melting endotherm of the produced cocrystals. A single and sharp endothermic peak was observed at 174.29°C in the thermogram (Fig. 3.11) of the extruded cocrystals processed with TSE which is quite similar to the prototype cocrystals (Fig. 3.12).

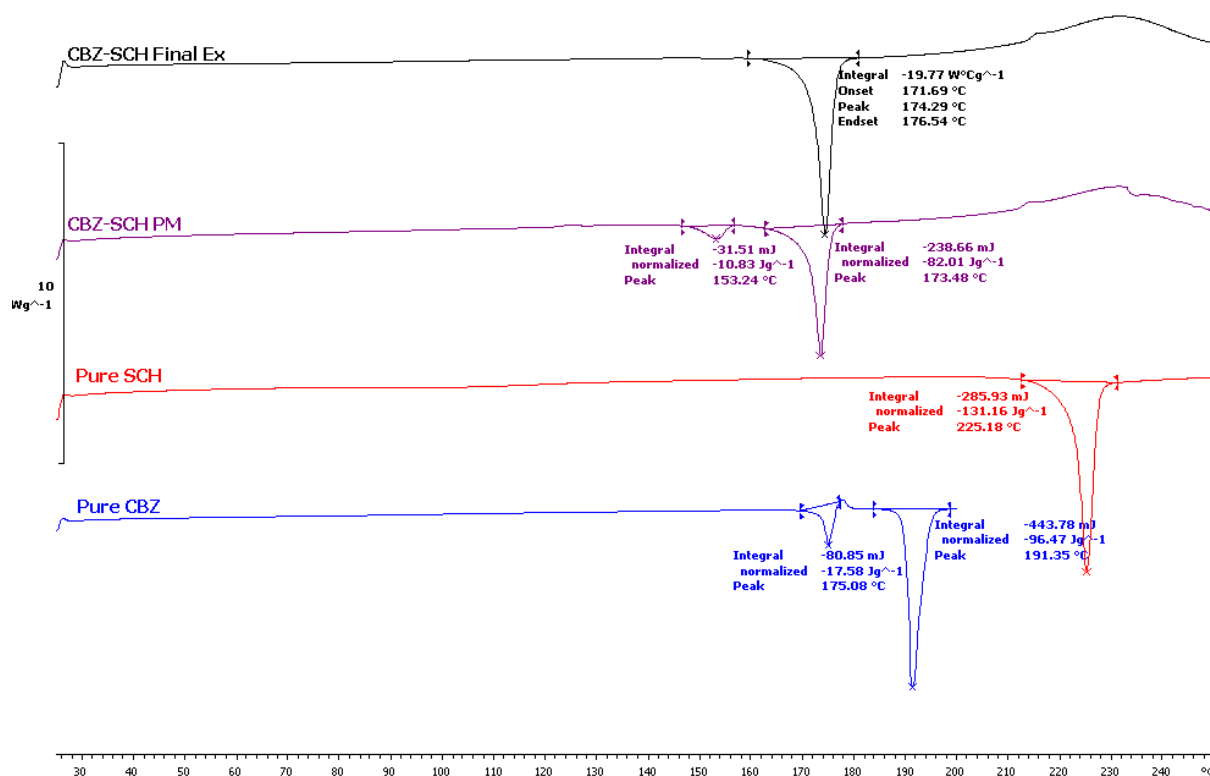


**Fig. 3.11.** DSC thermograms of bulk CBZ, bulk SCH, cocrystals processed by TSE and the PM.

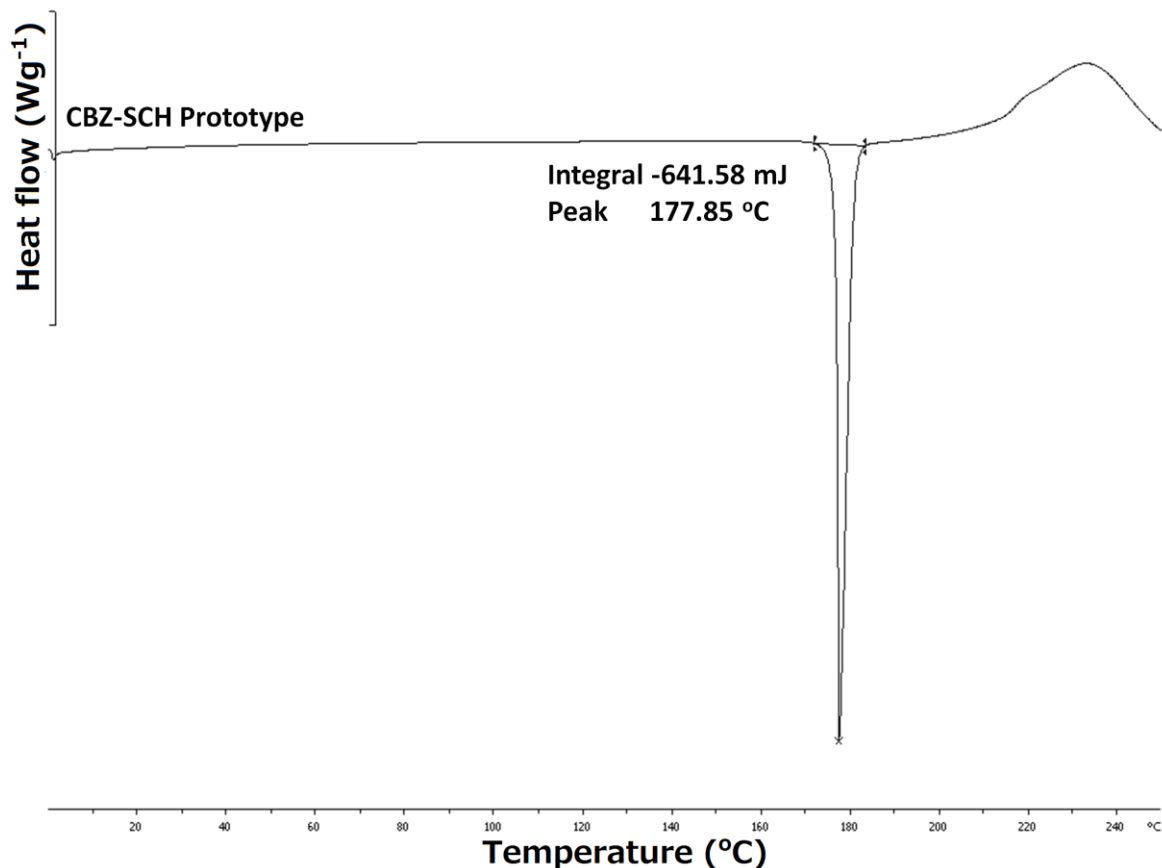


**Fig. 3.12.** DSC thermogram of CBZ-SCH prototype.

Furthermore, the data in **Fig. 3.13** shows the DSC thermograms of the materials collected from three different mixing zones during TSE processing. By comparing the thermograms of the samples collected from zone A and the PM it can be seen that they are almost identical suggesting no major crystal transformation of the processed blends. It can be observed that crystal transformation started at zone B by reducing the peak intensity at 154.22 $^{\circ}\text{C}$ .

In contrast, the thermal transitions of the processed materials collected from zone C presented a sharp melting peak at 174.04 $^{\circ}\text{C}$  which corresponds to the final melting point of the stable cocrystals but with no unreacted material. The complete formation of CBZ-SCH cocrystals occurred in zone C where the absence of the small endothermic peak is evident.

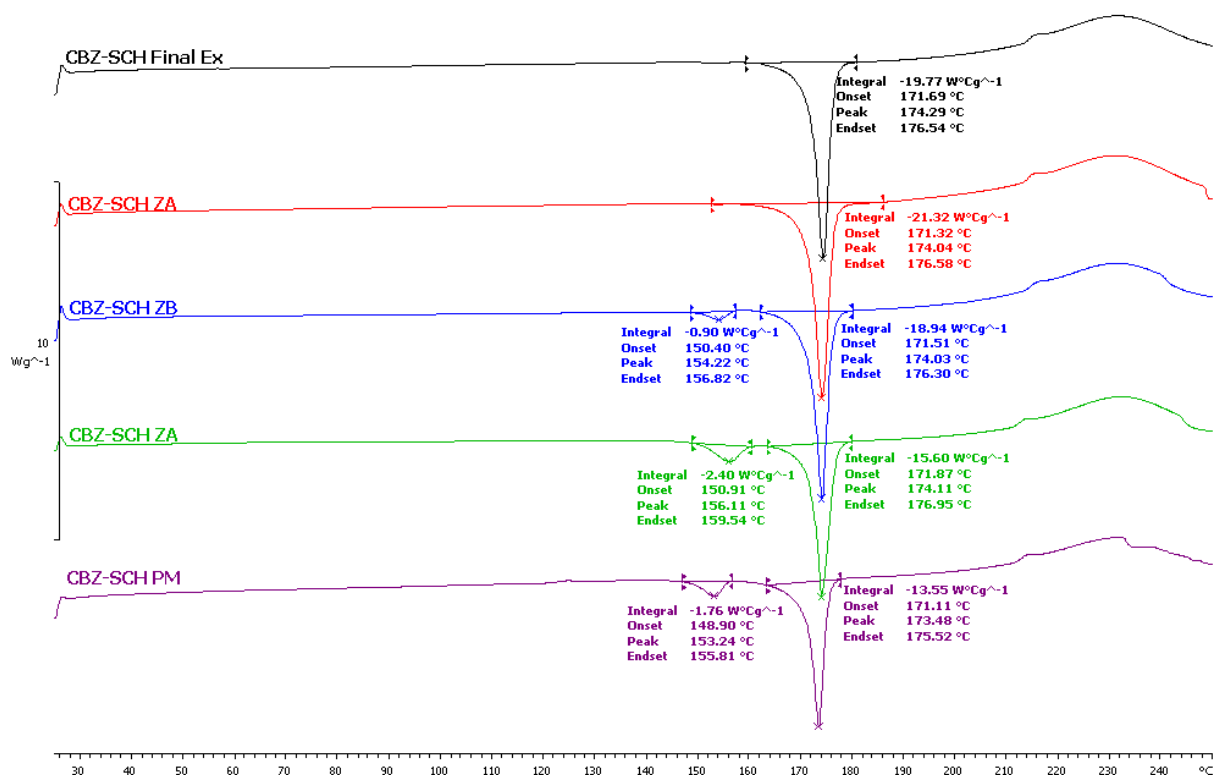


**Fig. 3.13.** DSC thermograms of samples were collected from different zones in the TSE, final extrudates and the PMs.

### 3.3.8. XRPD analysis

Samples were further analysed by XRPD to identify the diffraction patterns of the cocrystals produced by HME and chemical processing. As shown in **Fig. 3.15** the intense peaks of CBZ form III appear at  $13.07^\circ$ ,  $15.31^\circ$ ,  $19.49^\circ$ ,  $24.96^\circ$  and  $27.24^\circ$   $2\theta$  [37-38] while those of bulk SCH occur at  $9.56^\circ$ ,  $16.02^\circ$ ,  $19.13^\circ$ ,  $25.14^\circ$   $2\theta$  values, respectively.

In contrast, the diffraction peaks of the CBZ-SCH prototype (**Fig. 3.14**) appear at  $7.03^\circ$ ,  $13.67^\circ$ ,  $14.02^\circ$ ,  $14.95^\circ$ ,  $20.14^\circ$ ,  $21.45^\circ$ ,  $21.74^\circ$ ,  $23.43^\circ$ ,  $25.79^\circ$  and  $28.29^\circ$   $2\theta$  values and it is to be noted that they are completely different than those of the individual bulk substances.

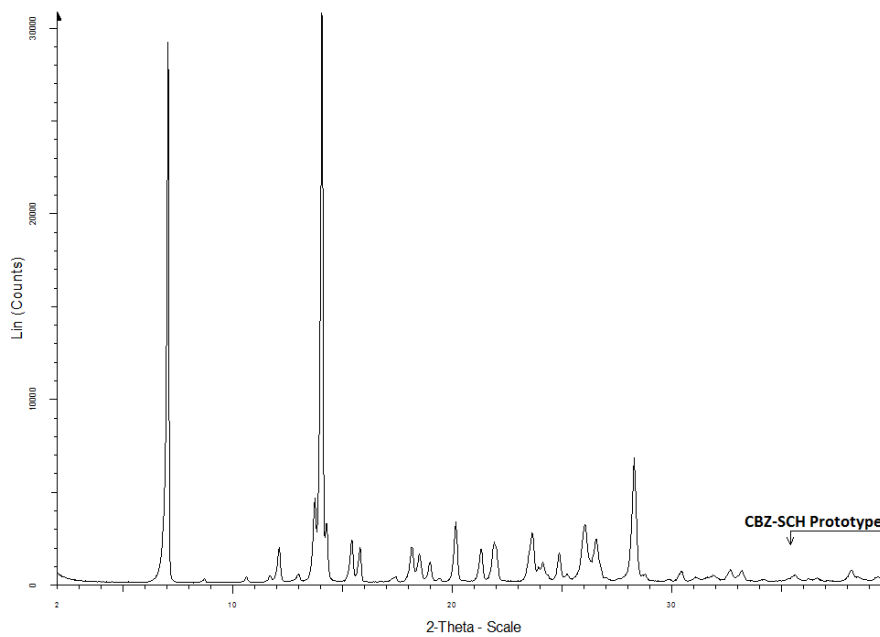


**Fig. 3.14.** X-ray diffractogram of CBZ-SCH prototype.

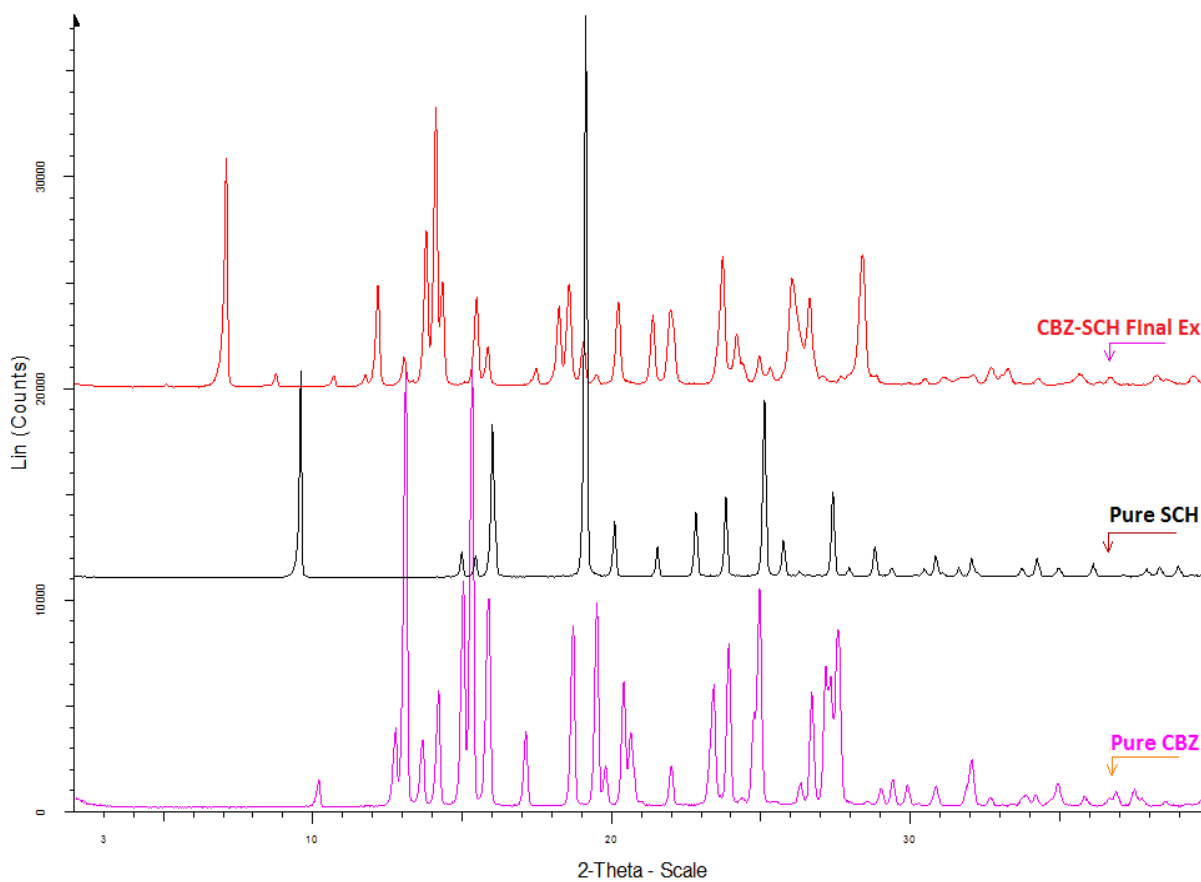


**Fig. 3.15.** X-ray diffractograms of CBZ (bulk), SCH (bulk), and CBZ-SCH cocrystal extrudates.

It can be clearly observed that the development of cocrystals began in the 2<sup>nd</sup> mixing zone of the HME barrel with the appearance of new intensity peaks at 7.03°, 18.24° and 28.29° 2θ values (**Fig. 3.16**). Both peaks with low intensity were also observed in the 1<sup>st</sup> mixing zone together with other characteristic peaks of bulk CBZ and TCA. It is clear that the interactions between the drug and co-former started in the mixing zone A while in the zone B, the peaks at 10.2° and 20.65°, disappeared. Finally, the cocrystals were successfully formed in the 3<sup>rd</sup> mixing zone (zone C) with the appearance of diffraction peaks at 7.03°, 18.24° and 28.29° 2θ values which are identical to those of the prototype and the disappearance of some characteristic peaks (9.53°, 9.10°, 17.11°, 20.65°, 22.78° and 27.35° 2θ values) of bulk compounds. Apparently, the screw configuration in zone B played a crucial role in the initiation of the cocrystallization process, while the placement of the mixing elements at 60 and 90° angles in zone C resulted in cocrystals with improved crystallinity.

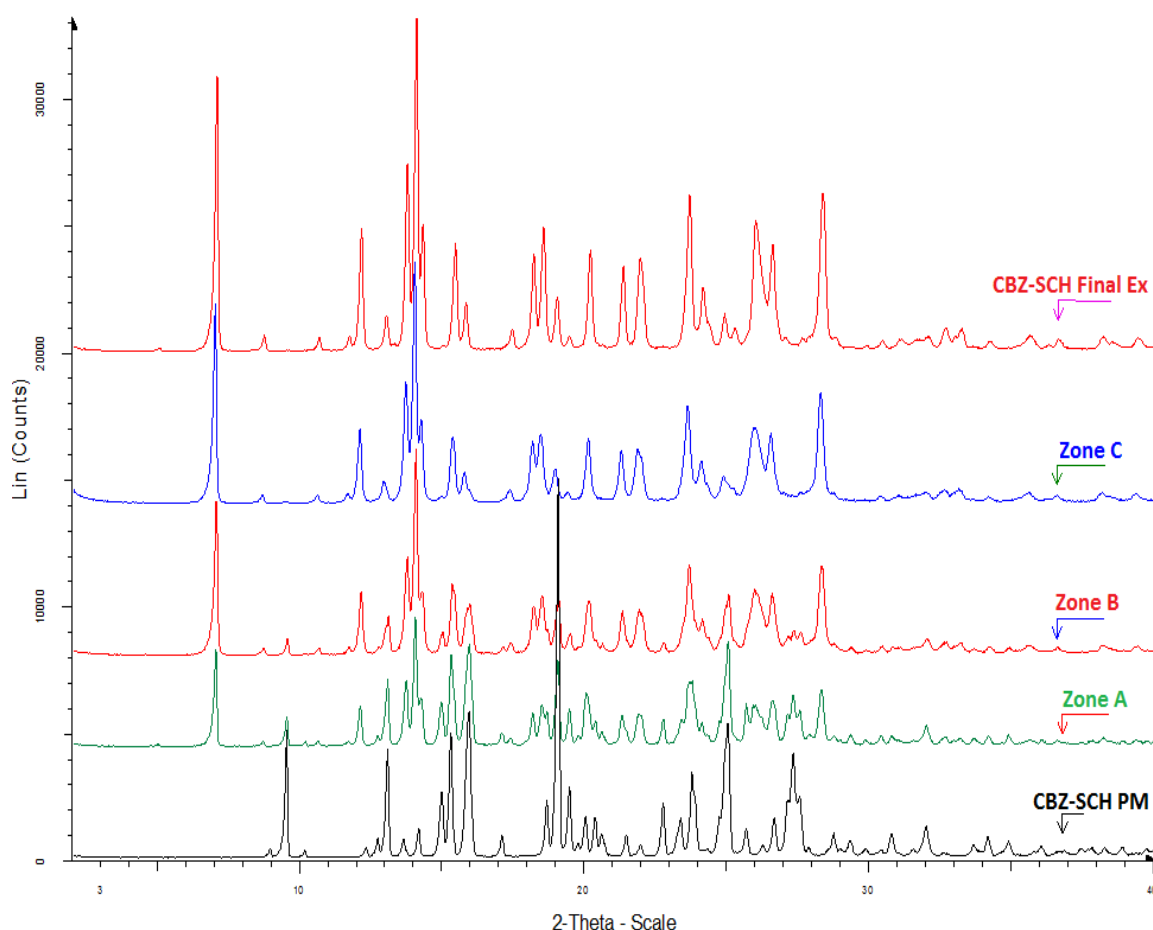


**Fig. 3.16.** X-ray diffractograms of the CBZ-SCH physical mixture, samples from the TSE barrel zones (A, B and C) and final extrudates.

### 3.3.9. In-line NIR monitoring

Off-line NIR spectra of CBZ, SCH and the physical mixture (PM) were measured to identify the characteristic bands attributed to the cocrystal. The NIR spectra of CBZ and SCH present characteristic bands at different wavenumbers regions between 7000-4500  $\text{cm}^{-1}$  (Fig. 3.17). The spectrum of the PM is represented by the combined spectra of the bulk materials.

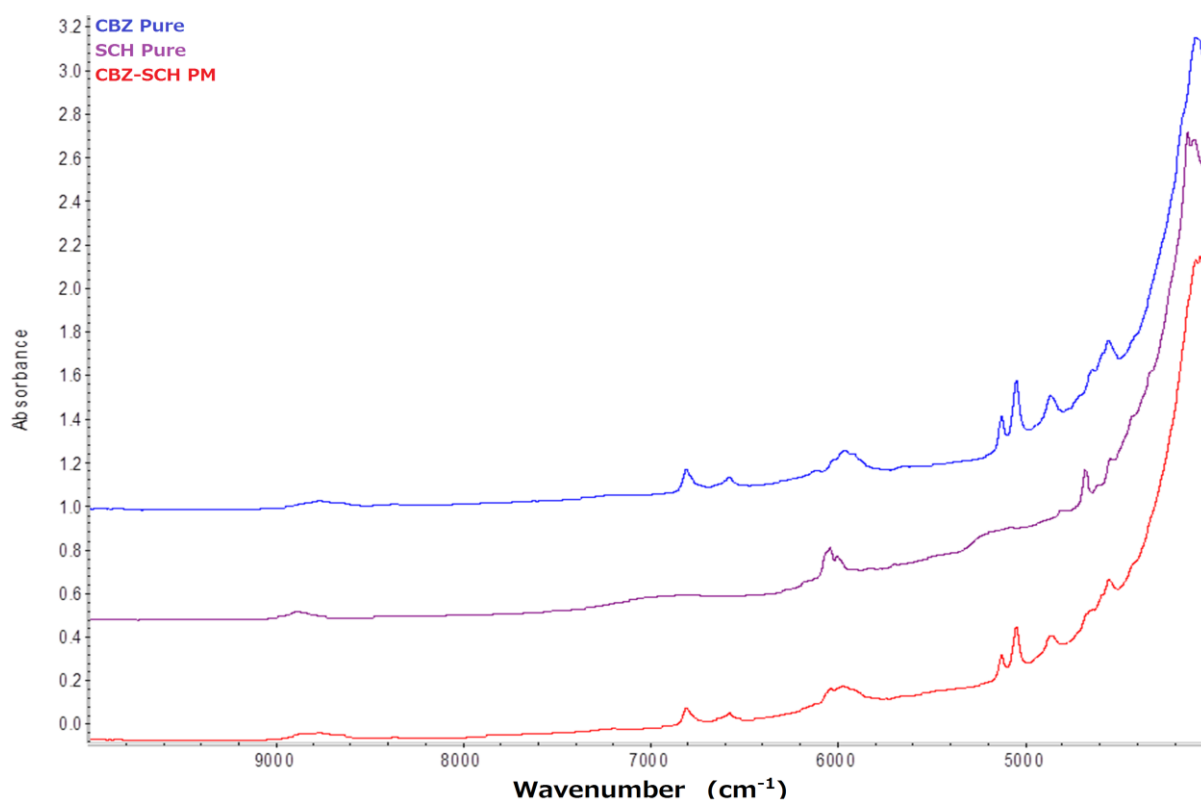


**Fig. 3.17.** NIR spectra of CBZ (bulk), SCH, and CBZ/SCH PM.

The second derivative NIR spectra of the PM, CBZ and the TCA coformer in the 6400-7100  $\text{cm}^{-1}$  region are shown in Fig. 3.18. The NIR spectrum of SCH is almost flat, no absorption band was observed whereas those of pure CBZ and the PM spectra are identical and overlapped but the band intensities are different.

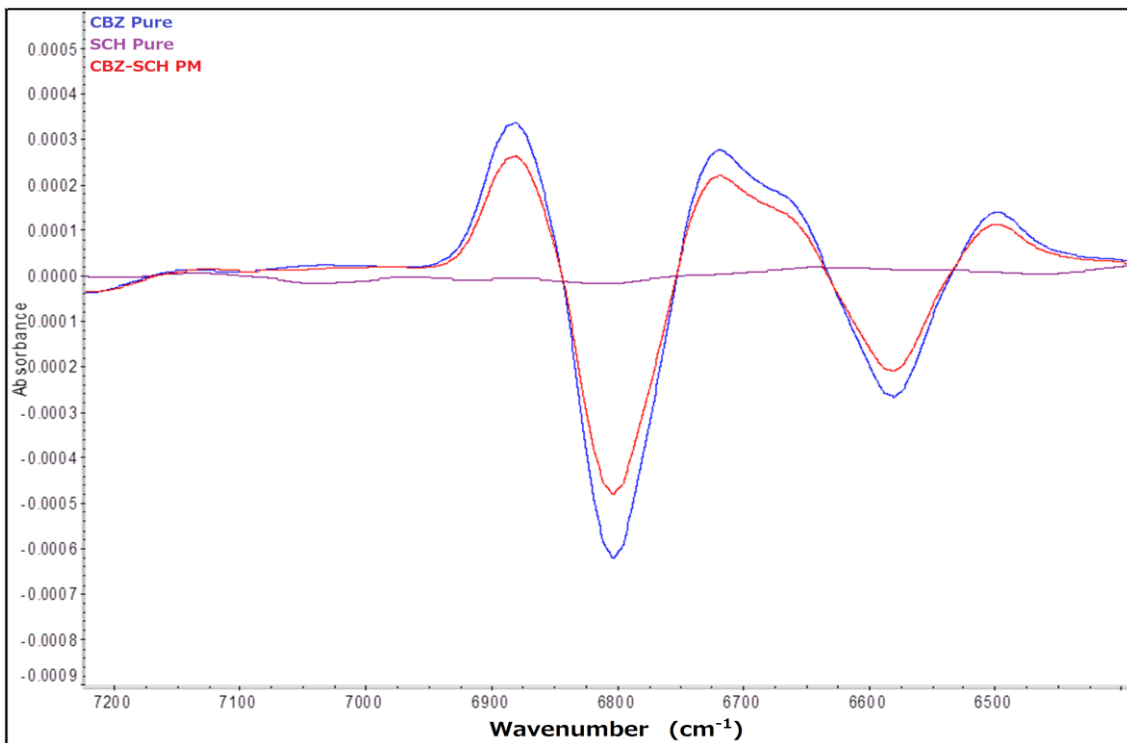


**Fig. 3.18.** Second derivatives NIR spectra of CBZ (bulk), SCH, and CBZ/SCH PM in the 6400-7100  $\text{cm}^{-1}$  wavenumber region.

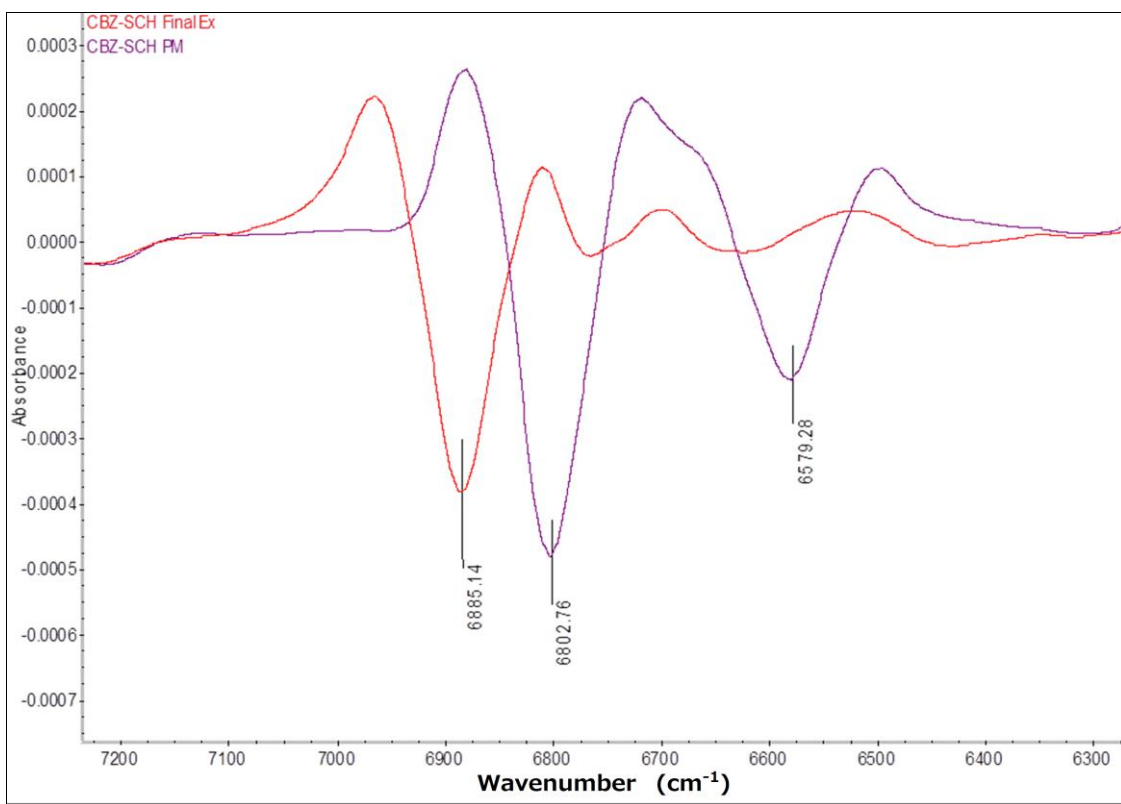


**Fig. 3.19.** Second derivative spectra of CBZ/SCH (PM) and the extruded cocrystals in the 6400-7100  $\text{cm}^{-1}$  wavenumber region.

**Fig. 3.19** shows the second derivative spectra of the PM and the extruded cococrystals that show significant differences due to the band shifts. The band observed at  $6579\text{ cm}^{-1}$  could be due to the N-H stretching first overtone of CBZ which has an intramolecular H-bond between the C=O and N-H of CBZ. This band reduced in intensity as the intermolecular H-bond formation occurred during extrusion and cococrystallization increased. Another band at  $6802\text{ cm}^{-1}$  was due to the N-H stretching first overtone. This was found to shift to  $6885\text{ cm}^{-1}$  as the H-bonds formed between CBZ and SCH. The new band became more intense as cococrystallization increased. The band shift to lower wavenumbers could be attributed to the formation of hydrogen bonding as a result of the formation of cococrystals between CBZ and SCH [34]. As the CBZ-SCH blends are transferred within the conveying and mixing zones of the HME barrel, the formation of cococrystals is expected to gradually take place along the barrel. In order to further study cococrystal formation, the NIR probe was carefully placed in the three mixing zones and the in-line scans were collected [33].

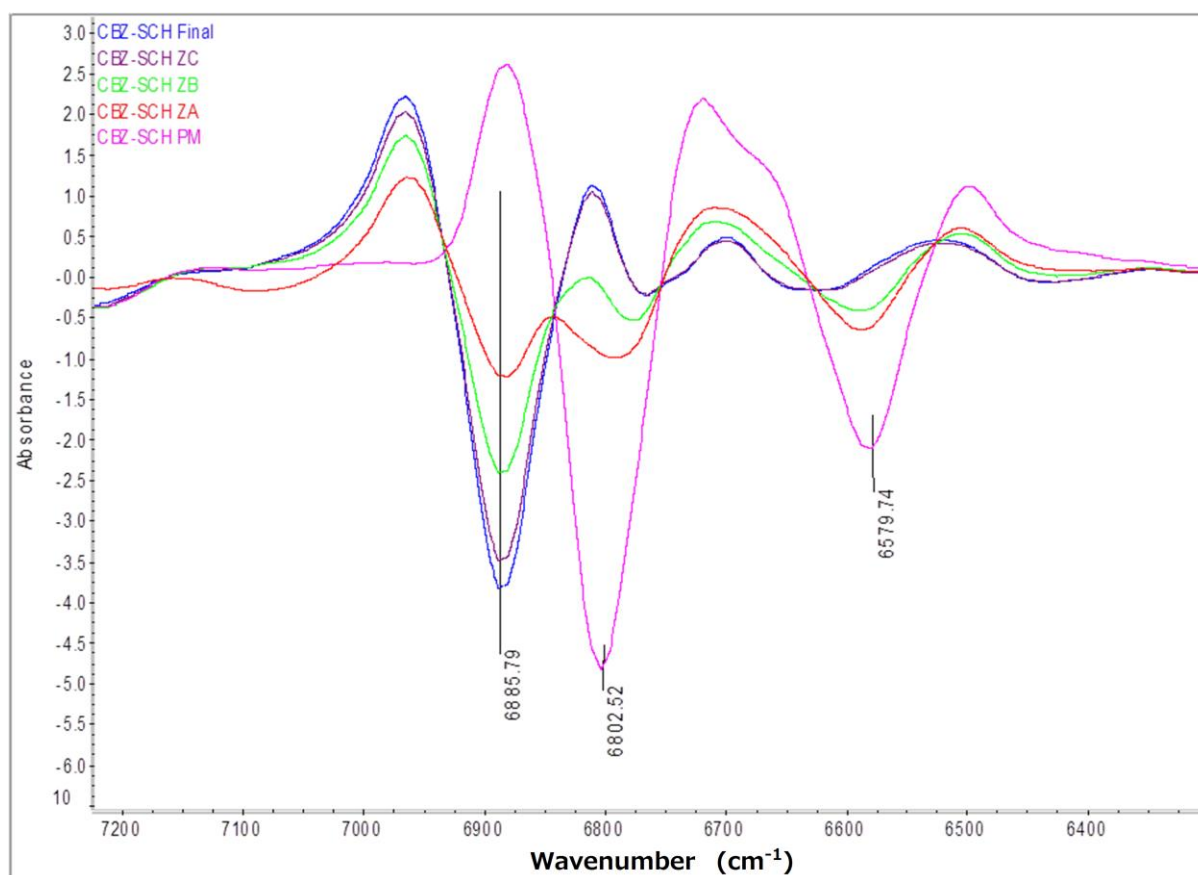


**Fig. 3.20.** Second derivative of in-line NIR spectra in the mixing zones (A, B, C), the TSE extrudates and the PM.

The data in **Fig. 3.20** shows the second derivative spectra of the three different mixing zones, the final extruded co-crystals compared to the PM. It is obvious that the formation of CBZ-SCH cocrystals starts in the first mixing zone and a band appears at  $6885\text{ cm}^{-1}$ . The spectra obtained for zones B and C shows an increase in the new band as the extrudate moves towards the end of the extruder. The off-line scan of the final extruded CBZ-SCH cocrystals present the highest intensity suggesting the completion of the process. These findings suggest that cocrystals were formed gradually due to the increasing mixing capacity across the three mixing zones.

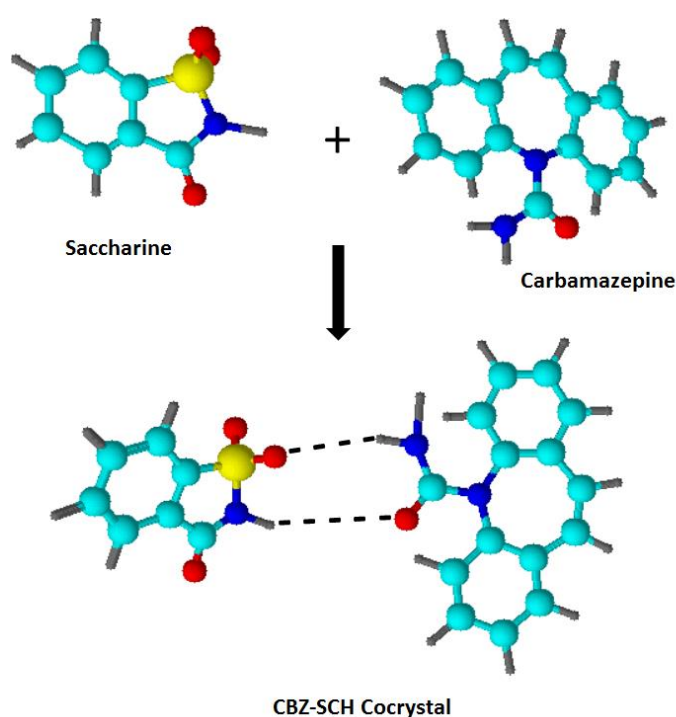


**Fig. 3.21.** Molecular modelling of the developed CBZ-SCH form I cocrystals depicting the hydrogen-bonding between the functional groups.

A schematic representation of the H-bonding between the CBZ and SCH molecules is depicted in **Fig. 3.21**. The X-ray diffractograms are in agreement with the Porter *et al.*, (2008) findings where the characteristic intensity peak at  $6.9^\circ 2\theta$  is related to the CBZ-SCH form I cocrystals [34]. In this instance the SCH N-H forms a H-bond with the CBZ carboxyl group while the CBZ amine group forms a H-bond with the S=O of SCH [35].

### 3.3.10. *In-vitro* dissolution studies

The *in-vitro* dissolution rate of the produced cocrystals was one of the main criteria to assess their performance. For this reason the dissolution patterns of all extrudates were compared to those of the bulk CBZ and the prototype.

As expected, the bulk CBZ showed a slow dissolution rate with approximately 60% of the drug being dissolved after 2 hr (Fig. 3.22). The CBZ dissolution rate in the PM also showed a low dissolution profile similar to the bulk substance without any significant difference suggesting that SCH does not affect the drug dissolution rates. As shown in Fig. 3.23, the TSE processed cocrystals gave increased dissolution rates compared to the prototype. As a result, faster dissolution rate has been observed for the extrudate cocrystals.

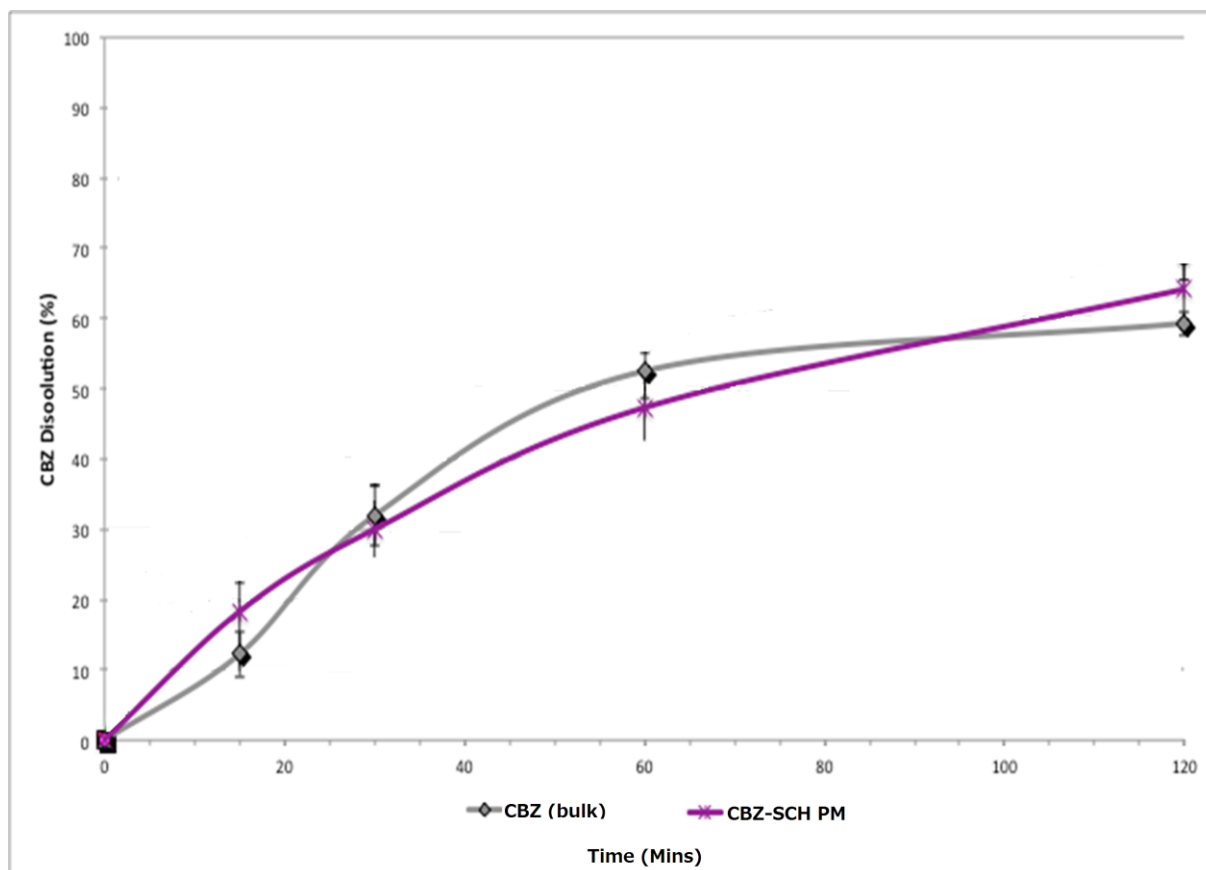
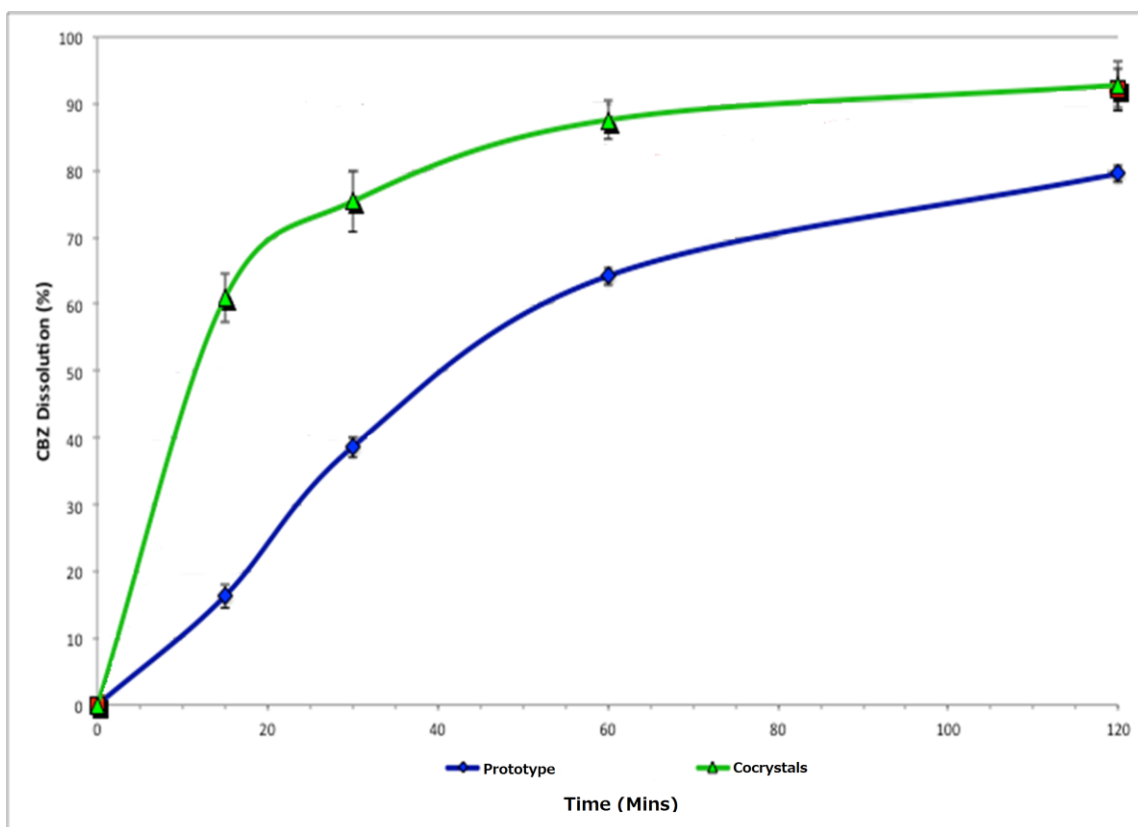


Fig. 3.22. Dissolution profiles of bulk CBZ and CBZ/SCH PM.



**Fig. 3.23.** Dissolution profiles of CBZ/SCH prototype and CBZ/SCH cocryystals processed via TSE.

### 3.4. Conclusions

Twin screw extrusion was used to produce cocryystals of CBZ-TCA and CBZ-SCH as a continuous manufacturing process. The cocrySTALLIZATION process were monitored using NIR probe inserted on to HME barrel during process and off-line NIR spectra were collected from bulk materials, physical mixtures and extruded cocryystals. It has been found that cocrySTALLIZATION occurred by the formation of H-bonds between drug and conformer, and this resulted in the formation of new vibrational band in the NIR spectra obtained from the cocryystals compared with physical mixtures. In-line NIR spectra collected from three different mixing zones confirmed that cocryystal formation starts to form at 2<sup>nd</sup> mixing zone of the HME barrel (zone B) and completely formed at the 3<sup>rd</sup> Mixing zone of the HME (zone C), The findings of the cocryystal formation via in-line NIR spectroscopy wre confirmed via XRPD and thermal analysis (DSC). Dissolution studies of the produced cocryystals showed improved drug release profiles compared with the prototype cocryystals produced by solvent evaporation method.

### 3.5. References

1. Bond AD, What is a co-crystal? *CrystEngComm*, 2007; **9**: 833-834
2. Desiraju GR, Crystal and co-crystal, *CrystEngComm*, 2003; **5**: 466-467.
3. Hickey MB, Peterson ML, Scoppettuolo LA, Morrisette SL, Vetter A, Guzmán H, Remenar JF, Zhang Z, Tawa MD, Haley S, Zaworotko MJ, Almarsson Ö, Performance comparison of a co-crystal of carbamazepine with marketed product, *European Journal of Pharmaceutics and Biopharmaceutics*, 2007; **67**(1): 112-119
4. McNamara D, Childs S, Giordano J, Iarriccio A, Cassidy J, Shet M, Mannion R, O'Donnell E, Park A, Use of a glutaric acid co-crystal to improve oral bioavailability of a low solubility API, *Pharmaceutcal Research*, 2006; **23**: 1888-1897
5. Good D, Rodriguez-Hornedo N, Solubility Advantage of Pharmaceutical Cocrystals, *Crystal Growth & Design*, 2009; **9**: 2252-2264.
6. Trask AV, Motherwell WDS, Jones W, Physical stability enhancement of theophylline via cocrystallization, *International journal of pharmaceutics*, 2006; **320**(1–2): 114-123.
7. Karki S, Friscic T, Fabian L, Laity PR, Day GM, Jones W, Improving mechanical properties of crystalline solids by cocrystal formation: new compressible forms of paracetamol, *Adv. Mater. (Weinheim Ger)*, 2009; **21**: 3905-3909.
8. Sun CC, Hou H, Improving Mechanical Properties of Caffeine and Methyl Gallate Crystals by Cocrystallization, *Crystal Growth & Design*, 2008; **8**: 1575-1579.
9. Desiraju GR, Supramolecular Synthons in Crystal Engineering? A New Organic Synthesis, *Angewandte Chemie International Edition in English*, 1995; **34**(21): 2311-2327.
10. Aakeroy CB, Champness NR, Janiak C, *CrystEngComm*, 2010; **12**: 22-43.
11. Lu E, Rodriguez-Hornedo N, Suryanarayanan R, A rapid thermal method for cocrystal screening, *CrysEngComm*, 2008; **10**: 665-668.
12. Guidance for Industry: Regulatory Classification of Pharmaceutical Cocrystals <http://www.fda.gov/downloads/Drugs/Guidances/UCM281764.pdf>
13. Yadav A, Shete A, Dabke A, Kulkarni P, Sakhare S, Co-crystals: A novel approach to modify physicochemical properties of active pharmaceutical ingredients, *Indian Journal of Pharmaceutical Sciences*, 2009; **71**: 359–370.
14. Hickey MB, Almarsson O, Peterson ML, Crystal engineering and crystallography in the pharmaceutical industry, *CrysEngComm*, 2012; **14**: 2349-2349

15. Friscic T, Trask AV, Jones W, Motherwell WDS, Screening for inclusion compounds and systematic construction of three-component solids by liquid-assisted grinding, *Angewandte Chemie International Edition*, 2006; **45**: 7546-7550.
16. Trask AV, Motherwell WDS, Jones W, Solvent-drop grinding: green polymorph control of cocrystallisation, *Chemical Communications*, 2004; 890-891.
17. Hsi KH, Chadwick K, Fried A, Kenny M, Myerson AS, Separation of impurities from solution by selective co-crystal formation, *CrysEngComm*, 2012; **14**: 2386-2388.
18. Alhalaweh AI, Velaga SP, Formation of Cocrystals from Stoichiometric Solutions of Incongruently Saturating Systems by Spray Drying, American Chemical Society, 2010
19. Trask A, Jones W, Crystal Engineering of Organic Cocrystals by the Solid-State Grinding Approach, In: ed. F. Toda, Springer Berlin Heidelberg, 2005; 41-70.
20. Aher S, Dhumal R, Mahadik K, Paradkar A, York P, Ultrasound assisted cocrystallization from solution (USSC) containing a non-congruently soluble cocrystal component pair: Caffeine/maleic acid. *European Journal of Pharmaceutical Sciences*, 2010; **41**(5): 597-602.
21. Padrela L, Rodrigues MA, Velaga SP, Matos HA, de Azevedo EG, Formation of indomethacin–saccharin cocrystals using supercritical fluid technology, *European Journal of Pharmaceutical Sciences*, 2009; **38**(1): 9-17.
22. Aakeroy CB, Forbes S, Desper J, The effect of water molecules in stabilizing co-crystals of active pharmaceutical ingredients, *CrysEngComm*, 2013; **14**: 2435-2443
23. Buanz ABM, Telford R, Scowen IJ, Gaisford S, Rapid preparation of pharmaceutical co-crystals with thermal ink-jet printing, *CrysEngComm*, 2013; **14**: 2404-2412.
24. Thorson MR, Goyal S, Gong Y, Zhang GGZ, Kenis PJA, Microfluidic approach to polymorph screening through antisolvent crystallization, *CrysEngComm*, 2012; **14**: 2404-2412
25. Sheikh AY, Abd Rahim S, Hammond RB, Roberts KJ, Scalable solution cocrystallization: case of carbamazepine-nicotinamide I, *CrystEngComm*, 2009; **11**: 501-5
26. Medina C, Daurio D, Nagapudi K, Alvarez-Nunez F, Manufacture of pharmaceutical co-crystals using twin screw extrusion: a solvent-less and scalable process, *Journal of Pharmaceutical Sciences*, 2010; **99**: 1693-1696.

27. Dhumal R, Kelly A, York P, Coates P, Paradkar A, Cocrystalization and Simultaneous Agglomeration Using Hot Melt Extrusion, *Pharmaceutical research*, 2010; **27**(12): 2725-2733.
28. Sekhon BS, Pharmaceutical co-crystals- a review, *Ars Pharmaceutica*, 2009; **50**: 99-117
29. CDER, 2004 Office of Pharmaceutical Sciences, Process and Analytical Technologies Initiative, <http://www.fda.gov/cder/OPS/PAT.htm>.
30. Saerens L, Dierickx L, Lenain B, Vervaet C, Remon JP, Beer TD, Raman spectroscopy for the in-line polymer–drug quantification and solid state characterization during a pharmaceutical hot-melt extrusion process, *European Journal of Pharmaceutics and Biopharmaceutics*. 2011; **77**(1): 158-163.
31. Peterson ML, Morissette SL, McNulty C, Goldsweig A, Shaw P, LeQuesne M, Monagle J, Encina N, Marchionna J, Johnson A, Gonzalez-Zugasti J, Lemmo AV, Ellis SJ, Cima MJ, Almarsson Å, Iterative High-Throughput Polymorphism Studies on Acetaminophen and an Experimentally Derived Structure for Form III, *Journal of the American Chemical Society*, 2002; **124**(37): 10958-10959.
32. Alles M, Velaga S, Alhalaweh A, Cornett C, Rasmussen MA, Berg Fvd, Diego HLd, Rantanen J, Near-Infrared Spectroscopy for Cocrystal Screening. A Comparative Study with Raman Spectroscopy, *Analytical Chemistry*, 2008; **80**(20): 7755-7764.
33. Kelly AL, Gough T, Dhumal RS, Halsey SA, Paradkar A, Monitoring ibuprofen–nicotinamide cocrystal formation during solvent free continuous cocrystallization (SFCC) using near infrared spectroscopy as a PAT tool, *International journal of pharmaceutics*, 2012; **426**(1–2): 15-20.
34. Porter III WW, Elie SC, Matzger AJ, *Crystal Growth & Design*, 2008; **8**(1): 14-16.
35. Grzesiak AL, Lang M, Kim K, Matzger AJ, Comparison of the four anhydrous polymorphs of carbamazepine and the crystal structure of form I, *Journal of Pharmaceutical Sciences*, 2003; **92**(11): 2260-2271.
36. Enxian L, Rodriguez-Hornedo N, Suryanarayanan R, *CrystEngComm*, 2008; **10**: 665-668.
37. Rustichelli C, Gamberini G, Ferioli V, Gamberini MC, Ficarra R, Tommasini S, *Journal of Pharmaceutical and Biomedical Analysis*, 2000; **23**(1): 41-54.
38. Grzesiak AL, Lang M, Kim K, Matzger AJ, *Journal of Pharmaceutical Sciences*, 2003; **92**: 2260-2271.

## **Chapter 4: Development and characterization of orally disintegrated tablets (ODTs) prepared by using sugar based cocrystals processed via hot-melt extrusion**

---

### **4.1. Introduction**

Starting from the plastics and rubber industry in the second half of the 19<sup>th</sup> century, and then the food industry, hot-melt extrusion (HME) has over the last three decades - also been introduced as a contemporary technique in the pharmaceutical industry [1]. HME offers many advantages over conventional pharmaceutical production methods, due to its versatility in embracing a wide range of applications. HME can be operated as a continuous and single step process. The foregoing together with the relatively short processing time, reduced labour costs/involvement arising from the ability to automate the process makes the technique particularly attractive for the production of pharmaceutical formulations [2-3]. Moreover, it is an eco-friendly tool because HME is a solvent free technology. HME has potential to be applied in continuous manufacturing for a wide variety of dosage forms and formulations, such as granules, pellets, tablets, capsules, implants, suppositories, stents, transdermal and transmucosal systems as well as ophthalmic inserts [4]. Formulations produced by using HME often exhibit an enhanced bioavailability of poorly water soluble drugs because of the dispersion of the API, at a molecular level, in the final dosage forms [5-7]. HME can also be combined with the Process Analytical Technology (PAT) tools in order to monitor and understand material processing and ensure the quality of the end product using science based knowledge and Quality by Design (QbD) approaches [8-11].

Cocrystals are crystals formed of two or more compounds. A cocrystal has a unique crystalline structure, which is different from the crystal structure of its components [12]. Pharmaceutical co-crystals can be defined as crystalline materials comprised of an API and one or more unique co-crystal formers, which are solids at room temperature [13]. Co-crystallization represents a viable means of enhancing the physical properties of active compounds such as solubility, dispersibility, wettability, anti-caking, anti-dusting, anti-separation, homogeneity, flowability and stability [14]. Pharmaceutical cocrystals can be produced using various conventional techniques such as solvent methods and particle size reduction methods [15]. Dhumul *et al.*, [16] have successfully prepared cocrystals of ibuprofen and nicotinamide (1:1 molar ratio) utilising melt extrusion process. Moradiya *et al.*, [17-18]

have reported the use of HME in order to enhance the bioavailability of the poorly water soluble drug carbamazepine by producing pharmaceutical cocrystals of carbamazepine-saccharine (1:1) and carbamazepine-*trans* cinnamic acid (1:1). They also used in-line NIR to monitor and understand the cocrystallization process during HME.

Cocrystal materials are not only produced in the field of pharmaceutical formulation. Cocrystalline sugars have also been shown to have superior properties compared to single sugars on their own. Cocrystalline sugar materials have been shown to exhibit superior solubility, flowability and possess better compressibility properties compared to single sugars [19]. Formation and characterization of cocrystals and their applications in scientific research has been described by Frankenbach [20]. Details of cocrystallizing sugars have been revealed by Geary *et al.*, [21]; they described the cocrystallization of various sugars such as glucose-sucrose, lactose-maltose/aspartame, lactose-galactose/glucose etc. Cocrystalline sugar alcohols are also reported to be formed between xylitol and sorbitol [22] as well as sorbitol and mannitol [23]; the cocrystals were produced by melt crystallization. The resultant cocrystal products were reported to be more easily formulated into tablets compared to their non-HME treated counterparts and to compound into chewing-gum as well as being easier to handle in the sweets industry and/or in terms of the composition of pharmaceutical formulations.

The development of oral disintegrating tablets (ODTs) has, over the last decade, received increased interest amongst academic researchers and the pharmaceutical industry. ODTs are designed to disintegrate or dissolve rapidly on contact with saliva, in the absence of additional water, compared to traditional tablet forms. ODTs provide several advantages as they combine the properties of both liquid and conventional tablet formulations [24-25]. HME has been successfully used to develop taste masked ODTs using ibuprofen with Eudragit EPO polymer [26].

In this study, we used three sugar alcohols (mannitol, xylitol and sorbitol) to produce cocrystals via HME which was coupled with in-line NIR to monitor and understand the process. The aim of this study was also to evaluate their compressibility in comparison to the marketed sugar binder, Starlac, for the development of a placebo and a drug loaded orally disintegrating tablets (ODTs).

## 4.2. Materials & methods

### 4.2.1. Materials

Pearlitol (mannitol, C<sub>6</sub>H<sub>14</sub>O<sub>6</sub>), sorbitol (C<sub>5</sub>H<sub>10</sub>O<sub>5</sub>), xylitol (C<sub>6</sub>H<sub>14</sub>O<sub>6</sub>) and Starlac were kindly donated by Roquette (Corby, UK). Paracetamol (PMOL) was kindly provided by Mallinckrodt Chemical Ltd (Canada). Mg-stearate and silica were obtained from Sigma-Aldrich (Dorset, UK). All samples were used as received.

### 4.2.2. HME

HME was performed using a Eurolab 16 mm twin screw extruder (Thermo Fisher Scientific, Germany). The hot-melt extruder was equipped with a DD Flexwall® 18 feeder (Brabender Technology, Germany), which was set in volumetric feeding mode.

**Table 4.1.** Compositions of formulations used for HME.

<b>Formulation No.</b>	<b>Pearlitol (w/w, %)</b>	<b>Sorbitol (w/w, %)</b>	<b>Xylitol (w/w, %)</b>	<b>Processing temperature of extruder barrel (°C) (feed point to die)</b>
<b>F1</b>	71	13	16	50/90/135/135/135/135/135/135/135
<b>F2</b>	60	25	16	
<b>F3</b>	78	13	9	
<b>F4</b>	74	24	2	
<b>F5</b>	85	13	2	50/90/110/135/165/165/165/165/140
<b>F6</b>	96	2	2	
<b>F7</b>	89	2	9	
<b>F8</b>	82	2	16	
<b>F9</b>	67	24	9	
<b>FA</b>	92	6	2	50/100/120/160/160/160/160/160/140
<b>FB</b>	86	2	12	
<b>FC</b>	88	0	12	

Three different sugar blend ratios (w/w) were extruded (**Table 4.1**), composed of pearlitol, sorbitol and xylitol. Prior to HME, all the formulations were blended in a TF2 Turbula mixer (Basel, Switzerland) at 100 rpm for 10 mins, in order to ensure homogeneous mixing of the physical blends.

#### **4.2.3. Scanning electron microscopy**

The morphology of all extruded samples, including the bulk sugars, was examined by SEM (Hitachi SU8030, Japan). Samples were placed on double sided carbon tape sticks on an aluminium stub and coated with a thin layer of chromium in an argon atmosphere at room temperature. An accelerating electron beam voltage of 2 kV was used to obtain the SEM images.

#### **4.2.4. Thermal analysis**

The physical state of the pure sugars and the granules (obtained by cutter milling the extrudates) were studied by differential scanning calorimetry (DSC) using a Mettler-Toledo 823e (Greifensee, Switzerland) differential scanning calorimeter. Samples were accurately weighed (2-3 mg), placed in aluminium pans and sealed. Measurements were carried out under an atmosphere of dry nitrogen using a flow rate of 50 mL/min. Samples were scanned at a heating rate of 10.0°C/min from 25°C to 190°C.

#### **4.2.5. X-ray powder diffraction**

XRPD was used to assess the crystalline state of the active substances in the extruded formulations. All formulations including pure sugars, physical mixtures and extruded formulations were evaluated using a Bruker D8 (Karlsruhe, Germany) Advance in theta–theta mode, using a Cu anode at 40 kV and 40 mA, parallel beam Goebel mirror, 0.2 mm exit slit, LynxEye Position Sensitive Detector with 3° opening and LynxIris at 6.5 mm and sample rotation of 15 rpm. The samples were scanned from 2 to 40° 2-theta with a step size of 0.02° 2-theta and a counting time of 0.2 s per step; 176 channels active on the PSD making a total counting time of 35.2 s per step.

#### **4.2.6. Near-infrared spectroscopy**

Diffuse reflectance near infrared spectroscopic measurements were performed continuously, in-line and non-invasively during HME using an Antaris MX Fourier Transform NIR Spectrometer (Thermo Scientific, UK). A fibre optic NIR probe was inserted in three

different mixing zones of the extruder barrel for in-line monitoring. Spectra were collected in 30 s in the 10000-4000  $\text{cm}^{-1}$  wavenumber region with a resolution of 16  $\text{cm}^{-1}$  and averaged over 32 individual scans. Off-line NIR measurements were also carried out, on all the samples, in order to collect the spectra of the pure materials and the finished products. Spectra were collected using Result Software (version 3.0, Thermo scientific, UK) and analysed by TQ analysis software (version 3.0, Thermo scientific, UK)

#### **4.2.7. Particle size analysis**

The particle size distribution was measured by laser diffraction (Mastersizer 2000, Malvern, UK) where 5 g of powders was placed in the dry powder feeder. Sampling time was set at 15 s, and each sample was measured three times.

#### **4.2.8. Flow properties and compressibility**

Compressibility index (Carr's index) values of different formulations were determined by measuring the tapped and bulk densities of the powders after subjecting them to 100 taps in a graduated measuring cylinder using the following relationship:

$$\text{Carr's index} = \left(1 - \frac{\rho_b}{\rho_t}\right) \times 100$$

Where  $\rho_b$  is the bulk density and  $\rho_t$  is the tapped density.

#### **4.2.9. Tablet preparation**

For the tablet compression, batches of F4-F7 and FA-FC were prepared using 250 mg of each mixture of extruded sugars without addition of any API (placebo formulations), whereas drug loaded formulations, using a 250 mg dose of the API (PMOL) combined with 250 mg of the extruded sugars (FA – FC) were also prepared. Another batch of tablets containing Starlac (commercial binder) with 250 mg of PMOL was also prepared for a comparative study. All excipients were passed through a mesh with an aperture of 500  $\mu\text{m}$  before use. The batches were blended with magnesium stearate (1%) and silicon dioxide (0.25%) in a Turbula TF2 mixer (Basel, Switzerland) for 5 minutes. Blends were directly compressed on a Flexitab tablet press (Oystar-Manesty, Germany) using 13 mm normal flat punches. Dwell time was set at 30 ms and the compaction force was varied from 5-20 kN to obtain the final tablets with a hardness of 5-15 kP.

#### 4.2.10. Tablet characterisation

Freshly prepared tablets were characterized according to the United States Pharmacopeia (USP 30-NF 25, 2007). For the weight uniformity test, ten tablets were weighed individually and the results were expressed as a mean value of the individual determinations. The thickness of 10 tablets was measured using a screw meter. The tablet hardness was measured with a Erweka hardness tester (Erweka, Germany). The disintegration time was evaluated using 6 tablets per formulation by employing a disintegrator tester (Erweka, Germany).

### 4.3. Results and discussion

#### 4.3.1. HME

The extrudates were collected as a molten mass from the end of the extruder as the die, which is normally placed at the end of the extruder to shape the extrudates, was removed. All the extrudates were cutter milled, to reduce the particle size, in order to obtain granules. During HME processing the screw configuration was adjusted to achieve homogenous mixing by assembling the kneading elements in three separate “mixing zones”, as shown in **Fig. 4.1**. The mixing zones were designed to obtain high mixing capacity whereas conveying elements have minimal mixing ability. The extruded samples were collected from each zone in order to investigate the effect of the kneading elements and provide a better understanding of cocrystallization process.

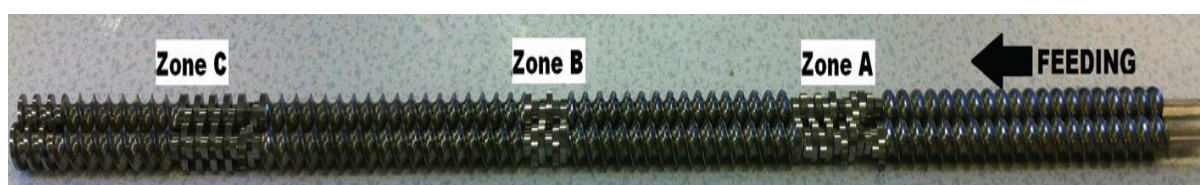


**Fig. 4.1.** Schematic of the extruder screw, indicating the mixing and collection zones (ZA-ZC) of the HME.

A wide range of formulations, F1-F9, composed of the three sugars at various weight ratios () was assessed for the formation of cocrystals. As explained below most of the formulations did not form sugar cocrystals. Only one formulation (F6) formed cocrystals after extrusion; formulations F3 and F4 exhibited low amounts of unreacted materials after extrusion. Three new formulations (FA-FC) were designed from an understanding of the data analysed from formulations F3, F4 and F6, and were further evaluated in order to optimize the quality of the cocrystals.

### 4.3.2. Scanning electron microscopy

The morphology of the bulk materials, physical mixtures, and the granules (cutter milled after extrusion) of FA-FC was examined using SEM (**Fig. 4.2**). Bulk pearlitol particles appeared to be of a cylindrical-like shape with rough surfaces; whilst sorbitol and xylitol displayed needle-shape and disc-shaped crystals, respectively. The physical mixtures and the extrudates were observed to be cylindrical-like in shape due to the high content of pearlitol within the formulations.

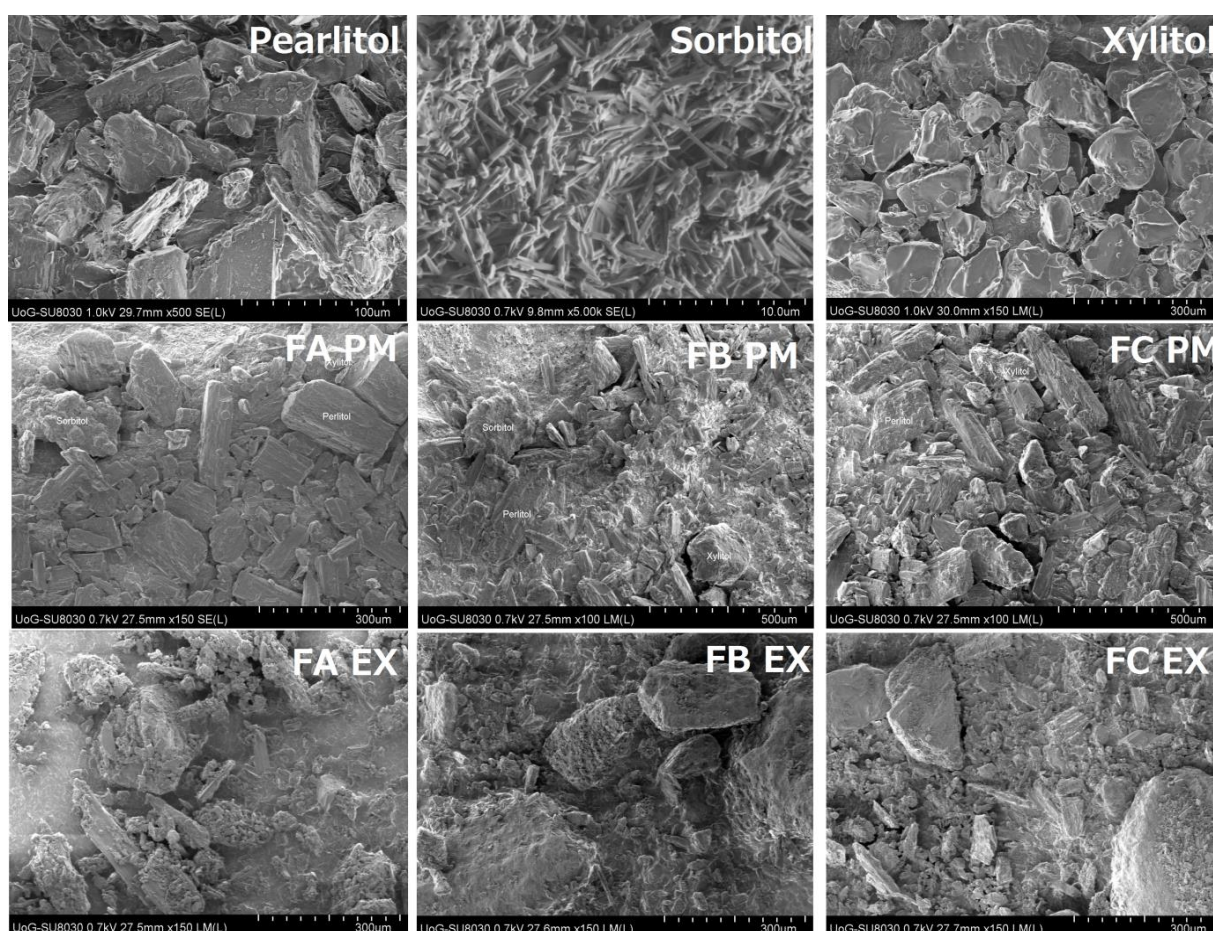


**Fig. 4.2.** SEM micrographs of bulk pearlitol, sorbitol, xylitol, physical mixtures (PMs) and the extruded formulations of FA, FB and FC.

### 4.3.3. Differential scanning calorimetry

DSC was employed to evaluate the solid state thermal properties of the pure components as well as the extruded cocrystals. Analysis of thermal transitions of the bulk sugars indicated that the melting peaks appeared at 166.72°C, 94.51°C and 97.79°C for pearlitol, xylitol and sorbitol, respectively (**Fig. 4.3**). The DSC thermograms of the initially extruded formulations

(F1-F9) showed the presence of unreacted bulk materials which indicates that, except for F6 cocrystals were not completely formed; however, F3 and F4 contained negligible amounts of unreacted materials after extrusion (Figs. 4.4 – 4.8). On the other hand, the presence of unreacted sugars was not observed in the DSC thermograms for the three newly designed formulations FA-FC (Figs. 4.10 - 4.12), which indicates that cocrystals were successfully formed using the sugars via HME.

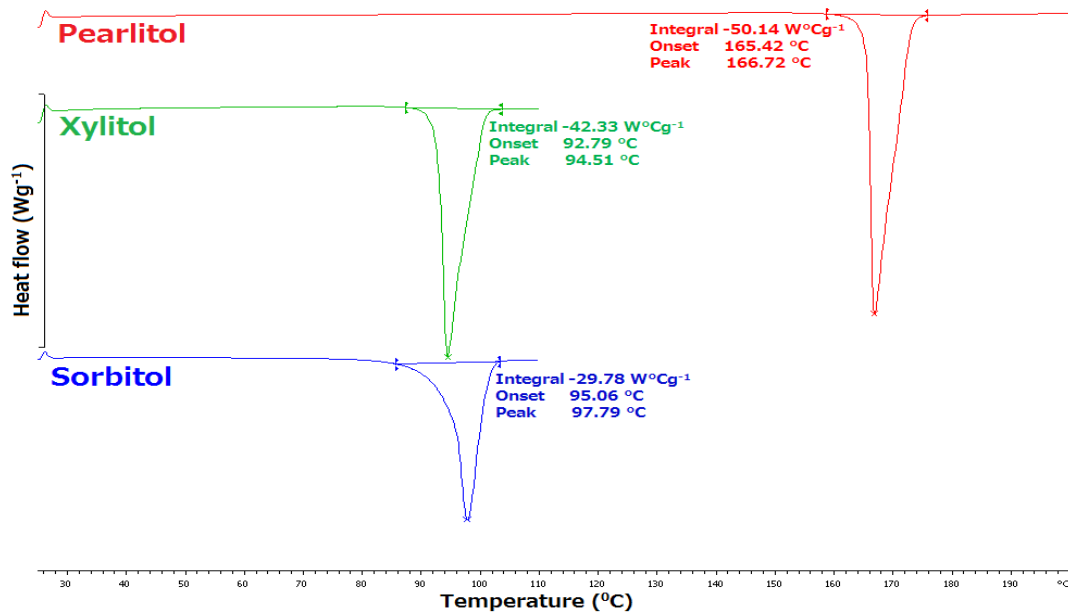


Fig. 4.3. DSC thermograms for pure (bulk) pearlitol, sorbitol and xylitol.

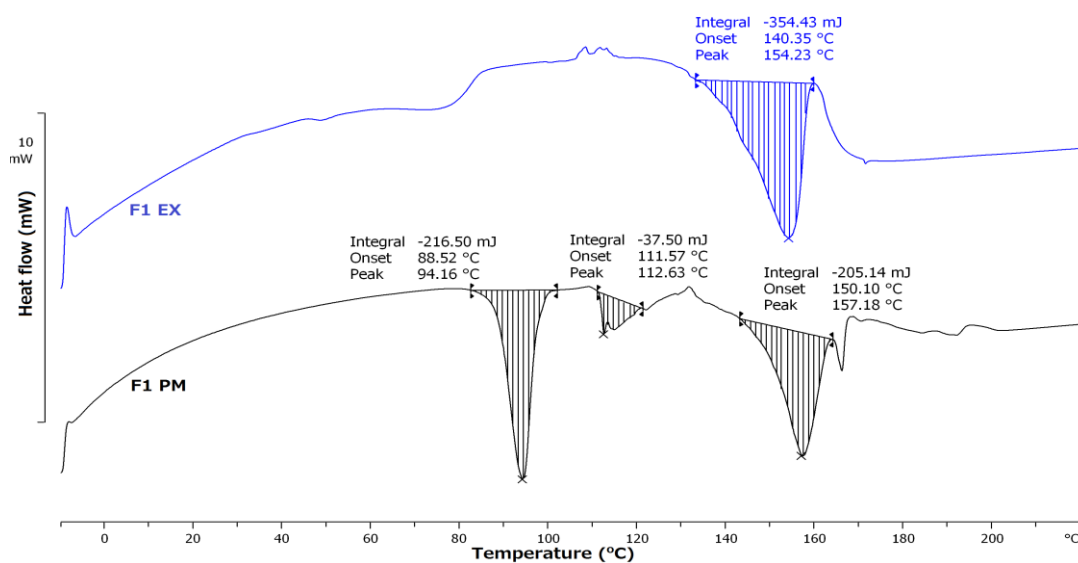
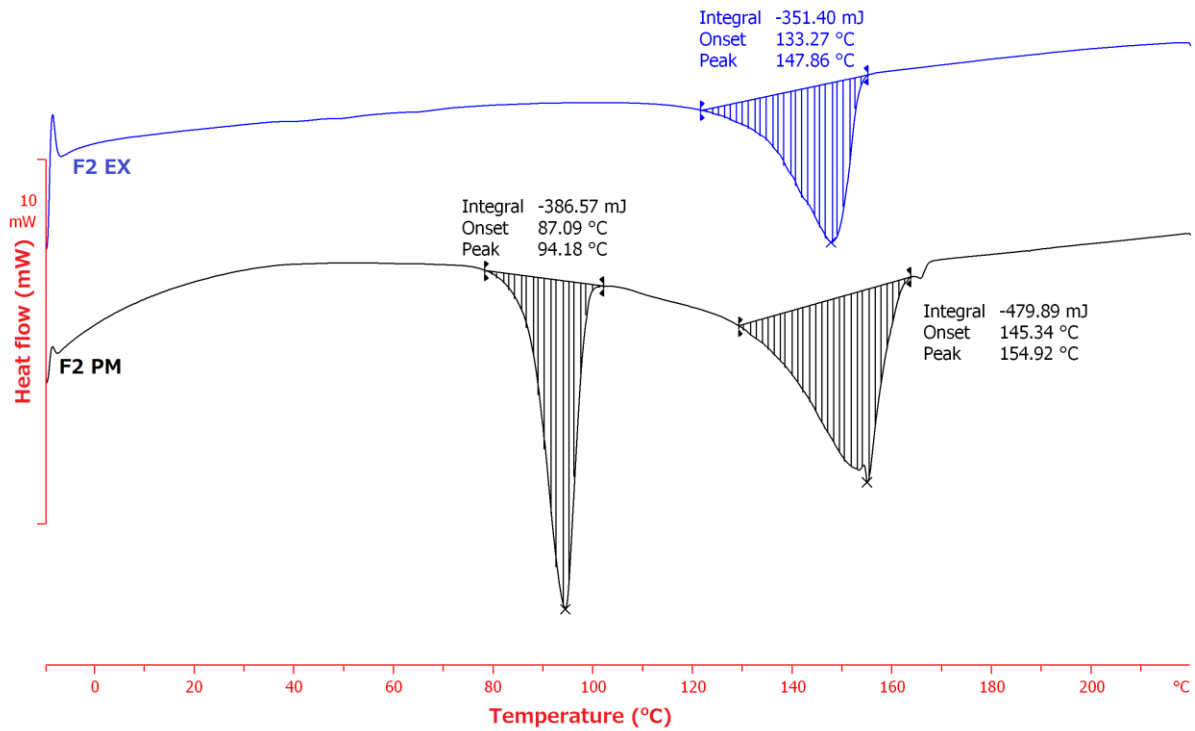
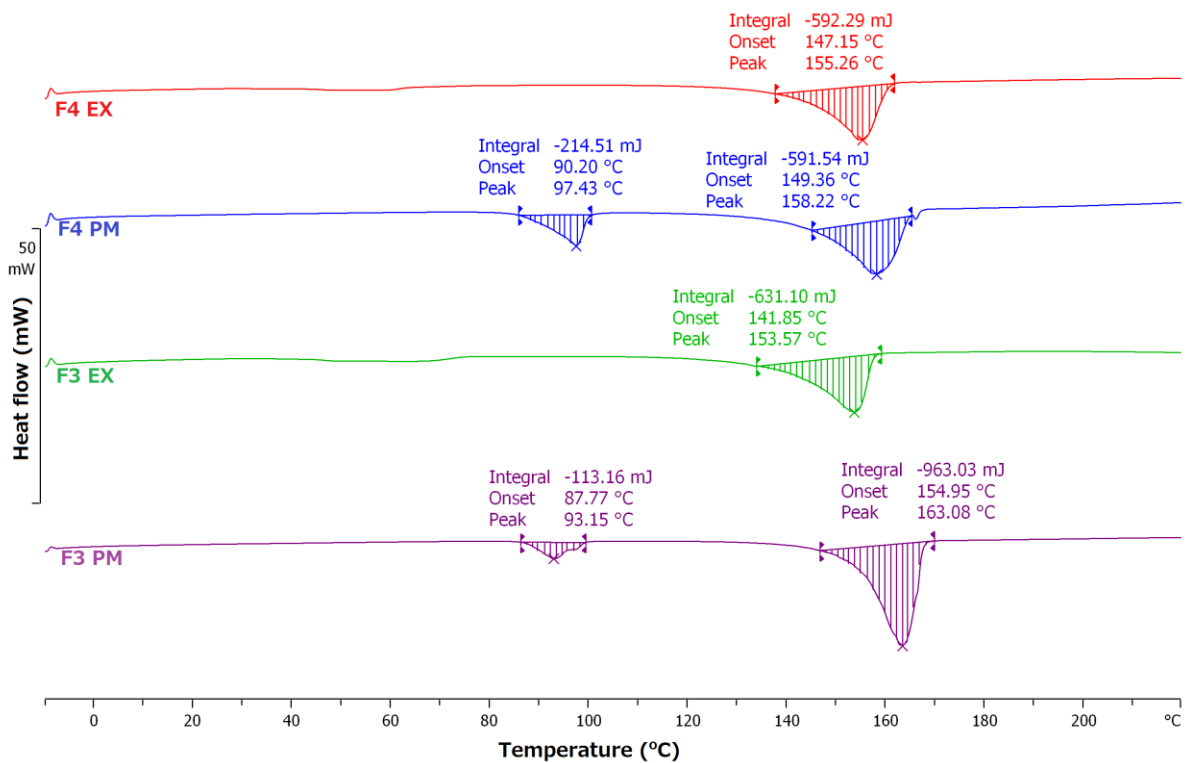


Fig. 4.4. DSC thermograms of a physical mixture of F1 and the extrudate.



**Fig. 4.5.** DSC thermograms of a physical mixture of F2 and the extrudate.



**Fig. 4.6.** DSC thermograms of physical mixtures of F3-F4 and the extrudates.

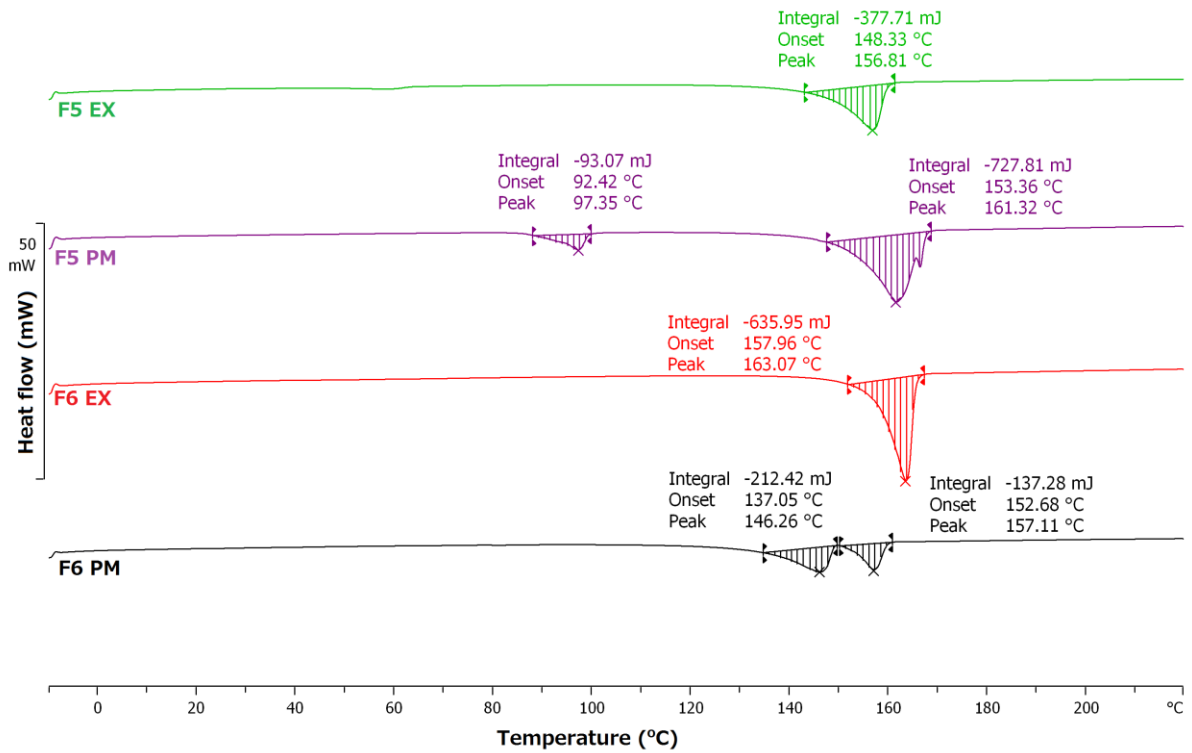


Fig. 4.7. DSC thermograms of physical mixtures of F5-F6 and the extrudates.

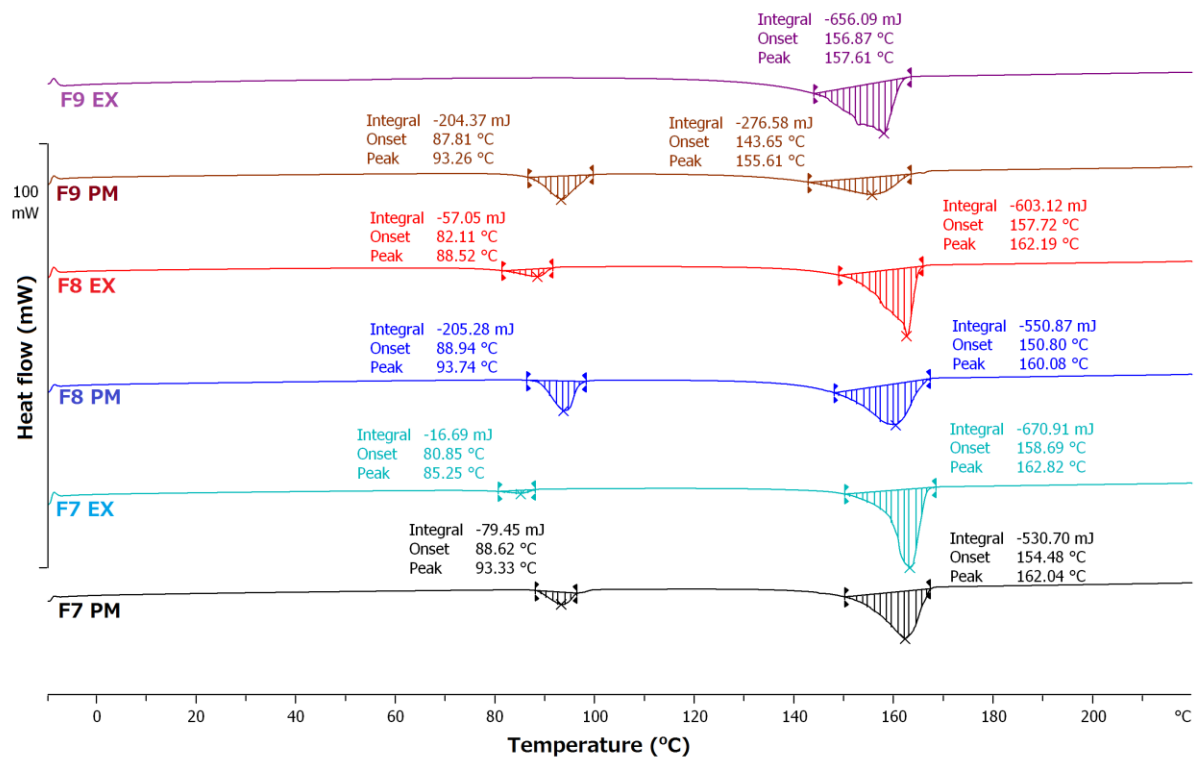
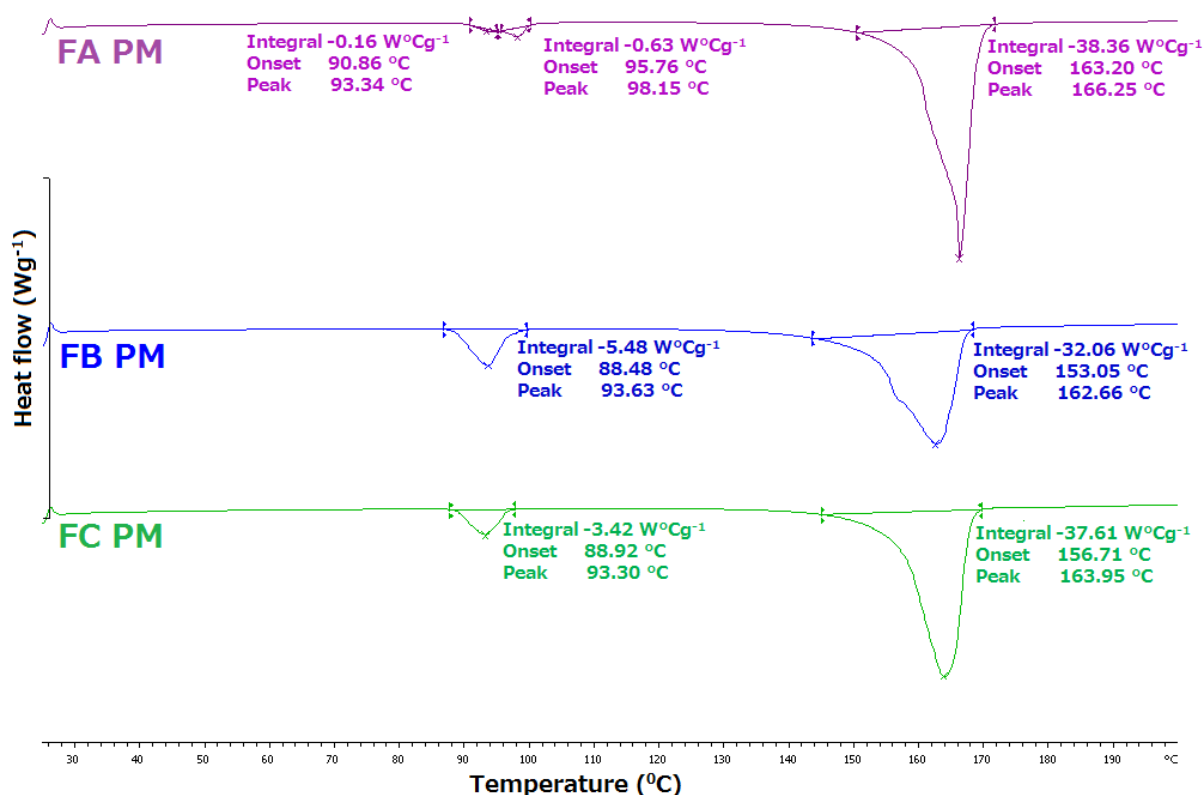


Fig. 4.8. DSC thermograms of physical mixtures of F7-F9 and the extrudates.

The physical mixture of FA (**Fig. 4.9**) showed two minor peaks at 93.35°C and 98.15°C due to the presence of xylitol and sorbitol, respectively while the peak at 166.25°C belonged to pearlitol. In contrast, FB and FC showed two endothermic transitions as FB contains small amounts (2%) of sorbitol whilst FC does not contain any sorbitol. Xylitol shows an endothermic transition at 93.63°C and pearlitol at 162.66°C, respectively in the physical mixture of FB. Similarly the physical mixture of FC shows endothermic transitions at 93.30°C and 163.95°C due to the presence of xylitol and pearlitol, respectively.



**Fig. 4.9.** DSC thermograms of the physical mixtures of FA, FB and FC.

A single endothermic transition at 163.39°C was observed in the thermogram (**Fig. 4.10**) of the FA extruded cocystals. Furthermore, samples collected from the different HME mixing zones (ZA, ZB and ZC) were also analysed using DSC in order to detect the progression of cocystal formation. The DSC thermograms of samples collected from different mixing zones (ZA, ZB and ZC) of the extruder barrel showed a single endothermic transition, which is similar to the thermogram of the final extrudates. This suggested that cocystal formation occurred from the very beginning of the extrusion process, i.e., in mixing zone A of the extruder.

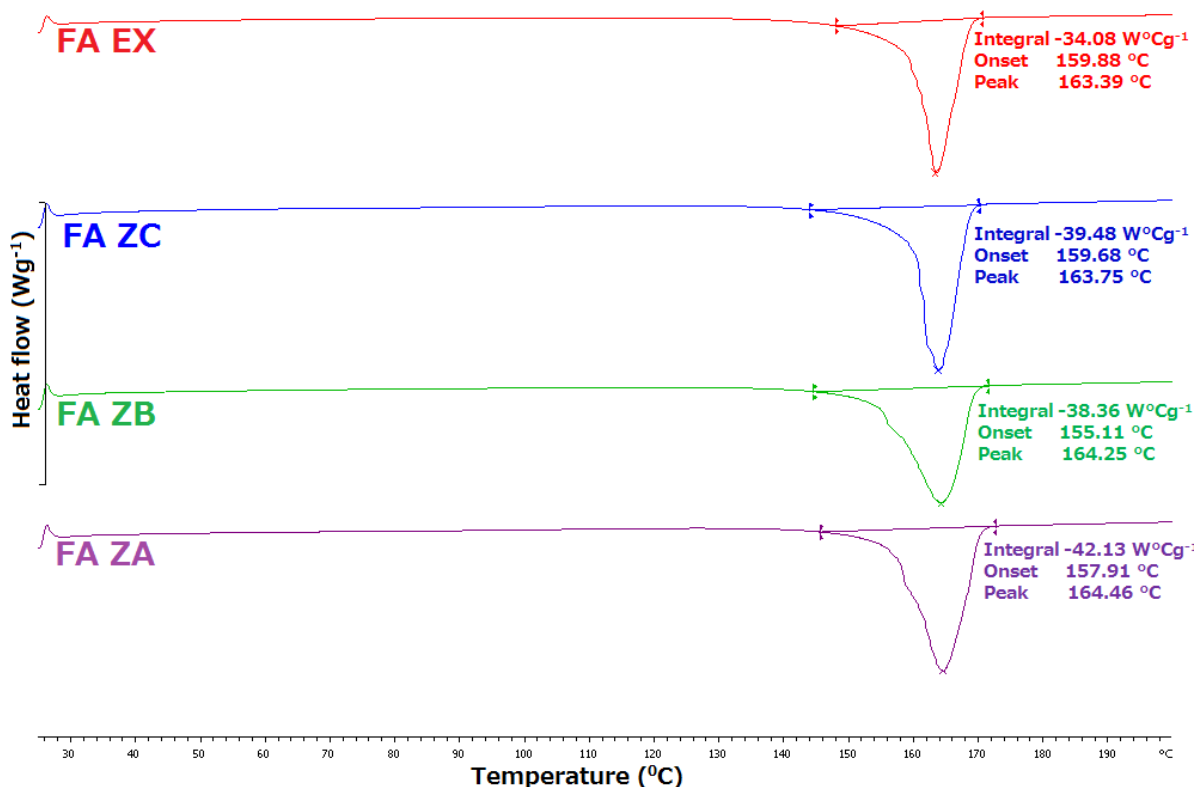


**Fig. 4.10.** DSC thermograms of samples collected from different mixing zones of the extruder barrel and the final extrudates of FA.

Similarly, single endothermic transitions at 158.43°C and 162.18°C were observed in the thermograms (**Fig. 4.11** and **Fig. 4.12**) of the extruded cocrystals of FB and FC, respectively. In contrast to formulation FA the cocrystals produced from formulations FB and FC were formed in the last mixing zone (ZC) of the extruder.

A comparison of the thermograms of the samples collected from mixing zones ZA and ZB and the physical mixtures show that they are almost identical suggesting no major crystal transformation of the processed blends. In contrast, the thermal transitions of the processed materials collected from mixing zone ZC presented sharp melting transitions at 158.43°C and 162.18°C (FB and FC, respectively) which corresponds to the final melting point of the stable cocrystals. The complete formation of cocrystals occurred in mixing zone ZC where the absence of any other endothermic peak is evident.

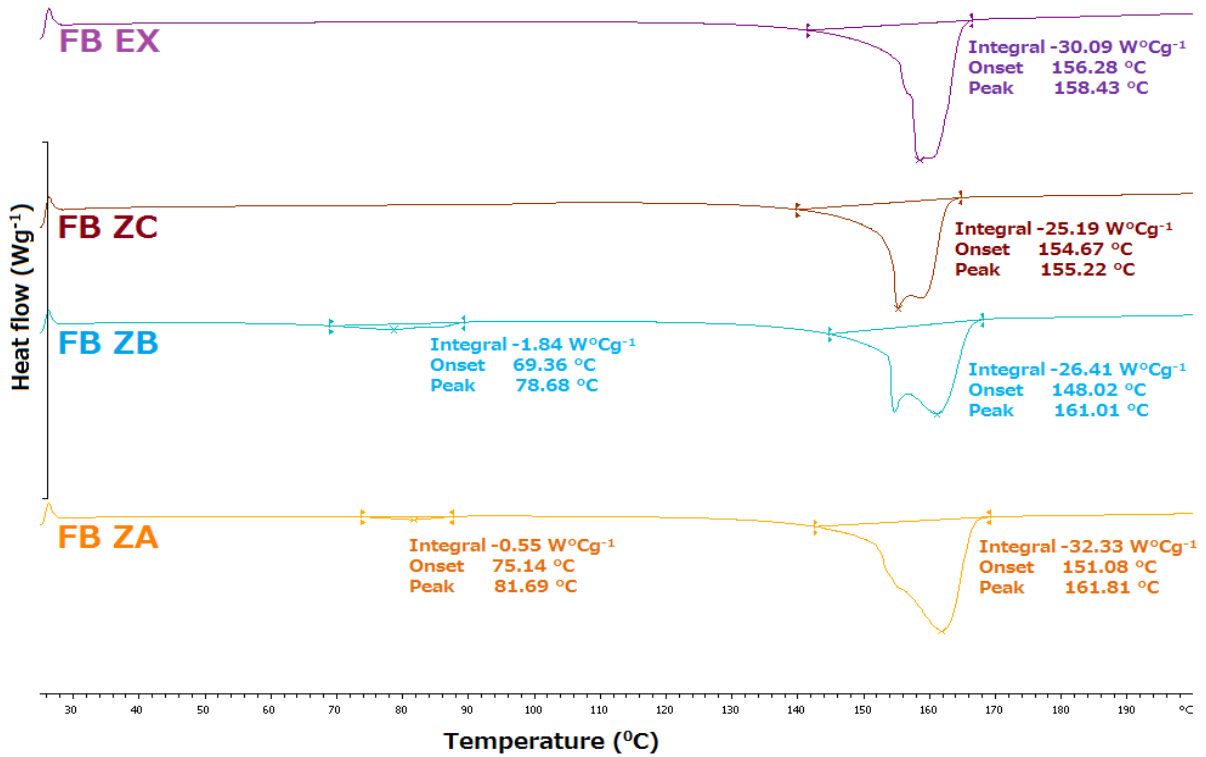


**Fig. 4.11.** DSC thermograms of samples collected from different mixing zones of the extruder barrel and the final extrudates of FB.

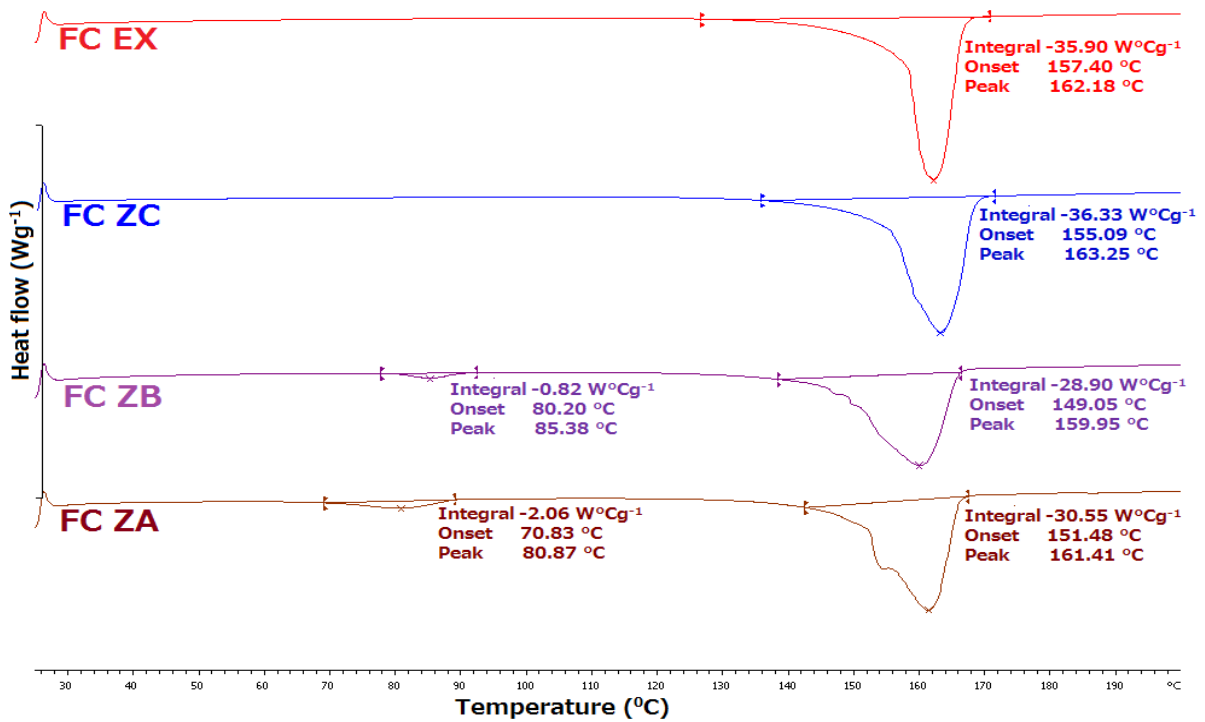


**Fig. 4.12.** DSC thermograms of samples collected from different mixing zones of the extruder barrel and the final extrudates of FC.

#### 4.3.4. X-ray powder diffraction

XRPD was used to investigate the crystalline state of the sugars. X-ray diffractograms of pure components are shown in **Fig. 4.13**. Bulk pearlitol displayed distinct peaks at 10.54°, 11.45°, 14.67°, 16.82°, 18.81°, 20.47°, 21.12°, 21.70°, 23.49°, 24.73°, 25.97°, 28.34°, 29.54°, 31.82°, 38.72° and 44.12° 2-theta values. Xylitol showed peaks at 14.06°, 14.61°, 17.67°, 19.88°, 22.22°, 22.58°, 23.66°, 28.24°, 29.35°, 30.2°, 31.07°, 31.6° and 35.24° 2-theta values and the peaks for sorbitol occurred at 7.32°, 11.32°, 11.78°, 16.94°, 17.67° and 18.74° 2-theta values.

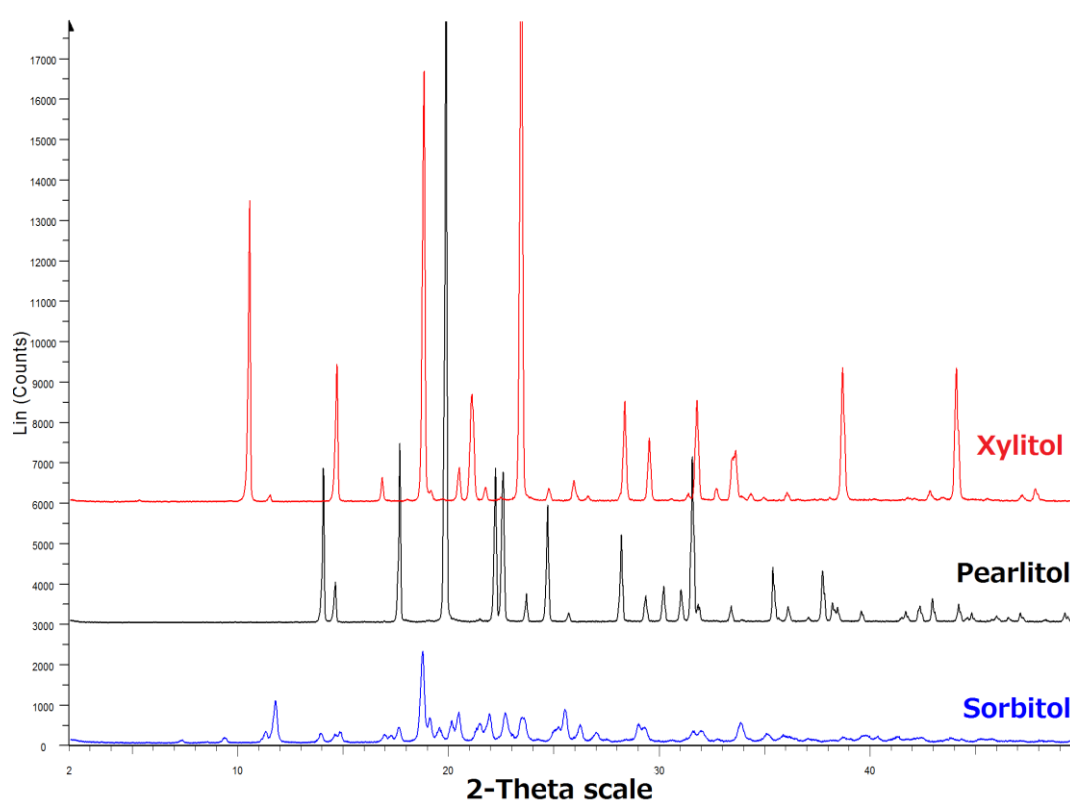


**Fig. 4.13.** XRPD profiles of pure (bulk) pearlitol, sorbitol and xylitol.

XRPD data of preliminary formulations (F1-F9) showed that there is formation of new peaks with lower intensities compared with the physical mixtures in conjunction with other characteristic peaks of pure materials which demonstrate the presence of impurities (or pure materials) in the extrudates, excluding F6 (**Fig. 4.14** and **Fig. 4.15**). However, XRPD profiles of FA-FC show the formation of new peaks with high intensity while the characteristic peaks for pure (bulk) materials disappear which demonstrates the formation of cocrystals after HME extrusion.

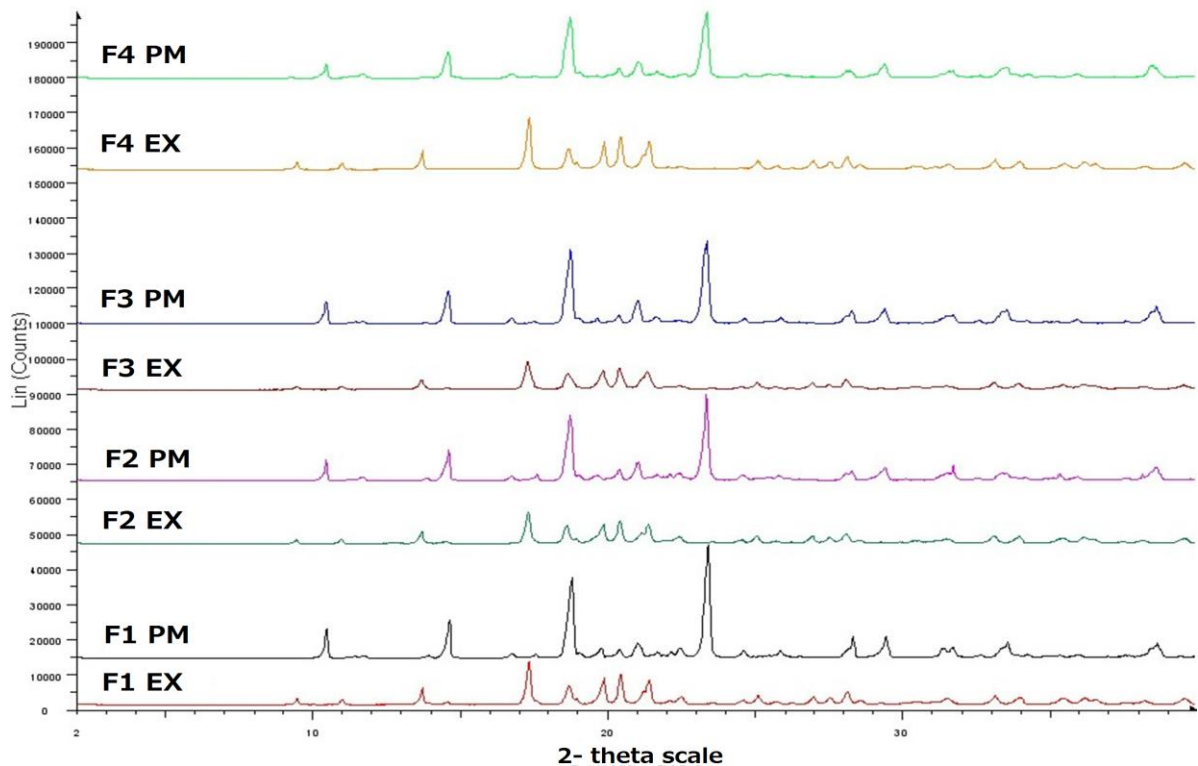


**Fig. 4.14.** XRPD profiles of the physical mixtures of F1-F4 and the extrudates.

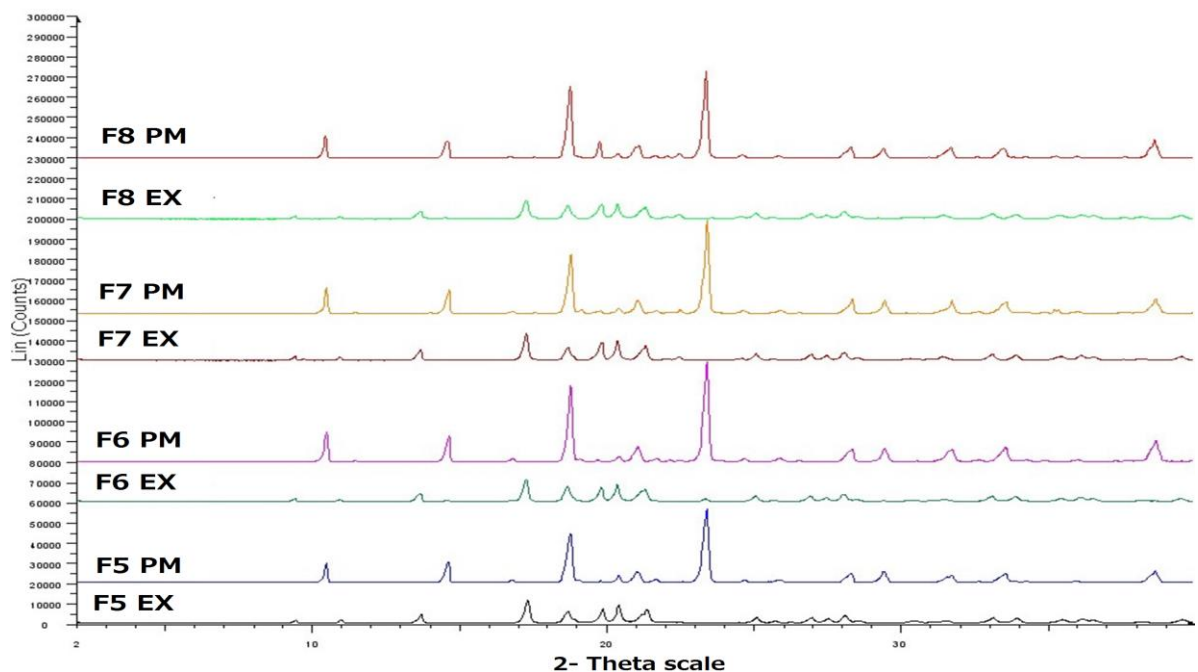


**Fig. 4.15.** XRPD profiles of the physical mixtures of F5-F8 and the extrudates.

The data in **Fig. 4.16** shows the development of cocrystals produced during extrusion of FA began in the third mixing zone (ZC) with the appearance of new intensity peaks at  $9.47^\circ$ ,

11.03°, 13.73°, 17.35°, 19.92°, 27.04°, 27.56°, 28.18°, 35.6°, 36.25° and 39.64°  $2\theta$  values. It is clear that the interactions between the sugars started in the third mixing zone; whilst diffractograms of samples collected from the second mixing zone (ZB) show that the peaks at 10.58°, 11.55°, 14.74°, 16.89°, 21.74° and 29.55°  $2\theta$  are not present and the intensity of some of the other peaks has been reduced. The cocrystals were successfully formed at the third mixing zone (ZC) with the appearance of new diffraction peaks at  $2\theta$  values which are identical to those of the diffractogram of the final extrudates. Apparently, the screw configuration in the mixing zone B plays a crucial role for the initiation of the cocrystallization process while the placement of the mixing element angles at 60 and 90° in mixing zone C resulted in cocrystals with improved crystallinity.

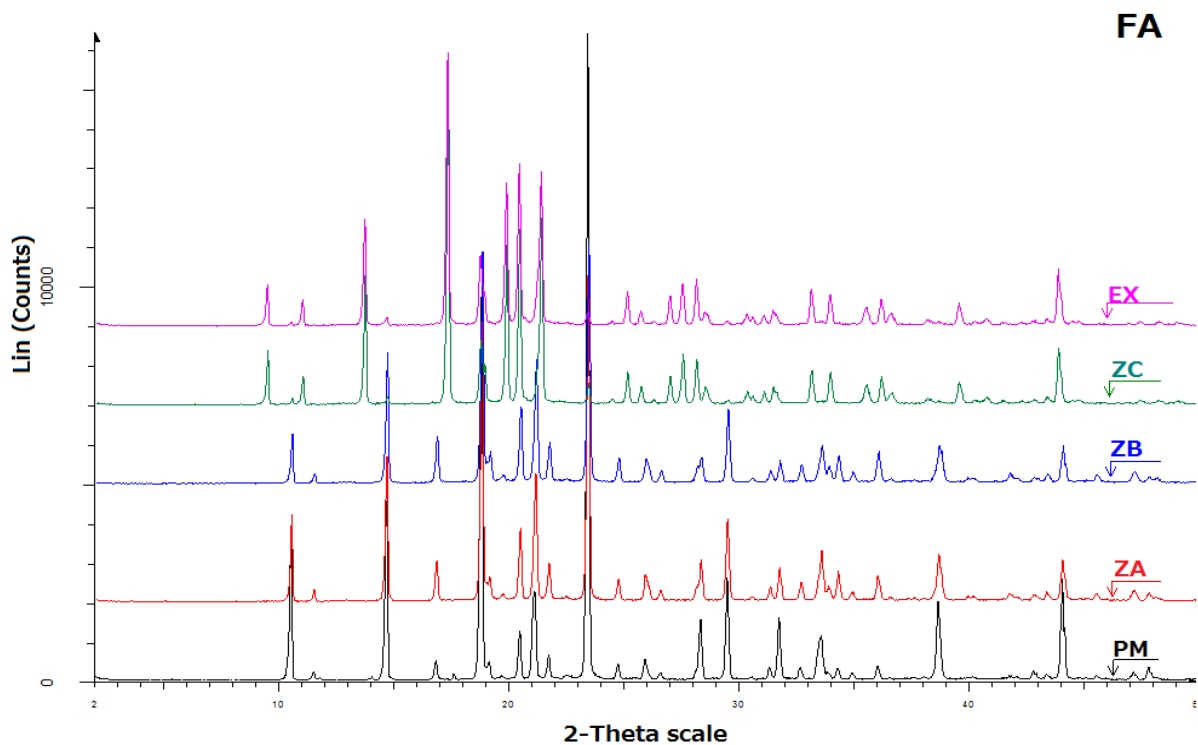


**Fig. 4.16.** XRPD profiles of a physical mixture and samples collected from three different mixing zones of extruder and final extrudates of FA.

Furthermore, a similar kind of progression pattern for cocrystal formation has also been found for two other formulations, FB and FC during extrusion (**Fig. 4.17** and **Fig. 4.18**). So it is clear that cocrystal formation occurred from the beginning of the second mixing zone (with the formation of new peaks of lower intensity and by the reduction in intensity of some peaks compared to the characteristic peaks of the pure materials) and cocrystallization is completed at the end of the extruder.

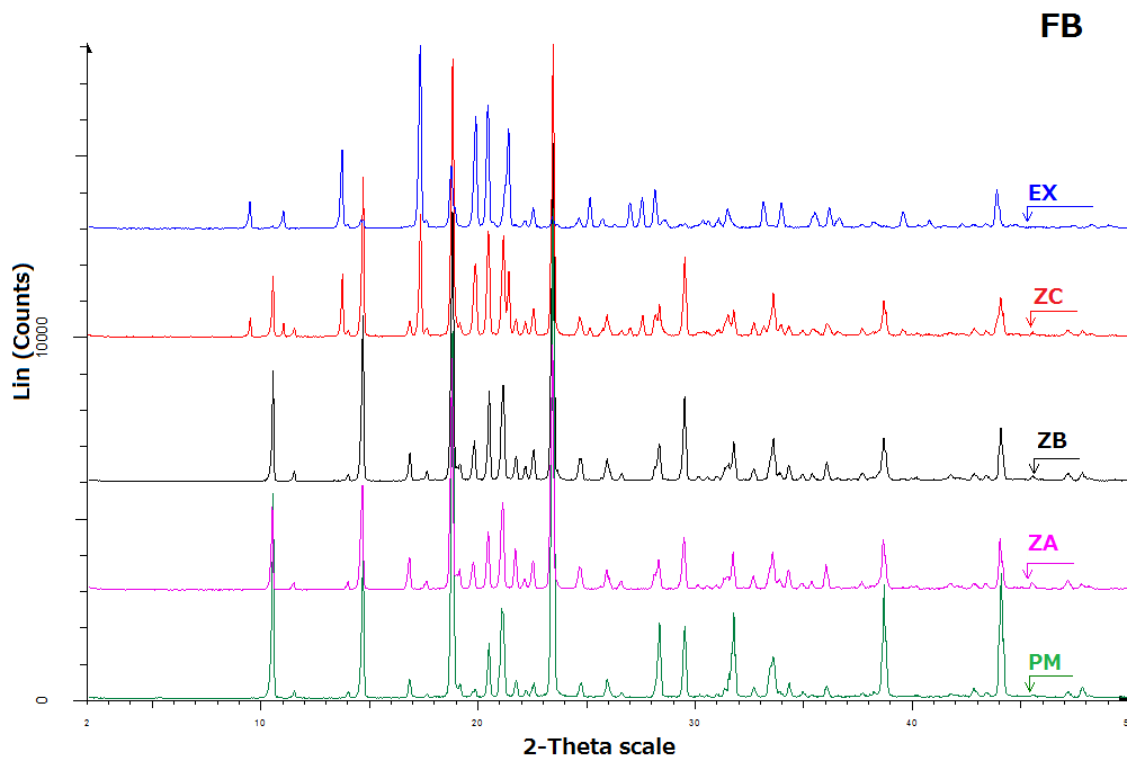


**Fig. 4.17.** XRPD profiles of a physical mixture and samples collected from three different mixing zones of extruder and final extrudates of FB.

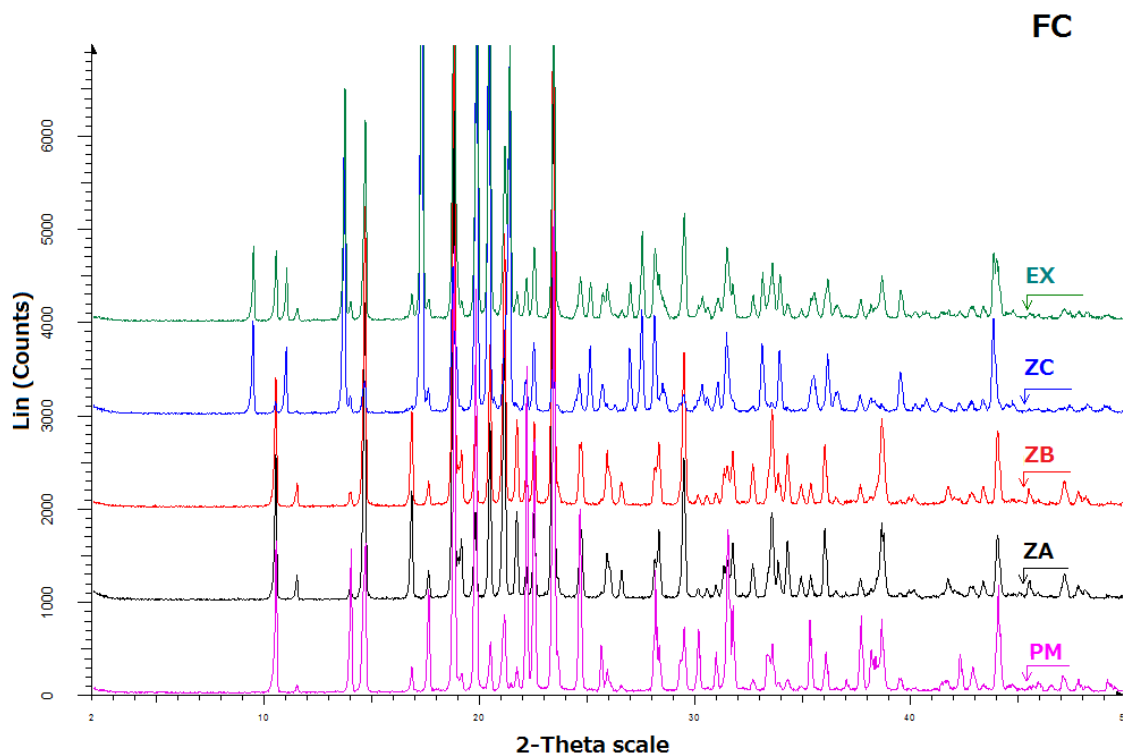


**Fig. 4.18.** XRPD profiles of a physical mixture and samples collected from three different mixing zones of extruder and final extrudates of FC.

### 4.3.5. In-line NIR monitoring

Off-line NIR spectra of pearlitol, sorbitol, xylitol and the physical mixtures were collected to identify the characteristic bands of these materials so that any new bands formed during extrusion could be attributed to the cocrystal. The NIR spectra of pure sugars and physical mixtures exhibit characteristic bands in the 7500-4000  $\text{cm}^{-1}$  wavenumber region (**Fig. 4.19**). The NIR bands of physical mixtures are overlaid with pearlitol bands due to the presence of the high content of pearlitol in the physical mixtures.

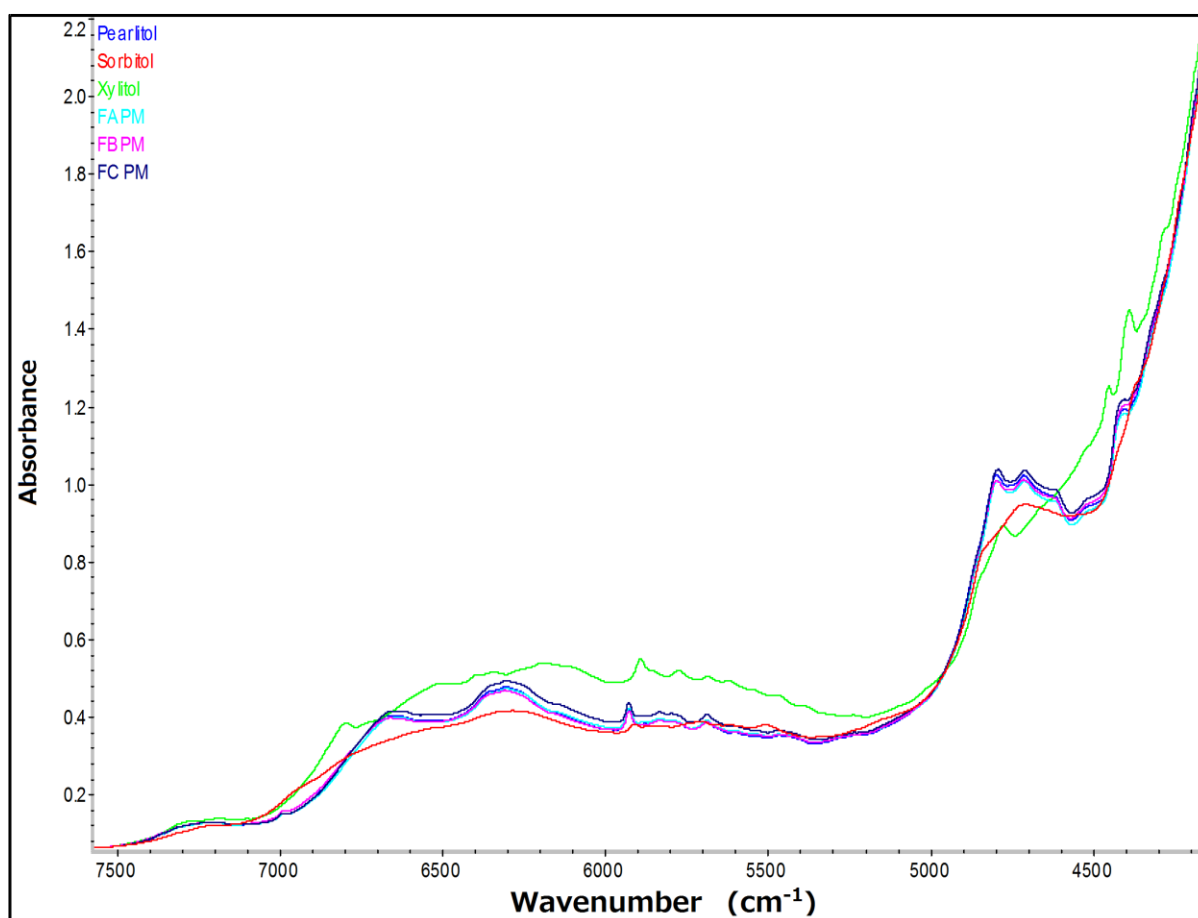


**Fig. 4.19.** Off-line NIR spectra of the pure (bulk) sugars pearlitol, sorbitol, xylitol and the physical mixtures of FA, FB and FC.

In-line NIR monitoring has also been performed during HME process to understand and monitor the cocrystallization process using sugars. **Fig. 4.20** shows the second derivative spectra of pearlitol, sorbitol, xylitol, a physical mixture and the extruded cocrystals of FA that show significant differences due to band shifts. The bands observed at 4412  $\text{cm}^{-1}$  and 5442  $\text{cm}^{-1}$  in the physical mixture are due to the OH stretching band of xylitol and sorbitol, respectively. These bands shifted towards 4389  $\text{cm}^{-1}$  and 5538  $\text{cm}^{-1}$  after extrusion which could

be due to the formation of H-bonds among the sugar moieties. The band shifting could be attributed to the formation of hydrogen bonding as a result of the formation of cocrystals between pearlitol, sorbitol and xylitol. It can also be seen from the spectra collected from the extruded cocrystal that there are two other new bands at 5748 and 4620  $\text{cm}^{-1}$ , which could also be due to the formation of H-bonds between the three sugar moieties.

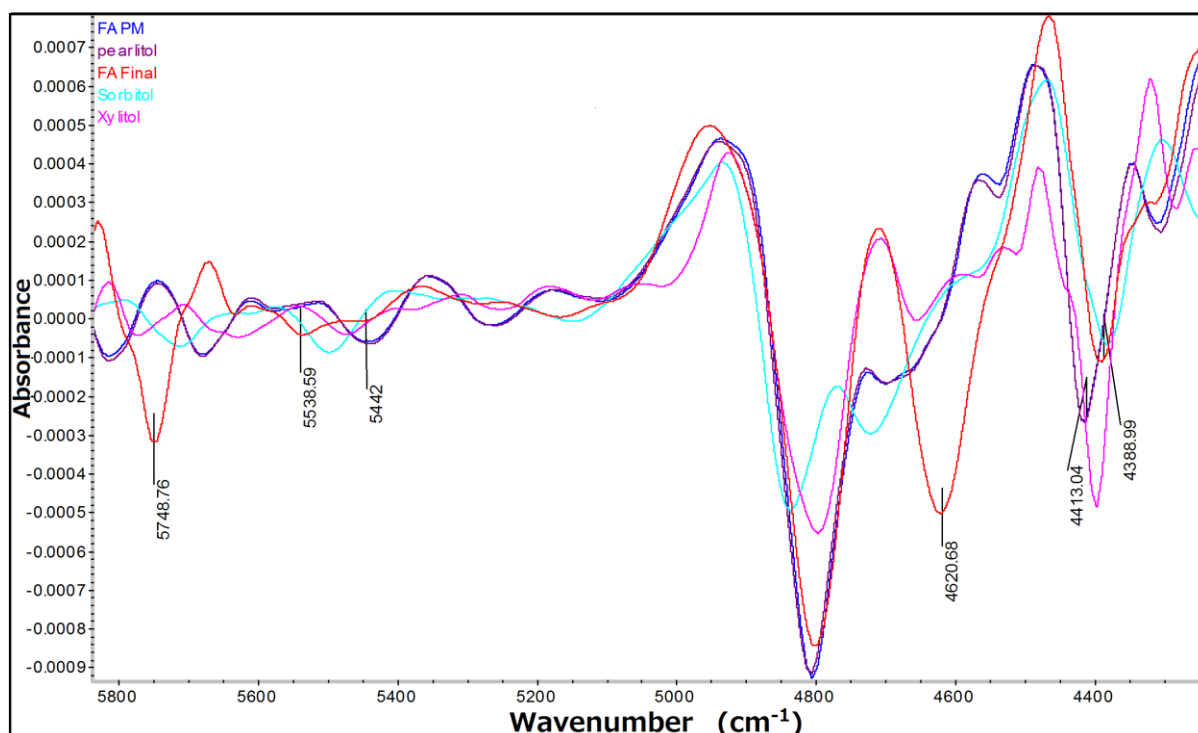


**Fig. 4.20.** Second derivative NIR spectra of raw materials (pearlitol, xylitol and sorbitol), a physical mixture and the extrudate of FA in the 5800 – 4300  $\text{cm}^{-1}$  wavenumber region.

As the physical mixture of FA are transferred within the conveying and mixing zones, the formation of cocrystals is expected to gradually take place along the barrel [27]. In order to further study cocrystal formation the in-line NIR probe was carefully inserted in the three mixing zones and spectra were collected [17-18]. **Fig. 4.21** shows the second derivative spectra collected from the three different mixing zones and the final extruded cocrystals compared to the physical mixture. Spectra collected at the first mixing zone (ZA) of the HME barrel were similar to the physical mixture indicating that no significant changes occurred. It was clear that the formation of cocrystals started in the second mixing zone of the HME barrel as the bands started to shift. The spectra obtained from mixing zone ZC of the HME barrel showed new vibrational bands as the extrudates moved towards the end of the extruder.

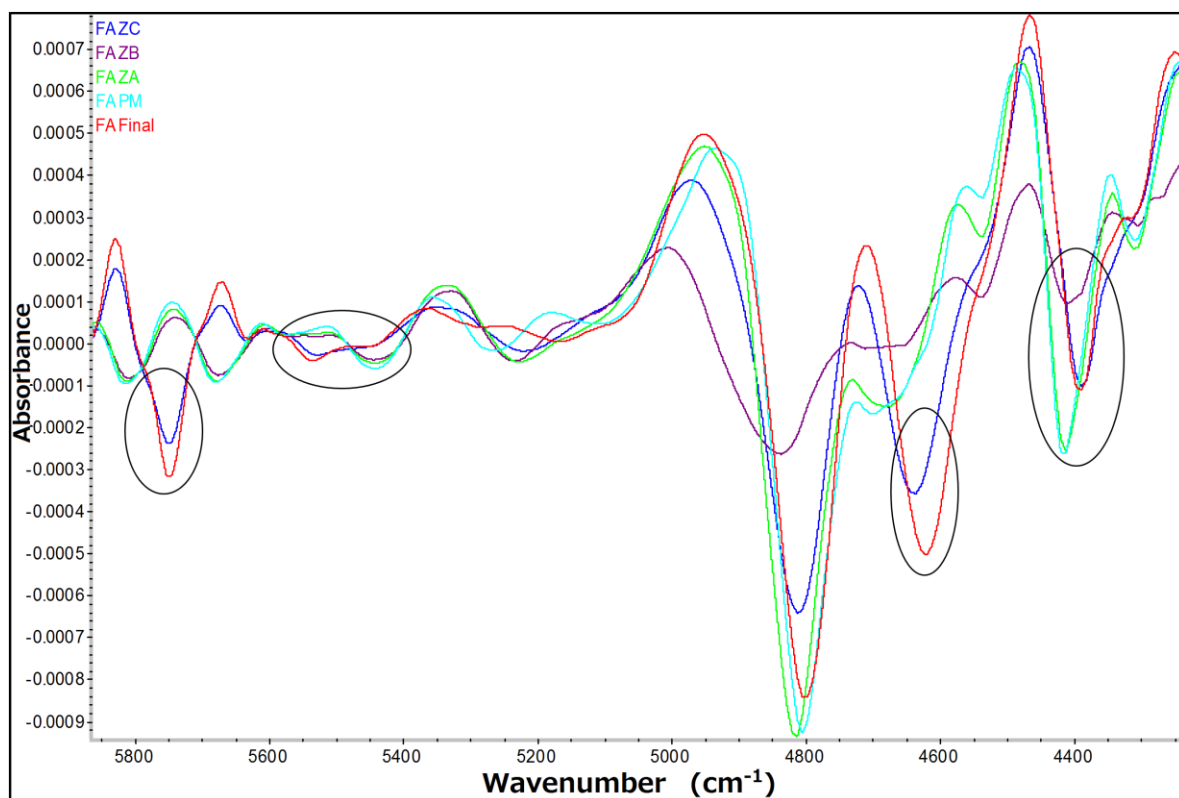


**Fig. 4.21.** Second derivative off-line NIR spectra of a physical mixture, in-line NIR spectra collected from different mixing zones during extrusion and the final extrudates of FA.

A similar kind of synthesis pattern of the cocrystals has also been detected using in-line NIR monitoring for the other two formulations (FB and FC; **Fig. 4.22** and **Fig. 4.23**). These finding suggests that cocrystals were formed gradually due to the increasing mixing capacity along the mixing zones of the HME.

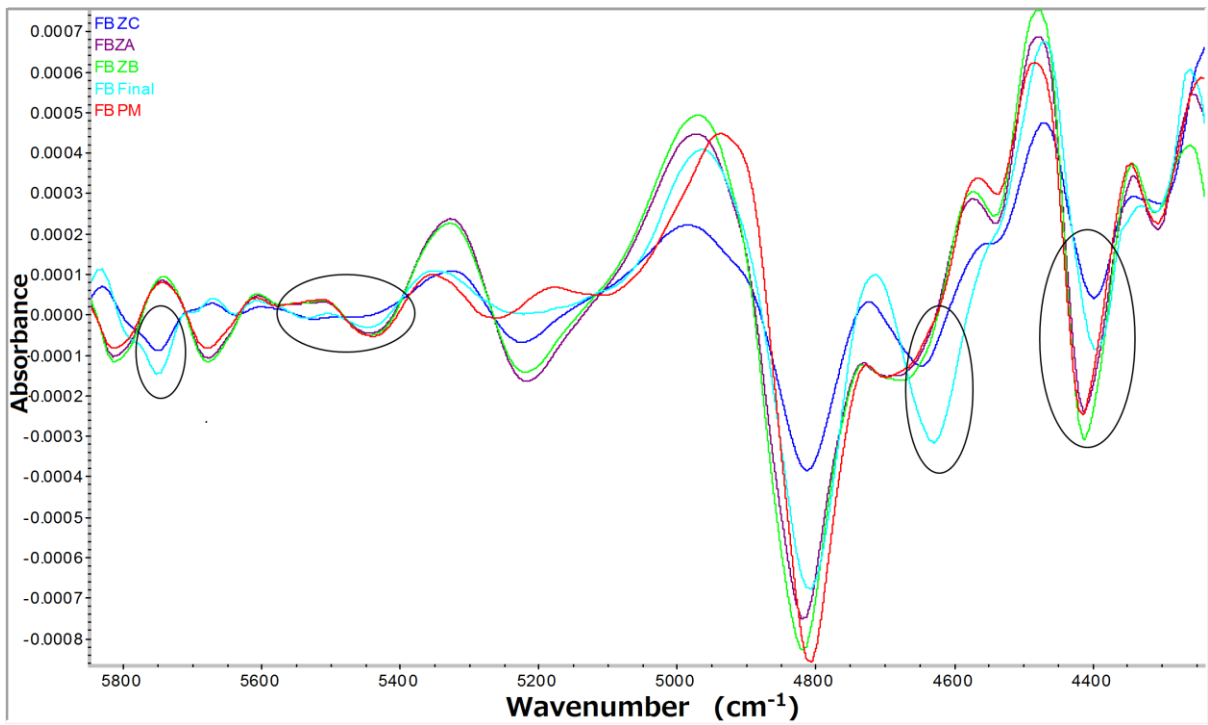


**Fig. 4.22.** Second derivative off-line NIR spectra of a physical mixture, in-line NIR spectra collected from different mixing zones during extrusion and the final extrudates of FB.

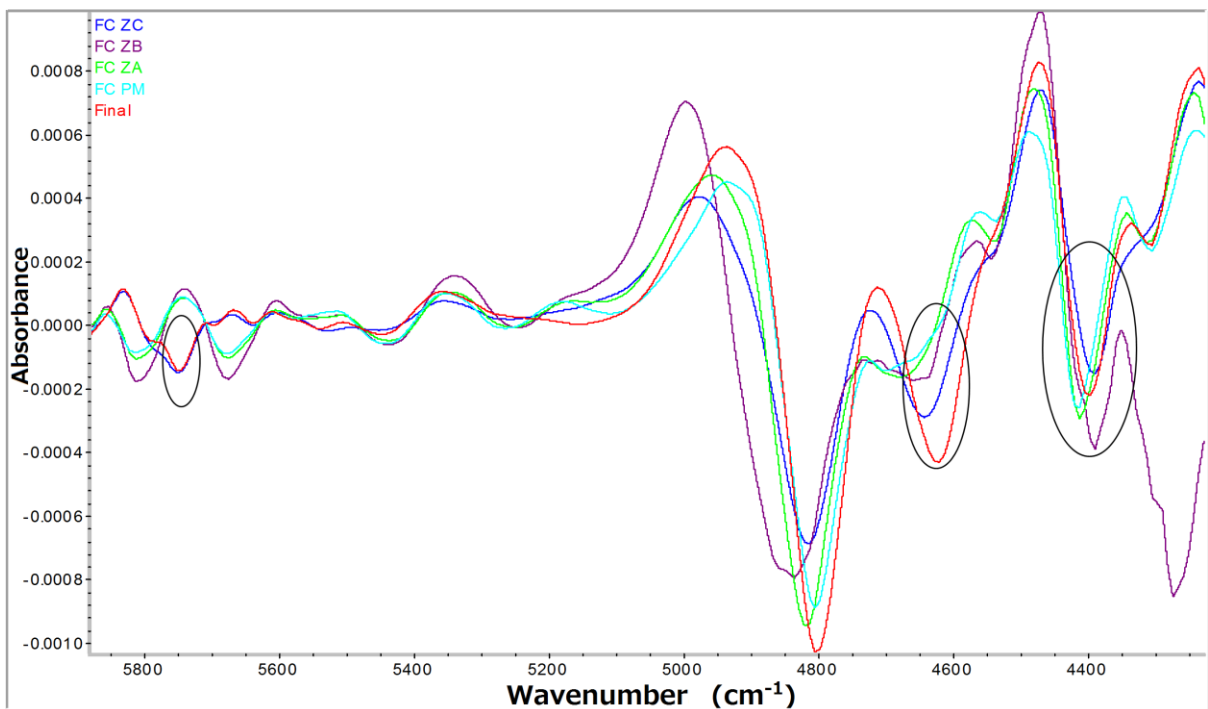


**Fig. 4.23.** Second derivative off-line NIR spectra of a physical mixture, in-line NIR spectra collected from different mixing zones during extrusion and the final extrudates of FC.

### 4.3.6. Particle size analysis

Cocrystals produced from formulations (FA-FC) after extrusion were then passed via a rotary cutter mill to grind them through a 250  $\mu\text{m}$  mesh to achieve less than 250  $\mu\text{m}$  particle sizes. The particle size distribution obtained (**Fig. 4.24** and **Fig. 4.25**) show a low fraction of fine particles with only less than 10% below 50  $\mu\text{m}$ . Similarly a small particle fraction of less than 10% was observed between 400-500  $\mu\text{m}$ . The majority of particles lay in the size of 100 – 250  $\mu\text{m}$  for all of the extruded formulations (FA, FB and FC).

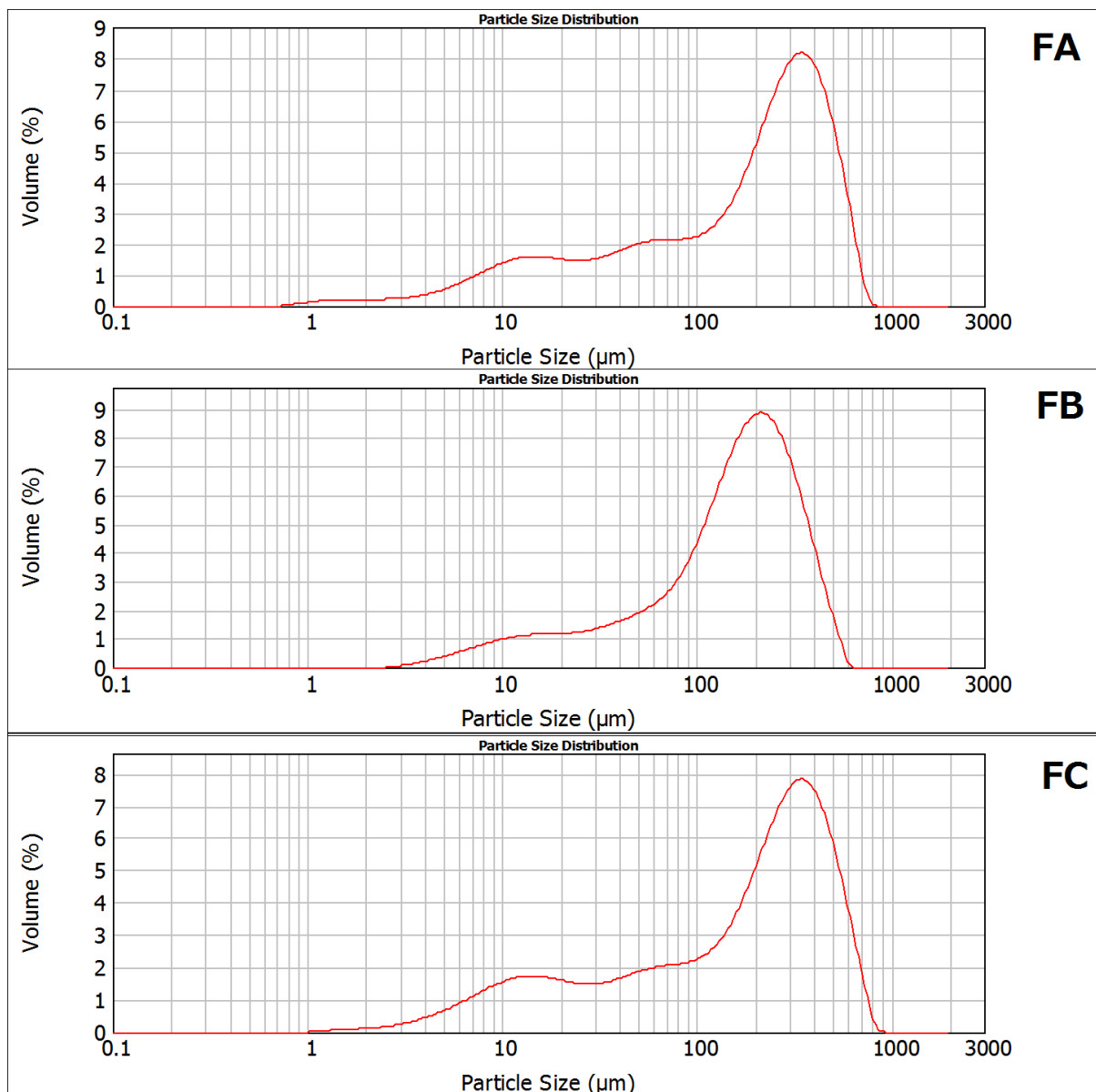


**Fig. 4.24.** Particle size distribution for the extruded formulations (FA-FC).

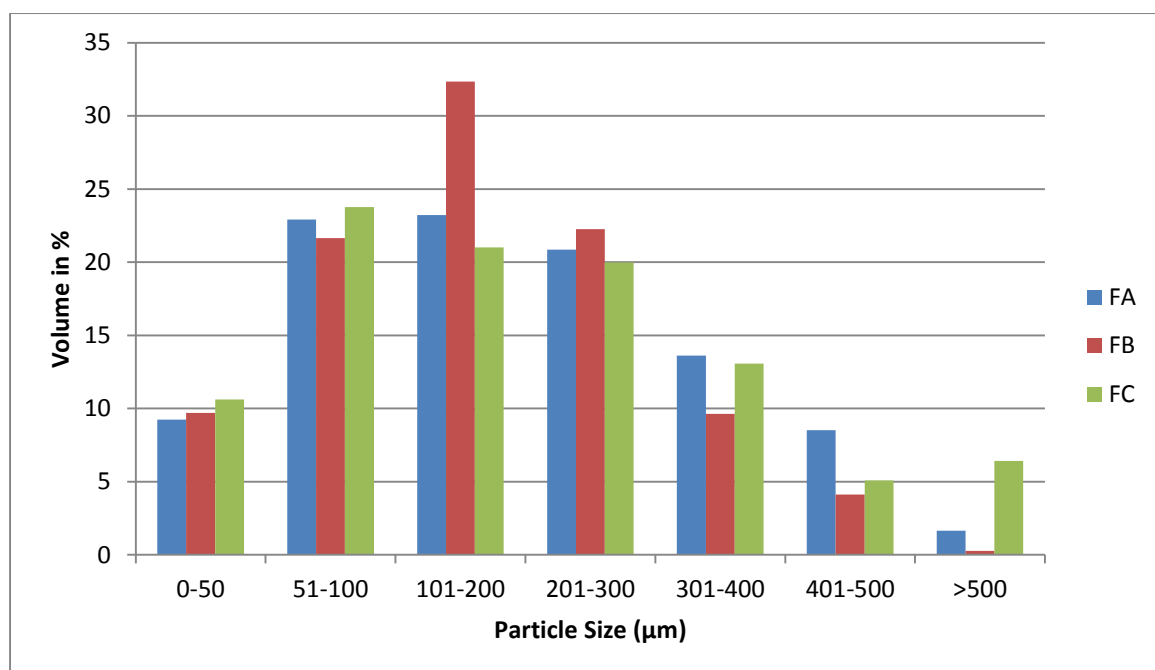


**Fig. 4.25.** Particle size distribution of micronized sugar cocrystals of the extrudates of FA-FC.

#### 4.3.7. Tablet preparation

The granules (cutter milled of the extrudates) of F1-F3 and F9 were not suitable for tableting due to stickiness of the powder and flow properties. The other extruded formulations (F4-F8 and FA-FC) were subjected to tableting without the addition of the API (placebo formulations). The formulations for the tablets were composed of 250 mg of extrudate granules with 1% Mg-stearate and 0.25% silica in each batch.

Furthermore, extruded sugar formulations (FA-FC) and Starlac (commercial binder) were blended with PMOL as an API and other ingredients prior to tableting. The composition of the batches comprising extruded sugars (FA-FC) for tableting with PMOL are shown in **Table 4.2**. The different mixtures of sugars are extruded as a molten mass and then cutter-milled to produce granules. Then PMOL and other excipients are added and then the formulation is tabletted.

All the placebo formulations (F4-F8 and FA-FC) and the PMOL loaded formulations (PLF1-PLF4) were characterized in terms of compressibility (Carr's index). It can be seen from the data in **Table 4.3**, all the batches showed excellent compressibility and flowability properties excluding F8, which gave us confidence to undertake tableting of the extruded formulations (F4-F7, FA-FC and PLF1-PLF4).

**Table 4.2.** Composition of tablet formulations blended with PMOL as an API (PMOL loaded formulations, PLFs)

<b>API/excipients</b>	<b>PLF1</b>	<b>PLF2</b>	<b>PLF3</b>	<b>PLF4</b>
FA	250 mg	-	-	
FB	-	250 mg	-	-
FC	-	-	250 mg	-
Starlac	-	-	-	250 mg
PMOL	250 mg	250 mg	250 mg	250 mg
Mg-stearate	1%	1%	1%	1%
Silica	0.25%	0.25%	0.25%	0.25%

**Table 4.3.** Compressibility properties of placebo formulations and PMOL loaded formulations.

	<b>Bulk density</b>	<b>Tapped density</b>	<b>Carr's index</b>
<b>Starlac</b>	0.60	0.66	9.09
<b>F4</b>	0.42	0.47	10.63
<b>F5</b>	0.41	0.48	14.58
<b>F6</b>	0.36	0.42	14.28
<b>F7</b>	0.37	0.43	13.95
<b>F8</b>	0.36	0.44	18.18
<b>FA</b>	0.54	0.62	12.12
<b>FB</b>	0.40	0.46	12.50
<b>FC</b>	0.54	0.64	14.71
<b>PLF1</b>	0.59	0.66	10.67
<b>PLF2</b>	0.60	0.66	9.37
<b>PLF3</b>	0.59	0.64	8.75
<b>PLF4</b>	0.58	0.63	9.40

### 4.3.8. Tablet characterization

Tablets made from placebo formulations (F4-F7 and FA-FB) and PMOL loaded formulations (PLF1-PLF3) were subjected to various product quality check including weight uniformity test, thickness, hardness, friability and disintegration test (**Table 4.4** and **Table 4.5**).

**Table 4.4.** Tablet characterization of placebo formulations and Starlac (no PMOL).

	<b>Compression force (kN)</b>	<b>Weight uniformity (mg)</b>	<b>Thickness (mm)</b>	<b>Hardness (Kp)</b>	<b>Friability (10<sup>-4</sup> g)</b>	<b>Disintegration time (sec)</b>
<b>F4</b>	5	260	2.75	10.1	-	>60
	10	260	2.64	14.8	-	>60
	15	230	2.29	14.2	4.3	>60
	20	220	2.26	12.3	4.3	>60
	25	260	2.55	13.3	3.3	>60
<b>F5</b>	5	290	2.96	10.0	4.6	80
	10	280	2.85	16.5	4.4	75
	15	310	3.06	23.3	3.8	>60
	20	300	2.88	22.4	3.0	>60
<b>F6</b>	2.5	200	2.53	2.8	11.5	50
	5	220	2.46	4.5	7.3	60-70
	10	210	2.20	7.5	3.7	60
	15	220	2.25	10.7	3.8	50-60
	20	210	2.16	11.2	4.4	60
<b>F7</b>	2.5	250	3.05	2.5	18.5	45
	5	240	2.70	4.5	14.6	60
	10	190	2.13	8.1	-	60
	15	210	2.23	10.8	8.5	60-70

	20	230	2.42	16.0	110.8	60-70
<b>Starlac</b>	2.5	260	3.32	0.6	-	40
	5	250	2.95	1.4	-	40-45
	10	240	2.62	3.6	32.2	35-40
<b>FA</b>	5	310	1.85	2.4	0	120
	10	300	1.64	3.3	0	120
	15	263	1.20	3.5	0.7992	120
<b>FB</b>	5	300	1.87	1.2	Tablet broken	120
	10	300	1.70	2.7		120
<b>FC</b>	5	293	1.78	0.6	Tablet broken	61
	10	277	1.65	1.2		120

All the tablets prepared without API (**Table 4.4**) shows similar values of weight and thickness. However, the hardness of the tablets varied with varying compression forces applied. It has been noticed that the higher the compression forces higher the hardness of the tablets, which suggests the good compactibility of the products. Interestingly FA-FC showed low hardness values compared with others (F4-F7). It has also been noticed that tablets prepared from FB-FC were broken during friability test.

All the tablets manufactured with API (PMOL loaded formulations with extruded sugar cocrystals, **Table 4.5**) also showed similar values of weight, thickness and hardness. All the tablets made from PLF1 and PLF4 had less visual defects (e.g. capping) whereas high visual defects were observed after compressing the batches PLF2 and PLF3. Capping occurred due to the stickiness of the materials with the upper punch. From the evaluation of the tablets it is clear that the PLF1 has better compressibility compared with the other two batches prepared from extruded sugars (PLF2-PLF3) and tablets prepared from commercial binder Starlac (PLF4). From the friability result it can be seen that PLF1 has lower friability than the PLF4 whilst few tablets were broken in case of PLF2 and PLF3.

**Table 4.5.** Tablet characterization of PMOL loaded formulations composed of extruded sugar cocrystals and Starlac.

	<b>Weight uniformity test (mg)</b>	<b>Thickness (mm)</b>	<b>Hardness (Kp)</b>	<b>Friability (%)</b>	<b>Disintegration time (sec)</b>
<b>PLF1</b>	516 ± 2.8%	3.17 ± 0.01	6.0 ± 0.8	0.045%	2 min 49 sec
<b>PLF2</b>	513 ± 3.6%	3.16 ± 0.03	6.4 ± 0.2	2 tablets broken	3 min 21 sec
<b>PLF3</b>	513 ± 2.8%	3.16 ± 0.03	6.4 ± 0.2	3 tablets broken	3 min 29 sec
<b>PLF4</b>	515 ± 3.0%	3.24 ± 0.09	6.1 ± 0.8	0.046%	2 min 58 sec

Disintegration time is a useful tool to quantify the water uptake into the tablet until complete disintegration is reached. This effect depends on the porosity of the tablet and on the wettability of the pores [28]. In this study, all tablets showed disintegration times above 60s, which are indicative of good characteristics for oral applications. Interestingly, in case of tablets prepared without API, placebo formulations (F4-F7) showed less disintegration time whilst FA-FC showed high disintegration time but the formulations (F4-F7) weren't formed any cocrystals after extrusion excluding F6. However, in case of tablets prepared with PMOL as an API, PLF1 showed better disintegration time compared with other formulations blended with PMOL (PLF2-PLF4). From this observation it can be concluded that using suitable sugar weight ratios in conjunction with precise HME processing parameters successful sugar cocrystals would be possible to made, and could have suitable tableting properties (compressibility, flow properties), friability and disintegrations time compared with commercial binders.

#### **4.4. Conclusions**

Cocrystals formed of three different sugars were successfully produced via HME processing. In-line NIR monitoring revealed the cocrystallization occurred due to the intense mixing of the materials while passing through the mixing zones of the extruder during HME, which has been confirmed by DSC and XRPD as reference methods. However, all of the extruded formulations after grinding showed excellent flow properties compared with the

commercial binder. Tablets prepared from the extruded grounded sugar cocrystals using specific weight ratios of sugars show good compressibility, friability and less disintegration time compared with tablets prepared from the commercial binder (Starlac).

#### 4.5. References

1. Almeida A, Claeys B, Remon JP, Vervaet C, Hot-melt extrusion developments in the pharmaceutical industry, In: Douroumis D, (ed.) Hot-melt extrusion: pharmaceutical application, Oxford, John Wiley & Sons Ltd, 2012: 43-69.
2. Maniruzzaman M, Boateng JS, Snowden MJ, Douroumis D, A review of hot-melt extrusion: process technology to pharmaceutical products. International Scholarly Research Notices, 2012, doi:10.5402/2012/436763.
3. Andrews GP, Jones DS, Hot melt extrusion- processing solid solutions? Journal of Pharmacy and Pharmacology, 2014; **66**(2): 145-147.
4. Repka MA, Battu SK, Upadhye SB, Thumma S, Pharmaceutical applications of hot-melt extrusion: Part II, Drug Development and Industrial Pharmacy, 2007; **33**: 1043–1057.
5. Kolter K, Karl, Gryczke A, Hot-Melt Extrusion with BASF Pharma Polymers: Extrusion Compendium, 2nd edn. Ludwigshafen: BASF SE Pharma Ingredients and Services, 2012.
6. Dhirendra K, Lewis S, Udupa N, Atin K, Solid dispersions: a review, Pakistan Journal of Pharmaceutical Sciences, 2009; **22**: 234–246.
7. Vasconcelos T, Sarmiento B, Costa P, Solid dispersions as strategy to improve oral bioavailability of poor water soluble drugs, Drug Discovery Today, 2007; **12**: 1068–1075.
8. Food and Drug Administration, 2004, <http://www.fda.gov/downloads/Drugs/GuidanceComplianceRegulatoryInformation/Guidances/ucm070305.pdf>.
9. EUFEPS QbD and PAT Sciences Network, <http://www.eufeps.org/PATnetwork.html>, 2010
10. De Beer T, Burggraeve A, Fonteyne M, Saerens L, Remon JP, Vervaet, C, Near infrared and Raman spectroscopy for the in-process monitoring of pharmaceutical production processes, International Journal of Pharmaceutics, 2011; **417**: 32– 47.

11. Saerens L, Vervaet C, Remon JP, De Beer T, Process monitoring and visualization solutions for hot-melt extrusion: a review, *Journal of Pharmacy and Pharmacology*, 2014; **66**(2): 180-203.
12. Atiipamula S, Chow PS, Tan RBH, Polymorphism in cocrystals: a review and assessment of its significance, *CrystEngComm*, 2004; **16**: 3451-3465
13. Qiao N, Li M, Schlindwein W, Malek N, Davies A, Trappitt G, Pharmaceutical cocrystals: An overview, *International Journal of Pharmaceutics*, 2011; **419**: 1-11.
14. Bhandari BR, Hartel RW, Co-crystallization of sucrose at high concentration in the presence of glucose and fructose, *Journal of Food Sciences*, 2002; **67**(5): 1797–1802.
15. Yadav AV, Shete AS, Dabke AP, Kulkarni PV, Sakhare SS, Co-crystal: A novel approach to modify physicochemical properties of active pharmaceutical ingredients, *Indian Journal of Pharmaceutical Sciences*, 2009; **71**(4): 359-370.
16. Dhumul RS, Kelly AL, Cocrystallization and simultaneous agglomeration using hot melt extrusion, *Pharmaceutical Research*, 2010; **27**(12): 2725-2733.
17. Moradiya H, Islam MT, Woollam GR, Slipper IJ, Halsey S, Snowden MJ, Douroumis D, Continuous cocrystallization for dissolution rate optimization of a poorly water-soluble drug, *Crystal Growth & Design*, 2014; **14**: 189-198.
18. Moradiya H, Islam MT, Halsey S, Maniruzzaman M, Chowdry B, Snowden MJ, Douroumis D, Continuous cocrystallisation of Carbamazepine and *trans*-Cinnamic acid via melt extrusion processing, *CrystEngComm*, 2014; **16**: 3573-3583.
19. Chen C, *International Sugar Journal*, 1994; **96**: 493-496
20. Frankenbach GM, (PhD thesis), The preparation and characterization of hydrogen-bonded cocrystals with application of material science, 1989.
21. Geary PM, (PhD thesis), The cocrystallisation of sugars by the supersaturation process, The University of Hull, 2008.
22. DuRoss JW, Melt cocrystallized sorbitol/xylitol compositions, US Patent 5158789A, 1991.
23. DuROss JW, Crystalline sugar alcohol containing uniformly dispersed particulate pharmaceutical compound, US Patent 5075291, 1989.
24. Habibh W, Khankarik R, Hontz J, Fast-dissolve drug delivery system, *Critical Reviews™ in Therapeutic Drug Carrier System*, 2000; **17**: 61-72.
25. Douroumis D, Practical approaches of taste masking technologies in oral solid forms, *Expert Opinion on Drug Delivery*, 2007; **4**: 417-426.

26. Gryczke A, Schminke S, Maniruzzaman M, Beck J, Douroumis D, Development and evaluation of orally disintegrating tablets (ODTs) containing Ibuprofen granules prepared by hot melt extrusion, *Colloids and Surfaces B: Biointerfaces*, 2011; **86**(2): 275-284.
27. Kelly AL, Gough T, Dhumal RS, Halsey SA, Paradkar A, Monitoring ibuprofen–nicotinamide cocrystal formation during solvent free continuous cocrystallization (SFCC) using near infrared spectroscopy as a PAT tool, *International journal of pharmaceuticals*, 2012; **426**(1–2): 15-20.
28. Luginbuhl R, Leuenberger H, Use of percolation theory to interpret water uptake, disintegration time and intrinsic dissolution rate of tablets consisting of binary mixtures, *Pharmaceutica Acta Helvetiae*, 1994; **69**(3): 127–134.

## Chapter 5: Implementation of transmission NIR as a PAT tool for monitoring drug transformation during HME processing

---

### 5.1. Introduction

Hot melt extrusion (HME) is an emerging processing technology for the development of solid drug dispersions embedded in a carrier matrix for the development of oral solid dosage pharmaceutical forms [1-3]. The technique has been adopted in pharmaceutical research due to its versatility and the several advantages that it offers compared to traditional manufacturing techniques. For example, HME is solvent free, a wide range of excipients can be processed, it is cost effective, and can be easily scaled-up with high throughput and operated in continuous mode [4]. HME has been utilized to enhance the dissolution rate of APIs by preparing solid dispersions [5, 6] where the drug is molecularly dispersed in the polymer matrix which leads to improved bioavailability [7, 8]. Hulsmann *et al.*, utilized HME to increase the rate of solubility of poorly water-soluble drugs, 17-estradiol hemihydrates [9, 10], using PEG 6000, PVP polymers or a vinylpyrrolidone-vinylacetate copolymer within the polymer matrix and by using sucroester WE15 or Gelucire® 44/14 as functional excipients. The formulation mixtures were extruded as rods, milled into granules and finally compressed into tablets. The solid dispersions thus formed exhibited a significant increase in dissolution rate compared to the pure (bulk) drug or to the physical mixtures. Sun *et al.*, prepared a semi-solid capsule containing a solid dispersion of nimodipine processed with Eudragit® E100 and Plasdone® S630 using a twin-screw extruder [11]. The extruded solid dispersion was formulated into gelatine capsules followed by *in vivo* studies in beagle dogs and compared with a marketed product of the same drug. The *in vivo* comparison revealed faster absorption of nimodipine for the hot-melt extruded formulations compared to the marketed product.

The Food and Drug Administration (FDA) introduced the concept of Process Analytical Technologies (PAT) in 2004 for a better fundamental scientific understanding of manufacturing processes [12, 13] and to ensure the final quality of the end product [14]. The aim of this initiative is to implement appropriate measurement tools, which can be placed at/in- or on-line for monitoring and data analysis via a scientific approach such as chemometrics and Quality by Design (QbD) approach to ensure production of in-process materials and the final quality of products [15].

HME is among the technologies that can be coupled with PAT tools for the development of pharmaceutical solid dosage forms. In-line reflectance NIR and in-line Raman spectroscopy have also been used as PAT tools in order to understand drug-polymer interactions and to validate a method for continuous API quantification during HME processing [16, 17]. The application of in-line NIR spectroscopy to monitor the extrusion process was demonstrated by Fischer *et al.*, [18] who successfully determined the content of ethylene vinyl acetate in a polypropylene matrix. Off-line and in-line reflectance NIR has also been used to monitor the formation of ibuprofen-nicotinamide [19], carbamazepine-saccharine [20] and carbamazepine-*trans*-cinnamic acid [21] cocrystals. In-line reflectance NIR was combined with a QbD approach for the optimisation of paracetamol sustained release formulations and the identification of the optimal extrusion parameters [22]. However, reflectance NIR contains large amount of noise in the spectra when monitoring a transparent formulation. In contrast, transmission NIR has also been reported for studies of single screw polymer extrusion of low [23] and high [24, 25] density polyethylene/polypropylene co-polymers. But, the use of transmission NIR for the characterization of an API extrusion processed via HME has not been reported. Using NIR as a non-destructive on-line monitoring tool for the impact of critical process parameters (feed-rate, screw speed, temperature) improves process efficiency and product quality as adjustments to the process can be made in real time when deviations in the process are detected during HME. This was shown by Coates *et al.*, [24] for polyethylene-propylene blends where rapid and accurate determination of the ethylene content is essential. Thus it is important to employ an analytical method, such as transmission NIR, for monitoring transparent extrudates of an API produced by HME [26].

In this study, a transmission NIR probe was used for in-line monitoring of transparent extruded film formulations; the NIR probe was inserted in a specially designed extrusion die. In addition HME processing was coupled with both transmission and reflectance NIR probes in order to provide a more detailed understanding of the physical transformations of the drug during extrusion. For the purposes of the study, indomethacin (IND) was extruded with the hydrophilic polymers Soluplus (SOL) or Kollidon VA64 (VA64) at various drug/polymer ratios. Previous studies showed that the extrusion of IND with these polymers leads to molecular solutions with improved drug dissolution rates compared to the bulk drug [7].

## 5.2. Materials and methods

### 5.2.1. Materials

Indomethacin (IND) was supplied by Tokyo Chemical Industry Co. Ltd (Tokyo, Japan), Soluplus (polyvinyl caprolactam-polyvinyl acetate-polyvinyl- glycol graft copolymer) and Kollidon VA64 (vinylpyrrolidone-vinyl acetate copolymer) were kindly donated by BASF (Ludwigshafen, Germany). HPLC solvents (acetonitrile, acetic acid) were of analytical grade and purchased from Fisher Scientific (Loughborough, UK). All chemicals were used as received.

### 5.2.2. Hot-melt extrusion process

HME was performed by using a Eurolab 16 mm twin screw extruder (Thermo Fisher Scientific, Karlsruhe, Germany). The HME extruder was equipped with a DD Flexwall® 18 volumetric feeder (Brabender Technology, Duisburg, Germany).

Seven different formulations of IND/SOL and IND/VA64, at different weight ratios, were extruded (**Table 5.1**). Prior to HME, the drug and polymer were blended in a Turbula TF2 mixer (100 rpm) (Basel, Switzerland) for 10 min in order to obtain a homogeneous mix. The barrel temperature profile was set at (50/100/120/135/145/150/150/150/140)°C (from feeder to die) for batches F1-F5 and at (50/100/120/150/150/150/150/150/140)°C for formulations F6 and F7.

A newly manufactured transmission die (**Fig. 5.1A**) was fitted at the end of the extruder barrel in order to collect in-line transmission NIR spectra (**Fig. 5.2**). The die was made of stainless steel, with a 1 mm die opening where the transmission NIR probe can be inserted and the distance between the incident and the transmitted radiation was therefore 1 mm (slit size) so that the infra-red radiation can pass through the transparent extrudates and be transmitted to the NIR detector.

**Table 5.1.** Composition of IND extruded formulations with SOL and VA64 at various drug: polymer ratios.

<b>Formulations</b>	<b>IND (% w/w)</b>	<b>SOL (% w/w)</b>	<b>VA 64 (% w/w)</b>	<b>Screw speed</b>
<b>F1</b>	20	-	80	50
<b>F2</b>	40	-	60	50
<b>F3</b>	20	80	-	50
<b>F4</b>	40	60	-	50
<b>F5</b>	50	50	-	50
<b>F6</b>	50	50	-	200
<b>F7</b>	50	50	-	400

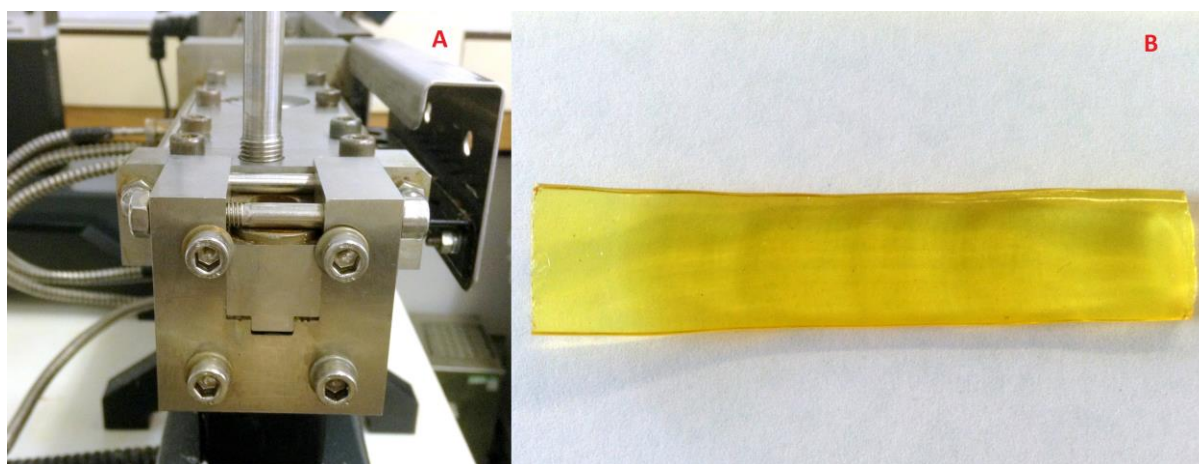


**Fig. 5.1.** The special die (A) made for in-line NIR monitoring via a transmission NIR probe and (B) an example of an extruded film.

### 5.2.3. Thermal analysis

The physical state of bulk IND, the physical mixtures and the granules prepared from extruded films were analysed by DSC using a Mettler-Toledo 823e (Greifensee, Switzerland) instrument. Accurately weighed samples (2-3 mg) were placed in aluminium pans and sealed. Measurements were carried out under a dry nitrogen gas atmosphere at a flow rate of 50 mL/min using a heating rate of 10.0°C/min from 0°C to 180°C.

Drug-polymer miscibility is related to the shift(s) in the melting endotherm or glass transition temperature of the drug [27]. Based on the Gordon-Taylor equation [28], if the drug and polymer are miscible then the mixture will show a single  $T_g$  that ranges between the  $T_g$  of the pure components and would depend on the relative proportion of each component. The  $T_g$  of the mixtures can be predicted using the Gordon-Taylor equation:

$$T_{g\text{ mix}} = \frac{w_1 \times T_{g1} + K \times w_2 \times T_{g2}}{w_1 + K \times w_2}$$

Where,  $T_g$  is the glass transition temperature,  $w_1$  and  $w_2$  are the weight fractions of components and  $K$  is calculated from the densities ( $\rho$ ) and  $T_g$  of the amorphous components:

$$K = \frac{T_{g1} \times \rho_1}{T_{g2} \times \rho_2}$$

### 5.2.4. X-ray powder diffraction

XRPD was used to assess the crystalline state of the IND, the physical mixtures and the hot-melt extrudates. All formulations including pure IND, physical mixtures and extruded formulations were evaluated using a Bruker D8 (Karlsruhe, Germany) Advance instrument in theta–theta mode, using a Cu anode at 40 kV and 40 mA, parallel beam Goebel mirror, 0.2 mm exit slit, LynxEye Position Sensitive Detector with 3° opening and LynxIris at 6.5 mm and sample rotation at 15 rpm. The samples were scanned from 2 to 40° 2-theta with a step size of 0.02° 2-theta and a counting time of 0.2 s per step; 176 channels active on the PSD making a total counting time of 35.2 s per step.

### 5.2.5. Near-infrared spectroscopy (NIR)

Transmission and reflectance NIR spectra were continuously collected in-line and non-invasively during hot-melt extrusion using a Fourier-Transform Antaris MX NIR analyser (Thermo Fisher Scientific, United Kingdom) equipped with an InGaAs detector, a quartz halogen lamp, and a fibre optic probe which was attached in the extrusion die. Spectra were collected every 1 min in the 10000-4000  $\text{cm}^{-1}$  wavenumber region with a resolution of 16  $\text{cm}^{-1}$  and averaged over 32 scans. A transmission probe was fitted at the end of the extruder orifice (die) and the reflectance probe was inserted in the first mixing zone of the extruder barrel (**Fig. 5.2**).

NIR data analysis was performed by using the Result Software (Version 3.0, Thermo Fisher Scientific, UK). Spectra collected in both diffuse reflectance and transmission modes usually require spectral pre-treatment before analysis. The degree of scattering depends on the wavelength of the incident radiation and the refractive index of the sample, which causes an uneven scatter over the whole spectrum. This can result in a baseline shift. Therefore, standard normal variate (SNV) correction was used before chemometric analysis of the spectra. Using SNV, unwanted scatter was removed from the raw spectra to prevent it from dominating over chemical information within the spectra. The result of SNV pre-processing is that each spectrum has the same offset and amplitude, eliminating difference in light scatter in the spectra from different samples, before developing the calibration model. Furthermore, second derivative pre-processing was undertaken after SNV correction. Second derivative NIR spectra magnify differences in spectral features, provide baseline normalisation and remove data offsets due to scattering effects and path length variation. For principal component analysis (PCA) and for the development of a partial least square (PLS) model, 10 spectra of each drug-polymer mixture were used. Prior to PCA and PLS, spectra were mean centred. The PLS model was developed by regressing the IND concentration ( $Y$ ) versus the corresponding in-line collected spectra ( $X$ ). This model was validated by using off-line NIR spectra collected for each drug-polymer mixture. These validation spectra were used to evaluate the predictive performance of the PLS model.

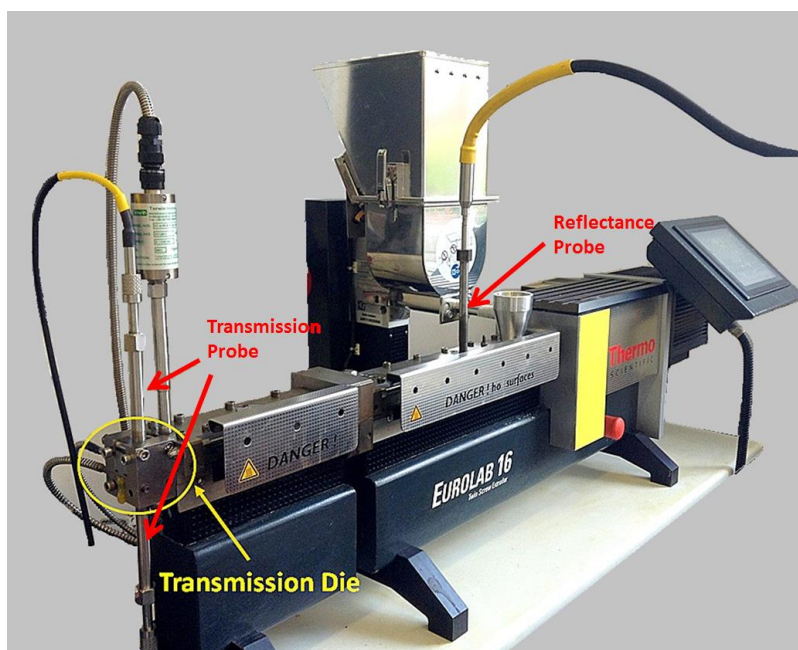


**Fig. 5.2.** In-line NIR probes (transmission and reflectance) attached to the HME.

### **5.2.6. Confocal Raman spectroscopy**

Raman mapping was performed using a Jobin/Yvon LabRam 320 instrument equipped with an Olympus microscope (Horiba, Japan) by means of a He-Ne ion laser ( $\lambda = 632.8$  nm) and 1800 l/nm. The experimental conditions were: 100 nm slit width, a 50 $\times$  Microsoft objective and 0.2 s acquisition times. Each spectrum was the mean of two. The sample profiling was performed at step increments of 8  $\mu\text{m}$  in the X–Y direction over an area of 2000 x 600  $\mu\text{m}^2$ . PCA was used for data analysis. Prior to the analysis, all spectra were base line corrected and normalised using the standard normal variates method (SNV) to avoid intensity deviation among the Raman spectra. The Raman chemical maps were constructed by using Solo + Mia software (Eigenvector, Research, Inc. Wenatchee, USA).

### **5.2.7. *In-vitro* drug release studies**

The release profiles for IND (bulk and granules produced from the extruded films using a cutter mill) were obtained using a Varian 705 DS dissolution paddle apparatus (Varian Inc. North Carolina, US). The analysis was carried out using dosage forms containing 50 mg of IND, in 900 mL of dissolution medium maintained at  $37.0 \pm 0.5^\circ\text{C}$  and agitated at 100 rpm. A phosphate buffer solution pH 6.8 was used the dissolution medium. At pre-established time intervals 5 mL samples were withdrawn from the dissolution medium, filtered through a 0.45  $\mu\text{m}$  mesh, and analysed using HPLC. All dissolution studies were performed in triplicate.

### 5.2.8. HPLC analysis

The release of IND, in the dissolution studies, was determined by using an Agilent Technologies HPLC 1200 series system equipped with a HICROM S50DS2, 5  $\mu\text{m}$  x 150 mm x 4 mm column using a 20  $\mu\text{l}$  injection volume and a detection wavelength of 298 nm. The mobile phase consisted of acetonitrile/water (1% acetic acid) (70:30 v/v). The flow rate was adjusted to 1.5 mL/min and the retention time of IND was about 4 min. A calibration curve for IND (10–50  $\mu\text{g}/\text{mL}$ ) was used to quantitate all the samples.

## 5.3. Results and discussion

### 5.3.1. Hot-melt extrusion process

The objective of this study was to investigate, for the first time, the implementation of in-line transmission and reflectance NIR probes in order to understand the transformation of the API (IND), in the presence of the polymers, from a crystalline phase to an amorphous phase during HME processing. The use of an NIR transmission probe for in-line monitoring during HME has not been previously reported and in this case it was used to record the NIR signals from molecular solutions or amorphous solid dispersions. It is known that a drug-polymer system is considered miscible if the difference between their solubility parameters is less than 7.0  $\text{MPa}^{1/2}$  [29]. Binary blends with differences in solubility parameters higher than 10  $\text{MPa}^{1/2}$  are likely to be immiscible. Maniruzzaman *et al.*, [7] showed that the solubility parameters for IND, VA64 and SOL are 22.84  $\text{MPa}^{1/2}$ , 19.63  $\text{MPa}^{1/2}$  and 19.40  $\text{MPa}^{1/2}$ , respectively. As the solubility parameter difference between IND and VA64 is 3.21  $\text{MPa}^{1/2}$  and that for IND and SOL is 3.44  $\text{MPa}^{1/2}$ , glassy solutions will be obtained during HME processing via sufficient miscibility of IND with both polymers. Using a die orifice (**Fig. 5.1A**) with a 1 mm slit size results in the production of IND/polymer extrudates in the form of transparent films (**Fig. 5.1B**). The film thickness was also 1 mm which facilitated the monitoring process using the in-line NIR transmission probe. Formulations F1-F5 were extruded at various drug-polymer ratios using a constant, low screw speed (50 rpm) in order to gain a better understanding of the transformations in the crystallinity of the API. However, higher screw speeds were applied for formulations F6 and F7 in order to monitor NIR signal variations related to the screw speed. Heil *et al.*, [30] observed that higher screw speeds result in greater variability in extrusion processing, whereas lower screw speeds provide better repeatability.

### 5.3.2. X-ray powder diffraction (XRPD)

XRPD analysis was performed in order to investigate the physical state of the bulk IND, drug–polymer physical mixtures and the hot-melt extruded samples. The data in **Fig. 5.3** shows the diffractogram of bulk IND with distinct intensity peaks at 10.17°, 11.62°, 17.02°, 19.60°, 21.82°, 23.99°, 26.61°, 29.37°, 30.32° and 33.55° 2 $\theta$  values whereas pure SOL and VA64 presented noisy signals due to their amorphous nature.

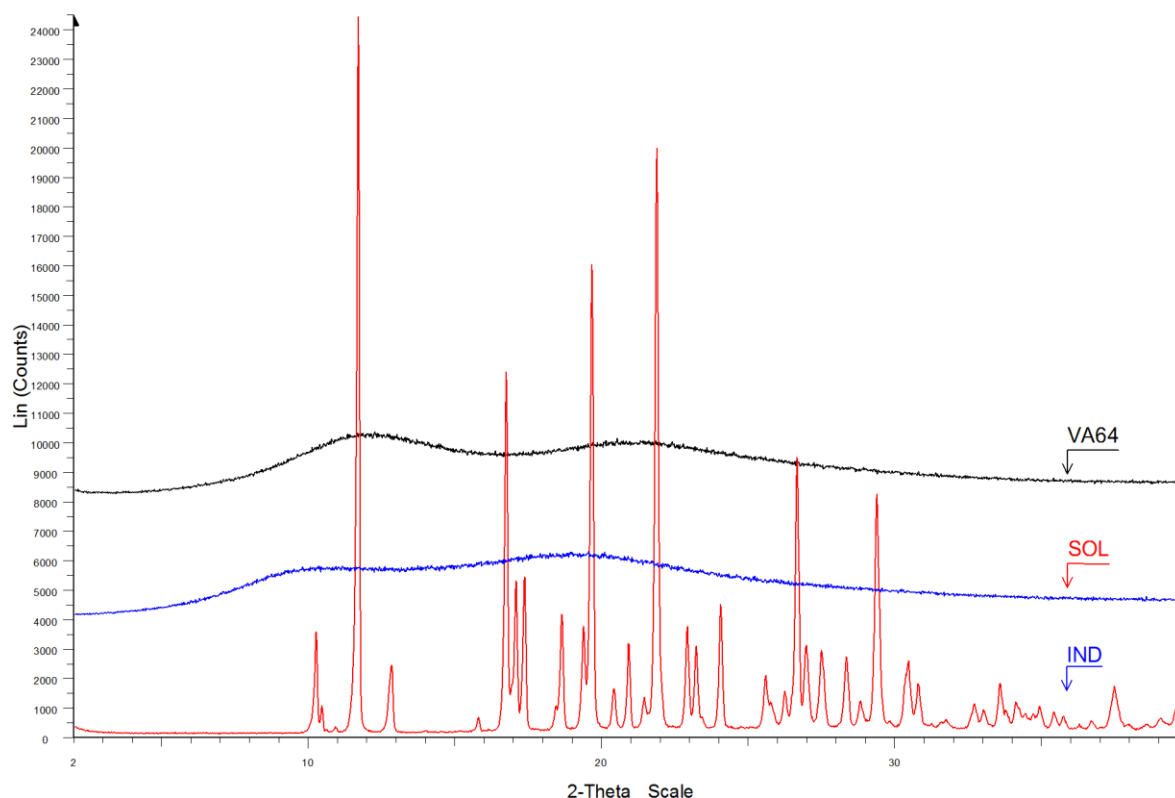


**Fig. 5.3.** XRPD profiles of bulk IND, SOL and VA64.

The physical mixtures of IND formulations with both SOL and VA64 polymers showed lower intensity peaks suggesting that they remained in the crystalline state at 20-50% loading (**Fig. 5.4**). In contrast, no distinct intensity peaks were observed in the diffractograms of all the extruded formulations, even at high drug loading (**Fig. 5.5**). The absence of high intensity IND peaks indicates the formation of a solid dispersion, where the drug is present in an amorphous state or molecularly dispersed into the polymer matrices.

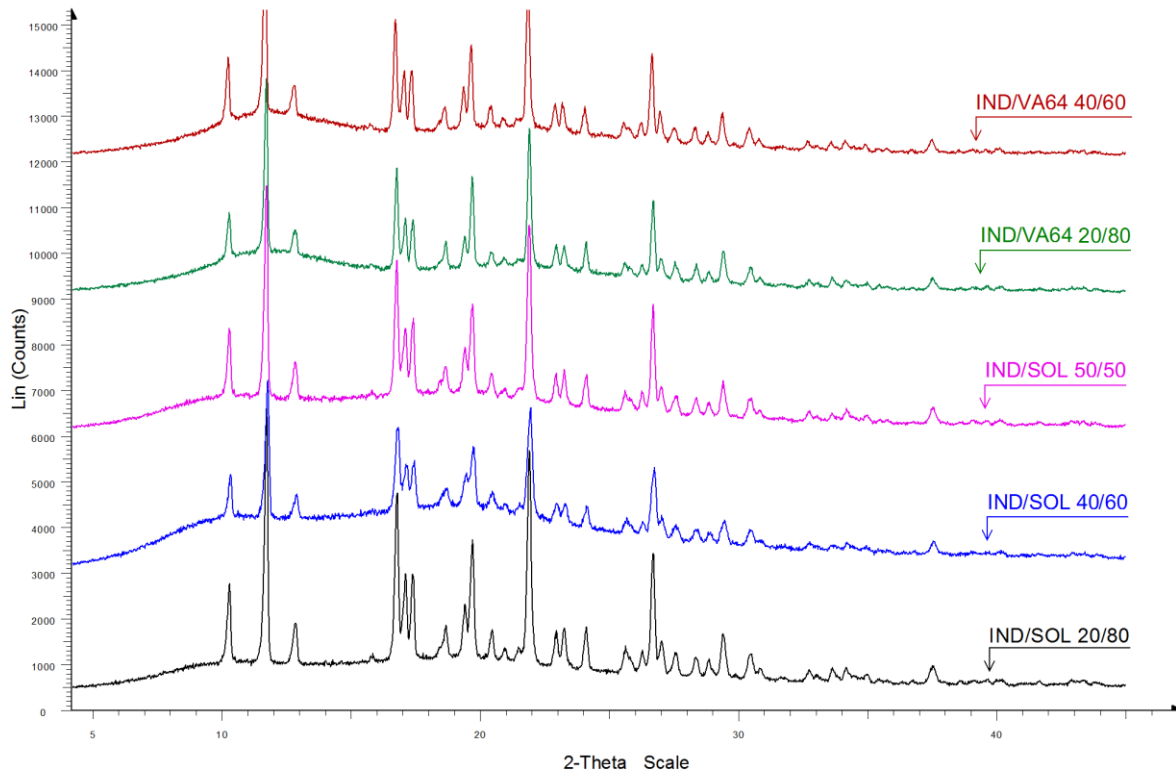


**Fig. 5.4.** XRPD profiles of physical mixtures of IND/SOL and IND/VA64.

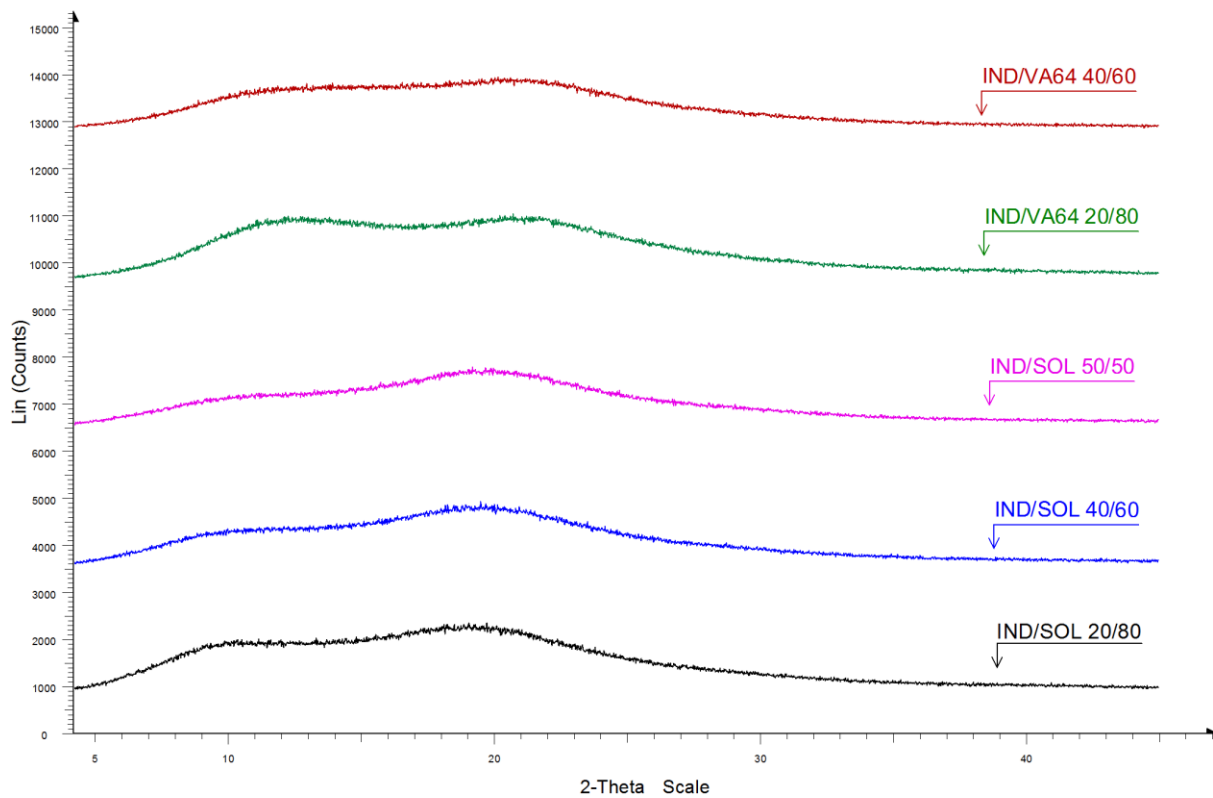


**Fig. 5.5.** XRPD profiles of IND/SOL and IND/VA64 extrudates.

### 5.3.3. Differential scanning calorimetry

Differential scanning calorimetry was also used to determine the physical state of IND within the extruded formulations and compared with those of the physical mixtures. As shown in the data in **Fig. 5.6**, the DSC thermograms of pure IND displayed sharp melting endothermic transitions at 161.08°C ( $\Delta H = 101.60 \text{ Jg}^{-1}$ ). The DSC thermograms of SOL and VA64 gave  $T_g$  values of 68.07°C and 104.99°C, respectively due to their amorphous nature (**Fig. 5.6**). Interestingly, the thermograms of the physical mixtures of all IND/VA64 and IND/SOL formulations showed broad endothermic transitions (**Fig. 5.7 - Fig. 5.8**).

The absence of a sharp melting peak for IND in the physical mixtures suggests that the API is partially dissolved within the polymer matrices. This behaviour is attributed to the both SOL and VA64 acting as solubilizers for a wide range of water insoluble drugs [33, 34].

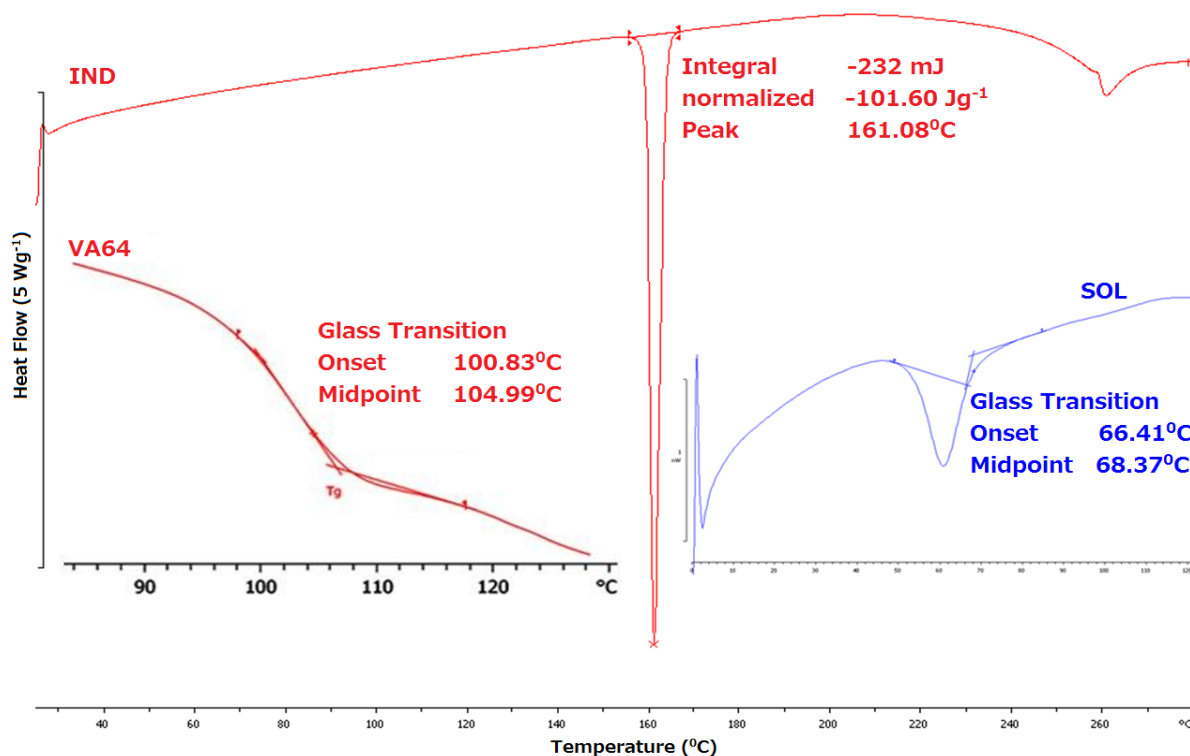


**Fig. 5.6.** DSC thermograms of bulk IND, SOL and VA64.

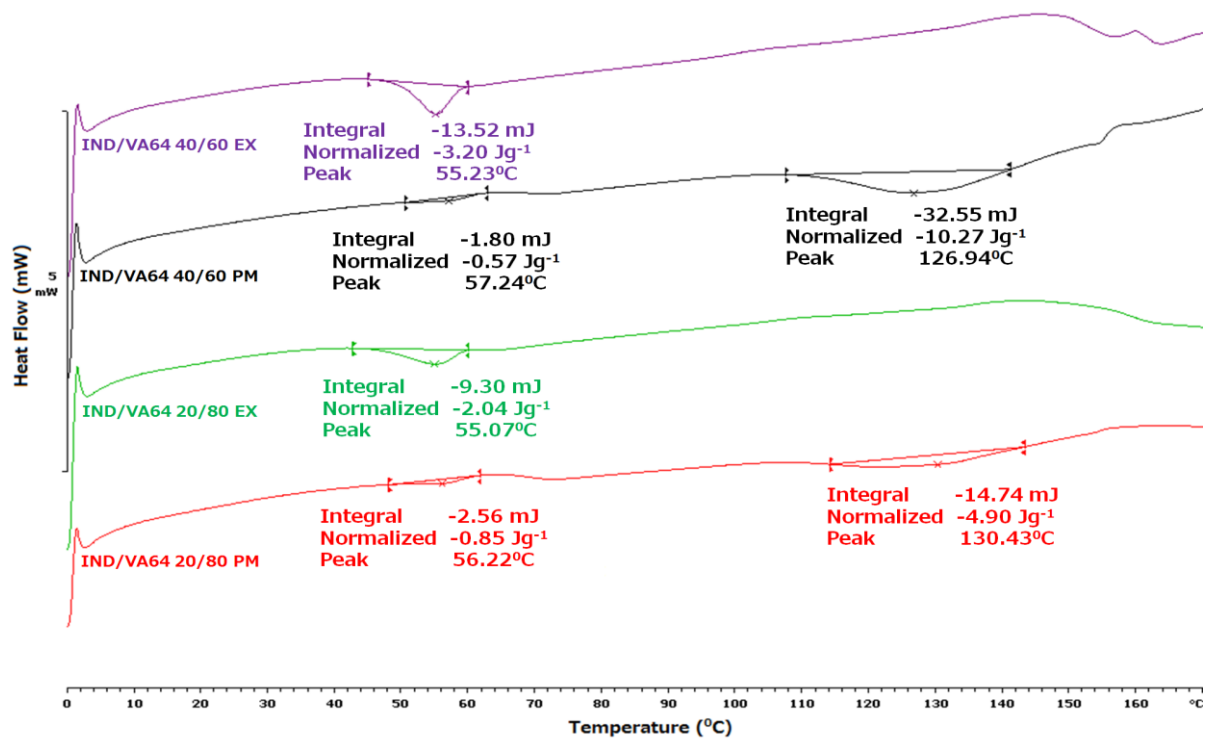


Fig. 5.7. DSC thermograms of physical mixtures of IND/VA64 and extruded formulations.

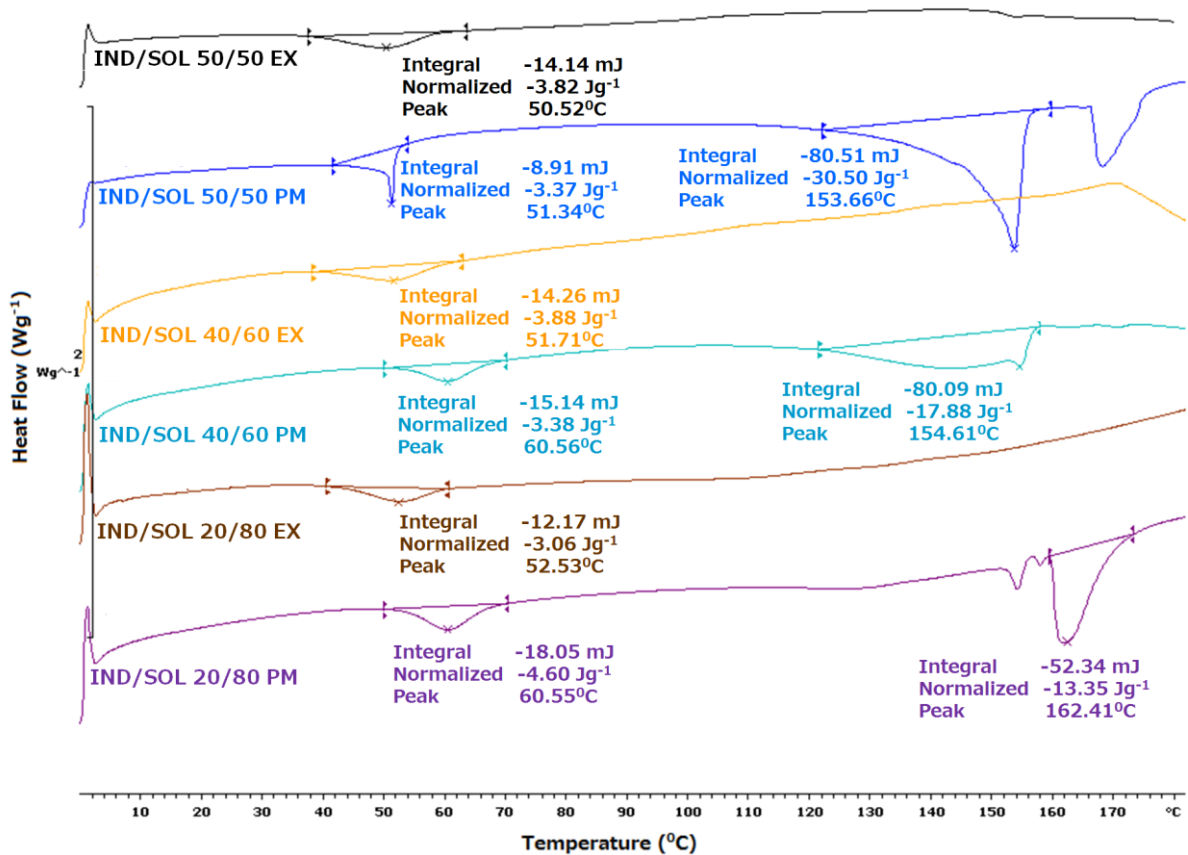


Fig. 5.8. DSC thermograms of physical mixtures of IND/SOL and extruded formulations.

However, a single  $T_g$  was observed in all thermograms for the extrudates indicating drug-polymer miscibility. According to the Gordon-Taylor equation, when two components of a mixture are miscible the single  $T_g$  of the extruded materials should be located between their  $T_g$  values [28]. By using the Gordon-Taylor equation the theoretical  $T_g$  of the drug-polymer blends was estimated (**Table 5.2**). In addition, the presence of a single  $T_g$  in all extruded samples suggests that the IND is molecularly dispersed within the polymer matrices. The incorporation of IND in both polymers lowers the  $T_g$  and allows the polymer chain segments greater freedom due to the fact that IND acts as a plasticizer.

**Table 5.2.** Melting endotherms and glass transition temperatures for bulk IND, SOL, VA64 and extrudates (EX).

Formulations	Melting Endotherms (°C)	Glass transition temperatures ( $T_g$ , °C)	Calculated $T_g$ (Gordon-Taylor equation) (°C)
<b>Bulk IND</b>	161.08	42.3	
<b>VA64</b>		104.99	
<b>SOL</b>		68.37	
<b>F1 PM</b>	130.43	56.22	82.99
<b>F1 EX</b>		55.07	
<b>F2 PM</b>	126.94	57.24	67.98
<b>F2 EX</b>		55.23	
<b>F3 PM</b>	162.41	60.55	61.48
<b>F3 EX</b>		52.53	
<b>F4 PM</b>	154.61	60.56	55.61
<b>F4 EX</b>		51.71	
<b>F5 PM</b>	153.66	51.34	52.99
<b>F5 EX</b>		50.52	

Densities ( $\rho$ ), IND=1.34 g/cm<sup>3</sup>; SOL=1.192 g/cm<sup>3</sup>; VA64=1.127 g/cm<sup>3</sup> [31, 32]

### 5.3.4. In-line NIR monitoring

Off-line NIR spectra of pure IND, SOL and VA64 and the physical mixtures of all the formulations were measured in order to identify the characteristic bands attributed to the pure samples. The pure compounds display characteristic NIR spectral band lies between 6300 – 5500  $\text{cm}^{-1}$  wavenumber region. Extrusion processes for all of the IND formulations were monitored by using both the in-line NIR transmission and reflectance probes. The probes were placed in two different positions of the extruder barrel. The reflectance NIR probe was fitted into the first mixing zone of the barrel and the transmission NIR probes inserted in the extruder exit die (**Fig. 5.2**). The rationale for using both probes was to provide a more detailed understanding of the drug transformations during extrusion. As the first mixing zone is near to the feed point, it was expected that physical mixtures of the formulations would not have melted in this zone of the extruder. This allowed the spectra to be collected using the reflectance NIR probe in this zone as the mixture would still be reflective. On the other hand, the extrudates converted to a transparent solution along the heated barrel so the spectra were collected using a transmission NIR probe located on the extruder die.

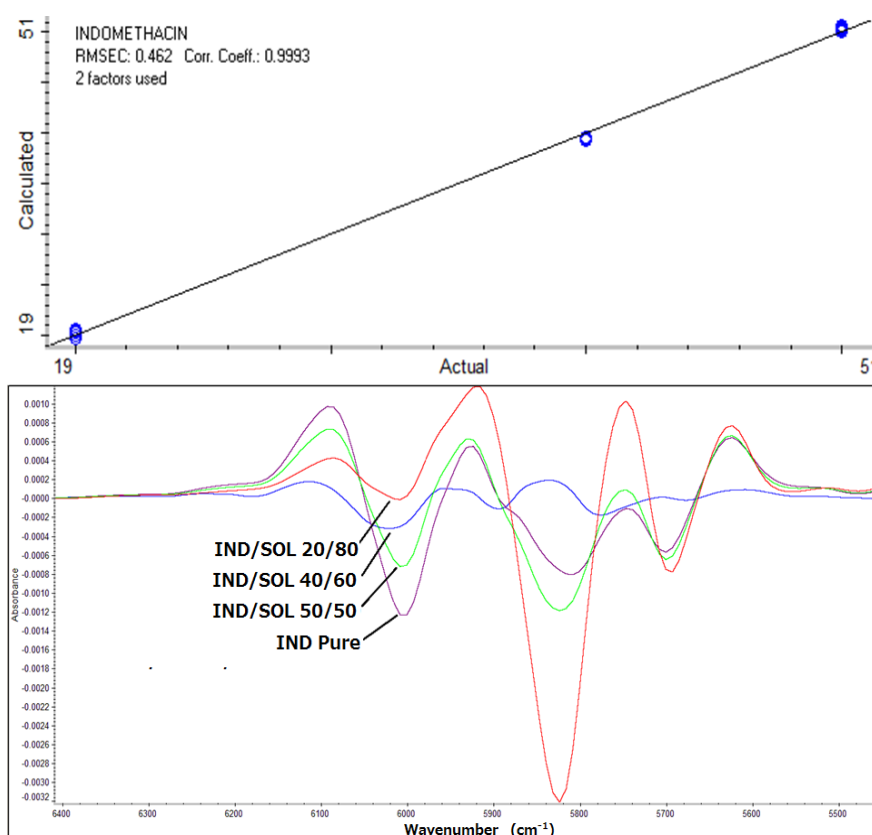


**Fig. 5.9.** Calibration plot (top) and second derivative NIR spectra (bottom) collected from extruded IND/SOL mixtures at different weight ratios and bulk IND.

A partial least squares (PLS) calibration model (**Fig. 5.9**) was developed using spectra collected from the in-line transmission NIR probe during IND/SOL (20%, 40% and 50%) extrusions to allow prediction of IND concentration in unknown samples during further HME processing ( $r^2= 0.9995$ ,  $SEC=0.379\%$ , 2 factors,  $6000\text{--}5500\text{ cm}^{-1}$  wavenumber range). There were significant changes in band intensity at different concentrations of IND (**Fig. 5.9**), where the band intensities increased with increasing concentrations of IND in the formulations.

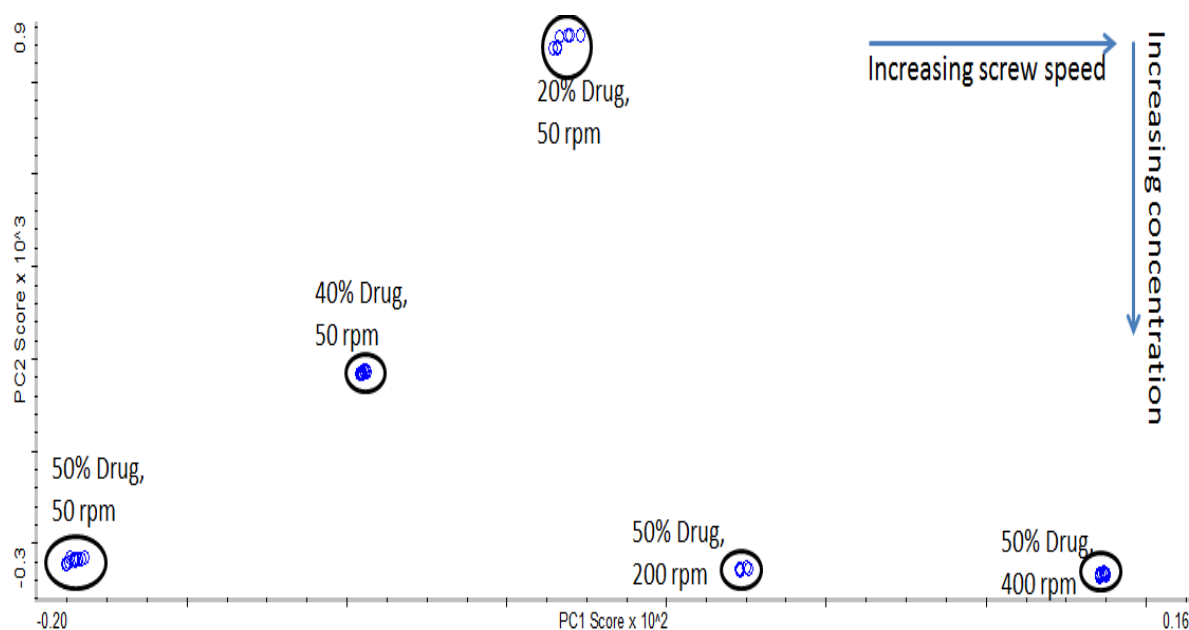


**Fig. 5.10.** Principal component score plot of NIR spectra from the in-line transmission probe data.

Two additional formulations (F6 and F7) were extruded in order to identify the effect of screw speed on the extrusion process; screw speeds of 200 rpm and 400 rpm were applied during IND/SOL (50/50, w/w) extrusion. Principal component analysis (PCA) was used to investigate whether or not NIR could be used to detect the results of changes in the screw speed of the extruder. PCA was applied over the  $6500\text{--}5500\text{ cm}^{-1}$  spectral range to 50 spectra (10 spectra each from IND/SOL formulations, F3-F7) resulting in a model with two PCs covering nearly all the spectral variations (99.04%). The PC scores plot obtained using constant process parameters (F3 – F5) and variable screw speeds (F6 and F7) are shown in **Fig. 5.10**. The PC scores plot clearly shows that the screw speed has a significant effect on the NIR spectra as samples were widely spread on the PC1 axis. The second PC was then used to describe the variation in the IND concentration. Ellipses were drawn around points in the PC score plot corresponding to specific production runs at constant IND concentration. However, the ellipses

were very similar in size which indicated that screw speed had very little influence on the homogeneity of the extrudates.

Moreover, the characteristic bands of IND in the NIR region ( $6100 - 5600 \text{ cm}^{-1}$ ) were significantly changed after extrusion. The data in **Fig. 5.11** shows the unprocessed pure IND bands, the PM of IND/VA64 (20/80, w/w), the reflectance NIR spectra collected from the first mixing zone and the spectra collected using the in-line transmission NIR probe at the die. It was clearly observed that IND had characteristic bands in this region. Interestingly the spectrum of the PM and the reflectance spectrum from the first mixing zone were similar which indicated that the PM had not started to melt in the first zone.

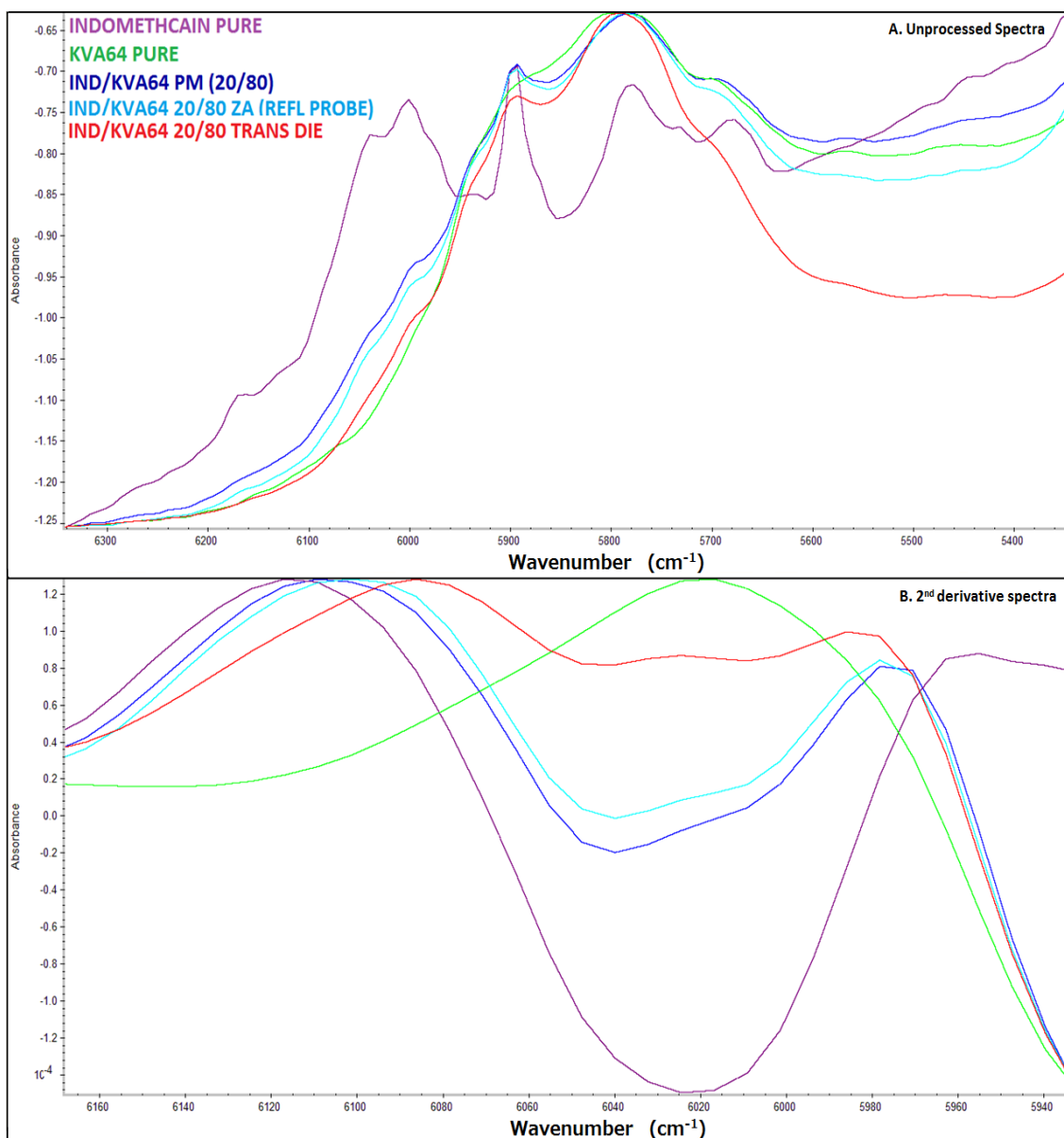


**Fig. 5.11.** Unprocessed and second derivative NIR spectra of IND/VA64 (20/80).

However, the spectra collected from the transmission NIR probe, during extrusion, showed that the IND bands were no longer present due to the IND being dispersed within the polymer matrix. Furthermore, the second derivative spectra also showed changes in the IND spectral profile due to changes in the crystallinity of the drug. The band at  $6020\text{ cm}^{-1}$  decreased in intensity in the PM due to the presence of either polymers compared to the bulk IND. This band was also slightly less intense from samples in the first mixing zone compared with the PM, whereas the spectra collected by in-line transmission NIR probe at the die showed that this band was absent. This change indicated that the crystalline IND was fully converted into the amorphous form and this conclusion was confirmed by the DSC and XRPD data. A similar conversion pattern was also found for the extrusion of IND/SOL (20/80, w/w) (**Fig. 5.12**).

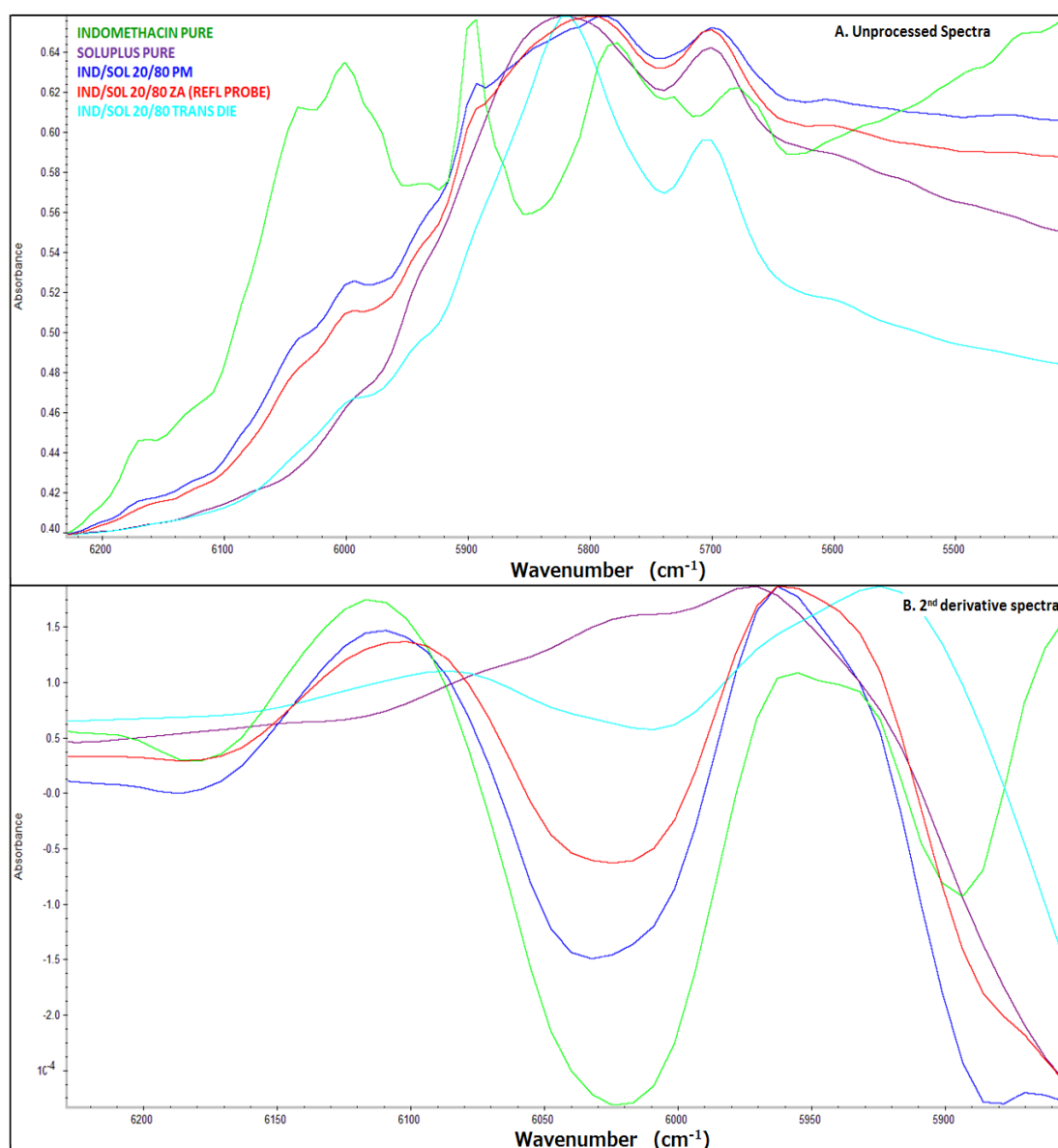


**Fig. 5.12.** Unprocessed and second derivative NIR spectra of IND/SOL (20/80, w/w).

However, when a high IND drug loaded mixture was extruded with VA64 and SOL, a similar kind of progression pattern was noticed (Fig. 5.13 and Fig. 5.14). The data in Fig. 5.15, shows that the band at  $6020\text{ cm}^{-1}$  is present in the PM and the spectra collected by the in-line reflectance NIR probe in the first zone due to the high amount of IND present during IND/SOL (50/50, w/w) extrusion. The in-line transmission NIR spectra showed significant changes in this band in both unprocessed and second derivative spectra. This is a clear indication of the conversion of crystalline IND to the amorphous state even when using high drug loaded IND during extrusion. The NIR data are in good agreement with the DSC thermograms and XRPD diffractograms obtained for the extrudates. The use of the transmission NIR probe proved helpful in monitoring the HME processing of molecularly dispersed IND/SOL and IND/VA64 that are in the form of clear and transparent extrudates. The use of the reflectance NIR probe for in-line monitoring of such extrudates would be very difficult, because of the high noise signals produced.

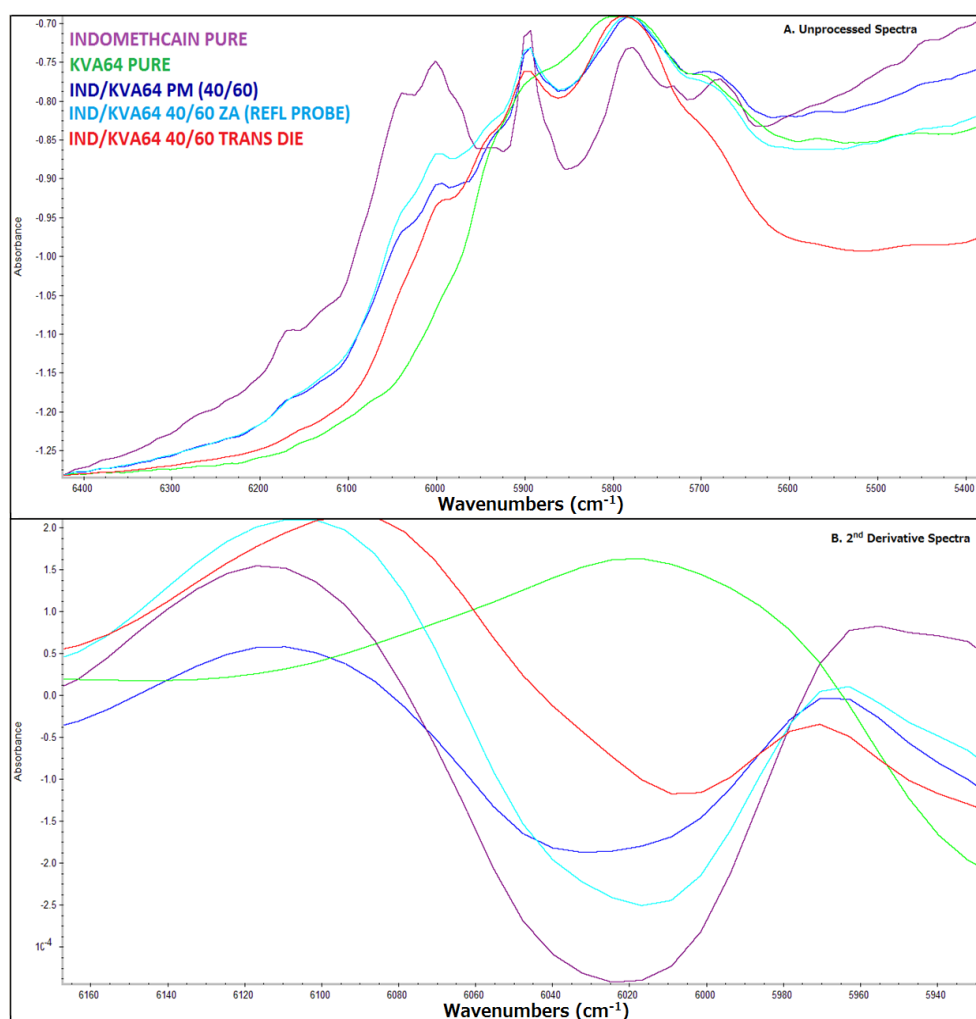


**Fig. 5.13.** Unprocessed and second derivative NIR spectra of IND/VA64 (40/60, w/w).

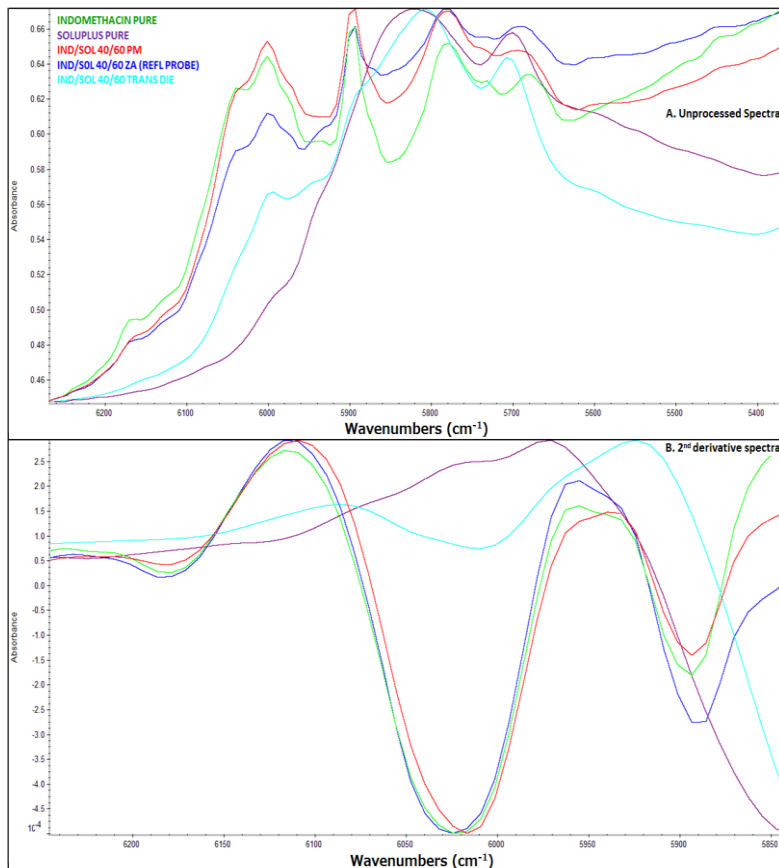


**Fig. 5.14.** Unprocessed and second derivative NIR spectra of IND/SOL (40/60, w/w).

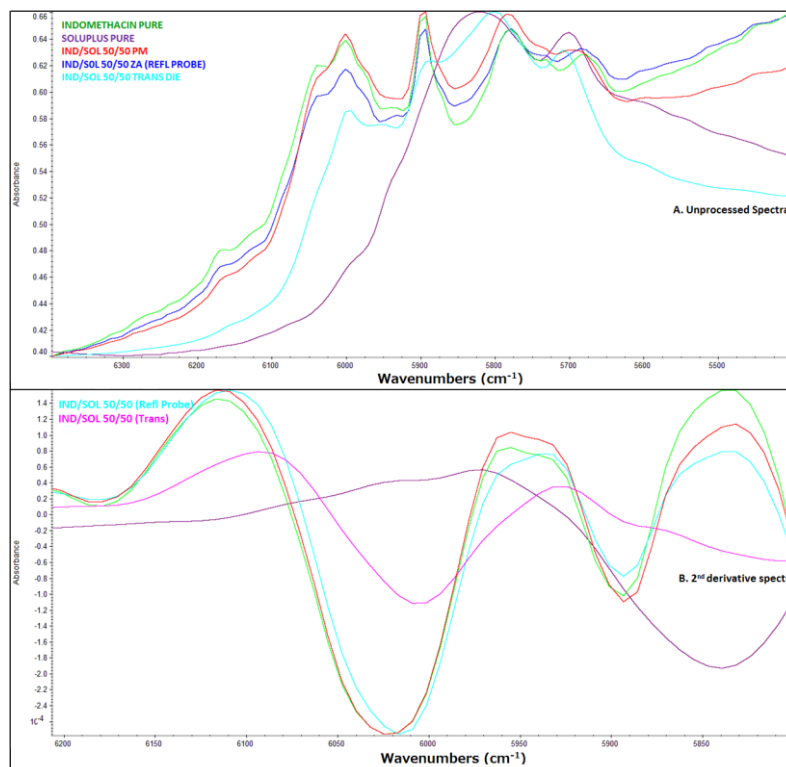


**Fig. 5.15.** Unprocessed and second derivative NIR spectra of IND/SOL (50/50).

### 5.3.5. Confocal Raman spectroscopy

The data in **Fig. 5.16** illustrates the Raman spectra of the pure compounds. Most of the Raman bands overlap or can be potentially overlapped in the extrudates due to the chemical environment. Hence, for example, the Raman bands of IND in the 1500-1720  $\text{cm}^{-1}$  wavenumber region, which correspond to C=O stretching, are overlapped with the broad bands of VA64 at 1650 and 1750  $\text{cm}^{-1}$ . Therefore, multivariate data analysis (namely PCA) which takes into account the whole spectrum was applied. The method does not require the pure spectra of the compounds which can change in the formulations due to molecular interactions. In PCA, the spectra are decomposed into principal components that reflect variations amongst the spectra. In principle, the Raman hyperspectral data set can be described as a linear combination of a small number of components and hence instead of observing the distribution of a particular band, the distribution of the entire spectrum which corresponds to a particular component is obtained.

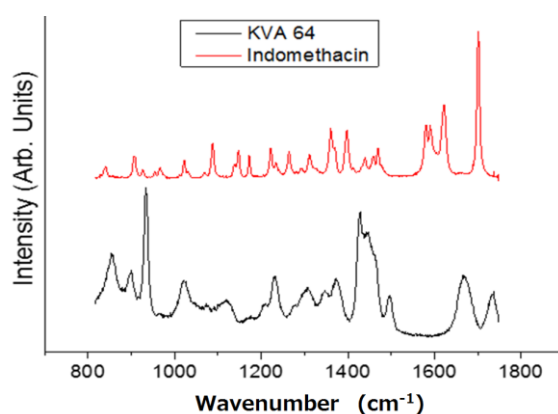


**Fig. 5.16.** Raman spectra of pure IND and VA64.

The data in **Fig. 5.17** shows the first principal component spectrum and the corresponding concentration map for the extruded IND/VA64 sample. The hyperspectral Raman data were decomposed into three PCs. There are various methods which can be used to determine the number of components present in PCA [35, 36]. The most common approach is the analysis of eigenvalues and by monitoring the values of the associated scores and loadings. It is quite likely that there are only two components present (**Fig. 5.17a**); which is expected as there are only two compounds present. This can be clearly confirmed by plotting the first three PCs where only the first PC has identifiable bands. The 2<sup>nd</sup> and 3<sup>rd</sup> PCs contain noise and the bands are too broad to extract any useful information (**Fig. 5.17b**). The first loading spectrum contains characteristic bands for both IND and VA64. It is worth mentioning that the carbonyl

band of IND at  $1710\text{ cm}^{-1}$  moves towards a lower wavenumber (**Fig. 5.17c**) indicating stronger interactions of the C=O group. It is possible for the carbonyl groups of IND to interact with the OH groups of other IND molecules via hydrogen bonding. In the amorphous state these interactions are stronger than in crystalline powder resulting in the movement of the C=O band to lower wavenumbers. Also, previous studies showed that the Raman bands of amorphous IND become broader [37] resulting in an overlap with the bands of VA64 rendering the analysis even more difficult (**Fig. 5.17b**). The concentration map for PC1 (**Fig. 5.17d**) shows the homogeneous distribution of the compounds.

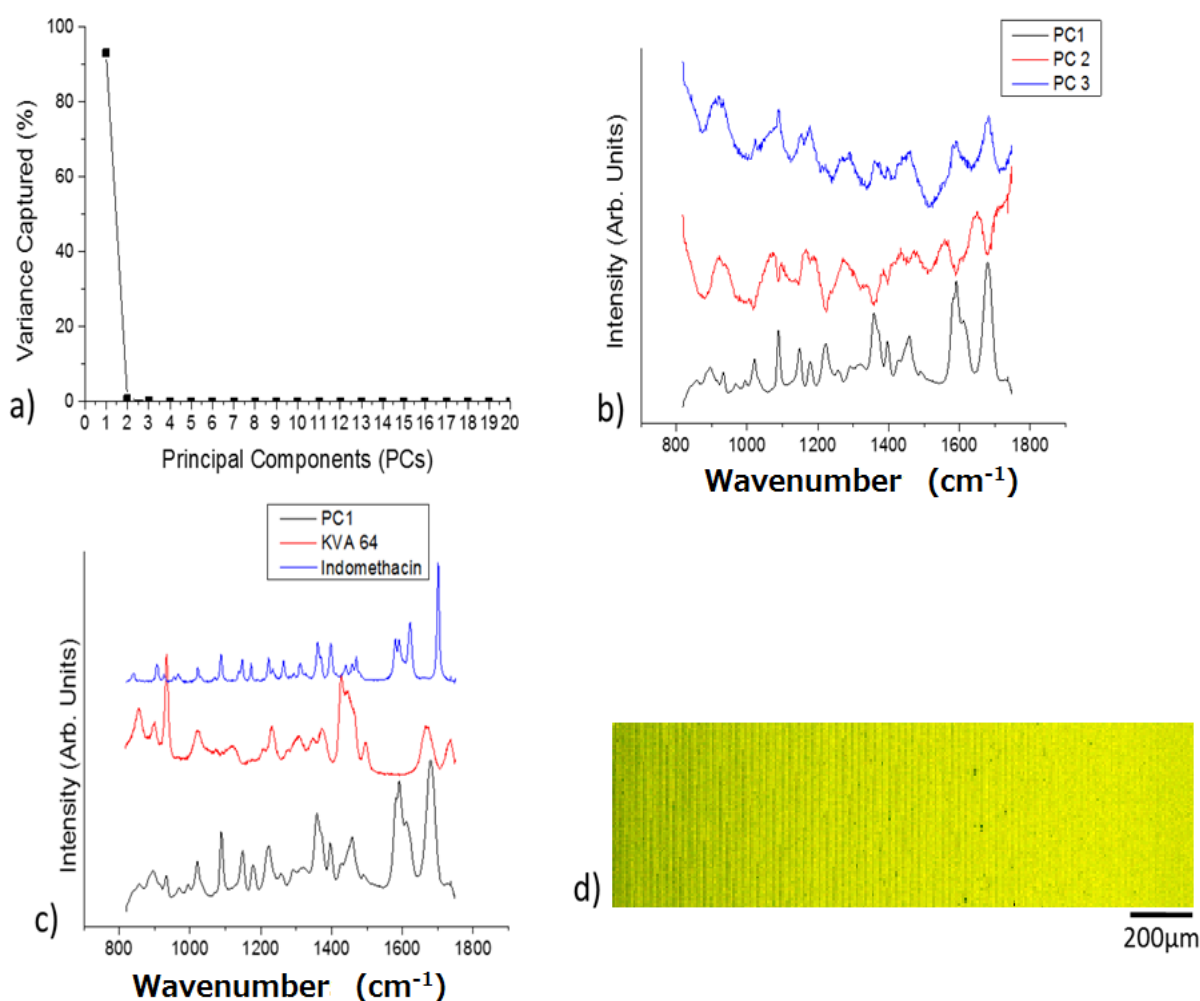


**Fig. 5.17.** a) Variation of eigenvalues with the principal components, b) comparison of first three PCs c) comparison of first PC with the spectra of IND and VA64 and d) chemical map of PC1.

### 5.3.6. *In-vitro* drug release studies

*In-vitro* drug release studies were performed in order to investigate the dissolution patterns of the extruded samples and the bulk IND. The dissolution profiles of bulk IND and extruded formulations with the highest IND loadings for VA64 and SOL are shown in **Fig. 5.18**. Due to low water solubility, the bulk IND powder showed very low dissolution rates compared with extruded formulations. IND/VA64 extrudates at 40:60 (w/w) ratios displayed a rapid dissolution rate, with 80% of the IND being released in 15 min while complete IND release was detected at 30 min. For the extruded IND/SOL granules 30% of the IND was released in the first 20 min and approximately 55% after 30 min. More than 80% IND was released after 90 min from the IND/SOL (50:50 w/w) extrudates. The dissolution studies revealed faster IND release rates with increasing loadings due to stronger drug/polymer interactions [38, 39]. However, dissolution studies performed at pH 1.2 showed negligible amount of IND release after 2 hr. These results are in agreement with previous studies [33, 34].

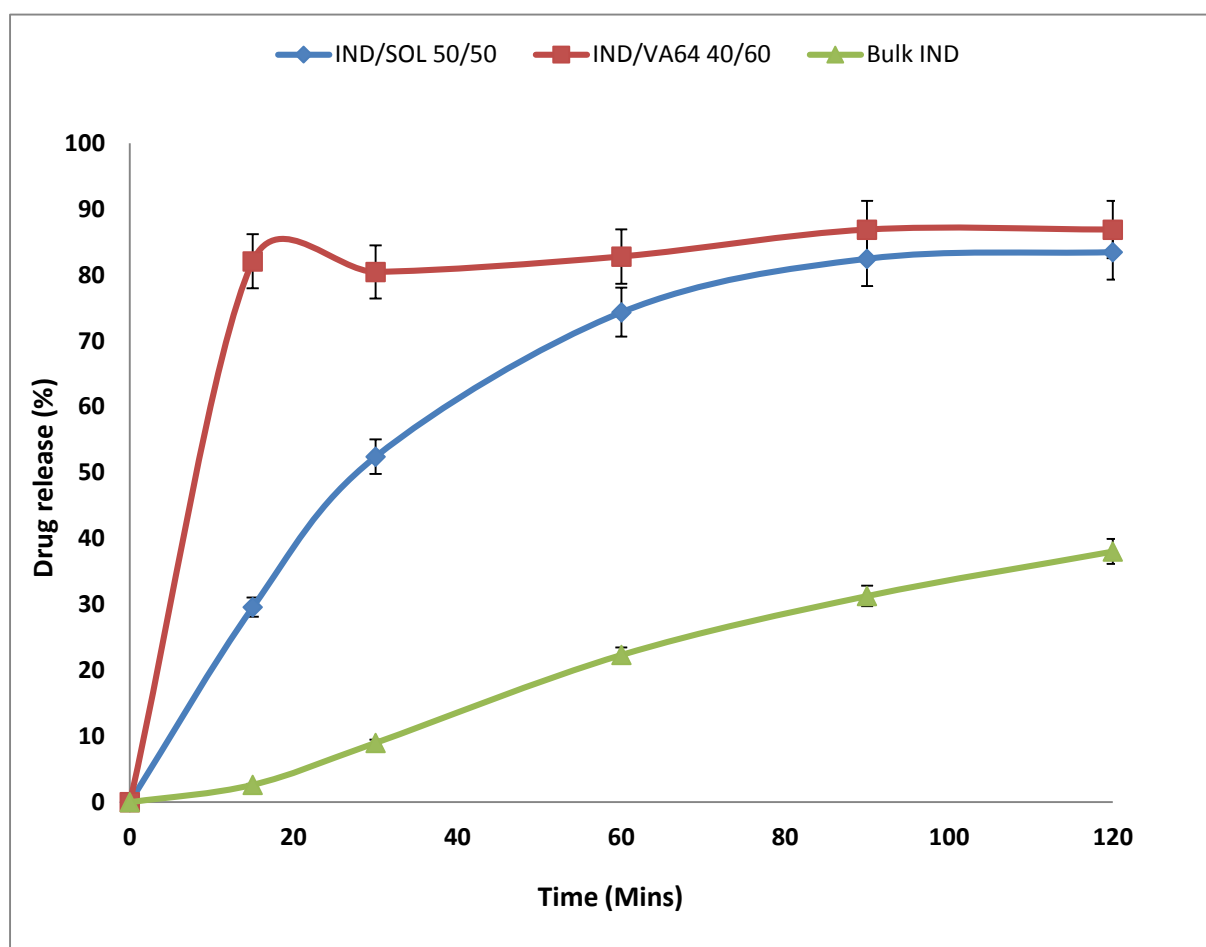


**Fig. 5.18.** Drug release profile of bulk IND, IND/SOL (50/50) and IND/VA64 (40/60).

## 5.4. Conclusions

In this study, in-line transmission and reflectance NIR probes were employed as PAT tools for monitoring the HME processing of IND/ SOL and IND/VA 64 extrudates. By using both the NIR probes it was possible to monitor the transformation of IND from the crystalline to the amorphous state at various drug/polymer ratios. An in-line reflectance NIR probe was used to collect NIR spectra of IND/polymer mixtures, at different weight ratios, in the first mixing zone of the HME. Via the use of a specially designed die an in-line NIR transmission probe was used to characterize extruded films constituted of the different ratios of IND and the two different polymers. Physicochemical characterization, using DSC and XRPD, of IND/polymer granules (obtained by cutter milling the extruded transparent films) confirmed the plasticization effect of IND and the manufacture of solid solutions with IND being molecularly dispersed in the polymer matrices. The PCA plots obtained from the NIR transmission spectra showed that a change in the screw speed of the extruder results in different NIR spectra. Confocal Raman spectroscopic data was used to show the homogeneity of the IND/polymer film extrudates. In conclusion the use of a transmission NIR probe proved to be a valuable PAT tool for monitoring and process understanding of HME molecular dispersions.

## 5.5. References

1. Maniruzzaman M, Boateng JS, Snowden MJ, Douroumis D, A review of hot-melt extrusion: process technology to pharmaceutical products. *International Scholarly Research Notices*, 2012; doi:10.5402/2012/436763.
2. Douroumis D, *Hot-melt extrusion: pharmaceutical applications*, Oxford, John Wiley & Sons Ltd. 2012.
3. Andrews GP, Jones DS, Hot melt extrusion- processing solid solutions? *Journal of Pharmacy and Pharmacology*, 2014; **66**(2): 145-147.
4. Almeida A, Claeys B, Remon JP, Vervaet C, Hot-melt extrusion developments in the pharmaceutical industry, In: Douroumis D, (ed.) *Hot-melt extrusion: pharmaceutical application*, Oxford, John Wiley & Sons Ltd, 2012: 43-69.
5. Jones DS, Margetson DN, McAllister MS, Yu T, Shu L, McCoy CP, Andrews GP, Thermodynamically stable amorphous drug dispersions in amorphous hydrophilic polymers engineered by hot melt extrusion, *Chemical Engineering Research and Design*, 2014; DOI:10.1016/j.cherd.2014.08.022.

6. Qi S, Belton P, Nollenberger K, Clayden N, Reading M, Craig DQM, Characterisation and prediction of phase separation in hot-melt extruded solid dispersions: A thermal, microscopic and NMR relaxometry study, *Pharmaceutical Research*, 2010; **27**: 1869-1883
7. Maniruzzaman M, Rana MM, Boateng JS, Mitchell JC, Douroumis D, Dissolution enhancement of poorly water soluble APIs processed by hot melt extrusion using hydrophilic polymers, 2013; **39**(2): 218-227.
8. Yang Z, Nollenberger K, Albers J, Moffat J, Craig D, Qi S, The effect of processing on the surface physical stability of amorphous solid dispersion, *European Journal of Pharmaceutics and Biopharmaceutics*, 2014; DOI:10.1016/j.ejpb.2014.07.013.
9. Hulsmann S, Backensfeld T, Keitel S, Bodmeier R, Melt extrusion – an alternative method for enhancing the dissolution rate of 17-beta-estradiol hemihydrate, *European Journal of Pharmaceutics and Biopharmaceutics*, 2000; **49**(3): 237 -42
10. Hulsmann S, Backensfeld T, Bodmeier R, Stability of extruded 17-beta-estradiol solid dispersions, *Pharmaceutical Development and Technology*, 2001; **6**(2): 223 -9.
11. Sun Y, Rui Y, Wenliang Z, Tang X, Nimodipine semi-solid capsules containing solid dispersion for improving dissolution, *International Journal of Pharmaceutics*, 2008; **359**(1-2): 144 -9
12. De Beer T, Burggraeve A, Fonteyne M, Saerens L, Remon JP, Vervaet, C, Near infrared and Raman spectroscopy for the in-process monitoring of pharmaceutical production processes, *International Journal of Pharmaceutics*, 2011; **417**: 32– 47.
13. Saerens L, Vervaet C, Remon JP, De Beer T, Process monitoring and visualization solutions for hot-melt extrusion: a review, *Journal of Pharmacy and Pharmacology*, 2014; **66**(2): 180-203.
14. EUFEPS QbD and PAT Sciences Network, <http://www.eufeps.org/PATnetwork.html>. 2010
15. Food and Drug Administration, 2004, <http://www.fda.gov/downloads/Drugs/GuidanceComplianceRegulatoryInformation/Guidances/ucm070305.pdf>.
16. Saerens L, Dierickx L, Quinten T, Adriaensens P, Carleer R, Vervaet C, Remon JP, De Beer T, In-line NIR spectroscopy for the understanding of polymer–drug interaction during pharmaceutical hot-melt extrusion, *European Journal of Pharmaceutics and Biopharmaceutics*, 2012; **81**: 230–237.

17. Saerens L, Seghera N, Vervaetb C, Remon JP, De Beer T, Validation of an in-line Raman spectroscopic method for continuous active pharmaceutical ingredient quantification during pharmaceutical hot-melt extrusion, *Analytica Chimica Acta*, 2014; **806**: 180-187.
18. Fischer D, Bayer T, Echhorn KJ, Otto M, In-line process monitoring on polymer melts by NIR spectroscopy, *Journal of Analytical Chemistry*. 1997; **359**: 74-77.
19. Kelly AL, Gough T, Dhumal RS, Halsey SA, Paradkar A, Monitoring ibuprofen–nicotinamide cocrystal formation during solvent free continuous cocrystallization (SFCC) using near infrared spectroscopy as a PAT tool, *International Journal of Pharmaceutics*, 2012; **426**: 15– 20.
20. Moradiya H, Islam MT, Woollam GR, Slipper IJ, Halsey S, Snowden MJ, Douroumis D, Continuous cocrystallization for dissolution rate optimization of a poorly water-soluble drug, *Crystal Growth Design*, 2014; **14**: 189-198.
21. Moradiya H, Islam MT, Halsey S, Maniruzzaman M, Chowdry B, Snowden MJ, Douroumis D, Continuous cocrystallisation of Carbamazepine and *trans*-Cinnamic acid via melt extrusion processing, *CrystEngComm*, 2014; **16**: 3573-3583.
22. Islam MT, Maniruzzaman M, Halsey S, Chowdhry B, Douroumis D, Development of sustained release formulations processed by Hot-melt extrusion by using a quality by design approach, *Drug Delivery and Translational Research*, 2014; **4**: 377-387.
23. Rohe T, Becker W, Kolle S, Eisenreich N, Eyerer P, Near infrared (NIR) spectroscopy for in-line monitoring of polymer extrusion processes, *Talanta*, 1999; **50**: 283–290.
24. Coatesa PD, Barnesa SE, Sibleya MG, Brown EC, Edwardsb HGM, Scowen IJ, In-process vibrational spectroscopy and ultrasound measurements in polymer melt extrusion, *Polymer*, 2003; **44**: 5937–5949.
25. Barnes SE, Brown EC, Sibley MG, Edwards HGM, Scown IJ, Vibrational spectroscopic and ultrasound analysis for in-process characterization of high-density polyethylene/polypropylene blends during melt extrusion, *Applied Spectroscopy*, 2005; **59**(5): 611-619.
26. Saerens L, (PhD Thesis), Spectroscopic process monitoring for quality assessment, visualization and understanding of pharmaceutical hot-melt extrusion, University of Ghent, 2013.

27. Mura P, Faucci MT, Manderioli A, Furlanetto S, Pinzauti S, Thermal analysis as a screening technique in preformulation studies on picotinamide solid dosage forms, *Drug Development and Industrial Pharmaceutics*, 1998; **24**: 747–756.
28. Forster A, Hempenstall J, Tucker, Rades T, The potential of small-scale fusion experiments and the Gordon-Taylor equation to predict the suitability of drug/polymer blends for melt extrusion, *Drug Development and Industrial Pharmacy*, 2001; **27**: 549–560.
29. Greenhalgh DJ, Williams AC, Timmins P, York P, Solubility parameters as predictors of miscibility in solid dispersions, *Journal of Pharmaceutical Sciences*, 1999; **88**: 1182-1190.
30. Heil C, Hirsch J, Improved process understanding and control of a hot-melt extrusion process with near-infrared spectroscopy, In: Douroumis D (ed.) *Hot-melt extrusion: pharmaceutical application*, Oxford, John Wiley & Sons Ltd, 2012: 333-353
31. Chokshi RJ, Sandhu HK, Iyer RM, Shah NH, Malick AW, Zia H, Characterization of physico-mechanical properties of indomethacin and polymers to assess their suitability for hot-melt extrusion process as a means to manufacture solid dispersion/solution, *Journal of Pharmaceutical Sciences*, 2005; **94**(11): 2463-2474.
32. Djuris J, Nikolakakis I, Ibric S, Djuric Z, Kachrimanis K, Preparation of carbamazepine-Soluplus® solid dispersions by hot-melt extrusion, and prediction of drug-polymer miscibility by thermodynamic model fitting, *European Journal of Pharmaceutics and Biopharmaceutics*, 2013; (**84**): 228-237.
33. Terife G, Faridi N, Wang P, Gogs CG, Hot melt mixing and foaming of Soluplus® and indomethacin, *Polymer Engineering & Sciences*, 2012; **52**(8): 1629-1639.
34. Forster A, Hempenstall J, Rades T, Characterization of glass solutions of poorly water soluble drugs produced by melt extrusion with hydrophilic amorphous polymers, *Journal of pharmacy and pharmacology*, 2000; **53**(3): 303-315.
35. Hancewicz T, Juan AD, Maeder M, Ferré RT, Local rank analysis for exploratory spectroscopic image analysis. Fixed Size Image Window-Evolving Factor Analysis, *Chemometrics and Intelligent Laboratory Systems*, 2005; **77**(1-2): 64-74.
36. Maeder M, Evolving factor analysis for the resolution of overlapping chromatographic peaks, *Analytical Chemistry*, 1987; **59**: 527-530.

37. Savolainen M, Heinz A, Strachan C, Gordon KC, Yliruusi J, Rades T, Sandler N, Screening for differences in the amorphous state of indomethacin using multivariate visualization, *European Journal of Pharmaceutical Sciences*, 2007; **30**: 113-123.
38. Gryczke A, Solubility parameters for prediction of drug/polymer miscibility in hot-melt extruded formulations, In: Douroumis D. (ed.) *Hot-melt extrusion: pharmaceutical application*, Oxford, John Wiley & Sons Ltd, 2012:71-92.
39. Leuner C, Dressman J, Improving drug solubility for oral delivery using solid dispersions, *European Journal of Pharmaceutics & Biopharmaceutics*, 2000; **50**(1): 47-60.

## Chapter 6: Prediction of polymorphic transformations of paracetamol in solid dispersions

---

### 6.1. Introduction

Solid dispersions have attracted considerable interest as an efficient means of improving dissolution rate and hence the bioavailability of the poorly soluble drugs. Solid dispersions are commonly used for the development of pharmaceutical dosage forms where a hydrophobic drug is dispersed molecularly in either amorphous or crystalline hydrophilic matrix [1]. There are several techniques were used for the preparation of solid dispersions including hot spin mixing [2], spray drying [3, 4], co-evaporation or co-precipitation [5], freeze-drying [6], supercritical fluid processing [7] and hot-melt extrusion (HME) [8, 9]. Over the last few decades, HME obtained significant attention for the development of pharmaceutical solid dispersions to increase the solubility and bioavailability of the hydrophobic drugs, taste masking of bitter APIs, and sustained release or controlled release formulations.

HME is advantageous over other conventional methods to develop solid dispersions. It offers solvent free process with reduced processing steps, easy to scale up, can be manufactured continuously and in/on-line monitoring is possible via process analytical technology tools such as NIR. HME contains a heated barrel which may have elevated temperature profile during processing to melt the drug and polymer. HME also contains several mixing zones with varying screw configuration which facilitate the homogenous mixing of the materials used during HME. Due to this high temperature and mixing zones there is possible molecular interactions of drug and polymer occurs which can affect the physicochemical properties. However, it is important to obtain not only a detailed understanding of the physicochemical properties of the drug in the extruded formulations after extrusion but also to understand and monitor during extrusion process, where possible drug transformations from crystalline to amorphous, polymorphic changes or molecular interactions may take place. Such knowledge is important as the solid-state properties of the drug can affect both the stability and the dissolution behaviour of the developed pharmaceutical formulations. The drug is dispersed in the polymer matrices by following ways, crystalline dispersions (substitutional and interstitial), molecular dispersions (continuous or discontinuous), and amorphous dispersions (the drug is present as a separate amorphous phase) [10, 11]. It has been reported that solid dispersions produced via HME can undergo phase separation either through crystallization or polymorphic changes of

the API [11]. Several analytical approaches have been developed to characterize the distribution of the drug(s) in the polymer matrices, phase separation phenomena, and amorphous/crystalline ratio of the drug [10, 11]. Furthermore, process analytical tools have been used to understand the transformation of drug and solid-state characterization of drug/copolymer blends during HME via in-line monitoring [12]. However, identification, prediction, and characterization of solid dispersions involving polymorphic transformations are difficult to undertake during the extrusion process and, to date, this topic has received little attention.

Studies of drug/polymer physical mixtures (PMs) may provide significant insights into the physical properties of the drug and possible transformations that can take place during HME. To characterize the solid-state pharmaceutical reactions including crystal transformations variable temperature X-ray powder diffraction (VTXRPD) has been reported previously [13, 14] which is a powerful tool that can be used to explore such changes as it can be used to facilitate the simultaneous quantification of multiple solid phases [15, 16].

The work reported in this chapter is to explore the identification of polymorphic transformation of paracetamol (PMOL) in the physical binary mixtures of drug and polymer via VTXRPD which is then compared with the NIR data obtained by monitoring in-line during the HME processing of the same drug and polymer blend extrusion. PMOL was selected as a model API as it exists in three polymorphic forms [9] namely Form I (monoclinic), Form II (orthorhombic), and Form III (unstable), in decreasing order of stability and melting point. This approach could potentially be employed as an effective tool to predict and characterize polymorphic transformations of drug substances for the development of solid dispersions via HME.

## **6.2. Materials and methods**

### **6.2.1. Materials**

Paracetamol was kindly donated by Mallinckrodt Chemical Ltd. (Covidien, UK). Soluplus® (SOL) and Kollidon® (VA64) were also donated by BASF (Germany). All materials were used as received.

### **6.2.2. Hansen solubility parameters ( $\delta$ ) and Flory–Huggins interaction parameter ( $\chi$ ): drug–copolymer miscibility**

Hansen solubility parameters were used to predict the miscibility of PMOL with the polymers in solid dispersions. The Hansen [19] solubility parameters ( $\delta$ ) of both the drug as

well as the polymers were calculated by considering their chemical structure. In order to determine the theoretical drug/polymer miscibility, the solubility parameters were calculated by using the Hoftyzer and van Krevelen method [19, 20] using the following equation:

$$\delta^2 = \delta_d^2 + \delta_p^2 + \delta_h^2 \quad (1)$$

Where,

$$\delta_d = \frac{\sum F_{di}}{V_i}, \delta_p = \frac{\sqrt{\sum F_{pi}^2}}{V_i}, \delta_h = \frac{\sqrt{\sum E_{hi}}}{V_i}$$

$i$  = structural groups within the molecule,  $\delta$  = the total solubility parameter,  $\delta_d$  = the energy from dispersion forces between molecules,  $\delta_p$  = the energy from the dipolar intermolecular force between molecules,  $\delta_h$  = the energy from hydrogen bonds between molecules,  $F_{di}$  = molar attraction constant due to molecular dispersion forces,  $E_{hi}$  = hydrogen bonding energy, and  $V_i$  = group contribution to molar volume.

The Flory–Huggins (F–H) interaction parameter ( $\chi$ ) of the model system was determined under two different conditions using the Nishi–Wang (Eq. (2)) [21] equation based on melting point depression data and Hildebrand and Scott (Eq. (3)) [22] correlations with the solubility parameters. The F–H interaction parameter ( $\chi$ ) for all of the drug/polymer binary mixtures was calculated by using the following equations. The value determined by Nishi–Wang represents the interactions between the two substances, specifically at the melting temperature, which may not be extrapolated to other temperatures.

$$\frac{1}{T_m} - \frac{1}{T_m^0} = -\frac{Rv_{drug}}{\Delta H_{drug}v_{poly}} \left[ \ln \phi_{drug} + \left(1 - \frac{1}{m_{poly}}\right) \times (1 - \phi_{drug}) + \chi_{drug-poly} (1 - \phi_{drug})^2 \right] \quad (2)$$

Where  $L$  is the molar volume of the repeating unit,  $m$  is the degree of copolymerization,  $N$  is the volume fraction, and  $\chi$  is the crystalline–amorphous copolymer interaction parameter.  $T_m$  and  $T_m^0$  are the temperatures of the crystalline melting peak of the pure drug and the melting peak of the drug in the presence of the polymer in the system, respectively.

The F–H interaction parameter ( $\chi$ ) can be also estimated by the method developed by Hildebrand and Scott using the following equation [22]:

$$\chi = \frac{v(\delta_{drug} - \delta_{poly})^2}{RT} \quad (3)$$

Where  $R$  is the gas constant,  $T$  is the absolute temperature, and  $v$  the volume per lattice site and  $\delta_{drug}$  and  $\delta_{poly}$  are the solubility parameters of drug and copolymers, respectively.

### 6.2.3. HME process

PMOL formulations, using either SOL or VA64, were carefully mixed in 100 g batches for 10 min each prior to extrusion. A Turbula TF2 Mixer (Basel, Switzerland) was used to thoroughly blend the powder formulations. The drug/polymer ratios (w/w, %) were used 40:60, 50:50, and 60:40 for both polymers. Extrusion of all PMOL-based formulations was performed using a Eurolab 16 twin screw extruder (Thermo Fisher, Germany) equipped with a 2 mm rod die with a screw speed of 50–100 rpm (feed rate 0.5–1 kg/h). The temperature profile used for all formulations was (50/100/115/120/120/120/120/120/120/120)°C (from feeding zone → die). The extrudates produced (strands) were milled for 5 min at 400 rpm by using a Pulverisette ball milling system using eight balls (1.5 cm diameter) (Retsch, Germany) to obtain granules (<500  $\mu$ m).

### 6.2.4. Thermal analysis (DSC and MTDSC)

A Mettler-Toledo 823e (Greifensee, Switzerland) differential scanning calorimeter (DSC) was used to carry out DSC scans of the pure API, PMs of API/polymers and API/polymer extrudates. Samples (3–5 mg) were placed in aluminium pans with pierced lids and sealed. The samples were heated at 1–10°C/min from 0°C to 220°C under an atmosphere of dry nitrogen. In addition modulated temperature differential scanning calorimetry (MTDSC) studies were performed from 20°C to 150°C with an underlying heating rate of 1°C/min. The pulse height was adjusted to 1°C–2°C with a temperature pulse width of 15–30 s.

### 6.2.5. Hot-stage microscopy

Characterization of PMOL in the molten polymeric carrier was assessed using hot-stage microscopy (HSM). During testing, an Olympus BX60 microscope (Olympus Corporation, Center Valley, Pennsylvania) with Insight QE camera (Diagnostic Instruments, Inc., Sterling

Heights, Michigan) was used to visually observe samples, whereas a FP82HT hot stage controlled by a FP 90 central processor (Mettler Toledo, Columbus, Ohio) was used to maintain temperatures between 20°C and 250°C. Images were captured under visible and polarized light using Spot Advance Software (Diagnostic Instruments, Inc.).

### **6.2.6. Variable-temperature X-ray powder diffraction**

Variable-temperature X-ray powder diffraction was used to determine the polymorphic behaviour of the pure PMOL as well as PMs and extruded samples of PMOL/copolymers using a Bruker D8 Advance (Germany) in theta–theta reflection mode. For the purpose of the study, a copper anode at 40 kV and 40 mA, parallel beam Goebel mirror, 0.2 mm exit slit, Lynx-Eye silicon strip position-sensitive detector (PSD) opening at 3° with 176 active channels, Lynx-Iris at 6.5 mm, and a secondary 2.5° Soller slit were used. Each sample was scanned from 2° to 40° 2-theta with a step size of 0.02° 2-theta and a counting time of 0.2 s per step; 176 channels active on the PSD resulting in a total counting time of 35.2 s per step. Variable temperature was achieved by using Anton Paar TTK450 non-ambient sample chamber with a maximum heating rate of 0.2° per second. Data collection was performed using DiffracPlus Commander, whereas the data manipulation and presentation were undertaken by using the EVA V.16 program [23].

### **6.2.7. In-line NIR spectroscopy**

Near-infrared spectrometry was performed during extrusion using an Antaris II NIR spectrometer (Thermo Scientific, UK) equipped with a halogen NIR source and InGaAs detector. The instrument utilized a fiber optic probe that was connected to the NIR spectrometer and used for in-line monitoring. NIR spectra were collected in real-time during the entire extrusion process via a fibre optic diffuse reflectance probe. All NIR in-line spectra were continuously collected using the Result Integration software (Version 3.0 Thermo Scientific). Each spectrum was acquired by averaging 32 scans with a resolution of 16 cm<sup>-1</sup> over the 4000–10000 cm<sup>-1</sup> wavenumber range. The acquisition of a full spectrum took approximately 16 s. The spectral pre-processing was performed using the TQ Analyst software (Version 8.6.12 Thermo Scientific).

## 6.3. Results and discussion

### 6.3.1. Solubility parameters

The miscibility of PMOL with SOL and VA64 was estimated by determining the Hansen solubility parameters using the Hoftyzer and Van Krevelen approach. The miscibility results from a balance between the energy of mixing released by intermolecular interactions of the components and the energy released by intramolecular interactions within the components [24, 25]. The theoretical approach using the solubility parameters suggests that compounds with similar  $\delta$  values are likely to be miscible. It is usually accepted that compounds with  $\Delta\delta < 7 \text{ MPa}^{1/2}$  are likely to be miscible and compounds with  $\Delta\delta > 10 \text{ MPa}^{1/2}$  are likely to be immiscible [24]. Thus, the solubility parameters provide a simple and generic approach for the development of solid dispersions.

**Table 6.1.** Calculated Hansen solubility parameters for PMOL and polymers.

Sample	$\delta_d$ (MPa <sup>1/2</sup> )	$\delta_p$ (MPa <sup>1/2</sup> )	$\delta_h$ (MPa <sup>1/2</sup> )	$\Delta \delta$
PMOL	19.43	9.71	13.88	-
SOL	15.14	0.45	12.18	6.34
VA	18.0	0.64	7.73	6.17

As shown in **Table 6.1**, the difference between the calculated solubility parameters of the polymers and the drug indicates that PMOL is likely to be miscible with both SOL and VA64. The miscibility of PMOL/VA64 is higher than that of PMOL/SOL as the  $\Delta\delta$  of the drug/copolymer formulations are 6.17 and 6.34 MPa<sup>1/2</sup>, respectively.

### 6.3.2. (F-H) theory for the prediction of drug/polymers interaction parameter

In order to determine the F-H interaction parameter ( $\chi$ ) [26–28] between PMOL and both polymers, the heat of fusion and melting temperatures of crystalline PMOL, as well as the glass transition temperature ( $T_g$ ) of both polymers were determined by DSC studies. The molar volumes of SOL, VA64, and PMOL were estimated from the functional group contributions of the chemical structures. The molecular volume calculated for PMOL is 120.95 cm<sup>3</sup>, whereas

those of SOL and VA64 are 380.04 (monomer) and 206.33 cm<sup>3</sup> (monomer), respectively. From Eqs. (2) and (3), the average value of  $\chi$  is calculated, as shown in **Table 6.2**.

**Table 6.2.** F–H interaction parameters for different melt extruded drug–polymer formulations.

Formulations	Volume Fractions (Drug/polymer) ( $\phi$ )	Nishi-Wang ( $\chi$ )	Hildebrand – Scott ( $\chi$ )
PMOL/SOL 40%	0.4:0.6	4.3±0.01	1.6
PMOL/SOL 50%	0.5:0.5	4.9±0.01	
PMOL/SOL 60%	0.6:0.4	6.0±0.01	
PMOL/VA64 40%	0.4:0.6	4.34±0.01	1.5
PMOL/VA64 50%	0.5:0.5	4.96±0.01	
PMOL/VA64 60%	0.6:0.4	5.98±0.01	

Generally, the negative values of the calculated interaction parameters indicate a net attraction force between two molecular compounds in a binary mixture, which is favourable for all compositions at the observed melting temperature of PMOL [29, 30]. Therefore, less positive values of  $\chi$  suggest stronger interactions between drug/polymers powders in the melting temperature (both drug and polymers). The data in **Table 6.2** show that both VA64 and SOL facilitate strong interactions with PMOL, which is in a good agreement with the predicted drug/copolymer miscibility estimated by the Hansen solubility parameters. Interestingly, by increasing the amount of PMOL in the SOL based formulations, the interaction strength increases. This could be attributed to the presence of a higher number of –NH groups and their contribution toward the interaction parameter compared with that of –COOH groups. The higher number of group contributors corresponding to the NH over –COOH molecules increases the net attraction forces between drug and polymer. It has previously been reported that interactions can take place between the amine group of the drug and the carboxyl group of the polymer [8, 9]. Similar trends have been observed for PMOL/VA64 formulations where interaction parameter increases with the increasing drug

content in the formulations. These findings together with the data obtained from Hansen solubility parameters complement each other suggesting good drug/polymer miscibility for PMOL/VA64 and PMOL/SOL formulations and possible drug–polymer interactions during extrusion processing. However, neither theoretical approach can predict possible polymorphic transformations in the melted state, apart from indicating possible drug/polymer interactions.

### 6.3.3. Thermal analysis

Differential scanning calorimetry studies were performed to investigate the physical state of PMOL within the polymer matrices [31]. The DSC thermogram of PMOL showed a sharp melting transition at 169.1°C ( $\Delta H$  137.00 J/g), which corresponds to polymorphic Form I (**Fig. 6.1**) [9]. In the case of SOL, an endothermic transition with a distinct step change was obtained at 68.4°C ( $\Delta H$  5.5 J/g), whereas for VA64 an endothermic transition was obtained at 105.5°C ( $\Delta H$  1.3 J/g); both endothermic transitions correspond to the  $T_g$  of the polymers.

**Table 6.3.** DSC data for PMOL, copolymers and HME extruded formulations.

Formulations	Glass transition/ enthalpy (°C)	Melting endotherm/ enthalpy (°C / $\Delta H$ , Jg <sup>-1</sup> )
PMOL	-	169.1/137.0
SOL	68.4	-
VA64	105.5	-
<b>Extruded formulations</b>		
PMOL/SOL 40%	70.8	141.3/9.7
PMOL/SOL 50%	59.5	144.6/6.4
PMOL/SOL 60%	81.8	150.8/11.6
PMOL/VA64 40%	52.9	137.0/13.3
PMOL/VA64 50%	105.8	131.3/7.2
PMOL/VA64 60%	102.2	123.3/5.5

The DSC scans of the PMOL/SOL extrudates (**Table 6.3**) showed melting endotherms at 141.3°C, 144.6°C, and 150.8°C that correspond to 40%, 50%, and 60% PMOL loadings,

respectively. The melting transitions detected are shifted to lower temperatures and the peak shapes are broader compared with those of pure PMOL suggesting the coexistence of amorphous and crystalline PMOL [11]. However, an increase in PMOL concentration in the extruded samples results in a higher fraction of crystalline drug in the polymer matrices. The melting transitions of PMOL between 141°C and 151°C indicate interactions between PMOL and the polymer [9–11].

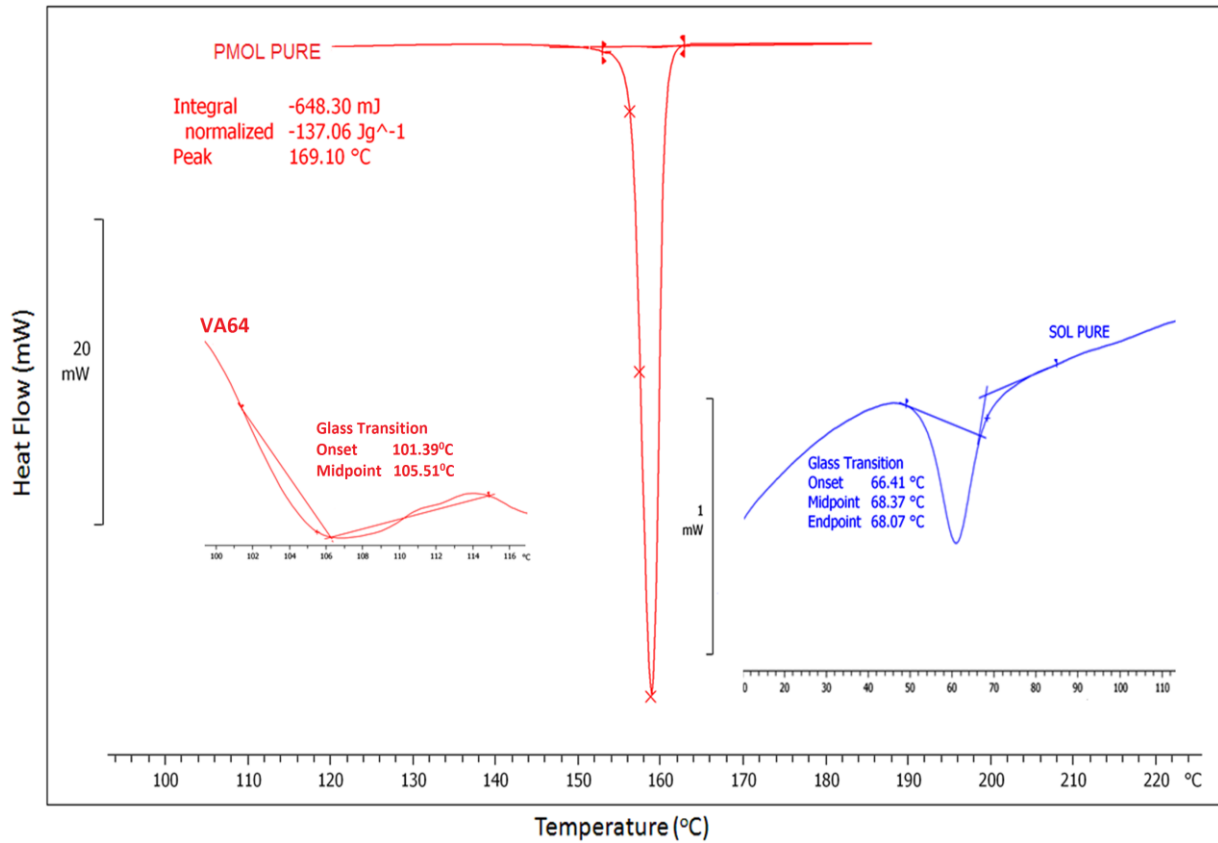


**Fig. 6.1.** DSC thermal transitions of PMOL and polymers.

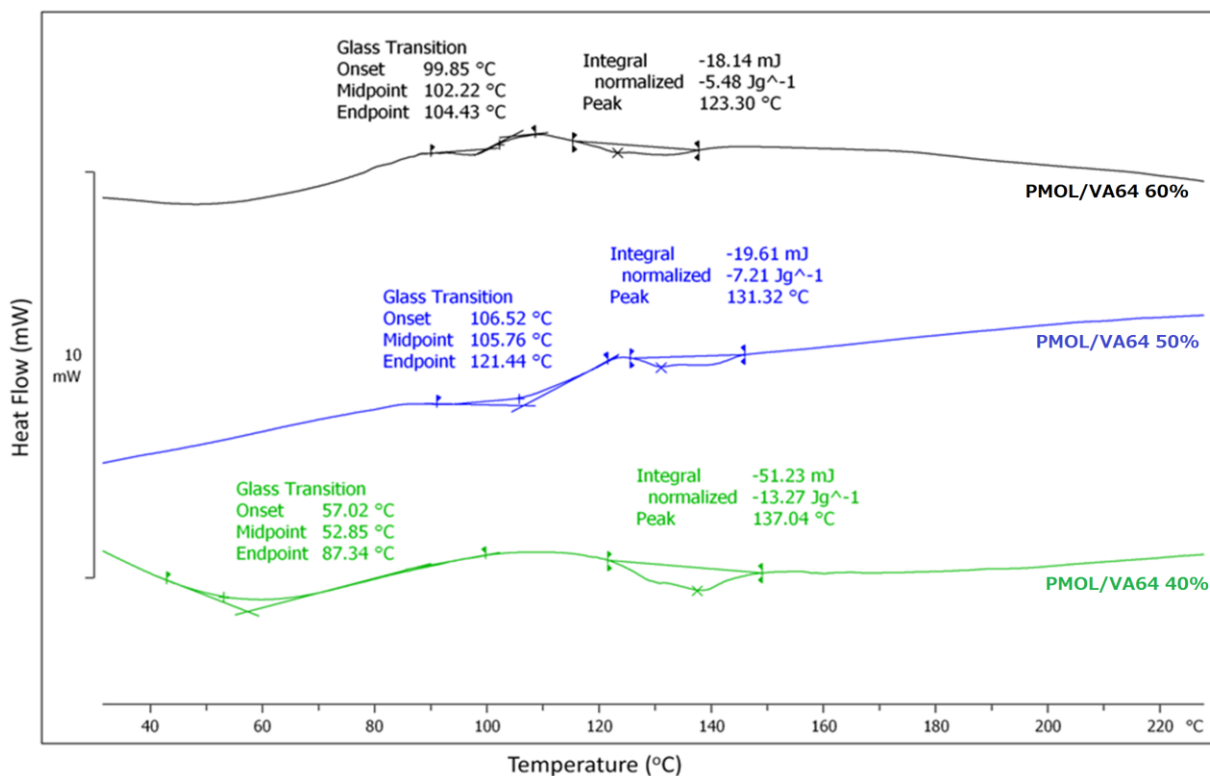


**Fig. 6.2.** Thermal transitions of PMOL-VA64 extruded formulations.

The PMOL/VA64 extrudates showed two endothermic transitions, one close to the  $T_g$  of bulk VA64 (105°C) and the other between 123°C and 137°C corresponding to the melting transitions of the drug, depending on the PMOL loadings. The  $T_g$  values range from 52°C to 102.2°C (**Fig. 6.2**) depending on the drug loadings. Similarly, the volume fraction of the PMOL is directly proportional to the amount of PMOL used and the melting transitions in the extruded formulations with SOL. Interestingly, a reverse effect was observed with the VA64 copolymer, where increasing fractions of PMOL resulted in lower drug melting points, due to the interaction of PMOL with the VA64 polymer.

Hot-stage microscopy studies were conducted to visually determine the thermal transitions and the extent of drug melting within the polymer matrices at different stages of heating. Images taken using HSM under optical light are shown in **Fig. 6.3**.

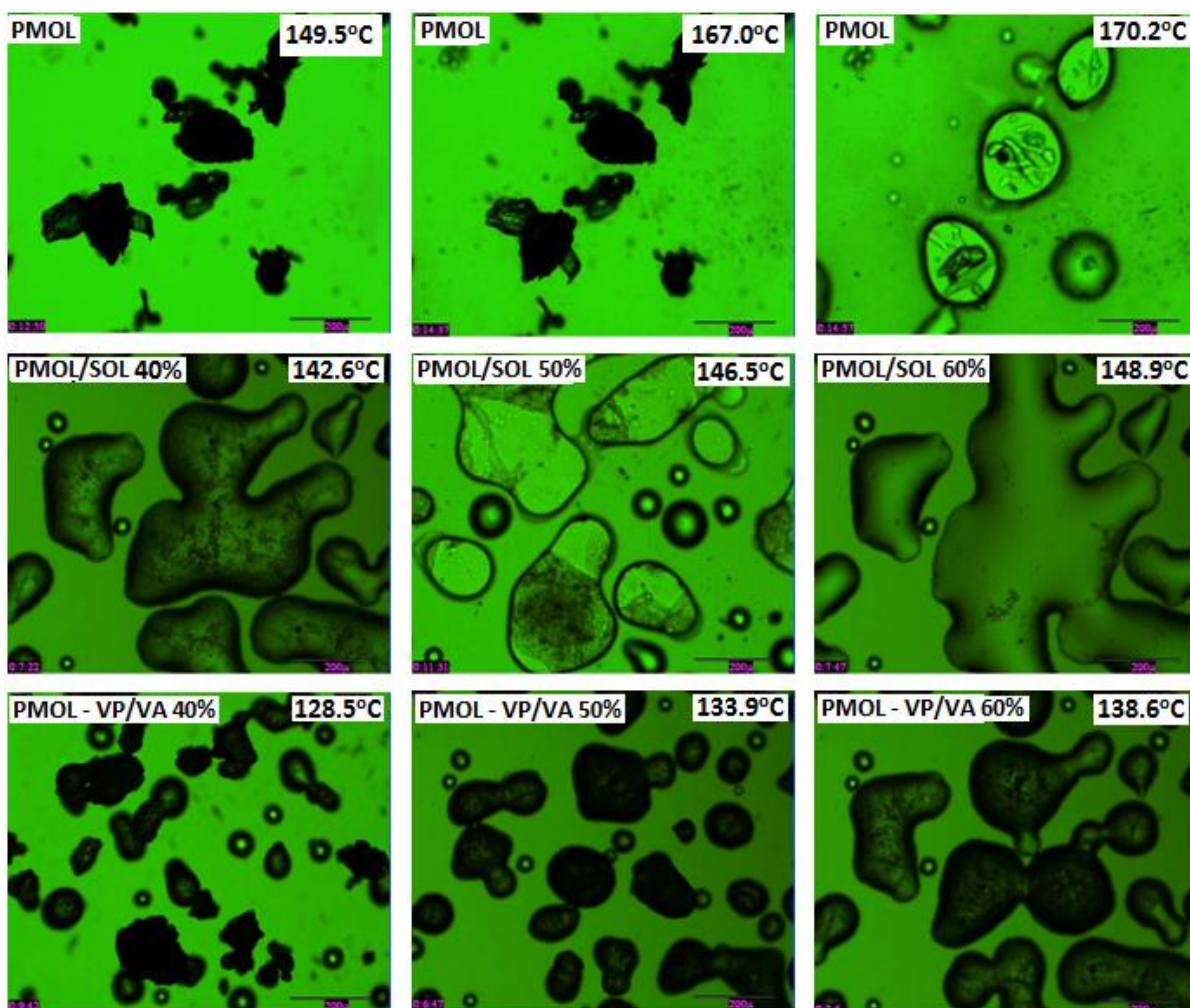


**Fig. 6.3.** HSM of pure PMOL and PMOL/SOL, PMOL/VA64 extruded formulations.

The bulk PMOL showed no change from 100°C to 169°C, which is in agreement with the DSC a result as no thermal transitions occurred until approximately 170.2°C. Similarly to the DSC thermograms, the PMOL/SOL extrudates showed nominal API melting until temperatures of 140°C– 142°C and thereafter showed extensive melting of the drug (**Fig. 6.3**). For the PMOL/VA64 extrudates, it was noted that PMOL started melting (and perhaps being solubilised) in the polymer matrix at 128°C or above. The differences observed between SOL and VA64 polymeric systems was mainly the temperature range where they started showing melting transitions. All formulations with VA64 displayed melting around 130°C, which is slightly lower than that observed for SOL (140°C) polymeric systems. This could potentially be attributed to the intermolecular interactions occurring during the extrusion processing.

#### 6.3.4. Variable-temperature X-ray powder diffraction

The main aim of the overall study was to investigate whether VTXRPD can be effectively used as a predictive tool for the determination of polymorphic transformations of drug/polymer systems prior to HME processing. For this reason, the effect of temperature on the polymorphic transformations of PMOL was investigated for bulk PMOL, PMOL/SOL, PMOL/VA64 PMs as well as the extruded formulations. These findings were then compared with the in-line NIR monitoring of the extruded formulations.

The standard XRPD profile for Form I (monoclinic) PMOL showed distinct crystalline peaks at 2-theta values of 12.11°, 13.82°, 15.52°, 18.20°, 20.42°, 23.51°, 24.39°, and 26.59° and a series of smaller (less intense) peaks at different 2-theta values ranging from 26.78° to 38.45° at ambient temperature. VTXRPD analysis of PMOL polymorph Form I clearly showed a peak shift as a function of increase temperature in the position of the 24.0° 2-theta indicative of some crystalline change (a distorted lattice on its way to becoming orthorhombic). This distortion of the lattice increases with increasing temperature at above 160°C (**Fig. 6.4**). A further increase in temperature led to the transformation of PMOL to polymorph Form II (orthorhombic), which was complete at 165°C (**Fig. 6.4**). The characteristic crystalline peak at 24.36° 2-theta for polymorphic Form I [32, 33] shifted to a new peak position at 24.03° 2-theta. This new peak displayed higher intensity than that at 24.36° and is strong evidence of the polymorphic transition from the monoclinic to the orthorhombic form.

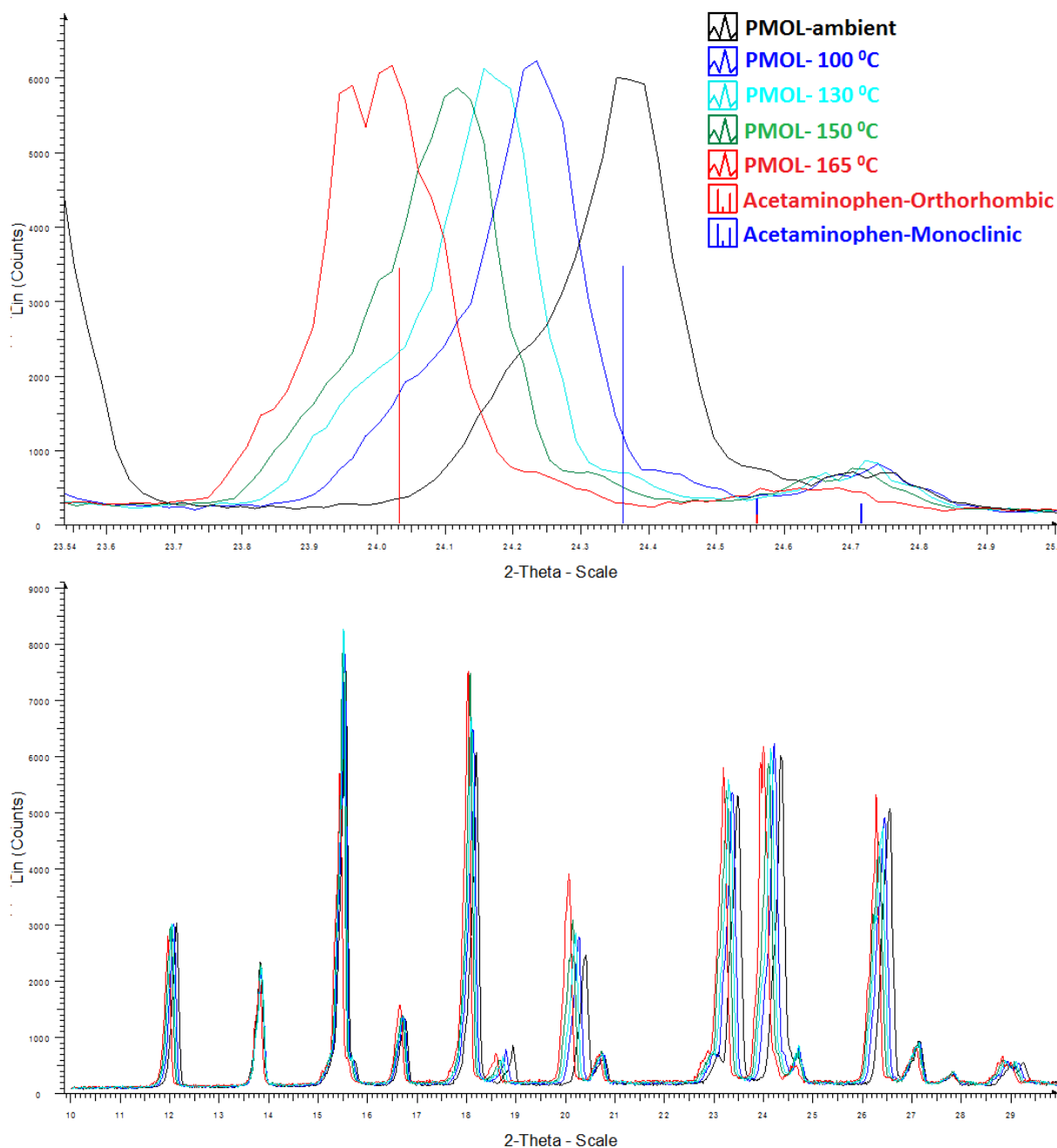


**Fig. 6.4.** VTXRPD diffractograms of bulk PMOL as a function of temperature.

Similar studies were undertaken for binary PMs and extruded formulations of PMOL/SOL and PMOL/VA64, **Fig. 6.5 – Fig. 6.8**. It is evident that both the SOL and VA64 play a key role in the PMOL polymorphic transformation where the critical transformation temperature is different to that of bulk PMOL. In the PMOL/SOL 40% PM, the characteristic peak at 24.4° 2-theta starts shifting with an increase in temperature and completely transforms at 112°C to a higher intensity peak at 24.0° 2-theta, which corresponds to the orthorhombic form (**Fig. 6.5**).

A further increase in temperature up to 120°C did not change the polymorphic form of PMOL (Form II) and then the XRPD peaks (e.g., 23.99°, 24.39° 2-theta) start decreasing in intensity even with a small temperature increase (e.g., 1°C increments). A similar thermal dependency was observed in the PMOL/SOL 40% extruded formulation (**Fig. 6.5**). The presence of SOL resulted in a significant reduction of the PMOL transformation temperature for polymorphic Form II. This observation is very important in relation to HME as it provides not only significant insights into the selection of extrusion temperature but also on the resultant nature of the extrudates.

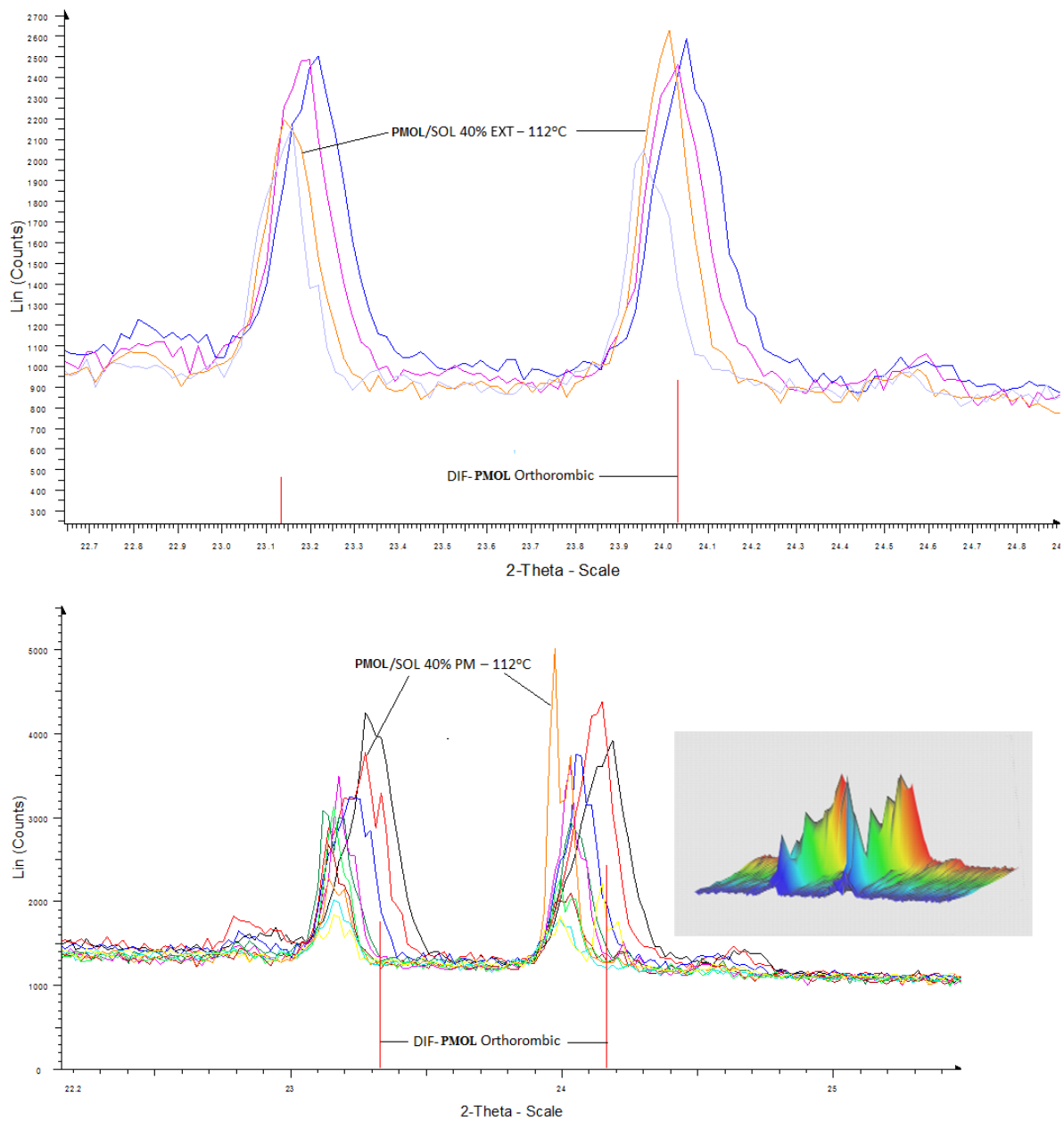


**Fig. 6.5.** VTXRPD diffractograms of PMOL/SOL 40% physical mixture (PM) and extruded formulations (EXT) at different temperatures (from ambient to 122°C).

Further VT-XRPD analysis was performed using PMOL/SOL 60% PM and extruded formulations where the temperature was increased up to 122°C and subsequently decreased to 100°C in order to investigate possible polymorphic transformations of PMOL (**Fig. 6.6**). Interestingly, as a result of the temperature increase a complete transformation of Form I PMOL to Form II was detected at 120°C (slightly higher than that of the PMOL/SOL 40% formulation), although the onset transformation temperature occurred at 112°C. The reason for the slight increase in the transformation temperature could be attributed to the increased amount of PMOL present in the PMOL/SOL 60% formulation. When the temperature was decreased from 120°C toward lower temperatures, a complete reverse transformation from Form II to Form I occurred. This observation indicates that the polymorphic transformation of PMOL in PMOL/SOL systems is reversible as a function of temperature.

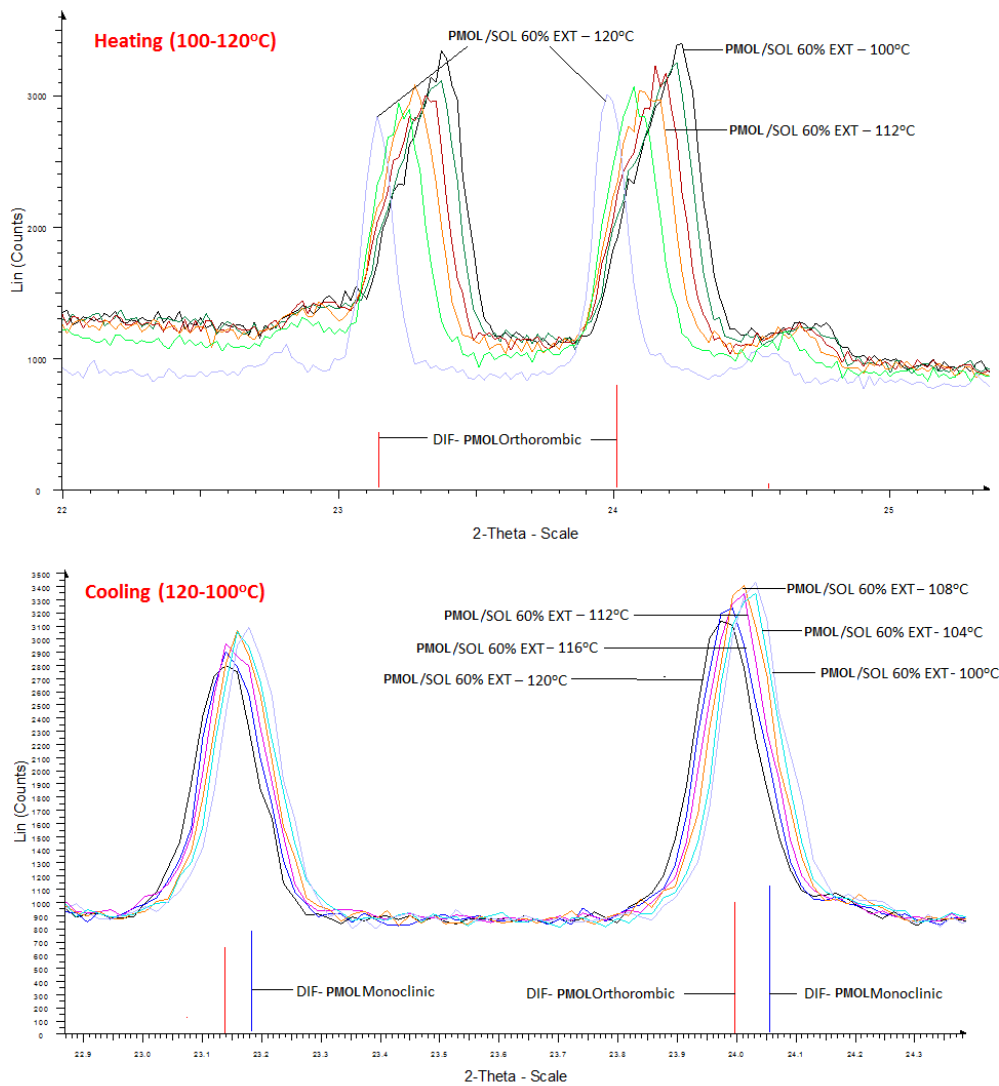


**Fig. 6.6.** VT-XRPD diffractograms of PMOL/SOL 60% extruded formulations at different temperatures (100-120°C; cooling and heating).

In the case of PMOL/VA64 60% extruded formulations, the diffraction pattern (ambient temperature) suggested the existence of Form I but as the temperature was increased a clear transformation to the orthorhombic form was found at 120°C and the characteristic diffraction peak shifted to 24.01° 2-theta, as shown in **Fig. 6.7**. Similar observations were made for other PM and extruded formulations in different drug loadings (e.g., PMOL/VA64 50% PM and extrudates).

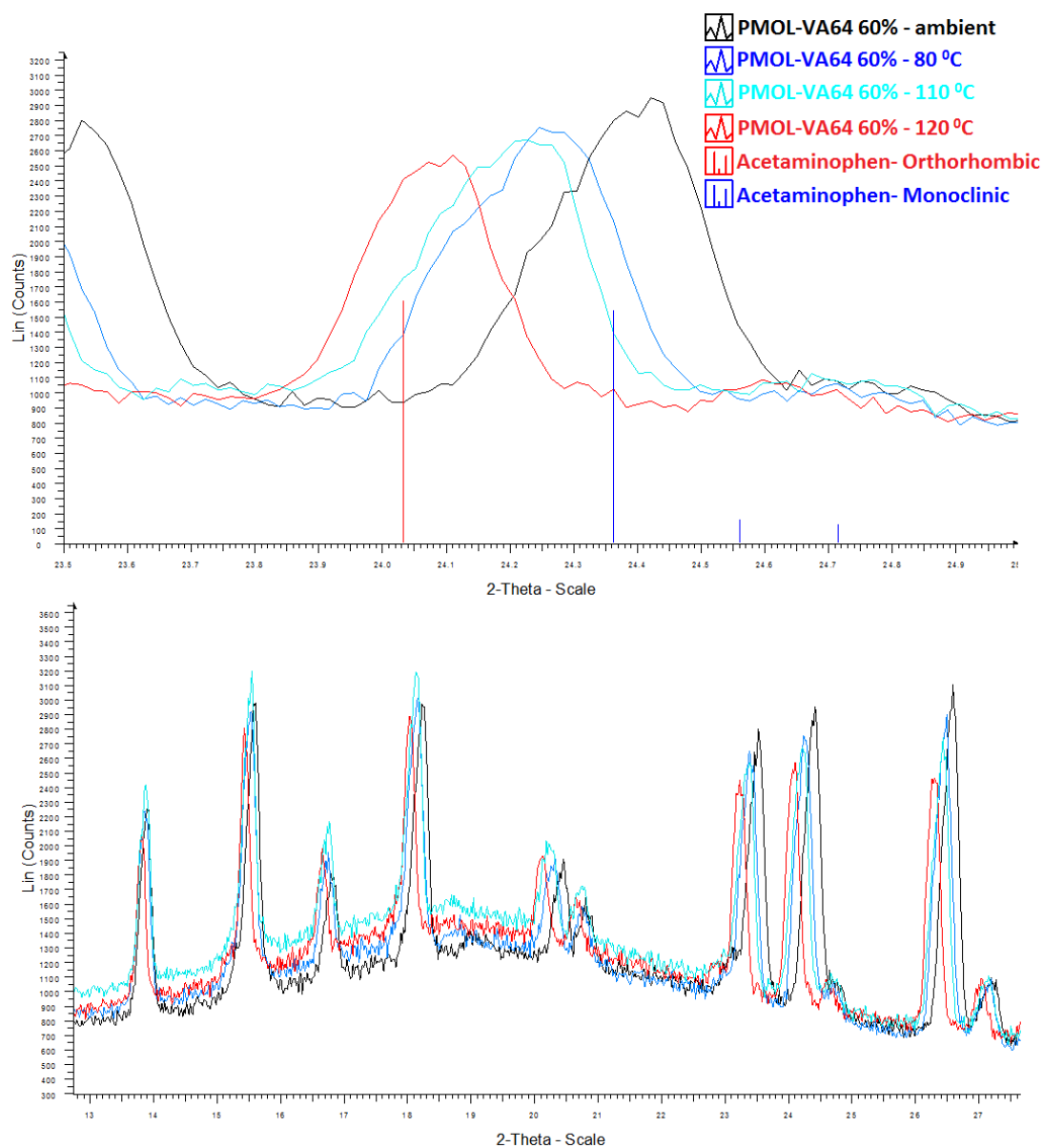


**Fig. 6.7.** VTXRPD diffractograms of PMOL-VA64 60% extruded formulations as a function of temperatures (from ambient to 122°C).

The PM of PMOL/VA64 40% formulation exhibited a transformation of PMOL at 120°C, which is higher in temperature than that of the PMOL/SOL 40% formulation (**Fig. 6.8**).

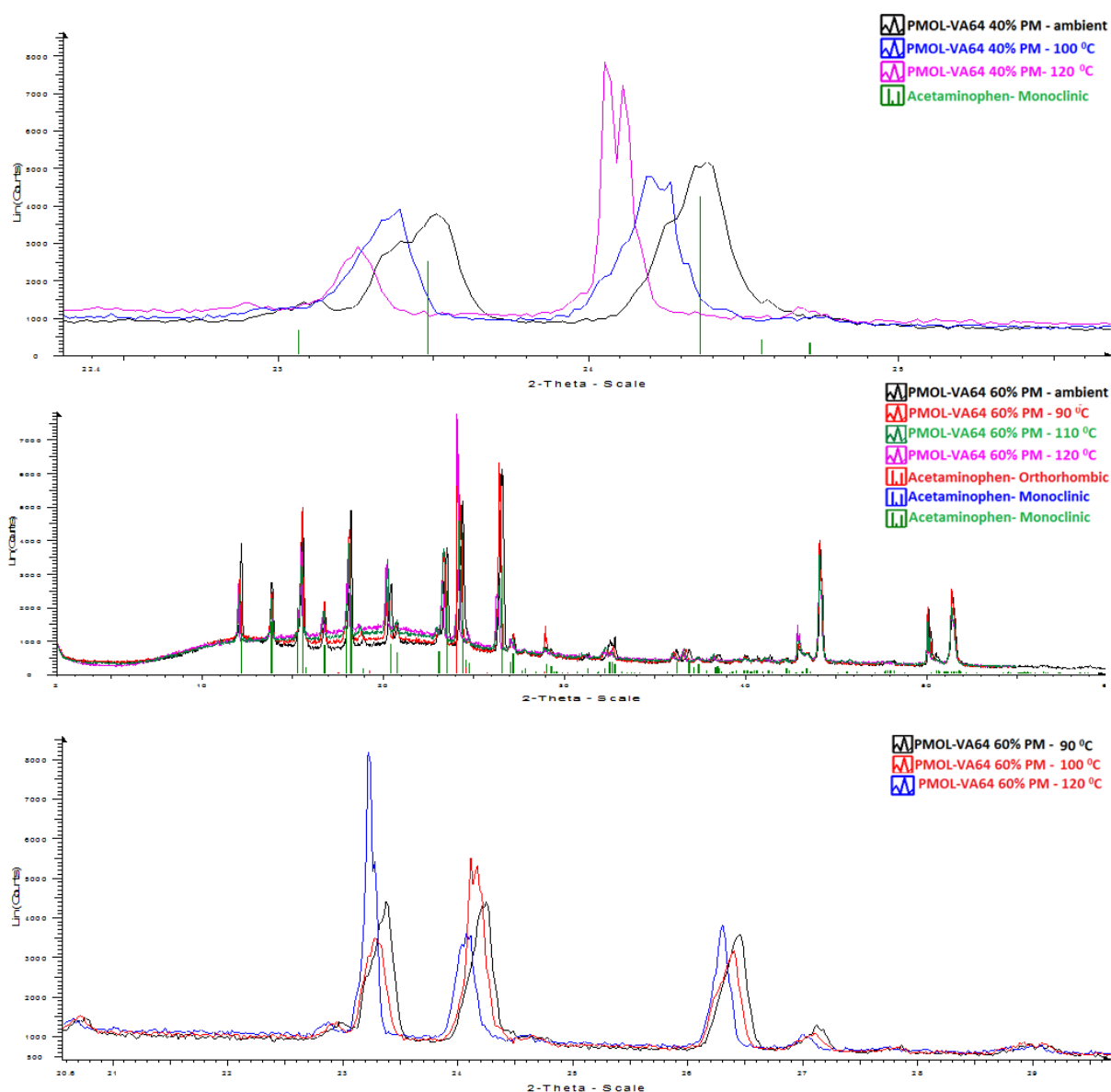


**Fig. 6.8.** VTXRPD diffractograms of PMOL-VA64 40% and 60% physical mixture (PM) at different temperatures (from ambient to 122°C).

This higher temperature could be due to the relatively higher  $T_g$  ( $\sim 105^\circ\text{C}$ ) of VA64 copolymer compared with the  $T_g$  of SOL ( $\sim 70^\circ\text{C}$ ). The exact temperatures at which the polymorphic transformations of PMOL from Form I to Form II were found in different formulations with both polymers are summarized in **Table 6.4**. The overall findings from VTXRPD analysis confirm that this technique can successfully be used as a predictive tool for extrusion processing and moreover to predict the possible temperature effects on polymorphic transformation of crystalline drugs, for example, PMOL. From the findings, it is clear that the drug loading plays a critical role in the polymorphic transformation temperature of PMOL Form I in PMOL/SOL systems. However, in the PMOL/VA64 formulations, the polymorphic

transformations occurred at 120°C regardless of the drug loadings. A quite similar study has been reported elsewhere for the prediction and analysis of the polymorphic transformation of mebendazole Form C by applying a similar approach [34].

**Table 6.4.** Polymorphic transformation temperatures of formulations physical mixtures (PMs) and extruded formulations (EX).

Formulations (PM and EXT) (w/w, %)	Temperature of polymorphic transformation (°C)
PMOL/SOL (40%)	112
PMOL/SOL (50%)	Starts at 112, completes at 116
PMOL/SOL (60%)	Starts at 112, completes at 120
PMOL/VA64 (40%)	120
PMOL/VA64 (50%)	120
PMOL/VA64 (60%)	120

### 6.3.5. In-line NIR spectroscopy monitoring

Near-infrared spectra of PMOL Form I were measured off-line to determine the characteristic vibrational bands attributable to this polymorph (**Fig. 6.9**). Subsequently, in-line NIR spectra of the PMOL/SOL 60% formulation were collected from different mixing zones during HME. The second derivative spectra in **Fig. 6.9a** show that there is a significant band shift between the NIR spectrum of PMOL Form I and the PMOL in the extruded formulation. The vibrational band due to the SOL in this region was flat indicating that it was not affecting the PMOL vibrational bands. It has been reported in previous NIR studies [35, 36] that the two polymorphs of PMOL (Form I and Form II) exhibit different vibrational band profiles. Similarly, from the data in **Fig. 6.9b**, it can be seen that the second derivative NIR spectra showed a significant band shift, notably between 6400 and 6300  $\text{cm}^{-1}$ , indicating that the polymorphic transformation of PMOL from its most stable Form I to the relatively less stable Form II takes place during the HME process at 120°C. From the results obtained, it can be concluded that the band shifts between the NIR spectra of PMOL Form I and the extrudates (PMOL/SOL 40%–60%) support the findings from the VTXRPD data with regard to the predictions of the polymorphic transformation of PMOL (from its Form I to Form II) during HME.

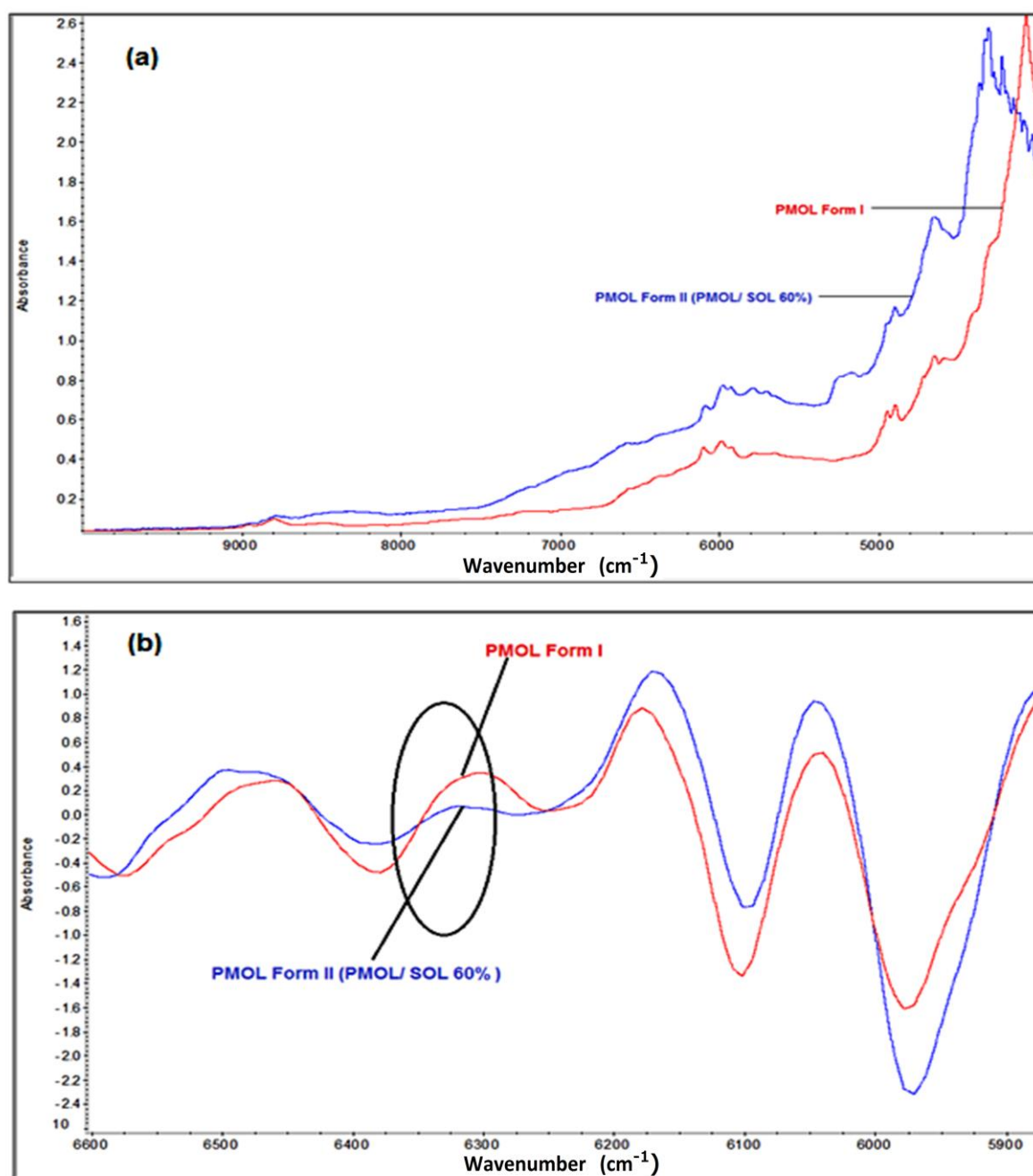


**Fig. 6.9.** (a) NIR spectra of PMOL pure Form I and PMOL extrudate at 120°C; (b) 2nd derivative NIR spectra.

## 6.4. Conclusions

In this study, VTMRPD was successfully implemented as an off-line predictive tool of drug transformation during HME processing. By observing the polymorphic transformations of PMOL and water-soluble polymers (SOL, VA64) PMs as a function of temperature, it was possible to identify identical trends for the extruded formulations of the same compositions. The study of the polymorphic transformations of PMOL in various formulations via VTMRPD

demonstrated that the stable Form I (monoclinic) of PMOL transformed to Form II (orthorhombic) depending on the applied temperature, the nature of the polymer used and the actual drug loading. The drug loading was found to affect the onset transformation temperatures for the PMOL/SOL blends but not for the PMOL/VA64, which was attributed to the different drug–polymer interaction strength. In-line NIR monitoring studies confirmed exactly the same transformations during the extrusion processing of PMOL/polymer formulations. In conclusion, VTXRPD can effectively be used as a predictive tool to monitor possible polymorphic transformation of APIs in solid dispersions but also as a valuable technique for the development of extruded formulations by potentially reducing processing times and experimentation. Most importantly, VTXRPD could provide excellent process understanding when combined with other analytical techniques, for example, in-line NIR.

## 6.5. References

1. Sekiguchi K, Obi N, Studies on absorption of eutectic mixtures. I. A comparison of the behavior of eutectic mixtures of sulphathiazole and that of ordinary sulphathiazole in man, *Chemical and Pharmaceutical Bulletin*, 1961; **9**: 866–872.
2. Srinarong P, deWaard H, Frijlink HW, Hinrichs WL, Improved dissolution behavior of lipophilic drugs by solid dispersions: The production process as starting point for formulation considerations, *Expert Opinion on Drug Delivery*, 2011; **8**(9): 1121–1140.
3. Alam MA, Ali R, Al-Jenoobi FI, Al-Mohizea AM, Solid dispersions: A strategy for poorly aqueous soluble drugs and technology updates, *Expert Opinion on Drug Delivery*, 2012; **9**(11): 1419–1440.
4. Jang DJ, Sim T, Oh E, Formulation and optimization of spraydried amlodipine solid dispersion for enhanced oral absorption, *Drug Development and Industrial Pharmacy*, 2013; **39**(7): 1133–1141.
5. Kushida I, Gotoda M, Investigation for the amorphous state of ER-34122, a dual 5 lipoxigenase/cyclooxygenase inhibitor with poor aqueous solubility, in HPMC solid dispersion prepared by the solvent evaporation method, *Drug Development and Industrial Pharmacy*, 2013; **39**(10): 1582–1588.
6. He X, Pei L, Tong HH, Zheng Y, Comparison of spray freeze drying and the solvent evaporation method for preparing solid dispersions of baicalein with Pluronic F68 to improve dissolution and oral bioavailability, *AAPS PharmSciTech*, 2011; **12**(1): 104–113.

7. Gong K, Viboonkiat R, Rehman IU, Buckton G, Darr JA, Formation and characterization of porous indomethacin-VA64 coprecipitates prepared using solvent-free supercritical fluid processing, *Journal of Pharmaceutical Sciences*, 2005; **94**(12): 2583–2590.
8. Maniruzzaman M, Rana MM, Boateng JS, Mitchell JC, Douroumis D, Dissolution enhancement of poorly water-soluble APIs processed by hot-melt extrusion using hydrophilic copolymers, *Drug Development and Industrial Pharmacy*, 2013; **39**(2): 218–227.
9. Maniruzzaman M, Boateng JS, Bonnefille M, Aranyos A, Mitchell JC, Douroumis D, Taste masking of paracetamol by hot-melt extrusion: An in vitro and in vivo evaluation, *European Journal of Pharmaceutics and Biopharmaceutics*, 2012; **80**(2): 433–442.
10. Qi S, Avasle P, Saklatvala R, Craig DQM, An investigation into the effects of thermal history on the crystallisation behaviour of amorphous paracetamol, *European Journal of Pharmaceutics and Biopharmaceutics*, 2008; **69**: 364–371.
11. Qi S, Gryczke A, Belton P, Craig DQM, Characterisation of solid dispersions of paracetamol and Eudragit® prepared by hot-melt extrusion using thermal, microthermal and spectroscopic analysis, *International Journal of Pharmaceutics*, 2008; **354**: 158–167.
12. Saerens L, Dierickx L, Lenain B, Vervaet C, Remon JP, De Beer T, Raman spectroscopy for the in-line copolymer–drug quantification and solid state characterization during a pharmaceutical hot-melt extrusion process, *European Journal of Pharmaceutics and Biopharmaceutics*, 2010; **77**: 158–163.
13. Rastogi SK, Zakrzewski M, Suryanarayanan R, Investigation of solid-state reactions using variable temperature X-ray powder diffractometry. I. Aspartame hemihydrates, *Pharmaceutical Research*, 2001; **18**: 267–273.
14. Rollinger JM, Burger A, Physicochemical characterization of hydrated and anhydrous crystal forms of amlodipine besylate, *Journal of Thermal Analysis and Calorimetry*, 2002; **68**: 361–372.
15. Rastogi SK, Zakrzewski M, Suryanarayanan R, Investigation of solid-state reactions using variable temperature X-ray powder diffractometry. II. Aminophylline monohydrate, *Pharmaceutical Research*, 2002; **19**: 1265–1273.

16. Li Y, Han J, Yang GG, Grant DJ, Suryanarayanan R, In situ dehydration of carbamazepine dihydrate: A novel technique to prepare amorphous anhydrous carbamazepine, *Pharmaceutical Development Technology*, 2000; **5**: 257–266.
17. Vercruyse J, Toiviainen M, Fonteyne M, Helkimo N, Ketolainen J, Juuti M, Delaet U, Van Assche I, Remonm JP, Vervaet C, De Beer T, Visualization and understanding of the granulation liquidmixing and distribution during continuous twin screw granulation using NIR chemical imaging, *European Journal of Pharmaceutics and Biopharmaceutics*, 2014; **86**(3): 383–392.
18. Hansen L, De Beer T, Pieters S, Heyden YV, Vervaet C, Remon JP, Montenez JP, Daoussi R, Near-infrared spectroscopic evaluation of lyophilized viral vaccine formulations, *Biotechnology Progress*, 2013; **29**(6): 1573–1586.
19. Hansen CM, The universality of the solubility parameter, *Industrial & Engineering Chemistry Research and Development*, 1969; **8**: 2–11.
20. Hoftyzer PJ, Krevelen DWV, *Properties of copolymers*. Amsterdam: Elsevier. 1976.
21. Nishi T, Wang TT, Melting point depression and kinetic effects of cooling on crystallization in poly(vinylidene fluoride)-poly (methyl methacrylate) mixtures, *Macromolecules*, 1975; **8**: 909–915.
22. Hildebrand J, Scott R, *Solubility of non-electrolytes*, 3rd ed. New York: Reinhold. 1950.
23. Kabekkodu SN, PDF-2 Release. Newtown Square, Pennsylvania: International Centre for Diffraction Data, 2008.
24. Hempenstall FJ, Tucker I, Rades T, Selection of excipients for melt extrusion with two poorlywater-soluble drugs by solubility parameter calculation and thermal analysis, *International Journal of Pharmaceutics*, 2001; **226**(1–2): 147–161.
25. Zheng X, Yang R, Tang X, Zheng L. Part I: Characterization of solid dispersions of nimodipine prepared by hot-melt extrusion, *Drug Development and Industrial Pharmacy*, 2007; **33**: 791–802.
26. Higgins JS, Lipson JES, White RP. A simple approach to copolymer mixture miscibility, *Philosophical Transaction of the Royal Society*, 2010; **368**: 1009–1025.
27. Paudel A, Nies E, Van den Mooter G, Relating hydrogenbonding interactions with the phase behavior of naproxen/PVP K 25 solid dispersions: Evaluation of solution-cast and quench-cooled films, *Molecular Pharmaceutics*, 2012; **9**(11): 3301–3317.

28. Tian Y, Caron V, Jones DS, Healy AM, Andrews GP, Using Flory–Huggins phase diagrams as a pre-formulation tool for the production of amorphous solid dispersions: A comparison between hot-melt extrusion and spray drying, *Journal of Pharmacy Pharmacology*, 2013; **66**(2): 256–274.
29. Zhao Y, Inbar P, Chokshi HP, Malick W, Choi DS, Prediction of the thermal phase diagram of amorphous solid dispersions by Flory– Huggins theory, *Journal of Pharmaceutical Sciences*, 2011; **100**(8): 3196–3207.
30. Janssens S, De Zeure A, Paudel A, Van Humbeeck J, Rombaut P, Van den Mooter G, Influence of preparation methods on solid state supersaturation of amorphous solid dispersions: A case study with itraconazole and eudragit E100, *Pharmaceutical Research*, 2010; **27**: 775–785.
31. Maniruzzaman M, Morgan DJ, Mendham AP, Pang J, Snowden MJ, Douroumis D, Drug–copolymer intermolecular interactions in hot-melt extruded solid dispersions, *International Journal of Pharmaceutics*, 2013; **443**(1–2): 199–208.
32. Rossi A, Savioli A, BiniM, Capsoni D, Massarotti V, Bettini R, Gazzaniga A, Sangalli ME, Giordano F, Solid-state characterization of paracetamol metastable polymorphs formed in binary mixtures with hydroxypropylmethylcellulose, *Thermochimica Acta*, 2001; **406**: 55–67.
33. Martino PD, Conflant P, Drache M, Huvenne JP, Guyot- Hermann AM, Preparation and physical characterization of forms II and III of paracetamol, *Journal of Thermal Analysis and Calorimetry*, 1997; **48**(3): 447–458.
34. De Villiers MM, Terblanche RJ, Liebenberg W, Swanepoel E, Dekker TG, Mingna S, Variable-temperature X-ray powder diffraction analysis of the crystal transformation of the pharmaceutically preferred polymorph C of mebendazole, *Journal of Pharmaceutical and Biomedical Analysis*, 2005; **38**: 435–441.
35. Wang IC, Lee MJ, Seo DY, Lee HE, Choi Y, Kim WS, Kim CS, Jeong MY, Choi GJ, Polymorph transformation in paracetamol monitored by in-line NIR spectroscopy during a cooling crystallization process, *AAPS PharmSciTech*, 2011; **12**(2): 764–770.
36. Khanmohammadi M, Garmarudi AB, Moazzen N, Ghasemi K, Qualitative discrimination between paracetamol tablets made by near infrared spectroscopy and chemometrics with regard to polymorphism, *Journal of Structural Chemistry*, 2010; **51**(4): 663–669.

## Chapter 7: Overall conclusions and future work

---

### 7.1. Overall conclusions

HME has already proved to be a robust method for producing numerous drug delivery systems and is a continuous manufacturing technique. Emerging analytical technologies have facilitated a range of testing approaches to assess critical material attributes of pharmaceutical products. Industry is moving towards the use of a continuous manufacturing paradigm. HME is one such operational technique, conducted in a continuous mode, which can be coupled with the PAT tools to function as part of the next generation technology to manufacture, control and ensure the final quality of pharmaceutical products. By insertion of in-line probes and spectral detectors it is possible to monitor, determine and understand compositional and process aspects of the molecular entities produced via HME. Conventionally, HME equipped with standard process monitoring sensors such as temperature and pressure probes has been used to control HME processes. However, these two probes do not give information about the critical quality attributes of the HME products and cannot ensure the pre-defined quality of the end products. So, the implementation of process monitoring using spectroscopic techniques such as NIR was evaluated in this research. NIR spectroscopy has been used in this research, to monitor and understand the final quality HME products using a QbD approach, cocrystallization, transformation of a drug from crystalline to amorphous states and to predict the polymorphic transformation of a drug during HME processing.

In-line NIR monitoring was successfully used during PMOL/EC/C888 extrusion to produce sustained release formulations. A fractional factorial design experiment using three dependent variables (screw speed, drug loading and feed rate) was designed prior to extrusion. A NIR probe was inserted in the HME die in order to monitor and collect spectra during extrusion. A PLS calibration model was developed using the collected spectra after processing via SNV, to predict PMOL concentration during HME. A PCA plot model has also been prepared which demonstrates that three formulations (F1, F4 and F5) amongst 11 formulations have very good repeatability in terms of PC scores. Extrudates were collected as 1 mm pellets using a pelletizer and then milled using a rotary cutter mill to produce particles of less than 250  $\mu\text{m}$  diameter, which were then blended with excipients to produce tablets. The freshly prepared tablets were then subjected to dissolution studies to evaluate their drug release patterns, and it was found that three formulations (F1, F4 and F5) showed sustained PMOL release for 12 h compared with the other formulations. Dissolution results were then inputted into the data analysis

software for statistical analysis and from the correlation analysis it was shown that drug loading, as a critical processing parameter, has a significant effect in dissolution studies, whilst the other two processing parameters (screw speed and feed rate) does not show any significant effect on the rate of drug release.

Cocrystallization process monitoring during HME was performed via in-line NIR spectroscopy as a PAT tool. Carbamazepine (CBZ) was selected as a model drug to produce cocrystals with two different coformers saccharine (SCH) and *trans*-cinnamic acid (TCA) and blended using 1:1 molar ratio. Various temperature profiles were applied for the production of cocrystals by HME, which demonstrates that temperature is a critical processing parameter. An in-line NIR probe was inserted in three different mixing zones of the HME barrel to collect spectra, and off-line NIR spectra of extruded cocrystals were also obtained. Cocrystallization occurred by the formation of H-bonds between the drug and coformer, and this resulted in the formation of a new vibrational band in the NIR spectra collected from the cocrystals compared with the spectra collected from the physical mixtures. The analysis of NIR spectra from different mixing zones and final extrudates demonstrated that the formation of cocrystals occurred after the 2<sup>nd</sup> mixing zone of the HME and gradually increased until the final extrudates. This analysis was confirmed by using DSC and XRPD as reference methods. Dissolution studies of the cocrystals showed improved drug release profiles compared with the prototype cocrystals produced via solvent evaporation.

In-line transmission and reflectance NIR probes were employed as PAT tools for monitoring the HME processing of IND/ SOL and IND/VA64 extrudates. By using both NIR probes (reflectance and transmission) it was possible to monitor the transformation of IND from the crystalline to the amorphous state at various drug/polymer ratios. An in-line reflectance NIR probe was used to collect NIR spectra of IND/polymer mixtures, at different weight ratios, in the first mixing zone of the HME. Via the use of a specially designed die an in-line NIR transmission probe was used to characterize extruded films constituted of the different ratios of IND and the two different polymers. Physicochemical characterization, using DSC and XRPD, of IND/polymer granules (obtained by cutter milling the extruded transparent films) confirmed the plasticization effect of IND and the manufacture of solid solutions with IND being molecularly dispersed in the polymer matrices. The PCA plots obtained from the NIR transmission spectra showed that a change in the screw speed of the extruder results in different NIR spectra. Confocal Raman spectroscopic data was used to show the homogeneity

of the IND/polymer film extrudates. Extruded formulations showed enhanced drug release properties compared with bulk IND, which is an agreement with previous studies. Therefore, the use of a transmission NIR probe proved to be a valuable PAT tool for monitoring and process understanding of molecular dispersions produced via HME.

Furthermore, in-line NIR was also used as a predictive tool together with VTXRPD during the polymorphic transformation of PMOL. VTXRPD was successfully implemented as an off-line predictive tool for drug transformation during HME processing. The study of the polymorphic transformations of PMOL in various formulations (different weight ratios of PMOL with SOL and VA64) via VTXRPD demonstrated that the stable Form I (monoclinic) of PMOL transformed to Form II (orthorhombic) depending on the applied temperature, the nature of the polymer used and the drug loading. The drug loading was found to affect the onset transformation temperatures for the PMOL/SOL blends but not for the PMOL/VA64, which was attributed to the differences in drug-polymer interactions. In-line NIR monitoring studies confirmed similar polymorphic transformations during the extrusion processing of PMOL/polymer formulations.

Cocrystals formed using three different sugar alcohols (mannitol, sorbitol and xylitol) were successfully produced via HME. In-line NIR monitoring revealed that cocrystallization occurred due to the intense mixing of the materials while passing through the mixing zones of the extruder during HME, which was confirmed by the use of DSC and XRPD data as reference methods. However, after grinding all of the extruded formulations showed excellent flow properties compared to the commercial binder (Starlac). Furthermore, the grounded sugar cocrystals, prepared using different weight ratios of sugars, were used to prepare tablets which exhibited good compressibility, friability properties and a decrease in disintegration time compared with tablets prepared from the commercial binder (Starlac).

## 7.2. Future work

The scope of NIR as a PAT tool in HME is broadening because of its flexibility to be used as a fast, non-destructive analytical tool. The results reported in this thesis demonstrate the successful implementation of NIR spectroscopy in HME processing of pharmaceuticals to produce sustained release formulations using a QbD paradigm, production of cocrystals, to monitor and understand the transformation of a drug from the crystalline to the amorphous state, and to predict polymorphic transformations. However, other PAT tools such as Raman spectroscopy and ultrasonic techniques could be used to investigate processing parameters in HME and quality attributes of the extrudates.

Future work using PAT tools in HME include the following.

- As HME is a continuous manufacturing technique, industries are moving towards this paradigm. Therefore, by implementing both in-line NIR and Raman spectroscopies it would be possible to scale-up laboratory based manufacturing processes to pilot scale, where NIR could be used as both a qualitative and quantitative tool to monitor and understand the process whilst Raman spectroscopy (on-line and off-line) could be used to detect any possible degradation of molecular entities as well as mapping and imaging the final products resulting from HME processing.
- Both in-line NIR and Raman spectroscopy could be coupled with HME to produce different delivery systems using a QbD approach to develop a design space using critical HME processing parameters and the critical quality attributes of the extrudates.
- Implementation of ultrasonic techniques in HME could be used to produce nanocrystals and in-line/off-line NIR and Raman spectroscopic techniques employed to characterize the nanocrystals during and after extrusion.
- To establish the cocrystal from the sugars, single X-ray crystallography would be helpful. A comparison study between conventional PMOL tablets with PMOL tablets produced from HME processed sugar cocrystal would be appropriate to evaluate the benefits of the sugar cocrystals. Stability will also important to understand the stability of the tablets.